

---

**From Lost Adhesion to Tumor Spreading –  
The Upregulation of IGF2BP1  
Controls a Targetable Mesenchymal Shift in  
Ovarian Cancer**

---

**Dissertation**

zur Erlangung des akademischen Grades

*doctor rerum naturalium*

(Dr. rer. nat.)

der

Naturwissenschaftlichen Fakultät I – Biowissenschaften

der Martin-Luther-Universität Halle-Wittenberg

vorgelegt

von Annekatriin Schott

geboren am 22.04.1993 in Rodewisch

1. Gutachter/in: Prof. Dr. Stefan Hüttelmaier

2. Gutachter/in: Prof. Dr. Sonja Keßler

3. Gutachter/in: Prof. Dr. Achim Aigner

Datum der Einreichung: 10.02.2022

Datum der öffentlichen Verteidigung: 05.10.2022

# TABLE OF CONTENT

1	INTRODUCTION.....	1
1.1	Epithelial ovarian carcinoma.....	1
1.1.1	Characterization of epithelial ovarian carcinoma and its heterogeneity.....	1
1.1.2	The vulnerability of EOC – from diagnosis, current therapy and targeting occurring resistances.....	4
1.2	From tissue integrity to cancer evolution and spreading.....	6
1.2.1	Epithelial-mesenchymal transition.....	6
1.2.2	Cell junctions.....	7
1.2.3	Adherens junctions in adhesion and cancer.....	8
1.3	The role of the oncogene SRC in cancer and therapy.....	13
1.3.1	SRC kinase activation and signaling during metastasis.....	13
1.3.2	Targeting SRC and ERK signaling in EOC.....	16
1.4	Conferring AJ-mediated signals to gene expression with the hippo pathway.....	17
1.5	Post-transcriptional regulation with the oncofetal IGF2BP1.....	19
1.6	Aims of the study.....	24
2	MATERIAL AND METHODS.....	25
2.1	Material.....	25
2.1.1	Chemicals and reagents.....	25
2.1.2	Bacteria strain.....	25
2.1.3	Cell lines.....	25
2.1.4	Primary and secondary antibodies.....	26
2.1.5	Plasmids.....	27
2.1.6	Oligonucleotides.....	28
2.1.7	Standard systems and Kits.....	31
2.1.8	Standard buffers.....	32
2.1.9	Devices.....	32
2.2	Cell biological methods.....	33
2.2.1	Cell culture.....	33
2.2.2	Transfections & reporter assays.....	33
2.2.2.1	siRNA transfection.....	33
2.2.2.2	Plasmid transfection.....	34
2.2.3	3D spheroid assays (growth, invasion).....	34
2.2.4	Inhibitor treatment.....	35
2.2.4.1	PP2, saracatinib, selumetinib, verteporfin and BTYNB.....	35
2.2.4.2	Emetine and actinomycin D.....	35

TABLE OF CONTENT

2.2.5	Protein labeling for translational monitoring.....	36
2.2.6	Establishment of CRISPR-Cas9 cell clones .....	36
2.2.7	Lentiviral transduction.....	37
2.3	Molecular biological methods .....	37
2.3.1	Cloning .....	37
2.3.2	Isolation of genomic DNA .....	38
2.3.3	RNA isolation .....	39
2.3.4	Reverse transcription & quantitative real-time PCR (qRT-PCR) .....	39
2.3.5	RNA-co-immunoprecipitation (RIP) .....	40
2.4	Protein-biochemical methods .....	40
2.4.1	Protein extraction, SDS-PAGE and Western Blot.....	40
2.4.2	Pull-down of active GTPases.....	41
2.4.3	Transcriptional monitoring with CLICK chemistry .....	41
2.4.4	Luminescence-based cell viability assay .....	42
2.4.5	Luminescence-based reporter assays.....	42
2.4.6	Quantitative proteomics .....	43
2.5	Microscopy.....	43
2.5.1	Bright field microscopy.....	43
2.5.2	Fluorescence microscopy with CLSM technique .....	43
2.5.3	Live-cell imaging via Incucyte S3.....	43
2.6	Mouse Xenograft studies and Ethics Approvals .....	44
2.7	Data analysis .....	44
2.7.1	NGS analysis.....	44
2.7.2	Functional enrichment analysis .....	45
2.7.3	Patient survival analysis .....	45
2.7.4	CLIP analysis.....	45
2.7.5	miRNA prediction.....	46
2.7.6	Synergy analysis.....	46
2.8	Statistics .....	46
3	RESULTS.....	47
3.1	The mesenchymal force of the proto-oncogenic mRNA binding protein IGF2BP1 in epithelial ovarian carcinoma .....	47
3.2	IGF2BP1 promotes AJ turnover without direct modulation of their mRNAs.....	53
3.3	IGF2BP1-dependent SRC activation mediates AJ disassembly.....	62
3.4	Overcoming contact inhibition of proliferation with IGF2BP1 by directly modulating YAP1 .....	69
3.5	Combined treatment of saracatinib and selumetinib effectively impairs IGF2BP1- driven invasive growth <i>in vitro</i> and <i>in vivo</i> .....	76

TABLE OF CONTENT

---

4	DISCUSSION.....	87
4.1	Upregulation of IGF2BP1 impairs AJ maintenance and promotes EMT in EOC .	88
4.2	The cooperation of the two oncogenic drivers SRC & IGF2BP1 .....	90
4.3	The strategies of IGF2BP1 to counter contact inhibition of proliferation.....	92
4.4	Targeted treatment strategies for IGF2BP1-driven ovarian tumors.....	96
5	SUMMARY .....	101
	REFERENCES .....	102
	APPENDIX.....	121
	Additional data .....	121
	List of figures.....	124
	List of tables .....	125
	List of abbreviations .....	126
	DANKSAGUNG .....	130
	CURRICULUM VITAE .....	131
	LIST OF PUBLICATIONS.....	132
	EIDESSTÄTTLICHE ERKLÄRUNG.....	133

# 1 INTRODUCTION

## 1.1 Epithelial ovarian carcinoma

### 1.1.1 Characterization of epithelial ovarian carcinoma and its heterogeneity

Epithelial ovarian carcinoma (EOC) is a female cancer. Although not one of the most common female cancer, it accounts with 207,252 deaths per 313,959 new cases in 2020 one of the highest death rates among gynecological malignancies (Sung et al., 2021). However, improvements in mortality remain dismal. Over the last decades, it appeared that EOC cannot be considered as a single disease. EOC are many diseases with genetic, histological, molecular and prognostic variations (Vaughan et al., 2011). Its complexity reaches from different cellular origins and histological subtypes with a varied mutational landscape over molecular subtypes associated with late diagnosis and rare therapy strategies (Bowtell et al., 2015).

For decades there is a debate about the cellular origin of EOC (Figure 1A). The recent understanding that separate lesions of origin resemble ovarian tumors has implemented the differentiated view on EOC as distinct disease entities. Thereby, the intensively discussed primary lesions of the different histological subtypes could be attributed to ovarian surface epithelium, cortical inclusion cysts, fallopian tube and endometrial epithelium (Karnezis et al., 2017). Based on this approach, major changes in histotype classification were established. According to the current report from the World Health Organization (WHO), EOC can be classified into five major histological subtypes (Figure 1B) including endometrioid, mucinous, clear cell, low-grade serous and high-grade serous (Kurman et al., 2014). Thereby, high-grade serous carcinoma (HGSC) represents the most common form of EOC diagnosed in about 70 % of the patients (Kobel et al., 2014; Prat, 2012) and associated with poor prognosis due to advanced stages at diagnosis, frequent metastatic spread and missing targeted therapy strategies (Bast et al., 2019; Bowtell et al., 2015; Prat, 2012). Today it is known that tubal lesions are considered as important sites of tumor initiation for a majority of HGSC cases. Moreover, strong evidence was found that BRCA (breast cancer 1)-mutated HGSC originates from the normal epithelium of distal fallopian tubes as well as some non-BRCA-associated carcinomas and implant on the ovary secondarily (Ahmed et al., 2012; Bowtell, 2010). However, precursor lesions seem to play an important role in initiation and often emerge with early occurring events like mutations.

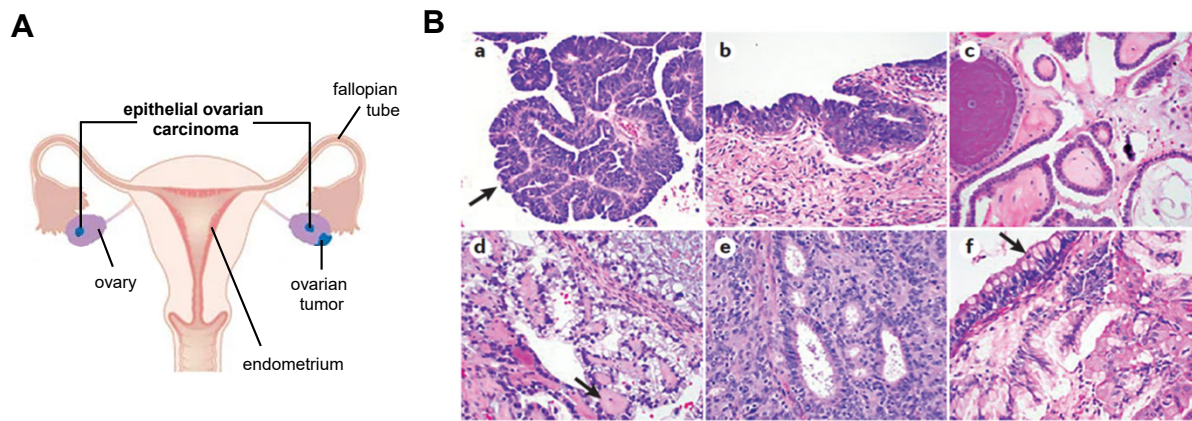


**Figure 1: Origin and histotypes of epithelial ovarian cancer (EOC).** (A) EOC derives from different origins, including ovary (ovarian surface epithelium), fallopian tube and endometrium, and consequently resembles different histological subtypes. Mucinous ovarian cancer mainly arises at the ovary but often also represents metastasis from the gastrointestinal tract. Endometrioid and clear cell cancer are referred to endometriosis. Low-grade serous carcinomas potentially derive from serous borderline tumors while the lesion identified for high-grade serous was the fallopian tube. Schematic modified from (Katopodis et al., 2019). (B) The different histotypes are visualized by immunohistochemistry (IHC) and displayed as follows (a) high-grade serous carcinoma (HGSC) (b) serous tubal intraepithelial carcinoma (STIC) which are potential precursors of HGSC (c) low-grade serous carcinoma (LGSC) (d) clear cell carcinoma (CCC) (e) endometrioid adenocarcinoma (f) mucinous carcinoma. Schematic from (Matulonis et al., 2016).

Although EOC shows a rare mutational landscape, some mutations can be almost exclusively assigned with one histological subtype. Especially, the most common form of EOC, HGSCs, exhibits widespread and ubiquitous TP53 mutations, a characteristic found in 97 % of all analyzed HGSC tumors (Ahmed et al., 2010; TCGA, 2011). TP53 mutation is the earliest occurring event in the evolution of HGSC which is detected so far. BRCA1 and BRCA2 germline mutations are defined in 13 % of HGSC (TCGA, 2011). In 50 % of all HGSC cases, deficiency of homologous recombination (HR) DNA repair pathway was observed which is partially linked to these early occurring mutations (TCGA, 2011) and makes HGSC to be prone for PARP (poly-ADP-ribose polymerase) inhibition (Bowtell et al., 2015). Beside this, HGSC is characterized by a frequent genomic instability and chromosomal alterations which are exclusively limited to the high-grade serous histotype and are essential for diagnosis (Prat, 2012). Notably, immunohistochemical assessment additionally improves the accuracy of histotype determination next to the WHO guidelines published in 2014 (Kobel et al., 2014; Kommoss et al., 2016; Kurman et al., 2014; Peres et al., 2018).

Concomitantly, HGSC can be subclassified into four relevant and distinct molecular subtypes with diverse microenvironmental involvement according to microarray-based gene expression profiling and unsupervised clustering of predominately serous tumors of the ovary, peritoneum and fallopian tube (Tothill et al., 2008). Several independent studies validated this molecular subtype classification by defining similar subtypes (Tan et al., 2013; TCGA, 2011). The different subtypes were summarized by Konecny et al. and collectively revealed a stroma reactive / mesenchymal (C1), an immunoreactive (C2), a differentiated (C4) and a mesenchymal / proliferative cluster (C5) (Konecny et al., 2016). Subtype C1 is

characterized by a stromal activation including intra-tumoral fibroblasts, vascular endothelial cells and pericytes leading to desmoplasia. This elevated stromal response thereby is associated with poor prognosis within this subtype. Enriched extracellular matrix production alters signaling networks as well as immune cell recruitment and function in C1. A targeted therapy of this subtype is currently addressed in the BEACON trial (ClinicalTrials.gov Identifier: NCT03363867). This phase II trial is evaluating the combination of cobimetinib, atezolizumab and bevacizumab targeting proliferation through MEK (mitogen-activated protein kinase kinase) as well as immune escape mechanism through PD-L1 (programmed cell death 1 ligand 1) and tumor vasculature through VEGF (vascular endothelial growth factor). In contrast to C1, a high T-cell infiltration seems to favor outcome and defines the immune reactive subtype C2. This subtype shows an elevated adaptive immune response and could be identified with markers for T-cell activation while a high expression of differentiation markers such as CA125 (cancer antigen 125) points to the C4 subtype (Tothill et al., 2008). The C5 subtype represents a dedifferentiated gene expression signature reflecting a mesenchymal shift and exhibits several over-expressed transcription factors and proliferative genes like HOX genes, HMGA2, TCF7L2, CDH2 and CDH3 (Konecny et al., 2016; TCGA, 2011; Tothill et al., 2008). Deregulation of MYCN, LIN28B, HMGA2 and the miRNA let-7 in this subtype was also shown in another study (Helland et al., 2011). Furthermore, an upregulation of WNT and cadherin signaling, a loss of E-cadherin-positive transmembrane contacts and low expression of differentiation marker CA125 and MUC1 are reported, implying a transition from epithelial to mesenchymal cell properties as a characteristic feature of this subtype (Tothill et al., 2008). Besides, the C5 subtype was characterized by a downregulation of immune markers and a low intra-tumoral and -stromal T-cell infiltration accompanied by a loss of immunogenicity (Tothill et al., 2008). This underpins the lowest survival rates observed for this subtype (Konecny et al., 2014) while targeted treatment strategies are still missing.

However, next to the molecular diversity between individual tumors, phenotypic, intra-tumoral heterogeneity occurs and leads to an inaccurate assessment of prognosis within the subtypes. This cellular plasticity in HGSC is based on a variety of infiltrated cells and multiple cell states instead of elicitation by genetic alteration (Hu et al., 2020). Therefore, a study using single cell sequencing investigated the classification of fallopian tube epithelial (FTE) cells, which represent the cellular origin of HGSC. This profiling broadened the view beyond genetic heterogeneity of HGSC and identified four subtypes of FTE cells. Linking the non-cancerous molecular markers of these subtypes to the cell state of corresponding cancer cells thereby defined a robust gene expression signature characterizing an EMT-high subtype of HGSC. Moreover, these EMT-high tumors were associated with poor prognosis (Hu et al., 2020). Notably, a connection of mesenchymal cell characteristics was



assigned for the C1 as well as C5 subtype (Konecny et al., 2016). Consequently, the linkage of phenotypic heterogeneity within tumors to the cells of origin thereby allows a more accurate prediction of tumor behavior and a better adaption of targeted therapy strategies (Hu et al., 2020).

### **1.1.2 The vulnerability of EOC – from diagnosis, current therapy and targeting occurring resistances**

Early diagnosis of EOC is still a problem due to its frequent asymptomatic progression. While LGSC, MC and EC are usually diagnosed in early stages, the majority (75 – 80 %), mainly comprising CCC and HGSC, are detected in advanced stages III-IV and are associated with metastatic spread (Bast et al., 2019; Prat, 2012). Overall survival within five years with advanced stage tumors is less than 30 % (Torre et al., 2018). Pre-operative screening is based on CA125 levels which exhibits a poor sensitivity for low volume tumors and raise too late in serum. Screening for CA125 over time and sequentially transvaginal sonography (TVS) is a more effective way with a higher specificity than single screening but needs to be improved for the detection at early stages to have an improvement on mortality (Bast et al., 2020). Besides, CA125 plasma levels vary among HGSC subtypes with the C5 subtype characterized by a low expression of the CA125 marker (Leong et al., 2015). To increase the sensitivity for early detection, additional markers are needed (Bast et al., 2020).

In case of abnormal pelvic mass, surgery is still the gold standard for histotyping and staging. Surgical tumor reduction and chemotherapy are the most important treatment strategies for ovarian cancer. Prognosis is based on residual tumor mass, stage at diagnosis and susceptibility to chemotherapy (Coleman et al., 2013). Recurrent disease occurs with an incidence of approximately 80 % and reflects with acquired chemoresistance an almost incurable state (du Bois et al., 2009).

According to WHO guidelines, a standard first-line combination therapy with paclitaxel and carboplatin, respective cisplatin, is recommended to be given to the patients. Frequent recurrence led to the establishment of a second-line treatment strategy where initial therapy is categorized into platinum-refractory, platinum-resistant and platinum-sensitive depending on the time between initial treatment and relapse. Second-line treatment is a combination of platinum-based chemotherapeutic and paclitaxel, gemcitabine, etoposide or doxorubicin for patients responding to the initial treatment (Kurman et al., 2014). In case of inefficient initial platinum-based treatment topotecan, gemcitabine or bevacizumab can be applied (Coleman et al., 2013).

While HGSC is initially highly responsive to platinum-based therapeutics, recurrent HGSC often develops resistances over time (Raja et al., 2012). Especially in widespread and advanced-stage diseases of HGSC resistances occur in up to 90 % of the patients

(Bowtell et al., 2015). Hence, it is a major advance that histotype-specific clinical trials are emerging aiming to replace the standardized therapy, which treated ovarian cancer to date only in general, with better targeted compounds and specifically address resistance mechanisms. Additionally, biomarkers for the selection of patients benefitting from individual therapies are needed.

Mutated BRCA in HGSC patients is one of the first established features which allows selective treatment of BRCA mutation carriers with PARP inhibitors. As part of the HR pathway, mutated BRCA leads to HR deficiency and DNA damage providing a basis for platinum sensitivity in highly proliferative cells. Subsequent PARP inhibition leads to further DNA damage resulting in cell apoptosis and thereby represents a new promising treatment strategy. Currently, different PARP inhibitors are studied and three are already approved like olaparib, rucaparib and niraparib in multiple settings showing different toxicity and application options (Mittica et al., 2018). Especially platinum-sensitive, recurrent patients with BRCA mutations benefit from a first-line maintenance therapy with PARP inhibitors after initial platinum-based treatment resulting in a substantially increased progression-free survival (PFS) (Kuroki and Guntupalli, 2020). There are further phase III trials with PARP inhibitors (PRIMA, PAOLA-1, VELIA) prolonging PFS in maintenance therapy irrespectively of the BRCA or HR mutation status and in combination with standard first-line platinum-taxane-based chemotherapeutics (Franzese et al., 2020).

Nevertheless, subsequent courses of platinum therapy as well as multiple and long-term therapy with PARP inhibitors lead to the establishment of resistances. Wide genomic instability and related copy number changes offer the potential for developing resistances. Mechanisms by which resistance is facilitated are manifold but worth to mention in this context is the restoration of BRCA function through secondary mutation and other components involved in HR like RAD51 (Bowtell et al., 2015; Kondrashova et al., 2017).

Specifically, in regard of targeting resistances, combinatorial treatment becomes essentially important. Platinum-resistant recurrence shows a quite low response rate to monotherapies and other standard platinum-free agents like paclitaxel, doxorubicin and topotecan (Gordon et al., 2001; Gordon et al., 2004; Markman et al., 2006). Novel combination approaches in treating platinum-resistant EOC are based on angiogenic targeting, immune checkpoint inhibition with monoclonal antibodies and kinase inhibitors (Katopodis et al., 2019; Kuroki and Guntupalli, 2020). For the combination of platinum-free agents with monoclonal antibodies like the anti-angiogenic bevacizumab (anti-VEGF) in the AURELIA phase III trial, an improvement of overall response rate and PFS was observed although overall survival remained unchangeably dismal (Pujade-Lauraine et al., 2014). Next to targeting the tumor vasculature, inhibiting mechanisms of immune escape within the tumor through the use of immune checkpoint inhibitors seems to be a promising tool

(Kuroki and Guntupalli, 2020). Preclinical observations have shown that anti-angiogenic therapy enhances T-cell infiltration within the tumor, promotes anti-tumor immunity and improves the effectivity of immune checkpoint blockade. Together with the reported high PD-L1 expression on tumor cells with deficiency in homologous recombination, this represents a rationale for PD-L1 inhibition within HGSC (Nero et al., 2021). Therefore, an ongoing phase II trial is currently evaluating the efficacy of the combination therapy of cobimetinib (MEKi), bevacizumab (VEGFi) and atezolizumab (PD-L1i) in patients with platinum resistant or refractory HGSC (BEACON trial, ClinicalTrials.gov Identifier: NCT03363867).

Besides, multiple preclinical studies reported that the SRC kinase confers resistance to taxane chemotherapeutics and highlighted benefits of its inhibition. Based on this, another phase III trial evaluated the combination of paclitaxel and the SRC inhibitor saracatinib. However, increasing the sensitivity to paclitaxel treatment with the addition of saracatinib remained unaccomplished in patients with platinum-resistant ovarian cancer (McNeish et al., 2014). Nevertheless, the SRC kinases possess a protruding role in the EMT process (Patel et al., 2016) and selected EMT-high tumors were above associated with poor prognosis (Hu et al., 2020). Referring to the EMT-high signature found in a subset of HGSC tumors (Hu et al., 2020), HGSC patients selected for an EMT-high subtype potentially benefit from the respective SRC inhibition.

In sum, there is an ongoing progress seen in developing new combinatorial treatment strategies, but the heterogeneity and plasticity of the tumor enables multiple adopting resistance mechanisms. The current need of subtype-specific identification of oncogenic drivers and targeted combination therapies are among the critical questions of ovarian cancer (Bowtell et al., 2015; Vaughan et al., 2011).

## **1.2 From tissue integrity to cancer evolution and spreading**

### **1.2.1 Epithelial-mesenchymal transition**

Since metastatic spread is a frequent problem in advanced stage HGSC, epithelial-to-mesenchymal transition (EMT) becomes important. EMT refers to the dynamic and reversible process where epithelial cells shift to a more mesenchymal phenotype and behavior coming along with increased migratory and invasive potential with concomitant reduced intercellular adhesion (Polyak and Weinberg, 2009). This process occurs during embryogenesis, wound healing, fibrosis, cancer progression and metastasis. The most common characteristics of EMT assembled by the EMT International Association are weakening of cell-cell adhesion and alteration of cell-matrix adhesion, cytoskeletal reorganization, changes in cell polarity, gain of cell motility and invasiveness (Polyak and Weinberg, 2009).

Epithelial cells are phenotypically characterized by an apical-basal polarity mediated by Par3 (PARD3), Crumbs (CRB1+3) and Scribble (SCRIB), cell-cell adhesion facilitated by tight junctions, adherens junctions and desmosomes, an extracellular matrix attachment, a cortical actin cytoskeleton and cytokeratin intermediate filament. Contrary, mesenchymal cells are defined by a front-back cell polarity, extracellular matrix degradation, migratory potential and vimentin-based intermediate filaments next to actin stress fibers. Cellular rearrangement such as detachment of E-cadherin from the plasma membrane are the earliest occurring events and often lead to a change in the expression of EMT transcription factors (TFs). SNAI1, SNAI2, TWIST1, ZEB1 and ZEB2 account as the key EMT-TFs which are also evolutionary conserved (Yang et al., 2020). Different signaling pathways convert extracellular signals into intracellular gene expression, confer transcriptional activation of these TFs and thereby maintain a mesenchymal cell state (Dongre and Weinberg, 2019).

Important to mention is that the process of EMT often results in an incomplete, intermediate cell state whereat gained mesenchymal and remaining epithelial properties are simultaneously present and can vary between different cells. This leads to a high phenotypic plasticity which is mediated by diverse stimuli of the cellular microenvironment and underlies an epigenetic, transcriptional and post-transcriptional regulation to maintain rapid adjustments. Which mechanisms are generally used and how stable these intermediate states are, remains unclear. Consequently, the complexity of EMT appearance, especially partial EMT, cannot be defined by only a few markers. It needs a cellular, molecular and functional characterization (Yang et al., 2020).

### **1.2.2 Cell junctions**

Cell junctions function as communication networks and barriers mediating adhesion between neighboring epithelial cells. A classification into communicating, occluding and anchoring junctions has therefore been established. The connexin-based gap junctions facilitate a chemical and electrical communication between neighboring cells by allowing an exchange of small molecules and ions through protein channels (Kumar and Gilula, 1996). Tight junctions are mainly composed of claudins, occludins and zonular occludens proteins and seal cells together to form a diffusion barrier across epithelium and maintain apical basolateral organization of membrane proteins (Balda and Matter, 2008). Adhesive, anchoring connections can be formed between cells and between cells and the extracellular matrix. Cell-matrix adhesion is assembled by integrin-based focal adhesion structures and hemidesmosomes enabling cellular attachment, migration and dynamic tissue rearrangement (Berrier and Yamada, 2007). Intercellular adhesion is constituted of cadherin-mediated adherens junctions or desmosomes linking contact sites to the actin cytoskeleton or intermediate filament system. While desmosomes mediate intercellular stability, adherens junctions transmit mechanical forces and extracellular stimuli into

intracellular signaling (Harris and Tepass, 2010; Hatzfeld et al., 2017). Disruption of these well-organized structures is part of the EMT process and represents the most obvious, phenotypic change providing the basis for a tumor to metastasize.

### 1.2.3 Adherens junctions in adhesion and cancer

Adherens junctions (AJs) mediate stable cell-cell adhesion within tissues while concomitantly underlying a dynamic, fine-tuned balance of permanent assembly and recycling (Kowalczyk and Nanes, 2012; Le et al., 1999). This enables a constant AJ maintenance while exhibiting a high plasticity allowing remodeling of adhesion and indirectly even movement through AJ dynamics. Moreover, these dynamic membrane structures also facilitate cell polarity, cell shape, tissue structure and stability as well as intercellular communication and contact inhibition of proliferation (McClatchey and Yap, 2012; Takeichi, 2014).

AJs are composed of transmembrane cadherins and intracellular catenins linked to the actin cytoskeleton (Figure 2A). Cadherins are important to facilitate homophilic calcium-dependent interaction between neighboring cells via five extracellular domains. Classical cadherins, important to highlight here, mainly comprise the epithelial cadherin (E-cadherin, CDH1) expressed in all epithelial tissues, the neuronal cadherin (N-cadherin, CDH2) found in neuronal and muscle tissue and the vascular epithelium cadherin (VE-cadherin, CDH5) present in endothelial cells (Harris and Tepass, 2010; Pokutta and Weis, 2007). A common characteristic is the ability of cadherin switching which occurs during the development as well as pathogenic processes like cancer evolution allowing cells to separate from each other due to its preference of homophilic cadherin-cadherin interaction (Halbleib and Nelson, 2006).

The most prominent switch is the exchange of CDH1 through CDH2 during the process of EMT (Halbleib and Nelson, 2006; Wheelock et al., 2008). Moreover, CDH1 was found to bind to the EGFR (epidermal growth factor receptor) and other growth factor receptors to facilitate growth suppression by inhibiting EGF signaling (Qian et al., 2004). A switch in membrane-bound cadherins will consequently alter growth stimulation. Hence, there are several studies indicating that CDH2 associates with FGFR (fibroblast growth factor receptor) preventing its internalization and thereby raising growth stimulation and consequently enabling tumor proliferation (Suyama et al., 2002; Wheelock et al., 2008). Along with this, a loss of CDH1 is associated with poor prognosis and clinical outcome (Faleiro-Rodrigues et al., 2004).

Next to the extracellular domain of cadherins mediating cell-to-cell adhesion, the cytoplasmic tail of all cadherins is highly conserved and associates with the armadillo domain of  $\beta$ -catenin (CTNNB1). Together with  $\alpha$ -catenin (CTNNA1) the adhesion structures are linked to the actin cytoskeleton (Pokutta and Weis, 2007). As stabilization factor, p120-

catenin (CTNND1) associates with different cadherins to prevent contact disassembly via clathrin-mediated endocytosis mediated by Numb and Hakai-dependent ubiquitination (Davis et al., 2003; Fujita et al., 2002; Ishiyama et al., 2010; Kourtidis et al., 2013; Kowalczyk and Nanes, 2012; Sato et al., 2011; Yap et al., 1998). Due to a lack of the catenin-typical armadillo domain, CTNNA1 is not able to directly bind cadherins (Coates, 2003). It was primarily thought that CTNNA1 directly binds CTNNB1 and links the AJ structure to the actin cytoskeleton but simultaneous binding of CTNNA1 to CTNNB1 and actin was conformationally excluded (Pokutta and Weis, 2007; Yamada et al., 2005). However, there is strong evidence that CTNNA1 certainly coordinates the actin dynamics and thereby facilitates the connection of AJ structures to the actin cytoskeleton during AJ assembly and rearrangement although the underlying mechanism is not precisely elucidated and validated yet (Adhikari et al., 2018; Chen et al., 2015; Desai et al., 2013; Drees et al., 2005; Hansen et al., 2013; Ishiyama et al., 2018).

The remodeling of actin dynamic also shapes the form and morphology of AJ appearance reaching from punctuate junctions to linear contacts. In epithelial tissue mature contacts exhibit linear actin filaments which are arranged in parallel to the plasma membrane. Punctuate junctions are characterized through a zipper-like contact structure facilitated by actin filaments terminating at the membrane-associated AJ complex and are mainly found in loose tissues, under tissue remodeling and often between mesenchymal cells (Takeichi, 2014).

Next to CTNNA1 also Rho-GTPases play a crucial role during actin remodeling, in actin polymerization as well as actomyosin contraction and AJ assembly (Takeichi, 2014).

The process of AJ assembly, based on different published models, was comprehensively summarized by Harris and Tepass et. al as well as Takeichi et al. and will be described in the following (Harris and Tepass, 2010; Takeichi, 2014) (Figure 2B). Assembly of AJs can be categorized in three fundamental steps: RAC-dependent initial clustering (I), RHO-dependent contact expansion (II) and AJ maturation (III). Association of cadherins and catenins already begins in the endoplasmic reticulum (ER) (Curtis et al., 2008). After their transport to the plasma membrane, cadherin-catenin complexes cluster and thereby induce the activation of the small GTPase RAC1 (Ras-related C3 botulinum toxin substrate 1) via its guanine nucleotide exchange factor (GEF) TIAM1 (T lymphoma invasion and metastasis-inducing protein 1) (Malliri et al., 2004; Nakagawa et al., 2001). Active RAC1 further recruits WAVE2 (WASP-family verprolin homologue 2) which activates ARP2/3 (actin-related protein 2/3) leading to actin polymerization and the formation of lamellipodia. These cell protrusions push the membrane outwards and promote initial cell-cell contact assembly (Yamazaki et al., 2007). In the next step, the fine-tuned balance between RAC1- and RHOA-dependent signaling, mediated through CTNND1 by recruiting the GTPase activating protein (GAP) p190RhoGAP, shifts to RHOA activation to facilitate

contact expansion (Wildenberg et al., 2006; Yamada and Nelson, 2007). At the same time, recruitment of Par3 (partitioning defective 3 homologue) to the site of contact initiation causes inhibition of RAC1 by sequestering TIAM1 (Chen and Macara, 2005). Concomitantly, the concentration of CTNNA1 at the membrane increases which leads to actin dimerization. These homodimers inhibit ARP2/3 and promote actin bundling (Drees et al., 2005; Yamada et al., 2005). Together with actomyosin, CTNNA1 reorganizes the actin network by promoting the formation of contractile actin bundles which results in contact maturation accompanied by shortening of the initial contacts (Drees et al., 2005).

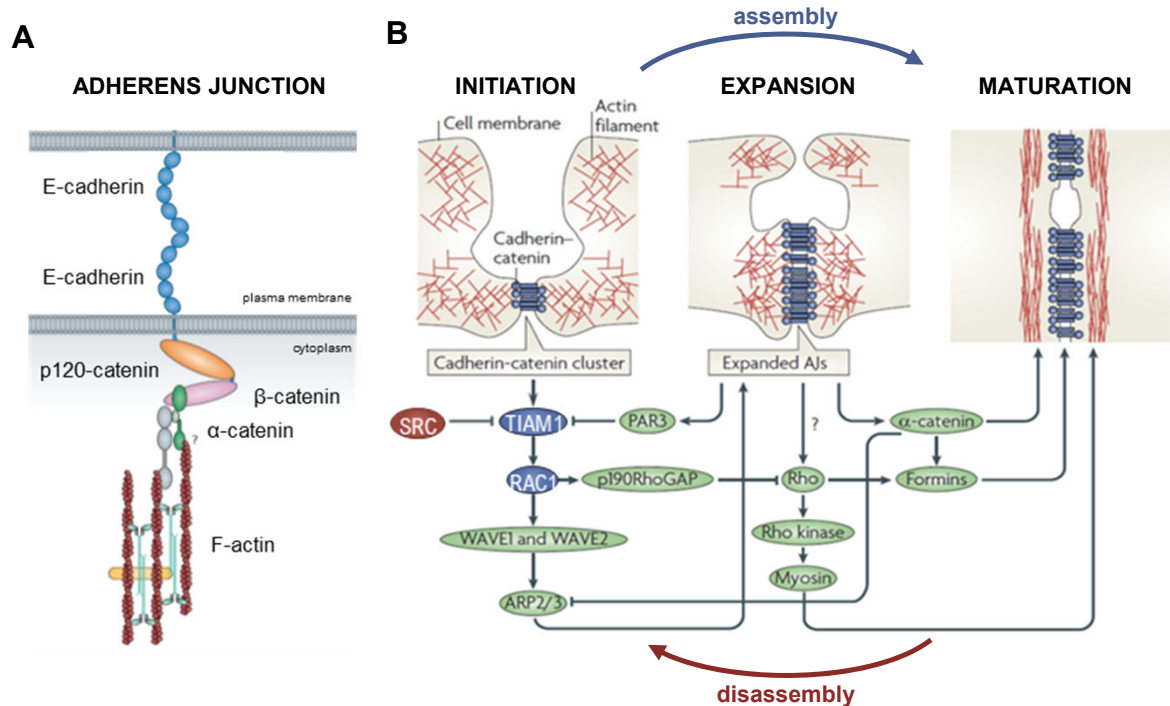


**Figure 2: Adherens junction assembly and disassembly.** (A) The core molecular structure of AJs comprises the calcium-dependent transmembrane cadherins (CDHs) which are linked to β-catenin (CTNNB1). This structure is stabilized by p120-catenin which binds to cadherin and CTNNB1. α-catenin (CTNNA1) connects AJs to actin cytoskeleton where it can either bind to CTNNB1 or actin and thereby mediates the linkage by a not yet fully elucidated mechanism. Schematic modified from (Takeichi, 2014). (B) The process of AJs assembly can be divided in three essential steps: RAC-dependent contact initiation, RHOA-dependent contact expansion and contact maturation. Initial clustering of cadherins and catenins stimulate RAC1 activation via TIAM1, this further recruits WAVE1/2 to drive ARP2/3-dependent actin polymerization for lamellipodia formation. In an PAR3- and p190RhoGAP-dependent manner, the mutual exclusive equilibrium between RAC1 and RHOA activity shifts to RHOA for contact expansion. CTNNA1 together with actinomyosin facilitate the formation of contractile actin bundles leading to contact maturation. AJs disassembly can be induced by various factors whereat SRC induced TIAM1 inhibition resulting in the AJs disruption is indicated here. Essential drivers of AJs assembly and disassembly interfering with each other are highlighted in blue (assembly) and red (disassembly). Schematic modified from (Harris and Tepass, 2010; Woodcock et al., 2009).

Next to their function in AJ structure, each protein fulfills a various role in the disassembled state with a diverse outcome for tumor progression. Especially the interconnected functions of cytoplasmic and nuclear catenins unroll an underestimated crosstalk between adhesion, migration and transcriptional regulation (McCrea and Gottardi, 2016). Cytoplasmic CTNNB1 can either be degraded or translocate to the nucleus. Degradation is mediated through GSK3B (glycogen synthase kinase 3 beta) which

phosphorylates CTNNB1 at Ser33, 37 and Thr41 in complex with AXIN and APC priming it for ubiquitination via BTRC ( $\beta$ -transducing repeat-containing protein) (Price, 2006). If canonical WNT signaling is stimulated, CTNNB1 translocates to the nucleus where it transduces the WNT signal and activates TCF/LEF1-driven (T cell factor/lymphoid enhancer factor family) transcription of proliferative genes (Willert and Jones, 2006).

Studies with CTNND1 demonstrated that it also responds to WNT signaling in a similar manner as CTNNB1 regarding its degradation or nuclear translocation with the difference of its isoform-specific sensitivity to WNT signals (Hong et al., 2016; Hong et al., 2010; Venhuizen et al., 2020). Nuclear CTNND1 was associated with anoikis resistance (Daniel and Reynolds, 1999; Park et al., 2005; van de Ven et al., 2015) and impairment of differentiation (Hosking et al., 2007; Lee et al., 2014). Next to its nuclear functions, CTNND1, as regulator of Rho family GTPases, seems to switch between facilitating contact stabilization and promoting cell migration in its cytoplasmic form by activating RAC1 and CDC42 (cell division cycle 42) and inhibiting RHOA (Cheung et al., 2010; Johnson et al., 2010; Noren et al., 2000).

Interestingly, a dual role is also found within RAC1. Depending on its activation factor, RAC1 can transfer upstream signals into differing cellular responses. In combination with the GEF TIAM1, RAC1 facilitates an early step in the process of AJ assembly inducing adhesion while an activation of RAC1 by PREX1 (Phosphatidylinositol 3,4,5-trisphosphate-dependent Rac exchange factor 1) promotes cell migration (Marei and Malliri, 2017).

In contrast to the other catenins, cytoplasmic CTNNA1 seems to function as tumor suppressor by inhibiting the WNT signaling through binding to APC and thereby promoting the degradation of cytoplasmic CTNNB1 (Choi et al., 2013). Additionally, CTNNA1 was shown to bind phosphorylated, cytoplasmic YAP1 (Yes-associated protein 1) to prevent its dephosphorylation and subsequent nuclear translocation for the stimulation of proliferative gene expression which will be assessed in more detail under 1.4 (Schlegelmilch et al., 2011; Silvis et al., 2011; Sun et al., 2014).

The switch between adhesion and the cytoplasmic respective nuclear function is tightly regulated on various levels such as transcription, by recycling via clathrin-mediated endocytosis, post-transcriptional and post-translational modifications or during the assembly process.

It is known that cadherins underlie a continuous recycling process via clathrin-mediated endocytosis allowing a constant exchange of cadherin proteins and a simple replacement by other cadherins. The expression of different cadherins between neighboring cells enables them to separate from each other which plays an important role during metastasis. Key modulators are the Rab proteins (Chung et al., 2014; Klymenko et al., 2017; Le et al., 1999; Wheelock et al., 2008). Beyond that, the post-translational phosphorylation represents an essential regulation mechanism of AJ modulation by influencing their protein-



protein interaction within contact structures. Phosphorylation is mainly facilitated through kinases phosphorylating either serine/threonine (Ser/Thr) or tyrosine (Tyr) residues (Bertocchi et al., 2012). Early studies showed that an overall inhibition of Tyr-kinases facilitated a cadherin-dependent AJ stabilization assigning Tyr-kinases an essential role in AJ turnover, especially for the SRC kinase (Matsuyoshi et al., 1992; Owens et al., 2000). Supporting this, overall inhibition of phosphatases led to a dramatic increase in cadherin and catenin phosphorylation resulting in the disassembly of cell colonies into single cells (Ozawa and Kemler, 1998). Contrary, phosphorylation was also seen having a positive, strengthening effect on adhesion in keratinocytes (Calautti et al., 1998).

With this dual view on phosphorylation events and their consequence for cell-cell adhesion, it is important to address phosphorylation sites in detail. Here, the focus is drawn on phosphorylation negatively associated with adhesion mediated by the SRC kinase. One of the most relevant phosphorylation sites displays the one within cadherins which disrupts their association with CTNNB1 and CTNND1 and subsequently AJ contact structures. It was described that SRC phosphorylation of CDH1 at Tyr860 leads to its degradation by facilitating binding of the E3 ligase Hakai to CDH1 for ubiquitinylation (Fujita et al., 2002). A conservation of this phosphorylation site was also found within CDH2 where this phosphorylation results in a dissociation of CTNNB1 from CDH2 within contact structures (Lilien et al., 2002; Qi et al., 2006). A similar event was described for the endothelial CDH5, where an Tyr658,731-phosphorylation reduces the interaction with CTNNB1 and CTNND1. Interestingly, this phosphorylation within CDH5 decreased the interaction with CTNND1 and thereby shifting the affinity of CTNND1 binding to CDH2 indicating a switch between vasculature establishment and migratory potential (Hatanaka et al., 2011; Potter et al., 2005). Furthermore, catenin phosphorylation also interferes with AJ maintenance. Phosphorylation of CTNNB1 at Tyr654 further disrupts AJs indicated by affecting its binding to CDH1 (Daugherty and Gottardi, 2007; Roura et al., 1999). CTNND1 is regulated in various ways including an interconnected feedback regulation between Ser/Thr- and Tyr-phosphorylation which seems to fulfill mutually exclusive functions. Notably, CTNND1 exhibits a phosphorylation domain containing eight tyrosine phosphorylation sites which can be induced by the SRC kinase (Mariner et al., 2001). Especially Tyr228 phosphorylation was mainly associated with a pro-tumorigenic role apart from adhesion (Kourtidis et al., 2015; Ma et al., 2012).

Not only direct phosphorylation of AJ proteins is responsible for AJ internalization and turnover. The SRC kinase is also involved in AJ disassembly by directly affecting the continuous assembly process through phosphorylating TIAM1 at Tyr384. This phosphorylation depicts a binding site for GRB2 (growth factor receptor bound protein). In complex with SOS1 (SOS Ras/Rac guanine nucleotide exchange factor 1) it stimulates ERK (extracellular signal-regulated kinases) activation which elicits proteolytic degradation of

TIAM1. Loss of TIAM1 enables a shift in AJ maintenance from the formation process to AJ turnover and is above required for cell migration (Woodcock et al., 2009). Besides, phosphorylation of RAC1 at Tyr64 is reported to be also directly conducted by SRC and FAK leading to its inactivation to control and balance cell shape and migration (Chang et al., 2011).

Thus, AJs are dynamic intercellular connections facilitating tissue integrity and signal transduction from the microenvironment to nuclear responses. Their high plasticity allows a constant adaption of adhesion and even cell movement regulated through GTPases and phosphorylation events involving the SRC kinase.

## **1.3 The role of the oncogene SRC in cancer and therapy**

### **1.3.1 SRC kinase activation and signaling during metastasis**

The SRC kinase is a non-receptor tyrosine kinase and refers to one of the oldest oncogenes which shows a high abundance and activation in a plethora of tumor entities and correlates with tumor progression (Summy and Gallick, 2003). Notably, SRC activity was frequently upregulated in ovarian cancer and associated with advanced stages (Simpkins et al., 2012; Wiener et al., 2003). Since a large set of SRC substrates were identified over the last decades, the kinase is involved in multiple cellular processes and signaling pathways. The historic discoveries describing SRC's molecular action mechanisms are summarized by Martin and Yeatman and will be reviewed in the following (Martin, 2001; Yeatman, 2004). To fulfill its functions, SRC facilitates transient protein-protein interactions with its substrates via its N-terminal SH3 and / or SH2 (SRC homology 3 + 2) domain to mediate tyrosine phosphorylation with its catalytic domain. While the SH3 domain is characterized to bind proline-rich motifs, the SH2 domain preferentially associates with phosphorylated tyrosine residues. SRC's kinase activity is positively and negatively controlled by its C-terminal regulatory domain exhibiting two Tyr-phosphorylation sites. While Tyr530 (human) interacts intramolecular with the SH2 domain to maintain an inactive, closed conformation of SRC, the phosphorylation of Tyr419 (human) is induced by an open conformation and is essential for the full activation of the SRC kinase (Figure 3).

Due to its wide cellular crosstalk, signaling- and location-specific regulation of SRC activity is important which is achieved by the numerous activation mechanisms and factors. The conformation-dependent activation of SRC can be promoted by direct dephosphorylation of Tyr527, most prominently by the phosphatases CSK (C-terminal SRC kinase) and PTPN1 (protein tyrosine phosphatase non-receptor type 1) opening the inactive, closed conformation (Bjorge et al., 2000; Okada, 2012). Recruiting of SRC to growth factor receptors like EGFR, FGFR, PGFR and HER2 (epithelial, fibroblast, platelet and human epithelial growth factor receptor) was also associated with stimulated SRC

activation (Bromann et al., 2004; DeMali et al., 1999; Landgren et al., 1995; Tice et al., 1999). Considering the low affinity interaction of Tyr530 with the intramolecular SH2 domain, a ligand with a high affinity either for the SH3 or SH2 domain can disrupt this interaction by competing for binding within these domains (Yadav and Miller, 2007). Reported SRC substrates are for instance PXN (paxillin), HCK, FAK (focal adhesion kinase) as well as the RNA-binding proteins hnRNPK (heterogeneous nuclear ribonucleoprotein K) and SAM68 (KHDRBS1) (Frisone et al., 2015; Moarefi et al., 1997; Ostareck-Lederer et al., 2002; Thomas et al., 1998; Weng et al., 1993; Yadav and Miller, 2007). In summary, promoting the opened conformational state of the SRC kinase enables autophosphorylation of Tyr419, essential for full kinase activity (Martin, 2001; Yeatman, 2004).

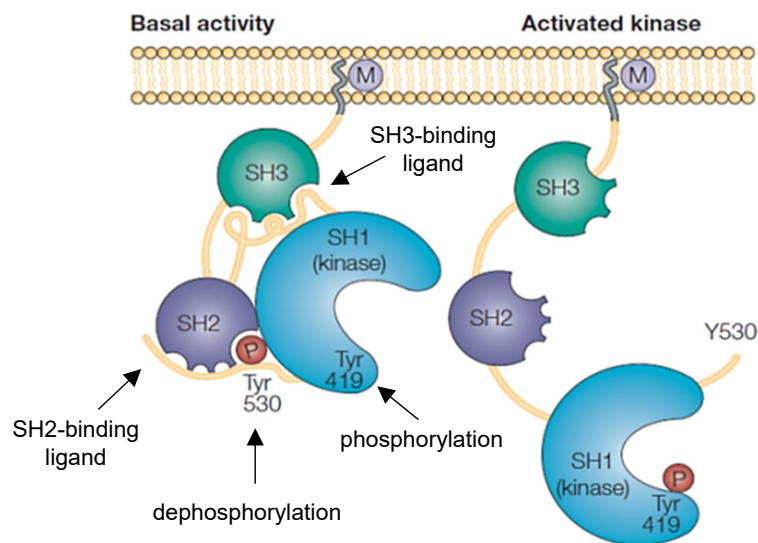


**Figure 3: Activation of the SRC kinase.** In its inactive form, the membrane bound SRC kinase exhibits a closed conformation interacting intramolecularly with a phosphorylation of tyrosine 530 (Y530) and its SH2 domain. Activation of SRC can be facilitated by different mechanisms including dephosphorylation of Y530, phosphorylation of Y419 or ligand binding to either SH2 or SH3 or both and thereby induces a conformational shift. The open conformation then enables autophosphorylation of Y419 which is essential for its full activity. Schematic modified from (Martin, 2001; Yeatman, 2004).

The main functions of SRC comprise the regulation of cell adhesion, the stimulation of cell migration and invasiveness and thereby enable metastasis while proliferation and tumor growth seems to remain unaffected by SRC (Boyer et al., 2002; Criscuoli et al., 2005; Guarino, 2010; Yeatman, 2004). Next to its destructive role for AJ-mediated cell-cell adhesion, SRC was further described to be part of the focal adhesion (FA) complex which mediates adhesion between cells and the extracellular matrix (ECM). Changing from a connective tumor to the spreading of single cells during metastasis requires the loss of intercellular adhesion followed by the modulation of integrin-based adhesion as described above (1.2.1) (Fincham and Frame, 1998). FAs are mainly composed of transmembrane integrins which are linked to the actin cytoskeleton via structural proteins like PXN, TLN1 (talin), VCL (vinculin), TNS1 (tensin) and ACTN1 ( $\alpha$ -actinin). Several signaling molecules are transiently recruited to the site of FAs mainly comprising tyrosine kinases and

phosphatases. The most prominent ones are SRC, FAK and CSK (Playford and Schaller, 2004; Wozniak et al., 2004). CSK and FAK are essential to activate and direct SRC SH2-dependently to its substrates within FAs. SRC then phosphorylates PXN, while interacting via the SH3 domain with a proline-rich motif, as well as CAS (CRK-associated substrate) (Weng et al., 1993; Wu et al., 2015; Xing et al., 1994). This phosphorylation of CAS and PXN creates docking sites for several SH2-containing proteins which further initiate integrin-mediated signaling and multiple other signaling cascades. The concomitant activation of Rho-GTPases has an extensive impact on the cytoskeletal and morphological remodeling including FA turnover which refers to the repetitive process of continuous formation and disruption of FAs, enabling cell motility and migration (Fincham and Frame, 1998; Playford and Schaller, 2004; Timpson et al., 2001; Weng et al., 1993; Wozniak et al., 2004; Wu et al., 2015; Xing et al., 1994; Yeatman, 2004). The ability of cells to migrate represents the basis for invasion. Thereby, SRC seems to mediate the activation of metalloprotease MMP-2 and expression as well as segregation of MMP-9, which are essential for the degradation of the ECM, indirectly via the FAK-SRC complex stimulating JNK signaling and RAC1 activation (Cortes-Reynosa et al., 2008; Guarino, 2010; Hsia et al., 2003).

As mentioned above, the SRC-driven phosphorylation followed by the recruitment of SH2-containing proteins assemble signaling complexes and transduce a network of signaling pathways. One pathway that can be further stimulated by SRC activation is the MAPK pathway (RAS-RAF-MEK-ERK pathway) indicated in several publications. (Hu et al., 2009; Stokoe and McCormick, 1997; Tran and Frost, 2003). SRC can stimulate RAF (rapidly accelerated fibrosarcoma) activation, directly or via repression of the RAF1 inhibitory protein PP2A, which further pronounce activity of MEK1/2 (mitogen-activated protein kinase kinase; MAP2K1/2) and, consequently, ERK1/2 (extracellular signal-regulated kinase 1/2; MAPK3/1) within a phosphorylation cascade. Classically, the pathway is stimulated by mitogen- and growth factor-induced signals, transduced by RAS GTPases activating the phosphorylation cascade which leads via RAF1 and MEK1/2 to the nuclear translocations of ERK1/2. Within the nucleus ERK triggers for instance TCF/SRF-driven transcription by indirectly enhancing the DNA binding activity of the TF SRF (serum response factor) and facilitates the phosphorylation of TCFs (ternary complex factors) which are required for the association with SRF (Lavoie et al., 2020). Inducing the transcription of a plethora of genes, however, ERK-stimulated gene expression essentially facilitates cell growth and proliferation. Due to the fine-tuned and complex regulation, the pathway thereby controls cell cycle and apoptosis. An upregulation of ERK activity was frequently observed in HGSC patients and associated with a simultaneous SRC activation (Simpkins et al., 2018).

### 1.3.2 Targeting SRC and ERK signaling in EOC

Early studies with an ovarian cancer cell line have shown that an inhibition of SRC modulated cell shape, decreased the invasive potential and reduced anchorage-independent growth which is a characteristic feature of cell detachment (Konecny et al., 2009). Mouse models even indicate a decreased tumor growth in the absence of SRC activity (Wiener et al., 1999). Additionally, the SRC inhibitor saracatinib was shown to exhibit anti-tumor activity in HGSC preclinical studies with mouse xenografts (Simpkins et al., 2012). Clinical trials (ClinicalTrials.gov Identifiers: NCT01196741, NCT00610714) further investigated saracatinib in combination with paclitaxel and additionally carboplatin in ovarian cancer but failed to essentially improve PFS and overall survival. There was also no improvement on the activity of paclitaxel in patients with platinum-resistant ovarian, fallopian tube or primary peritoneal cancer (McNeish et al., 2014). Following studies indicated that the initially seen benefits were shadowed by occurring resistances to saracatinib. Addressing the molecular mechanism in ovarian cancer cell lines, revealed that saracatinib resistance was driven by the activation of MAPK signaling (RAS-RAF-MEK-ERK pathway) accompanied by a reduction of NF1 (neurofibromin 1) expression and elevation of HER2 (human epidermal growth factor receptor 2) and ISNR (insulin receptor). Inhibition of MEK with selumetinib diminished ERK activity and proved beneficial for re-sensitizing saracatinib-resistant cells. Even synergistic effects were observed for the combination of saracatinib and selumetinib in 2D colony growth assays with resistant and sensitive cells providing a potential combination strategy in treating ovarian cancer. Additionally, the lack of suitable biomarkers for this combination therapy is highlighted and further investigations of markers for patient selection for clinical trials are requested (McGivern et al., 2018).

Based on these *in vitro* experiments, another study demonstrated a co-activation of SRC and ERK in 31 % of HGSC tumor samples from the TCGA and associated the increased activity with poor prognosis and survival. Moreover, dual inhibition of SRC and MEK using saracatinib and selumetinib decreased tumor volume and latency compared to monotherapies *in vivo* by the targeting tumor-initiating stem cells (Simpkins et al., 2018). Similarly, another *in vivo* experiment treating nude mice, suffering from SK-OV3 and OVCAR-3-based tumors, with saracatinib and selumetinib could verify the effects of a combined treatment compared to the respective monotherapies. A subsequent immunohistochemical analysis of the initiated tumors for SRC and ERK activity revealed an upregulation of CDH1 exclusively after dual treatment indicating a reversion of the SRC- and ERK-induced EMT seen in their study (Fang et al., 2017). Notably, selumetinib was also already tested individually in a clinical trial (ClinicalTrials.gov Identifier: NCT00551070) to control tumor growth and was shown to be well tolerated in patients with ovarian and peritoneal tumors suggesting it for further application in combination therapies (Farley et

al., 2013). Notably, preclinical studies have shown that MEK inhibition additionally sensitizes for PARP inhibition (Sun et al., 2020).

However, inhibition of SRC and ERK essentially targets two major regulators, involved in EMT and proliferation, with tremendous impact on tumor growth and metastasis (Lavoie et al., 2020; Patel et al., 2016). Especially, the deregulation of SRC leads to AJs turnover and thus to lost adhesion enabling tumor spreading (Matsuyoshi et al., 1992; Woodcock et al., 2009) as well as loss of contact inhibition of proliferation which in turn favors proliferation and tumor growth (McClatchey and Yap, 2012).

#### **1.4 Conferring AJ-mediated signals to gene expression with the hippo pathway**

The hippo pathway is an important signaling pathway connecting AJs to gene expression in a density-dependent manner mediating contact inhibition of proliferation (CIP) to sustain tissue homeostasis. Contact inhibition refers to the regulatory mechanism which arrests cell growth when cells come in contact with each other and reach a certain density, important to limit organ growth and during regeneration (McClatchey and Yap, 2012). Uncontrolled growth is a characteristic of tumors to continue cell growth under high density conditions and accounts as a cancer hallmark (Hanahan and Weinberg, 2011). So it appears obvious that the pathway was found to be deregulated in a variety of tumors (Han, 2019). In the view of ovarian cancer, an upregulated expression of the main effector of a dysregulated hippo pathway YAP1 was associated with poor prognosis in HGSC (Cho et al., 2017; Wang et al., 2020). Also, YAP's nuclear activity was found to decrease survival and could be connected with resistance to current chemotherapeutics in ovarian cancer (Hall et al., 2010; Xia et al., 2014; Zhang et al., 2011). Considering the mutational background of TP53 in HGSC and the evidence of a crosstalk between YAP1 and TP53, it is tempting to speculate that deficient TP53 protein affects correct YAP1 protein localization, stability and thus its transcriptional activity (Raj and Bam, 2019).

The hippo pathway is highly conserved in mammals and consists of a core signaling cascade including MST1/2 (macrophage stimulating 1 and 2 or serine threonine kinase 4 and 3, STK4/STK3), SAV1 (salvador family WW domain containing protein 1), MOB1A/B (MOB kinase activator 1 A/B) and LATS1/2 (large tumor suppressor kinase 1 and 2) to control YAP1/WWTR1 (Yes-associated protein 1 / WW domain containing transcription regulator 1; TAZ) (Figure 4). The kinases MST1/2 and subsequently LATS1/2 facilitate phosphorylation of YAP1 at Ser127 to sustain the cytoplasmic retention of the YAP1/WWTR1 complex. In contrast, unphosphorylated YAP1/WWTR1 translocates to the nucleus and acts as a transcriptional co-activator of TEAD1-4-driven (TEA domain transcription factor 1 - 4) gene expression (Yu and Guan, 2013). Moreover, YAP1/WWTR1

seems to stimulate a negative feedback loop by directly stimulating in combination with TEADs LATS2 expression and concomitantly its activation by NF2 induction (Moroishi et al., 2015). Several studies postulated gene signatures associated with YAP1/WWTR1-driven gene expression referring to various cellular processes and signaling pathways (Galli et al., 2015; Stein et al., 2015; Wang et al., 2018; Zanconato et al., 2015) pathways. The most validated transcriptional targets of TEAD-driven gene expression are: BIRC2/5, CCN1/2, BDNF, FGF1, EGF, AREG and AMOTL2 associated with cell proliferation and survival (Hansen et al., 2015; Zhao et al., 2010). Next to the major TFs, also SMADs, RUNX, PAX and TP63/73 are reported to be activated by YAP1/WWTR1 (Hansen et al., 2015). Notably, although sharing high similarities in regulation and on their transcriptional targets, YAP1 and WWTR1 are described to differ primarily in their significance on downstream functions. The effect on cell spreading, migration and proliferation and even target gene expression was much stronger triggered by YAP1 compared to WWTR1 (Plouffe et al., 2018).

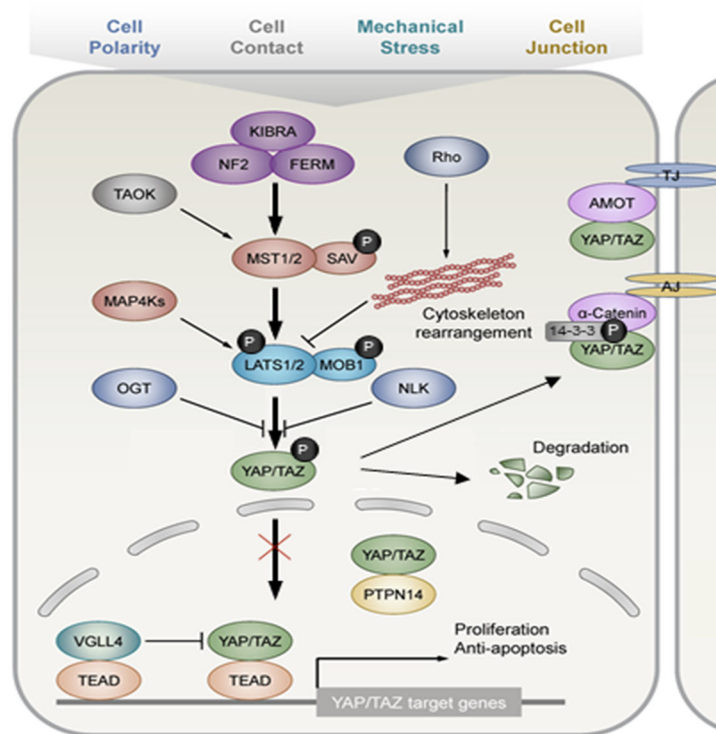


**Figure 4: The hippo pathway and its extracellular stimulation.** Hippo signaling is sensitized to different extracellular stimuli from the microenvironment including mechanical stress, cell contact, cell polarity mediated through different polarity complexes and cell-cell junctions such as tight junctions (TJs) and adherens junctions (AJs). The TJs associated protein AMOT as well as the AJs protein CTNNA1 thereby contribute to YAP's cytoplasmic retention. Extracellular stimuli are mainly transduced by the complex of WWC1 (KIBRA), NF2 (Merlin) and FRMD6 (FERM) to activate the core components of the hippo pathway. The core signaling cascade mediates phosphorylation through its kinases MST1/2 and LATS1/2 together with the adapter proteins SAV and MOB1 aiming to phosphorylate YAP/TAZ for its cytoplasmic retention or further degradation. Unphosphorylated YAP/TAZ translocates to the nucleus to associate with the TFs TEAD1-4 to activate transcription of proliferative and anti-apoptotic genes. VGLL4 and PTPN14 inhibit YAP/TAZ stimulated gene expression within the nucleus as well as several other factors located in the cytoplasm. Schematic modified from (Kim and Jho, 2018).

Due to its importance on tissue integrity, the mechanisms regulating the hippo pathway are quite diverse and mainly depend on extracellular stimuli. Especially, intracellular junctions, AJs as well as TJs are essential for transducing extracellular signals to the hippo pathway while their disruption leads to the nuclear localization of YAP1/WWTR1. Early studies have already connected cadherin structures in mediating contact inhibition of proliferation and linked their disruption to YAP1 activity (Kim et al., 2011; Yu and Guan, 2013). FRMD6 (FERM Domain Containing 6; also known as Ex) and NF2 (neurofibromin 2; also known as Merlin) co-localize with AJs, in complex with WWC1 (WW domain-containing protein 1; also known as KIBRA). In the Expanded-Merlin-KIBRA complex they recruit LATS1/2 and SAV1 to activate the hippo pathway (Kim and Jho, 2018; Yu and Guan, 2013). Additionally, MOB1 was also found to exclusively be activated at the plasma membrane (Ho et al., 2010). CTNNA1 was shown to associate with phosphorylated YAP1 at Ser127 via the 14-3-3 proteins preventing the nuclear localization of the YAP1/WWTR1 complex and thereby controlling its activity (Ren et al., 2010; Schlegelmilch et al., 2011; Silvis et al., 2011; Zhao et al., 2007).

Next to the junctional-driven regulation of the hippo pathway, different polarity complexes are also important to sustain apical basal polarity and YAP1/WWTR1 cytoplasmic retention (Martin-Belmonte and Perez-Moreno, 2011). For instance, the Crumbs (CRB) polarity complex including AMOT was linked to YAP1/WWTR1 cytoplasmic localization under dense conditions via TJs. Besides the classical regulation via the NF2/WWC1 complex and the hippo pathway, YAP1/WWTR1 seems also to be sensitive for ECM modulation, remodeling cell shape and consequently actin structure and the concomitant adjustment of mechanical tension involving RHOA, independent of LATS1/2 (Dupont et al., 2011; Zhao et al., 2012). Above, there are several hints that YAP1 activity can also be controlled apart from the hippo pathway. One example is SRC. The kinase was described to phosphorylate LATS1 to inhibit its function in the hippo pathway, but also direct phosphorylation within the transcription activation domain of YAP1 which uncouples YAP1 activity from the hippo pathway (Li et al., 2016; Si et al., 2017).

## **1.5 Post-transcriptional regulation with the oncofetal IGF2BP1**

RNA binding proteins (RBPs) essentially regulate post-transcriptional events by the formation of highly dynamic ribonucleoprotein complexes (RNPs) and binding a plethora of RNAs modulating RNA processing, localization, stability, translation and degradation (Gerstberger et al., 2014; Hentze et al., 2018). From the site of transcription within the nucleus to the site of translation and degradation in the cytoplasm, mRNAs are escorted by a variety of RBPs within the RNP complex. Although RBPs do not possess any enzymatic activity, they are able to control mRNA fate in all by the ability to recruit specific modulators.



The caging of mRNAs in RNPs in antagonism to miRNAs allows a fast and specific regulation and adaption of gene expression to the cellular microenvironment and signaling stimuli which is especially important for cancer evolution and metastasis. Over the last decades, only a few mRBPs were reported to be dysregulated in a variety of human cancers but the majority were associated with the regulation of a broad network of cellular processes and signaling cascades (Muller-McNicoll and Neugebauer, 2013; Pereira et al., 2017).

One of these mRBPs are the insulin-like growth factor 2 mRNA binding proteins (IGF2BPs) which constitute a protein family upregulated in a variety of solid tumors and are associated with differentiation, cell polarization, migration, proliferation and metabolism (Bell et al., 2013). Reported in various fields of research, the protein family is found under several synonyms including the human IMPs or IGF2BPs, the murine CRD-BP (coding region instability determinant binding protein), the chicken orthologs KOC (KH-domain-containing protein over-expressed in cancer) and ZBP1 (zipcode binding protein 1) as well as Vg1-RBP/Vera and VICKZ (Doyle et al., 1998; Havin et al., 1998; Mueller-Pillasch et al., 1999; Nielsen et al., 1999; Ross et al., 1997). All three orthologs share a relative high sequence homology but exhibit a distinct expression pattern which is conserved across species. Of the three family members (IGF2BP1 – 3), IGF2BP2 shows a ubiquitous occurrence in adult tissue. In contrast, IGF2BP1 and IGF2BP3 are termed as ‘oncofetal’ proteins based on their high expression during embryonic development while their abundance is lost during the process of cell differentiation and is with a few exceptions absent in adult tissue. Re-expression or *de novo* synthesis was observed in several tumor entities and is mainly associated with poor prognosis (Bell et al., 2013; Degrauwe et al., 2016b; Yaniv and Yisraeli, 2002; Yisraeli, 2005). So far, about the regulation of IGF2BP’s transcriptional expression is little known. Described regulators of IGF2BP1 expression are MYC and presumably CTNNB1 which were shown to induce IGF2BP1 transcription while IGF2BP2 expression is associated with HMGA2 (high mobility group AT-hook 2) (Cleyneen et al., 2007; Gu et al., 2009; Noubissi et al., 2010). Additionally, the MYC-enhanced IGF2BP1 transcription leads to a positive feedback regulation by the stabilization of MYC mRNA through IGF2BP1 proteins (Kobel et al., 2007; Lemm and Ross, 2002; Weidensdorfer et al., 2009). Obviously, a positive feedback mechanism is similarly described for CTNNB1 while a negative feedback regulation of CTNNB1 was observed via the IGF2BP1-driven stabilization of BTRC mRNA inducing CTNNB1 degradation (Gu et al., 2008; Noubissi et al., 2006).

The almost exclusively cytoplasmic proteins possess a conserved domain structure containing two N-terminal RNA recognition motif (RRM) and four C-terminal hnRNPK homology domains (KH). RNA binding is mainly facilitated via the KH domains and for IGF2BP1 it is additionally shown that it likely associates in a 3’UTR-dependent manner. The often underestimated RRM domains were reported to be involved in the protein associations

within the RNP complex and contribute to its stability although their whole function is not completely elucidated yet (Bell et al., 2013; Conway et al., 2016; Farina et al., 2003; Nielsen et al., 2004; Wachter et al., 2013). Moreover, in recent years RNA modifications emerged as important features within mRNPs whereas N6-methyladenosine (m6A) represents one of the most prevalent modifications. The IGF2BPs were identified to recognize these modifications and promote stabilization and translation of their target mRNAs in an m6A-dependent manner (Huang et al., 2018; Muller et al., 2019).

Focusing on IGF2BP1, several RNA targets were identified by cross-linking immunoprecipitation (CLIP) studies followed by sequencing of the bound RNAs (Conway et al., 2016; Hafner et al., 2010; Van Nostrand et al., 2016). Experimentally validated genes are linked to oncogenic as well as tumor-suppressive properties and comprise for instance KRAS, (Mongroo et al., 2011), CTNNB1 (Gu et al., 2009), LEF1 (Zirkel et al., 2013), MKI67 (Gutschner et al., 2014), GLI (Noubissi et al., 2009), CD44 (Vikesaa et al., 2006) and E2F1 (Muller et al., 2020). Thus, IGF2BP1 seems to stabilize these mRNA targets and thereby enhance their protein expression. Moreover, IGF2BP1 was suggested to be involved in facilitating drug resistance to the current therapy of ovarian cancer. IGF2BP1 was proposed to downregulate let-7 miRNAs and concomitant stabilize MDR1 (multidrug resistance 1) mRNA which is frequently observed after chemotherapy of relapsed patients and negatively correlated with PFS (Boyerinas et al., 2012; Sparanese and Lee, 2007). Besides, IGF2BP1 was shown to promote the expression of the cancer-related RBP LIN28B (Lin-28 homolog B) which suppresses the maturation of the miRNA let-7 and thereby reduces let-7 targeting of IGF2BP1 mRNA. Together, LIN28B and IGF2BP1 enhance the expression of the TF HMGA2 (high-mobility group AT-hook 2). The IGF2BP1-dependent recruitment of these two let-7 target mRNAs in RNPs prevents them from let-7 miRNA attack and shields from the miRISC (miRNA-induced silencing complex). This interplay of downregulated let-7 synthesis, mRNA binding and subsequent protection of all three mRNAs from let-7-driven gene silencing leads to an upregulation of these proteins in a synergistic manner (Busch et al., 2016). Similarly, deregulation of MYCN, LIN28B, HMGA2 and let-7 was also seen in the molecular subtype C5 of HGSC (Helland et al., 2011). Next to HMGA2, IGF2BP1 was described to further stabilize the transcription factors MYC and SRF which further pronounce its oncogenic character by inducing the transcription of several oncogenes (Huang et al., 2018; Muller et al., 2019). Some of the SRF target genes including PDLIM7 and FOXK1 were additionally stabilized by IGF2BP1 as well as the upstream factor MAPK1 (ERK2) which in turn stimulates TCF/SRF-driven gene expression (Lavoie et al., 2020; Muller et al., 2018; Muller et al., 2019). Preventing miRNA-directed silencing of its bound mRNAs through binding and / or stably sequestering them within the RNP complex seems to be a general mechanism by which IGF2BP1 promotes mRNA stability and regulates

mRNA fate of its targets (Elcheva et al., 2009; Goswami et al., 2010; Muller et al., 2018; Muller et al., 2019; Weidensdorfer et al., 2009).

Another function of IGF2BP1 seems to be the transport and spatial regulation of translation of the bound ACTB ( $\beta$ -actin) mRNA. IGF2BP1 was found to direct ACTB mRNA in developing neurons and primary fibroblasts to sites of active actin polymerization like protrusions (Farina et al., 2003; Huttelmaier et al., 2005). The association of the RBP with the zipcode of the 3'UTR of the ACTB mRNA already occurs within the nucleus to prevent its early translation in the cytoplasm and enable the cytoskeletal transport. Localized to the cell periphery, the SRC kinase phosphorylates IGF2BP1 to trigger the release of the bound ACTB mRNA. The spatial induced translation of ACTB leads to an increase of the local ACTB concentration within protrusions contributing to the cytoskeletal remodeling and actin-driven migration in an IGF2BP1-dependent manner (Farina et al., 2003; Huttelmaier et al., 2005; Oleynikov and Singer, 2003). Similar mechanisms are reported for IGF2BP orthologs with different kinases which suggests a central role for phosphorylation events in releasing bound mRNAs and disassemble RNP complexes (Dai et al., 2011; Git et al., 2009).

In detail, the association of IGF2BP1 with SRC was identified to interact via a proline-rich SH3 binding motif located in the linker region between KH2 and KH3 of IGF2BP1. This VP<sub>4</sub>SS motif is identically found within the SRC substrate and cell adhesion protein paxillin (PXN) and is highly conserved across species (Huttelmaier et al., 2005; Weng et al., 1993). Referring to the role of SRC in FA turnover and the spatial induction of ACTB translation together with IGF2BP1, this collectively enables cytoskeletal rearrangement which is important during cancer migration and invasion. Further impact of IGF2BP1 on cytoskeletal modulation was drawn with the observation that IGF2BP1 accumulates at the leading edge of lamellipodia, co-localizes together with ACTB and is essential during lamellipodia formation (Vainer et al., 2008). Loss of function analysis additionally revealed that IGF2BP1 modulates several mRNAs involved in adhesion to the extracellular matrix and thereby regulating invadopodia formation through the stabilization of the CD44 mRNA (Vikesaa et al., 2006). Next to its impact on invasion, the post-transcriptional control of mRNAs involved in migration was also mediated IGF2BP1-dependent (Oberman et al., 2007). In tumor-derived cells IGF2BP1-driven inhibition of MAPK4 (mitogen-activated protein kinase 4) translation leads to a shift of the cellular balance of F-actin and G-actin enabling cell migration through the mobilization of G-actin polymerization. Concomitantly, stabilization of PTEN (phosphatase and tensin homolog) mRNA through IGF2BP1 increased the expression of PTEN which antagonized PIP<sub>3</sub> (phosphatidylinositol-3,4,5-trisphosphat) signaling. The thereby obtained asymmetric distribution of the endogenous PIP<sub>3</sub> and PIP<sub>2</sub> (phosphatidylinositol-4,5-bisphosphat) equilibrium enhanced cell polarization through constraining RAC1 activation. Together, this increased velocity and sustained a persistence of cell migration in dependence on IGF2BP1 (Stohr et al., 2012).

The proposed association of IGF2BP1 in adhesion (Conway et al., 2016) was further linked to an IGF2BP1-driven promotion of mesenchymal properties in studies with melanoma-derived cells. The transcriptional regulators of EMT-driven gene expression, LEF1 (lymphoid enhancer binding factor 1) and SNAI2 (snail family transcriptional repressor 2), were bound and stabilized by IGF2BP1 to enhance their protein expression. In turn LEF1 enforced the transcription of the mesenchymal ECM protein FN1 (fibronectin 1) and SNAI2 which induced a mesenchymal cell morphology. A knockdown of IGF2BP1 reverted the effect, promoted CTNNB1-positive cell-cell contact formation and reduced cell migration (Zirkel et al., 2013). Taken together, through its RNA binding capacity the oncofetal IGF2BP1 is involved in the regulation of multiple cancer-associated processes like migration and invasion, therefore it modulates adhesion by promoting mesenchymal cell properties including stem cell renewal (Degrauwe et al., 2016b).

In accordance, IGF2BP1 seems to force tumor progression and its expression correlates with poor prognosis within various cancer entities like neuroblastoma, colorectal cancer, breast cancer, melanoma, non-small lung cancer and epithelial ovarian carcinoma (Bell et al., 2015; Dimitriadis et al., 2007; Fakhraldeen et al., 2015; Fortis et al., 2017; Kato et al., 2007; Kobel et al., 2007). In detail, *de novo* synthesized IGF2BP1 was observed in 69 % of the analyzed tumors of ovarian cancer and correlated with high-grade and high-stage resulting in reduced PFS and overall survival (Kobel et al., 2007). Furthermore, IGF2BP1 was shown to be one of the highest upregulated RBPs in hepatocellular carcinoma and anaplastic thyroid carcinoma (Gutschner et al., 2014; Haase et al., 2021). Its potential in tumor initiation was recently demonstrated with transgenic mice where IGF2BP1 expression was induced in their mammary epithelial cells. After approximately one year, 95 % of all mice developed tumors (Hamilton et al., 2013; Tessier et al., 2004). Similarly, *in vivo* models have shown that a depletion of IGF2BP1 reduces tumor growth next to the *in vitro* studies which observed decreased spheroid growth, invasion and migration in the absence of IGF2BP1 compared to its IGF2BP1-expressing control (Busch et al., 2016; Muller et al., 2018; Stohr et al., 2012).

Due to its oncogenic potential and its lost expression in healthy adult tissue, IGF2BP1 represents an interesting target for a selective treatment of IGF2BP1-positive tumors within patients. The recently developed small molecule inhibitor BTYNB specifically inhibits the binding of IGF2BP1 to its target mRNAs as shown for MYC as well as E2F1 and thereby reduces cell proliferation in ovarian cancer- and melanoma-derived cells (Mahapatra et al., 2017) as well as tumor growth *in vivo* (Muller et al., 2020). Inhibition of IGF2BP1 seems to be promising in targeted cancer therapy. The further development of IGF2BP1-specific inhibitors, their clinical evaluation and the selection of patients benefitting from this therapy remains to be addressed in the future. Two studies already emphasize IGF2BP1 as a putative biomarker for subtype-specific patient selection. The rare anaplastic thyroid

carcinoma (ATC) accounts for the most lethal carcinomas of the thyroid due to a lack of reliable diagnostic markers and precise treatment. IGF2BP1 represents a robust marker to distinguish ATC from other thyroid malignancies with a potential for future therapy (Haase et al., 2021). Moreover, the de-differentiated, mesenchymal C5 subtype of the most frequent histotype of ovarian cancer, HGSC, was recently in cooperation with this study associated with an enhanced IGF2BP1 abundance in comparison to the other subtypes. Thereby, IGF2BP1 expression was shown to correlate with the C5 signature in three independent datasets and immunohistochemical staining revealed a significant upregulation of IGF2BP1 within tumors linked to the C5 subtype (Bley et al., 2021).

In conclusion, the profound and exclusive role of IGF2BP1 within tumors can be benefitting in further evaluations of targeted therapy.

## 1.6 Aims of the study

Epithelial ovarian carcinomas (EOCs) and especially in its most frequent histotype, high-grade serous carcinomas (HGSCs), represent a complex malignancy due to its heterogeneity, frequent metastatic spread at diagnosis and its occurring resistances to standard therapies. The fast adaption of the tumor to its microenvironment and dissemination of single cells during metastasis underly a broad network of signaling cascades transducing extracellular signals into intracellular gene expression and remodeling processes. Intercellular junctions and its intracellular communication via SRC and Hippo signaling cascades thereby play a substantial role. The oncofetal mRNA binding protein IGF2BP1 shows a subtype-specific upregulation in HGSC and above it is associated with cancer progression. As a post-transcriptional regulator IGF2BP1 can modulate gene expression by controlling a network of mRNAs acting in distinct pathways. To understand HGSC with its low mutational burden, it is worth to draw attention on alternative regulatory strategies like RBPs de-regulated in HGSC to connect post-transcriptional control of gene expression with signaling networks and cancer properties. The oncogenic drivers SRC and IGF2BP1 were seen to be upregulated in EOC and several studies indicated towards their ability to modulate adhesion in various ways. During my master's thesis and based on previous NGS and quantitative proteomic analysis of our working group, we got first insights in the interference of IGF2BP1 with AJs. This study aims at elucidating the role of IGF2BP1 in controlling SRC-directed AJ disassembly *in cellulo* and *in vivo* in ovarian cancer and identifies a novel RNA-independent mechanism of IGF2BP1's directed control of SRC activation. It uncovers the IGF2BP1-guided connection of SRC, ERK and HIPPO signaling networks to promote EMT, growth and invasion to propose alternative treatment strategies for IGF2BP1-expressing HGSC tumors.

## 2 MATERIAL AND METHODS

### 2.1 Material

#### 2.1.1 Chemicals and reagents

Chemicals were obtained from Thermo Fisher, Roth and Sigma Aldrich unless otherwise stated. Cell culture dishes were delivered by Techno Plastic Products and Corning while cell culture medium, FBS, Opti-MEM, Trypsin and transfection reagents were supplied by Thermo Fisher and Biochrome. Restriction enzymes, corresponding reaction buffers, DNA markers and ladders were purchased from New England Biolabs and Promega. For further cloning, ligase enzyme and reaction buffer from Roche were used. Master mix for qRT-PCR was acquired from High Qu GmbH. Protein and RNA ladder were produced by New England Biolabs.

#### 2.1.2 Bacteria strain

Transformation of cloned plasmids was performed in the bacteria strain *Escherichia coli* TOP10 (genotype: F-mcrA  $\Delta$ (*mrr-hsdRMS-mcrBC*)  $\Phi$ 80*lacZ* $\Delta$ M15  $\Delta$ *lacX74 recA1 deoR araD139  $\Delta$ (*ara-leu*)7697 *galU galK rpsL* (StrR) *endA1 nupG*) and cultivated in LB culture medium (Luria Bertani – 1 % (w/v) Trypton, 0.5 % (w/v) yeast extract, 1 % (w/v) NaCl). For selection of recombinant bacteria populations LB culture medium was supplemented with antibiotics (30  $\mu$ g/mL Kanamycin or 150  $\mu$ g/mL Ampicillin). Beside the liquid culture, 1.5 % (w/v) Agar was added for bacteria cultivation on LB plates.*

#### 2.1.3 Cell lines

**Table 1: Overview of parental cell lines.**

cell line	origin	distributer	Cat. No.	publication
ES-2	ovary	ATCC	CRL-1978	(Lau et al., 1991)
NIH:OVCAR-3	ovary	CLS	300307	(Hamilton et al., 1983)
COV-318	ovary	Sigma Aldrich	07071903	(van den Berg-Bakker et al., 1993)
TOV-112D	ovary	ATCC	CRL-11731	(Provencher et al., 2000)
A2780	ovary	Sigma Aldrich	93112520	(Behrens et al., 1987; Hamilton et al., 1984)
CAOV-3	ovary	ATCC	HTB-75	(Fogh, 1986)
SK-OV-3	ovary	CLS	300342	(Fogh et al., 1977)
OAW-28	ovary	Sigma Aldrich	85101601	(Wilson et al., 1996)
OVCAR-5	ovary	CLS	300228	(Hamilton et al., 1984; Johnson et al., 1997)

OVCAR-8	ovary	CLS	300298	(Hamilton et al., 1984)
ID8	ovary (murine)	Sigma Aldrich	SCC145	(Roby et al., 2000)
ID8-TP53-KO	ovary (murine)	Iain McNeish	-	(Walton et al., 2016; Walton et al., 2017)
ID8-TP53- IGF2BP1-KO	ovary (murine)	Iain McNeish	-	(Walton et al., 2016; Walton et al., 2017)
HEK293T	kidney	ATCC	CRL-11268	(DuBridgE et al., 1987; Graham et al., 1977)

**Table 2: Generated cell clones by CRISPR-Cas9 system.**

cell clone	parental cell line	reference
ES-2 IGF2BP1 knockout	ES-2	Dr. Marcell Lederer
ES-2 YAP1-3'UTR deletion	ES-2	this study

### 2.1.4 Primary and secondary antibodies

**Table 3: Primary antibodies for Western blot and immunofluorescence staining.**

primary antibodies	species	company	Cat. No.
IGF2BP1 (6A9)	mouse	BSBS AB facility	Previously described (Stohr et al., 2012)
IGF2BP1	mouse	MBL	RN001M
CDH2 (8C11)	mouse	Santa Cruz	sc-53488
CTNNB1 (D10A8)	rabbit	Cell Signaling	8480
CTNNB1	mouse	Santa Cruz	sc-7963
CDH1 (EP700Y)	rabbit	Abcam	ab40772
CTNND1; pp120	mouse	BD Biosciences	610133
phospho-CTNNB1 (Ser33/37, Thr41)	rabbit	Cell Signaling	9561
phospho-CTNND1 (Tyr228)	mouse	BD Biosciences	612536
phospho-SRC (Tyr416) (100F9)	rabbit	Cell Signaling	2113
SRC (L4A1)	mouse	Cell Signaling	2110
phospho-ERK1/2; phospho-p44/42 MAPK (Thr202/Tyr204) (E10)	mouse	Cell Signaling	9106
ERK1/2; p44/42 MAPK (137F5)	rabbit	Cell Signaling	4695
KRT8	rat	TROMA-1 hybridoma cell supernatant	Previously described (Brulet et al., 1980)
VIM	mouse	BD Biosciences	550513
ACTB	mouse	Sigma Aldrich	A5316

VCL	mouse	Sigma Aldrich	V9131
GAPDH	rabbit	Bethyl	A300-641A
RPL7	rabbit	Bethyl	A300-741A
YAP1	mouse	Santa Cruz	sc-101199
ZEB2	rabbit	Bethyl	A302-474A
TWIST1	rabbit	Santa Cruz	sc-15393
SNAI1	rabbit	Cell Signaling	3879
SNAI2	mouse	Sigma Aldrich	WH0006591M5
RAC1	mouse	BD Bioscience	610650
GFP (for RIP)	mouse	Roche	11814460001
GFP	mouse	Santa Cruz	sc-9996

Secondary antibodies are either coupled with fluorescent dyes for Western blot detection via the LiCOR scanner or linked to a fluorophore for microscopical imaging (Table 4).

**Table 4: Secondary, fluorescence labelled antibodies for Western blot detection and immunofluorescence imaging.**

<b>secondary antibodies for Western blotting</b>	<b>company</b>	<b>Cat. No.</b>
IRDye 680RD Donkey anti-Rabbit IgG	LI-COR	926-68073
IRDye 680RD Donkey anti-Mouse IgG	LI-COR	926-68072
IRDye 800CW Donkey anti-Mouse IgG	LI-COR	926-32212
IRDye 800CW Donkey anti-Rabbit IgG	LI-COR	926-32213
IRDye 800CW Donkey anti-Rat IgG	LI-COR	926-32219
<b>secondary antibodies for immunostainings</b>	<b>company</b>	<b>Cat. No.</b>
Alexa Fluor 647 AffiniPure F(ab') <sub>2</sub> Fragment Donkey Anti-Rabbit IgG (H+L)	Dianova	711-606-152
Alexa Fluor 647-AffiniPure F(ab') <sub>2</sub> Fragment Donkey Anti-Mouse IgG (H+L) (min X)	Dianova	715-606-150
Alexa Fluor 488-AffiniPure F(ab') <sub>2</sub> Fragment Donkey Anti-Rabbit IgG (H+L) (min X)	Dianova	715-546-150
Alexa Fluor 488-AffiniPure F(ab') <sub>2</sub> Fragment Donkey Anti-Rabbit IgG (H+L) (min X)	Dianova	711-546-152

### 2.1.5 Plasmids

A variety of commercially available vectors (Table 5) were used directly, handled as cloning vectors, or inserted with different sequences (Table 6) for over-expression, CRIPSR-Cas9 systems, virus production, reporter plasmids or normalization.



**Table 5: Commercial plasmids.**

plasmids	resistence	company	Cat. No.
pCR®-blunt	Kanamycin	ThermoFisher Scientific	K270020
pmirGLO Dual luciferase	Ampicilin	Promega	E1330
pLVX	Ampicilin	Clontech	632164
pAc/pEGFP-C2	Kanamycin	Clontech	632481
pCDNA3.1_Cas9_T2A_GFP	Ampicilin	Hüttelmaier group	originated from Addgene Cat#128047
psg_RFP_BbsI	Ampicilin	Hüttelmaier group	–
pNL3.1 [Nluc minP]	Ampicilin	Promega	N1031
pGL4.54 [luc2/TK]	Ampicilin	Promega	E5061
pLenti-YAP1-3'UTR-Luc	Kanamycin	Applied Biological Materials Inc.	based on m012
pRL	Ampicilin	Promega	E2231
pMD2G	Ampicilin	Addgene	12259
psPAX2	Ampicilin	Addgene	12260
pCW57.1	Ampicilin	Addgene	41393

### 2.1.6 Oligonucleotides

All oligonucleotides, siRNAs and sgRNAs were ordered from Eurofins Genomics GmbH and Microsynth AG.

Oligonucleotides for cloning (Table 6) served for the generation of different constructs and were inserted into suitable, commercial vectors (Table 5). Generation of plasmids for protein or protein motif over-expression were performed. Reporter plasmids were cloned with indicated 3'UTRs or binding motifs. Besides, plasmids for CRISPR-Cas9-mediated 3'UTR deletions were established.

Table 6: Oligodesoxynucleotides for cloning.

insert	vector	sequence sense / antisense (5' - 3' )	restriction site
CTNNB1 - 3' UTR s	pmirGLO	CCGAATTCATCATCCCTTTAGGTAAGAAGTTTTAAAAAGC s GGGTCCGACCAATCGAATGAAATTAAGATTTAATTCTGAACC as	EcoRI-Sall
CDH2 - 3' UTR s	pmirGLO	CGGAATTCACCTTCAGGGTGAACCTGGTTTTTTGG s CGCTCGAGCACCAAGATCCAAAATTAGCATTTTATTTCAG as	EcoRI-XhoI
IGF2BP1 over-expression	pLVX and pAcGFP-C2	GGGAATTCATGAACAAGCTTTACATCGGCAACC s GGCTCGAGTCACTTCCCTCCGTGCCCTGGGCCCTGGTTACTCTG as	EcoRI-XhoI (XhoI in Sall in pAcGFP-C2)
IGF2BP1 ΔSH3 mutant (VP <sub>4</sub> SS replaced by GS)	pLVX and pAcGFP-C2	ATCGAATTCATGAACAAGCTTTACATCGGCAAC s AACGGATCCCTGCGCTGGATGAAGCTGGGAAAAG as GCAGGATCCGTTACTGGGGCTGCTCCCTATAGCTCC s AGCCTCGAGTCACTTCCCTCCGTGCCCTGGGCCCTG as	EcoRI-BamHI BamHI-XhoI (XhoI in Sall in pAcGFP-C2)
VP <sub>4</sub> SS motif of IGF2BP1	pAcGFP-C2	AATTCAGCGCAGTCCCGCCGCTCCAGCAGCC s TCGAGGCTGCTGGGAGGGCGGGACTGCGCTG as	BamHI-XhoI (XhoI in Sall in pAcGFP-C2)
YAP1 - 3' UTR depletion	psg1 psg2	CACCGATCTAAGGAGACACATGCAC s AAACGTGCATGTGTCTCCTTAGATc as CACCGTAAGAGCATGCTCATATGTT s AAACAACAATATGAGCATGCTCTTAc as	EcoRI-XhoI
YAP-TAZ binding motif	pNL3.1 [Nluc minP]	CTAGAAAGTTGAGACACATCCACACATTCACCTTGAGACACATCCACA CATTCCACTGCTCTAGACGTCAs AGCTTGACGCTAGAGCAGTGAATGTGTGGAATGTGTCTCAAGCTGCAGTGGAA TGTGTGGAATGTGTCTCAACTTT as according to Addgene plasmid #34615 and (Dupont et al., 2011)	XbaI-HindIII

**Table 7: Oligodesoxynucleotides for qRT-PCR.**

gene	sequence sense (5' – 3')	sequence antisense (5'– 3')
RPLP0	CCTCATATCCGGGGGAATGTG	GCAGCAGCTGGCACCTTATTG
GAPDH	CAACGAATTTGGCTACAGCA	AGGGGAGATTCAGTGTGGTG
HIST1H2AC	TTTCTCGTGAGCTTAGGCCG	CCTTGCTTACCACGTCCAGA
HIST2H3A	TGTTCAAGTTCCTCGTCGTTG	GCGGTCCTCGAGTATCTGAC
IGF2BP1	TAGTACCAAGAGACCAGACCC	GATTTCTGCCCGTTGTTGTC
LIN28B	ATGCAGAAGATCACTCCGTTCC	CACCAGGTCCTGTTACCCG
HMGA2	CCTAAGAGACCCAGGGGAAG	TCTTCGGCAGACTCTTGTGA
CTNNB1	TCGAAATCTTGCCCTTTGTC	ATCCCGAGCTAGGATGTGAA
CDH2	CCATCACTCGGCTTAATGGT	GATGATGATGCAGAGCAGGA
YAP1	TCCCAGATGAACGTCACAGC	TAACTGGCTACGCAGGGCTA
ERK2	TGGAGCAGTATTACGACCCG	AACACCGATGTCTGAGCACG

Single siRNAs as well as siRNA pools were transfected. A benefit of equally pooled siRNAs with different sequences against the target sequence is the reduction of off-target effects.

**Table 8: Oligonucleotides for siRNA-mediated inhibition of gene expression.**

siRNA	sequence (5' – 3')
control siRNA (siC)	UUGUACUACACAAAAGUACUG
IGF2BP1 siRNA pool (sil1)	CCGGGAGCAGACCAGGCAA UGAAUGGCCACCAGUUGGA CCAGGCAAGCCAUCAUGAAGCUGAA GGCUGCUCCCUAUAGCUCCUUUAUG GGGAAGAGCUGGAGGCCUA CCAUCCGCAACAUCACAAA AAGCTGAATGGCCACCAGTTG AACACCTGACTCCAAAGTTG GTATGGTACAGTAGAGAAC CCUGAAGAAGGUAGAGCAA GUUCGUAUGGUUAUCAUCA GUGAACACCGAGAGUGAGA

**Table 9: sgRNAs for establishment CRISPR-Cas9-mediated cell clones.**

target of sgRNA	sequence (5' – 3')
YAP1-3'UTR sgRNA-1	F D F F J W D D J D J F D W J F W F D W D W J W W # # AAACAACATATGAGCATGCTCTTAC as
YAP1-3'UTR sgRNA-2	F D F F J D W F W D D J J D J D F D F D W J F D F # # AACCGTGCATGTGTCTCCTTAGATC as
IGF2BP1-CDS sgRNA-1	CACCGAATGGCACCCACATACTGGG s AAACCCAGTATGTGGGTGCCATTC as
IGF2BP1-CDS sgRNA-2	CACCGTGCATAGGAAGGAGAACGC s AAACGCGTTCTCCTTCCTATGCAC as

All hybridization probes were labelled with fluorescence dyes (DyLight).

**Table 10: Oligonucleotides for sequencing.**

Purpose	amplification	sequence (5' – 3')
gPCR YAP1- 3'UTR	3'UTR YAP1	CCCACAAAACAATATGAATATGGAGATCTT s1 GCAGAACCGTTTCCAGACTACC s2 GGAAAGAATATATTTGAACCACATAAACAAACAAAAGG as

### 2.1.7 Standard systems and Kits

All standard systems and Kits were used according to the manufacturer's instructions unless otherwise stated.

**Table 11: Commercial kits used.**

Kit	company	Cat. No.
DC Protein Assay	Bio-Rad	5000111
CellTiter-Glo® Luminescent Cell Viability Assay	Promega	G7570
Dual-Glo® Luciferase Assay System	Promega	E2920
Nano-Glo® Luciferase Assay System	Promega	N1110
Phusion® High-Fidelity PCR Kit	New England Biolabs	E0553
Zero Blunt® PCR Cloning Kit	Thermo Fisher	K27002
Wizard SV Gel and Clean-Up System	Promega	A9281
QIAprep® Spin Miniprep Kit (250)	Qiagen	12123
QIAGEN Plasmid Midi Kit (100)	Qiagen	12143
Click-iT® Biotin Protein Analysis Detection Kit	Thermo Fisher	C33372
Matrigel	Corning	354234
Cultrex® 10X Spheroid Formation ECM	Trevigen	3500-096-01

### 2.1.8 Standard buffers

**Table 12: Composition of standard buffers.**

PBS (phosphate buffered saline; 0.01 M)	137 mM NaCl 2.7 mM KCl 10 mM Na <sub>2</sub> HPO <sub>4</sub> 2 mM KH <sub>2</sub> PO <sub>4</sub>
PBST (phosphate buffered saline-Tween)	0.01 M PBS 1% Tween-20
TAE (Tris/Acetate/EDTA)	40 mM Tris 20 mM Glacial acetic acid 1 mM EDTA
NuPAGE (transfer buffer)	50 mM Tris 40 mM Glycerin 0.04 % SDS 10 % Methanol
Ponceau-S	0.1 % Ponceau-S 5 % acetic acid
TRIZOL	0.8 mM Guanidine thiocyanate 0.4 mM Ammonium thiocyanate 0.1 mM Sodium acetate (pH 0.5) 5 % Glycerin 48 % Roti®Aqua Phenol
Total lysis buffer	50 mM Tris (pH 7.4) 50 mM NaCl 1 % SDS 2 mM MgCl <sub>2</sub>
5x MLB (pH 7.5)	125 mM HEPES 750 mM NaCl 5 % NP-40 50 mM MgCl <sub>2</sub> 5 mM EDTA 10 % Glycerol
10x lysis buffer (RIP)	100 mM HEPES (pH 7.0) 1.5 M KCl 50 mM MgCl <sub>2</sub> x 6H <sub>2</sub> O 5 % NP-40

### 2.1.9 Devices

**Table 13: Manufacturer's list of used devices.**

Microscopy	Nikon TE-2000E Leica SP5X Leica SP8X Sartorius Incucyte S3® Nikon TS-100
Flow cytometer	BD FACS Melody MACSQuant® Analyzer 9 Miltenyi BioTec
Luminescence	Promega GloMax® Discover 96 well Microplate Reader

Spectroscopy	Tecan Infinite 2000, 96 well Microplate und Nanodrop
SDS-PAGE	Life Technologies NuPAGE® Bis-Tris Electrophoresis System
Western blot	XCell II™ Mini-Cell Blot Module (Thermo Fisher)
Infrared scanner	LiCOR Odyssey Infrared Scanner
qRT-PCR	Roche Light Cycler 480 II
Thermocycler	Eppendorf Mastercycler Nexus II (96well)
Agarose gel electrophoresis	BioRad Mini-Sub® Cell GT Cell
UV Crosslinker	Biostep® Crosslinker 254nm
Centrifuges	Heraeus Biofuge Stratos Heraeus Biofuge fresco Eppendorf MiniSpin
Cell counter	Biorad T-20

## 2.2 Cell biological methods

### 2.2.1 Cell culture

All adherent ovarian cancer cell lines and HEK293T cells were cultivated at 37°C and 5 % CO<sub>2</sub> in Gibco™ DMEM (*Dublecco's modified Eagle's medium*; Thermo Fisher; ES-2, NIH-OVCAR-3, COV-318, TOV-112D, CAOV-3, SK-OV-3, OAW-28, OVCAR-5, OVCAR-8, HEK293T) or Gibco™ RPMI-1640 (*Roswell Park Memorial Institute*; ATCC modification; Thermo Fisher; A2780). The medium was supplemented by 10 % fetal bovine serum (FBS; Thermo Fisher) and 1 % GlutaMAX (L-Alanyl-L-glutamine; Thermo Fisher). Similarly, the murine ovarian surface epithelium cells, ID8, were cultivated in DMEM as well but supplemented with only 4 % FBS and additionally contained ITS (insulin-transferrin-selenium; Thermo Fisher). For re-plating, cells were washed with PBS and removed from cell culture dishes by adding 0.05 % Trypsin and 0.4 mM EDTA in PBS and resuspended in the corresponding medium. Afterwards, cells were seeded for cultivation, assays or transfections. A re-authentication of ES-2 and NIH:OVCAR-3 cell lines were performed by Eurofins Genomics using AmpFIST® Identifier® Plus PCR Amplification Kit (Thermo Fisher). Testing for mycoplasma was frequently utilized by PCR (polymerase chain reaction) with the 2x PCR mix (Roche) and the following primers (5'–3'): GTGGGGAGCAAAYAGGATTAGA (s) and GGATGATGATTTGACGTCRT (as).

### 2.2.2 Transfections & reporter assays

#### 2.2.2.1 siRNA transfection

For gene silencing by siRNAs (Table 8), cells were seeded and directly transfected using liposome-based transfection reagent Lipofectamine RNAiMAX, generally with 5x10<sup>5</sup>

cells per 6-well with 30 pmol siRNA and 7  $\mu$ l RNAiMAX according to the manufacturer's protocol. Cells reached confluency 24 h post transfection and were therefore splitted for a variety of assays ensuring comparable transfection efficacies in all measurements. Cells were harvested 72 h post transfection to analyze the cells in different assays. Reporter assays (2.2.2.2) with knockdown cells only differed in a re-transfection (Table 5; Table 6) 24 h after siRNA transfection with Lipofectamine 3000 for additional 48 h.

#### 2.2.2.2 Plasmid transfection

All plasmid transfections were carried out with the liposome-based Lipofectamine L2000 or L3000 depending on prior transfections and followed the manufacturer's instructions. Reporter plasmid transfections with pmirGLO, pLenti or pNL3.1 (Table 5, Table 6) were performed by adding 1  $\mu$ l Lipofectamine L3000 and 0.5  $\mu$ l Lipofectamine P3000 and 100 ng plasmid DNA to a 24-well cavity with  $1 \times 10^5$  cells. In detail, for analyzing 3'UTR luciferase reporter activity of CDH2 and CTNNB1, 100 ng of the pmirGLO reporter was transfected which contains a firefly luciferase for the measurement of the reporter activity and an additional renilla luciferase as an internal control. Next to 100 ng of the 3'UTR luciferase reporter pLenti-YAP1-3'UTR-Luc, 20 ng of a plasmid coding for a renilla luciferase (pRL) was co-transfected for normalization. To monitor the transcriptional activity of YAP1 with a YAP1/WWTR1-responsive reporter system, four repetitive TEAD binding sites were inserted in the Nanoluc luciferase containing pNL3.1 plasmid and transfected (100 ng) together with 10 ng of the control plasmid pGL4.54 coding for a firefly luciferase. Reporter assays were analyzed 48 h post plasmid transfection. For transfection of an over-expression, cells were seeded 12 h prior to transfection,  $5 \times 10^5$  cells per 6-well. Transfection was carried out with indicated plasmid concentrations and 5  $\mu$ l Lipofectamine L2000 for 48 h.

#### 2.2.3 3D spheroid assays (growth, invasion)

For the analysis of tumor-cell phenotypes, 3D growth and 3D invasion assays were performed. Accordingly,  $1 \times 10^3$  cells were seeded in 50  $\mu$ l growth medium into a round bottom ultra-low attachment plate (Corning; Cat#7007). When indicated, siRNA-mediated knockdown was transfected 24 h prior seeding otherwise stable cell lines were used. Cultrex® 10X Spheroid Formation ECM (Trevigen; Cat# 3500-096-01) was added to all cell lines except ES-2 and NIH:OVCA3. After seeding, cells were gently centrifuged for 5 min at 500 g and spheroid formation took place overnight. For invasion assays, 50  $\mu$ l Matrigel (Corning, Cat# 354234) was added to preformed spheroids and centrifuged again for 5 min at 300 g and 4°C. After polymerization of the Matrigel at 37°C for 1 h, 100  $\mu$ l growth medium supplemented with indicated final inhibitor concentration was added. In case of 3D growth assays, volume was adapted with growth medium to reach the same 200  $\mu$ l in total

for each 96-well. Subsequently, imaging of preformed spheroids was started by the Incucyte S3 device and proceeded for the stated time periods. Images were analyzed by spheroid segmentation with the Incucyte software. First images served as normalization control, in detail growth area or invasion front after stated time periods were calculated to spheroid input or body. Next to image analysis, viable cells of 3D growth assays were measured by CellTiter-Glo® (Promega) (2.4.4).

## 2.2.4 Inhibitor treatment

### 2.2.4.1 PP2, saracatinib, selumetinib, verteporfin and BTYNB

The activity of different signaling molecules was reversibly reduced with the usage of the respective small molecule inhibitors in cell culture and corresponding effects were analyzed in a variety of assays for indicated time.

Initially, PP2 (Sigma Aldrich; Cat#P0042) served as inhibitor for SRC phosphorylation by competing for the binding site of ATP in the SRC kinase resulting in inhibited SRC activity. For efficient inhibition, the manufacturer's recommended IC<sub>50</sub>-concentration of 100 nM was used.

Further studies were performed with saracatinib (Selleckchem; Cat#S1006), a more potent SRC inhibitor, that is already in clinical trials (ClinicalTrials.gov Identifiers: NCT01196741; NCT00610714; (McNeish et al., 2014). Aside, MEK activity was highly and selectively inhibited by selumetinib (Selleckchem; Cat#S1008) with current clinical application (ClinicalTrials.gov Identifiers: NCT00551070; NCT03162627). Without clinical consideration in cancer therapy yet, the small molecule inhibitor verteporfin (Selleckchem; Cat#S1786) was applied to interfere with the TEAD-YAP1 association while BTYNB (Biomol; Cat#Cay25623) was used to selectively inhibit IGF2BP1 function (Mahapatra et al., 2017). For all investigated inhibitors, EC<sub>50</sub>-concentrations in 2D or 3D were measured in advance. Therefore, 2x10<sup>3</sup> cells were seeded in a 96-well flat bottom plate (2D) or 1x10<sup>3</sup> cells in an ultra-low attachment round bottom plate (3D) and 12 different inhibitor concentrations were added. After three days in total, overall cell confluency was monitored as well as viable cells were determined by the luminescence-based reagent CellTiter-Glo® (Promega) (2.4.4) and EC<sub>50</sub>-concentration were calculated with the sigmoidal, 4PL-fit by GraphPad Prism software 9.2.0. For normalization, cell confluency of day 1 or luminescence quantification of seeded cells served as input control.

### 2.2.4.2 Emetine and actinomycin D

Emetine is known to block protein biosynthesis by binding to the 40S ribosomal subunit while actinomycin D inhibits DNA transcription. To study protein and RNA turnover, 2.5x10<sup>5</sup> cells were seeded in 6-wells 24 h after siRNA transfection, cultivated for 48 h and finally treated with 100 µM emetine (Sigma Aldrich) or 5 µM actinomycin D (Sigma Aldrich) for



indicated time points. Alterations in protein and mRNA abundance upon treatment were then determined by Western blotting or qRT-PCR.

### 2.2.5 Protein labeling for translational monitoring

Analysis of density-dependent differences in translation required labeling of the total amount of newly synthesized proteins. Therefore, cells were seeded in different densities,  $2 \times 10^5$  and  $6 \times 10^5$  cells per 6-well, and cultivated for 48 h. Afterwards, normal growth medium was replaced by methionine-free medium for 30 min and 50  $\mu$ M methionine analog Click-iT® AHA (L-azidohomoalaine; Thermo Fisher) was added for 2 h. Subsequently, incorporated AHA in newly synthesized proteins were labelled with Biotin by the Click-iT® Biotin Protein Analysis Detection Kit (Thermo Fisher) and further analyzed by Western blotting (2.4.1).

### 2.2.6 Establishment of CRISPR-Cas9 cell clones

For CRISPR-(clustered regularly interspaced short palindromic repeats)-Cas9-mediated knockout cell clones or complete deletion of 3'UTRs, two sgRNAs were designed including a PAM motif (NGG) and 20 nucleotides complementary to a genomic region downstream and upstream of the target sequence. After hybridization of ordered oligonucleotides, annealed sgRNAs were cloned into the psg-RFP vector via BbsI (2.3.1). Simultaneous transfection of overall 0.5  $\mu$ g sgRNA containing and 0.5  $\mu$ g Cas-9 coding plasmids to  $3 \times 10^5$  cells in a 12-well cavity was performed with Lipofectamine 3000 according to manufacturer's instructions. Single cell sorting with the flow cytometer BD FACS Melody served for selection of GFP- and RFP-double positive cells 48 h post transfection. Co-expression of RFP (sgRNA containing plasmid) and GFP (Cas9-coding plasmid) indicated effective transfection of both plasmids. To avoid cell contamination of single cell clones, normal growth medium was supplemented with 1 % penicillin-streptomycin and 0.1 % tetracycline. Approximately 3 weeks after sorting, CRISPR-Cas9-mediated deletions were tested by PCR of genomic DNA from single cell clones (2.3.2) with Q5 Hot Start High-Fidelity DNA Polymerase master mix (New England Biolabs) according to manufacturer's instructions. Different oligonucleotides were designed to verify 3'UTR deletion via a genomic PCR (gPCR) (Table 10). Therefore, one oligonucleotide pair (Table 10 s2 and as) bound outside the target 3'UTR and amplified the whole 3'UTR if present. In case of a deletion of the target 3'UTR a small PCR product was amplified. For the second oligonucleotide pair the same antisense oligonucleotide was used while the sense oligonucleotide was created to bind within the 3'UTR. Consequently, if the 3'UTR is present, a small product was amplified with the second oligonucleotide pair (Table 10 s1 and as) while a deletion of the target 3'UTR results in no product amplification. Amplified product length and appearance were evaluated by 1 % agarose gel electrophoresis analog to 2.3.1.

After successful testing, Sanger sequencing of 200 µg genomic DNA with corresponding oligonucleotides used in gPCR verified tested cell clones (Table 10).

### **2.2.7 Lentiviral transduction**

Over-expression of several wild type or mutant proteins was established by cloning the coding sequence into the pLVX vector (Table 5, Table 6) as described in 2.3.1. Permanent DNA transfer into the cells was accomplished by lentiviruses. For production of lentiviral particles, HEK293T cells were transfected with plasmids expressing viral envelope proteins (pMD2G), packaging proteins (psPAX2), Tet repressor protein (pCW57.1) and the plasmids encoding the GFP-fused protein of interest (pLVX). Over-expression of GFP alone served as a positive control. In a 6 cm cell culture plate  $3 \times 10^6$  cells were seeded 24 h prior transfection of 4 µg pLVX, 3 µg psPAX2, 1.2 µg pMD2G with Lipofectamine 3000 according to manufacturer's instructions. The virus containing growth medium was harvested 24 h and 48 h after transfection. Subsequently, virus was titrated to calculate optimal infection rate by adding four different virus concentrations to  $5 \times 10^4$  HEK293T cells in a 24-well plate and measuring infection rate via the fluorescence of the over-expressed target protein by the flow cytometer MACSQuant® Analyzer 9. Lentiviral transduction was carried out with  $5 \times 10^4$  cells and the appropriate amount of virus in 500 µL growth medium in a 24-well plate for 48 h. Finally, cells were washed four times with PBS and sorted for GFP-positive cells with the BD FACS Melody. For 3 passages, sorted cells were supplemented with 1 % penicillin-streptomycin and 0.1 % tetracycline to avoid bacterial contamination upon sorting.

## **2.3 Molecular biological methods**

### **2.3.1 Cloning**

The generation of plasmids followed two standardized cloning strategies, direct insertion of annealed oligonucleotides into target vectors or insertion of template-amplified PCR products into a cloning vector with further subcloning into target vectors.

The former strategy was used to establish sgRNA plasmids, reporter plasmids with binding elements as Nluc or protein motif containing plasmids. Annealing was performed with 5 µL of each oligonucleotide (Table 6) exhibiting sticky ends with restrictions sites and 10 µL water. Starting with an incubation at 95 °C for 5 min, proceeded with 65 °C for 5 min and finally cooled down to room temperature to allow optimal hybridization. Hybridized oligonucleotides were further ligated into the target vector. Therefore, 3 µg target vector was digested with 1 µL of each restriction enzymes corresponding to restriction sites of the oligonucleotides (Table 6) with 10x Cutsmart™ buffer (NEB) and separated by agarose gel electrophoresis. Using 1 % agarose gels (pegGOLD Universal Agarose, peglab) with ethidium bromide, samples were running with 6x Gel Loading Dye Orange (NEB) and

Quick-Load® 2-Log DNA Ladder (NEB) in TAE buffer at 120 V. Separated DNA fragments were visualized by UV light, extracted and purified with Wizard SV Gel and Clean-Up System (Promega). Ligation was realized with 2.5 µg of the respective vector, 7.5 µg insert in total, 0.8 µL T4 ligase (1 U/µL, Roche, Cat#10716359001) and 1.2 µL corresponding 10X ligase buffer for 1 h. After a 20 min incubation step of the ligated plasmid with the bacteria strain *Escherichia coli* TOP10, transformation was carried out with a heat shock at 42 °C for 50 sec followed by 2 min on ice. Subsequently, bacteria were cultivated in 800 µL LB medium at 37 °C for 1 h. For the selection of positive colonies, bacteria were plated on LB-agar plates containing either 100 mg/mL Ampicillin or 50 mg/mL Kanamycin and incubated at 37 °C overnight. Verified positive clones by PCR were further cultivated in liquid LB medium with the respective antibiotics (30 µg/mL Kanamycin or 150 µg/mL Ampicillin) at 37° C overnight to subsequently isolate DNA of the cloned plasmids from these liquid cultures with the QIAprep® Spin Miniprep Kit (250) or QIAGEN Plasmid Midi Kit (100). For verification of correct insertion, generated plasmids were sequenced from Eurofins Genomics GmbH.

The latter cloning strategy was applied to generate plasmids for protein over-expression or cloning entire 3'UTRs into reporter plasmids. Therefore, the target sequence was amplified by PCR with Phusion® High-Fidelity PCR Kit (DNA Polymerase 2 U/µL; NEB) with 0.5 µg genomic DNA or cDNA as template in a total volume of 25 µL. Appropriate oligonucleotides for PCR were flanked by restriction sites (Table 6). Amplified products were size separated by agarose gel electrophoresis and purified with the with Wizard SV Gel and Clean-Up System (Promega) as mentioned above. Purified PCR products were inserted into the pCR blunt vector using Zero Blunt® PCR Cloning Kit (Thermo Fisher) following the manufacturer's protocol. After ligation, bacterial transformation, bacteria cultivation on agar plates, selection and verification of positive clones by PCR, subsequent liquid cultures, plasmid isolation and Sanger sequencing for correct insertion were carried out as described above. The cloned plasmid was further digested using the indicated restriction sites to cut off the inserted fragment, purify it by agarose gel electrophoresis and sub-clone it into the target vector following the same protocol of ligation, bacterial transformation, bacteria cultivation, selection and verification of positive clones and plasmid isolation of subsequent liquid bacteria cultures.

Detailed cloning strategies for respective generated plasmids can be retained from listed, commercial vectors (Table 5) and used oligonucleotide sequences with indicated restriction sites (Table 6, Table 9).

### 2.3.2 Isolation of genomic DNA

For the isolation of genomic DNA, cells of a 6-well plate were lysed with 500 µL total lysis buffer (Table 12) and 5 µL proteinase K (NEB, Cat# P8107) and incubated for 1 h at

55 °C. Precipitation of genomic DNA was accomplished by adding isopropanol. Precipitated DNA was washed twice with 80 % ethanol, centrifuged at 14800 rpm for 5 min, dried and resuspended in approximately 70 µL nuclease-free water. Concentration was measured by nanodrop system with Tecan Infinite 2000 spectrometer. Isolated DNA was analyzed by PCR followed by 1 % agarose gel electrophoresis and by Sanger sequencing described in 2.2.6.

### 2.3.3 RNA isolation

Total RNA was extracted with Trizol (Table 12). In detail, a confluent 6-well plate was harvested in 1 mL Trizol and phase separation was accomplished by adding 200 µL chloroform followed by centrifugation at 1300 rpm for 10 min at 4 °C. RNA from the aqueous phase was precipitated with 500 µL isopropanol at room temperature for 30 min in a fresh tube. Pelleted RNA, 14800 rpm at 4 °C for 10 min, was washed twice in 80 % ethanol, dried and resuspended in 20 µL nuclease-free water. Determination of RNA quality and concentration were realized by Tecan Infinite 2000 spectrometer. Isolated RNA served for reverse transcription combined with qRT-PCR.

### 2.3.4 Reverse transcription & quantitative real-time PCR (qRT-PCR)

From 2 µg isolated RNA cDNA was synthesized based on random priming or dT priming for RNA decay studies. Initially, denaturation and annealing of RT primers were performed at 65 °C for 5 min and cool down to 4 °C. A master mix consisting of 4 µl 5x M-MLV Reverse Transcriptase buffer (Promega), 1 µl dNTPs (10mM) und 0.5 µl M-MLV Reverse Transcriptase (Promega, Cat# M1701, 200U/µL) was added to the denature RNA. Reverse transcription was carried out in a 3-step protocol: primer elongation at increasing temperatures from 20 °C to 25 °C to 30 °C every 5 min, reverse transcription at 42 °C for 1 h followed by transcriptase inactivation at 75 °C for 15 min.

Changes in RNA abundance of a variety of cellular studies including RNA turnover was precisely determined by qRT-PCR (quantitative real-time polymerase chain reaction) with SYBRgreen technology on a LightCycler 480 II (Roche) using a 384-well plate. Equal amounts of ORA qPCR Green ROX L Mix (HighQu) with 0.2 µM of each oligonucleotide were mixed with transcribed and diluted (1:10) RNA in a total volume of 5 µL. Oligonucleotides were designed with Primer-BLAST from NCBI (National Center for Biotechnology Information) to amplify the gene of interest spanning exon-exon borders. PCR reaction started with initial activation of polymerase at 95 °C for 5 min, followed by 50 cycles of denaturation at 95 °C for 10 sec, oligonucleotide annealing at 60 °C for 10 sec, elongation at 72 °C for 20 sec and ended up with a melting curve from 55 °C – 95 °C to evaluate specificity of amplified products. During amplification the SYBRgreen fluorescent dye intercalated into newly synthesized double-stranded DNA and fluorescence was

quantified. The second derivative maximum was used to determine the cycle of quantification ( $C_g$ ). Calculations, based on  $\Delta C_g$ - or the  $\Delta\Delta C_g$ - method (Livak and Schmittgen, 2001), reflected changes in RNA abundance relative to one or two different control parameters, as it is pointed out in the following formula. In this study, endogenous RNA transcripts (RPLP0, GAPDH, HIST1H2AC, HIST2H3A) and control populations served for normalization (Table 7).

Formula for  $\Delta\Delta C_g$  analysis:

$$\text{relative mRNA level} = 2^{(-((C_{gX}-C_{tN})_{\text{population}} - ((C_{gX}-C_{gN})_{\text{control population}})))}$$

$X$  – target transcript  
 $N$  – transcript for normalization

### 2.3.5 RNA-co-immunoprecipitation (RIP)

This approach investigates associations between a target protein and the bound RNAs. Confluent 10 cm cell culture plates were harvested, cell number was adapted to the lowest concentration, cells were lysed in 700  $\mu\text{L}$  1x lysis buffer (Table 12) containing 0.5 % NP-40 one ice for 10 min and centrifuged at 14800 rpm for 10 min to pellet cell debris. At the same time, Dynabeads® Protein G (Thermo Fisher, Cat#10004D) were incubated with 4  $\mu\text{L}$  GFP antibody for 10 min. For immunoprecipitation of the target protein, 500  $\mu\text{L}$  supernatant were added to 15  $\mu\text{L}$  GFP-coupled Dynabeads® Protein G and rotated for 30 min. The respective cell lysate served as input control for normalization. After 3 washing steps with 1x lysis buffer with 0.5 % NP-40 protein-RNA complexes were eluted in 100  $\mu\text{L}$  lysis buffer containing 1 % SDS at 65 °C for 5 min. One fifth of the pulldown elute was directly used to verify pulldown efficiency by Western blotting with respect to the respective input controls. For the remaining four fifth total RNA was isolated by the addition of 1 mL Trizol followed by an RNA purification described before (2.3.3). Transcript specific co-purification of putative target mRNAs was measured by qRT-PCR (2.3.4) in respect to input and control pulldown samples, both used for normalization.

## 2.4 Protein-biochemical methods

### 2.4.1 Protein extraction, SDS-PAGE and Western Blot

For analysis of protein abundance or protein turnover, cells were harvested with a rubber policeman to minimize degradation of transmembrane proteins 48 h after seeding an over-expression or 72 h after a siRNA transfection. Addition of phosphatase inhibitors (Sigma Aldrich, Cat#P0044 and Cat# P5726) was accessed whenever the phosphorylation status of proteins was analyzed. Total protein was extracted from pelleted cells with total lysis buffer for 10 min (Table 12) supplemented with 0.5 % Benzodase (Merck Millipore,

Cat#70746) to digest genomic DNA. Protein concentration was determined with the Lowry-based colorimetric DC Protein Assay (BioRad) measuring absorbance at 650 nm with GloMax® 96 well Microplate Luminometer (Promega). Equal amounts of protein extracts were mixed with 4x NuPAGE® LDS sample buffer (Thermo Fisher) and denatured at 65 °C for 10 min. Size separation of proteins on a NuPAGE® Novex® 4-12% Bis-Tris protein gel (Thermo Fisher) was performed with the corresponding NuPAGE® MOPS SDS running buffer based on SDS polyacrylamide gel electrophoresis (SDS-PAGE). Western blotting by a wet tank system transferred separated proteins onto a nitrocellulose membrane (Amersham Bioscience) using NUPAGE blotting buffer with 10 % methanol. Protein transfer was evaluated by Ponceau staining followed by blocking with 10 % milk in PBST or 5 % BSA (bovine serum albumin) in PBST for phosphorylated proteins. Protein abundance was detected using respective primary antibodies and fluorescence-labelled secondary antibodies (Table 3, Table 4). Fluorescence intensities were visualized at 680 nm or 800 nm with the Odyssey Infrared Imaging System (LI-COR) and quantified via the Image Studio™ Software (LI-COR) with respect to the loading control and control sample.

#### **2.4.2 Pull-down of active GTPases**

To monitor the activity of the GTPase RAC1, GTP-bound RAC1 was pulled and its abundance was subsequently analyzed by Western blot similarly to the here reported experiment (Wolf et al., 2006). For the pull-down cultured cells were harvested with a cell scraper and lysed in MLB (Table 12) while constantly working under ice-cold conditions. After removing cell debris by centrifugation at 14,000xg for 5 min, 20 µL of 0.5 M EDTA was added to 500 µL cell extract. For the generation of a positive control, 500 µL cell extract was substituted with 5 µL of 100XGTPyS resulting in a final concentration of 100 µM GTP while the negative control was mixed up to 1 mM GDP content. Controls were incubated for 30 min at 30 °C under brief agitation and reaction was stopped by adding 32 µL of 1 M MgCl<sub>2</sub> (60 mM final concentration) under ice-cold conditions. The pull-down of RAC1 was performed by incubating the cell extracts with 40 µL agarose beads, exhibiting the GTPase protein binding domain of the GEF TIAM1, for 45 min at 4 °C, followed by pelleting the beads by brief centrifugation for 10 sec and washing the beads three times with MLB. Bound RAC1 was released by adding 40 µL 2x Laemmli sample buffer and boiling it for 5 min. Addition of 2 µL dithiothreitol prior boiling improves the release from the beads. The abundance of released RAC1 was analyzed by Western blot.

#### **2.4.3 Transcriptional monitoring with CLICK chemistry**

Investigation of density-dependent changes in total translation rate was accomplished by labelling newly synthesized proteins with a methionine analog (2.2.5) and then covalently linking it with biotin for detection. Using Click-iT® Biotin Protein Analysis Detection Kit

(Thermo Fisher) total protein was commonly extracted from AHA-treated cells and Cu<sup>2+</sup> ion catalyzed biotinylation reaction was performed with 25 µL protein extract (3-4 µg/µL). Covalently labelled proteins were separated by SDS-PAGE, transferred by Western blotting and visualized with IRDye® 800CW Streptavidin (LI-COR) using Odyssey Infrared Imaging System (LI-COR). Total newly synthesized protein amount was quantified with corresponding software and normalized to total protein amount of ponceau staining as well as VCL and ACTB.

#### **2.4.4 Luminescence-based cell viability assay**

Luminescence-based measurements were performed determining viable cells by CellTiter-Glo® Luminescent Cell Viability Assay (Promega). Cell viability of 3D growth assays (2.2.3) and EC<sub>50</sub>-calculations (2.2.4.1) were analyzed by adding 50 µL reagent to a rest volume of 100 µL of growth medium per 96-well. After a 10 min incubation step, 100 µL lysate was transferred into white GloMax® 96-well microplate (Brand) and luminescence was monitored with the GloMax® (Promega) based on the ATP level. The luciferase thereby catalyzed the oxidation of luciferin using the cellular ATP and resulting in light emission. Consequently, the measured emitted light is proportional to the ATP concentration and thus to the number of living cells. For normalization, luminescence quantification of seeded cells served as input.

#### **2.4.5 Luminescence-based reporter assays**

Reporter activity was investigated by luminescence-based measurements in a biological system using Dual-Glo® or Nano-Glo® Luciferase Assay System. Reporter activity reflecting binding of 3'UTRs (pmirGLO, pLenti-YAP1-3'UTR-Luc with pRL) was assessed by Dual-Glo® system. Besides, transcriptional activity correlating with responsive promoter driven luciferase expression (pNL3.1 with pGL4.54) was reported by Nano-Glo® system. Depending on expressed luciferase, Dual-Glo® system recognizes firefly and renilla luciferases while Nano-Glo® system monitored NanoLuc® and firefly luciferases. The latter ones served for normalization of the reporter signal next to control plasmids or control populations. Luminescence measurement of firefly luciferase was performed by adding an amount of Dual-Glo®/Nano-Glo® reagent equal to volume of growth medium to cells followed by a 10 min incubation and transferring 50 µL to white GloMax® 96-well microplate (Promega) in duplicates. Afterwards, 50 µL Dual-Glo®/Nano-Glo® Stop&Glo® buffer containing corresponding Stop&Glo® substrate (1:100) was added to monitor renilla/NanoLuc® luminescence 10 min later.

### 2.4.6 Quantitative proteomics

Quantitative proteomics were carried out by Dr. Nadine Bley and Dr. Christian Ihling according to the previously described protocol (Bley et al., 2021).

## 2.5 Microscopy

### 2.5.1 Bright field microscopy

Bright field imaging served to visualize cell morphology using a Nikon TE-2000-E microscope with a 20x objective and phase contrast. Representative images are shown.

### 2.5.2 Fluorescence microscopy with CLSM technique

Localization of different proteins and intercellular interactions were investigated by confocal laser scanning microscopy (CLSM) including immunofluorescence staining of fixated cells, visualization by microscopy and quantification of intensities by ImageJ.

All cells were cultured for 48 h on cover slips which were prior incubated in 40 % (v/v) ethanol and 60 % (v/v) hydrochloric acid. After cultivation, cells were fixed with 4 % PFA/PBS solution (Sigma Aldrich, Cat#HT5012-1CS) for 1 h and permeabilized with 0.5 % (v/v) Triton X-100 in PBS for 5 min. Unspecific binding was blocked with 1 % BSA in PBS for 30 min. Sequential incubation of primary (1:50 – 1:200) and secondary fluorophore-linked antibodies (1:500) (Table 3, Table 4) as well as Phalloidin-TRITC (tetramethyl rhodamine B isothiocyanate; Sigma Aldrich, Cat# P1951) was performed in blocking solution, each for 1 h with two washing steps in between. Staining of nuclei was realized using DAPI (4',6-diaminidino-2-phenylindole; 1:10000) in PBS for 5 min. Cover slips were washed in water and dehydrated by adding > 99 % ethanol and mounted with ProLong™ Diamond Antifade Mountant (Thermo Fisher, Cat# P36970).

Imaging was performed with the Leica SP5X or SP8X confocal microscopes using a 63x oil objective. Fluorophores were excited with a white light laser while DAPI was excited with a diode laser (405 nm), emitted fluorescence was exposed to HyD detectors. Sequential images were acquired with standardized settings.

Image analysis via ImageJ was applied to compare cellular to transmembrane protein localization as previously described (Rietscher et al., 2018). Therefore, ratios of grey value intensities from 15 different intercellular connections of three independent images were calculated.

### 2.5.3 Live-cell imaging via Incucyte S3

To monitor 3D growth and invasion, bright field and fluorescence images were taken by the Incucyte S3 device after certain time intervals choosing from 4x, 10x or 20x



objectives. Image analysis including spheroid segmentation for 3D experiments and confluence masks for 2D studies was carried out by the Incucyte software. Representative images are shown.

## 2.6 Mouse Xenograft studies and Ethics Approvals

The local ethical review committee of the Martin Luther University Halle-Wittenberg granted permission for the mouse xenograft studies and animals were handled according to their guidelines. The immunodeficient athymic nude mice (FOXN1<sup>nu/nu</sup>) were obtained from Charles River. GFP or GFP-IGF2BP1 over-expressing ES-2 cells labelled with iRFP were pre-treated with 3  $\mu$ M saracatinib and 3  $\mu$ M selumetinib or DMSO for 48 h. Subsequent  $7.5 \times 10^4$  living cells (determined by Trypan Blue counting) suspended in 50 % Matrigel (Sigma Aldrich) and 50 % FBS-free DMEM and further supplemented with the inhibitors at the previous concentrations were injected intraperitoneal (IP) into six-week-old, female nude mice having five mice per condition. Tumor growth of isoflurane-anaesthetized mice was monitored weekly by near-infrared imaging with the Pearl imager (LI-COR) and quantified with the Image Studio software (LI-COR). Mice were sacrificed when tumor size reached termination criteria after 2 weeks. Animal handling and experiments were carried out by Simon Müller with assistance of Tommy Fuchs.

## 2.7 Data analysis

### 2.7.1 NGS analysis

Different RNA sequencing data obtained from several platforms including TCGA (The Cancer Genome Atlas) with 374 ovarian serous cystadenocarcinomas from the GDC portal (<http://portal.gdc.cancer.gov>), 133 normal ovary tissue samples from the GTEx portal (The Genotype-Tissue Expression; [gtexportal.org](http://gtexportal.org)) and CCLE with 45 ovarian cancer cell lines (Cancer Cell Line Encyclopedia; <http://portals.broadinstitute.org/ccle>) from the Broad Institute. Genes differentially expressed between TCGA cancer tissues and GTEx normal tissues was determined by Dr. Markus Glaß using the R-package edgeR v3.28.0. (Robinson et al., 2010) applying TMM normalization on raw count data. RNA expression values were obtained as CPM (counts per million mapped reads) values.

High and low IGF2BP1-expressing groups of the TCGA data were separated by the value of 5 RSEM (RNA-seq by expectation maximization) which approximately corresponds to the 3. quartile. Cell line expression data was downloaded as TPM (transcripts per million mapped reads) from the CCLE, and mutational data was obtained via the R-package depmap v1.0.0 (<http://depmap.org>).

Total RNA sequencing of IGF2BP1-3-depleted versus control ES-2 cells was prepared

by Dr. Nadine Bley and performed by Dr. Knut Krohn (IKFZ Leipzig, Germany; GEO: GSE109604) as well as conducted through Simon Müller and Dr. Andreas Dahl (NGS Facility University of Dresden, Germany; GEO: GSE116059) and analyzed by Dr. Danny Misiak and Dr. Markus Glaß. Therefore, Cutadapt was used to clip remaining sequencing adapters, TopHat2 to map reads to the human genome (UCSC GRCh37/hg19) R-package edgeR v3.28.0. (Robinson et al., 2010) to calculate differential gene expression applying TMM normalization on raw count data. RNA expression values were obtained as FPKM (fragments per kilobase million mapped reads) values.

### 2.7.2 Functional enrichment analysis

Gene set enrichment analysis using pre-ranked data were performed with the GSEA v4.0.3 software selecting either the Hallmark or the KEGG pathways gene sets from MSigDB (Liberzon et al., 2015). A permutation number of 1000 was applied, and classical enrichment statistics were elected. Gene annotation enrichment analyses (GAEA) were performed using Cytoscape v3.8.0 and the ClueGO plugin v2.5.7. selecting for KEGG pathways. A right-sided hypergeometric enrichment was applied and a cutoff-value for Benjamini-Hochberg corrected p-values of 0.05 was set. A gene set analysis with r2 (<http://r2.amc.nl/>) of positive correlated genes with a single gene was performed by using the KEGG gene set, a cutoff value of 0.05 and displaying over-represented pathways.

### 2.7.3 Patient survival analysis

Associations between patient overall survival and the expression of different genes were generated by using the Kaplan-Meier analysis from KM plotter (<https://kmplot.com/analysis/>) referring to microarray-based data of 1435 patients in total diagnosed with ovarian carcinoma (Gyorffy et al., 2012) including the Australian data set from Tothill et al. (Tothill et al., 2008).

### 2.7.4 CLIP analysis

Publicly available data of enriched CLIP hits for the proteins IGF2BP1-3 were obtained from ENCODE (<http://www.encodeproject.org/>; identifiers: ENCFF486BXN, ENCFF976DBP, ENCFF435MEM, ENCFF701YCW) and GEO (Gene Expression Omnibus; <http://www.ncbi.nlm.nih.gov/geo/>; identifiers: GSM2071742 and GSM2071745) consisting of PAR-CLIP, eCLIP and iCLIP studies (Conway et al., 2016; Degrauwe et al., 2016a; Hafner et al., 2010; Van Nostrand et al., 2016) in four different cell lines (HEK293, H9 hESCs, HepG2, K562). Dr. Markus Glaß and Dr. Danny Misiak downloaded and mapped the data to all annotated genes of the human genome (hg19) as previously described (Glass et al., 2021; Muller et al., 2018).

### 2.7.5 miRNA prediction

The prediction of putative miRNA binding site refers to the TargetScan database (<http://TargetScan.org>).

### 2.7.6 Synergy analysis

Synergy of different drug combinations was assessed with the SynergyFinder (<https://synergyfinder.fimm.fi/>) using a drug matrix where each drug varied in concentration. The recommended four-parameter logistic regression (LL4) for sigmoid curves was chosen as algorithm for curve fitting. Synergy scores were calculated based on different models: HSA, Bliss and ZIP. Each model compares responses of a measured response to an expected reference response. The reference models therefore assume no combinatorial effect between the drugs. The HSA (highest single agent) model expects a combination response which is equivalent to the maximum of the single drugs. The Bliss independence model refers to the basis of independent acting drugs and their individual response can be multiplied for their maximum combination effect. The ZIP (zero interaction potency) model compares potency between drug combination with the assumption that non-interacting drugs do not influence the potency of each other. The synergy score assumes synergy above 10, antagonism below -10 and additivity between -10 and 10.

## 2.8 Statistics

All experiments were performed at minimum in three independent, biological replicates unless otherwise stated. Statistical significance was tested by Student's *t*-test or Mann-Whitney Rank-Sum test depending on data distribution and is indicated in the diagrams as followed: \*  $p < 0.05$ ; \*\*  $p < 0.01$ ; \*\*\*  $p < 0.001$ .

## 3 RESULTS

### 3.1 The mesenchymal force of the proto-oncogenic mRNA binding protein IGF2BP1 in epithelial ovarian carcinoma

High-grade serous ovarian carcinoma (HGSC) is a complex disease due to its cellular heterogeneity and its rare mutational landscape. To understand this disease in its complexity, a broad view beyond the genomic level and the classical oncogenic factors is needed and different molecular mechanisms for adaption and cancer progression need to be considered. All cellular processes are regulated on various levels as epigenetics, transcription, post-transcriptional basis and translation. Here, the focus is drawn on mRNA binding proteins which are post-transcriptional regulators that can modulate gene expression by controlling a complex network of mRNAs acting in distinct pathways.

A comparison of RNA sequencing data from the TCGA including high-grade serous and endometrioid ovarian tumor samples (TCGA-OV) to normal ovarian tissue data from GTEx was drawn and the 10 most up- and downregulated mRBPs from all cancer-associated mRNA binding proteins reviewed in (Pereira et al., 2017) are highlighted. Interested in proto-oncogenic mRBPs, three of them (LIN28B, IGF2BP3 and IGF2BP1) emerged to exhibit a high deregulation in ovarian carcinoma indicated by fold change (FC; Figure 5A). Taking a closer look, next to the FC and the false discovery rate (FDR), to the hazard ratios (HRs) of these three proteins in the ovarian cancer cohort on KM plotter (Gyorffy et al., 2012), all of them correlate with a poor prognosis. Corresponding HRs for all mRBPs are indicated by bubble size whereat IGF2BP1 appears to be the one with the highest shift in mortality rate (Figure 5B), consistent with previous findings (Busch et al., 2016; Kobel et al., 2007; Muller et al., 2018). The PFS rate of 228 patients with a high IGF2BP1 expression compared to 255 patients with low IGF2BP1 expression was determined with 14.2 months versus 21 months resulting in a significant HR of 1.57 (Figure 5C). The distribution of IGF2BP1 expression is not only raised in ovarian carcinoma compared to normal ovarian tissue, but it also seems to split into two distinct populations within the TCGA ovarian cancer cohort (Figure 5D). Optimal separation of these populations was achieved at around 5 RSEM which almost corresponds to the 3rd quartile. A significant difference in the median expression of these two populations was determined, with a median of 7.2 RSEM in the IGF2BP1-high expressing group and a median of 1.5 RSEM in the IGF2BP1-low expressing group (Figure 5E). Performing a gene set enrichment analysis (GSEA) for the hallmark gene sets with the FCs of these two populations reveals an upregulation of several gene sets including the 'EMT' gene set with a significant normalized enrichment score (NES) of 2.95 (Figure 5F). This fits to the previous association of IGF2BP1 with a mesenchymal shift in cell lines of different entities (Zirkel et al., 2013). In the

regulation of EMT, different signaling pathways play an important role to confer extracellular signals to the transcriptional level. Therefore, an additional GSEA with the KEGG (Kyoto Encyclopedia of Genes and Genomes) gene sets was performed and the NES with the corresponding FDRs of the significant enriched, cancer-associated gene sets are shown (Figure 5G). Moreover, a gene annotation enrichment analysis (GAEA) of significant IGF2BP1-correlated genes and an r2 gene set analysis with positive IGF2BP1-correlated genes of the TCGA-OV cohort with the KEGG gene sets were investigated. Here, the indicated 'significance score' refers to the amount of analysis (GSEA, GAEA, r2 analysis) in which each shown gene set was ranked under the significant gene sets, reaching from 1 to 3, depicted by the bubble size in the diagram (Figure 5G). Next to a high association with the cell cycle gene set, already reported in (Muller et al., 2020), essential IGF2BP1-dependent signaling pathways are the Hippo, WNT and MAPK signaling pathway while the Hedgehog signaling pathway was only enriched in one out of the three analyses. Furthermore, in the GAEA and r2 analyses the DNA repair pathway or Fanconia anemia pathway also seems to play an essential role in ovarian cancer which matches with the genomic instability reported in HGSC tumors. For further details, the ranking of the significant enriched, cancer-associated gene sets of each analysis are displayed separately in the Appendix (Figure 35). Apart from this, the Hippo as well as the WNT pathway are both associated with intercellular adhesion mediated by adherens junctions maintaining an important part in EMT. Moreover, an enrichment of WNT and cadherin signaling in the mesenchymal, IGF2BP1-associated C5 subtype of HGSC tumors was reported (Bley et al., 2021; Tothill et al., 2008).

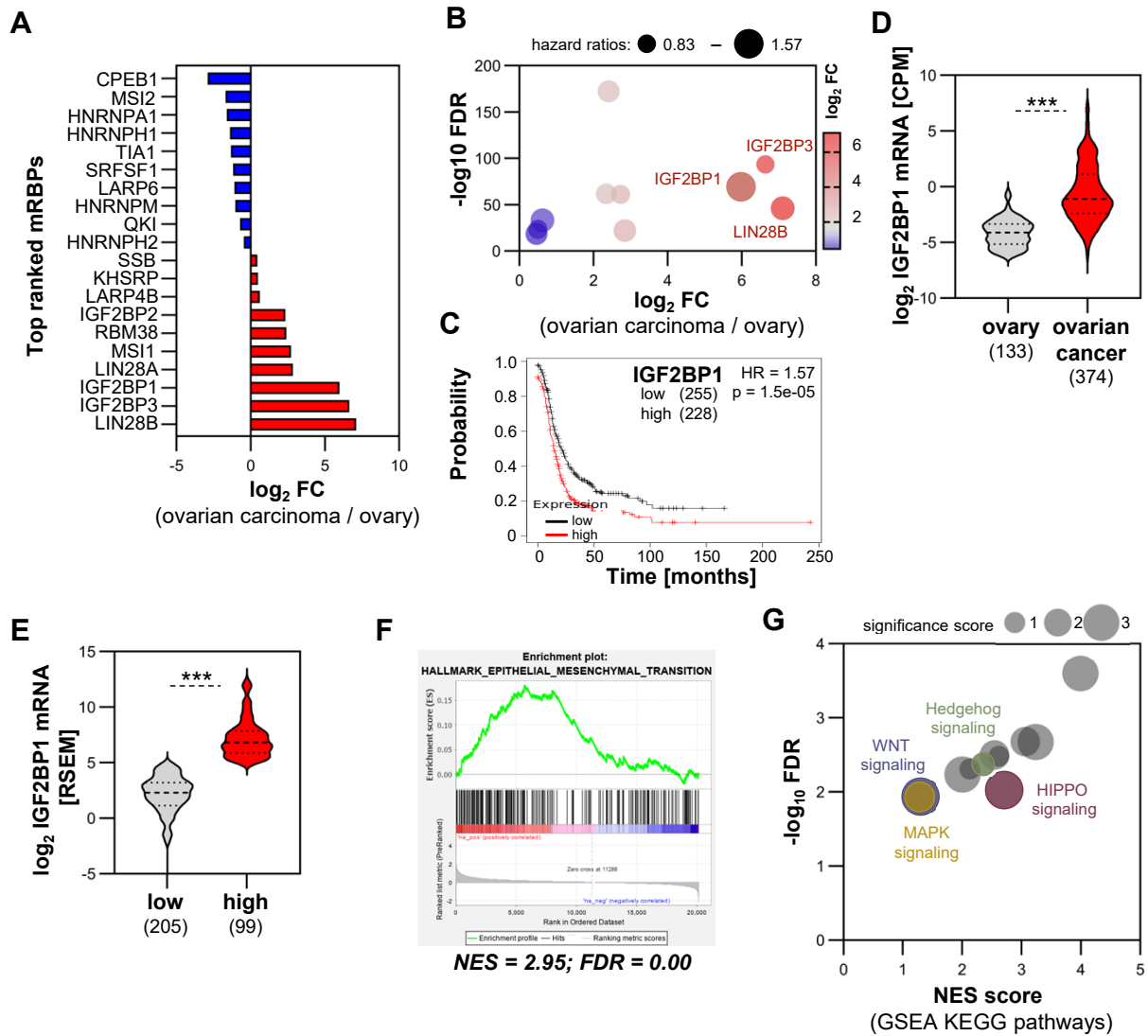


**Figure 5: The proto-oncogenic mRNA binding protein IGF2BP1 suffers from a high re-expression in ovarian carcinoma and is associated with EMT as well as various cancer signaling pathways.** (A) Expression of the cancer-associated mRBPs reported by (Pereira et al., 2017) was analyzed by comparing RNA sequencing data from the TCGA-OV cohort with the GTEx data of normal ovary tissue. The top 10 positive (red) and 10 negative (blue) shifted mRBPs are displayed. (B) FC expression of the top 10 upregulated mRBPs from A with their corresponding FDRs are shown. The bubble size depicts the respective hazard ratios (HRs) of each mRBP in the ovarian cohort from KM plotter. (C) The progression-free survival curve from KM plotter of the mRBP with the highest HR, IGF2BP1, is displayed. The tumor cohort is divided in a low and high IGF2BP1 expressing group containing 255 versus 228 samples. (D) Expression values of IGF2BP1 within normal ovarian tissue from the GTEx data is displayed next to its abundance in the TCGA-OV cohort. (E) The TCGA-OV cohort is splitted into high and low IGF2BP1-expressing tumors (cut-off 5 RSEM). (F) GSEA with pre-ranked log<sub>2</sub>FCs of the IGF2BP1 high expressing group vs. low expressing group from (E) was performed with the hallmark gene sets. The EMT gene set as one of the most significantly upregulated gene sets is shown as enrichment plot. (G) NES scores and the corresponding FDRs of significant cancer-associated KEGG pathways from a GSEA with the FCs between the IGF2BP1 high and low expressing group are displayed. KEGG gene sets, which were additionally significant upregulated in a GSEA with significant IGF2BP1-correlated gene and in an r<sup>2</sup> analysis with positive IGF2BP1-correlated genes of the TCGA-OV cohort, are indicated by bubble size. The ‘significance score’, reaching from one to three, reflects the number of gene ontology analysis that identified the respective gene set as significantly enriched. Statistical significance was assessed by Student’s *t*-test. \*\*\* *p* < 0.001.

Referring to the HGSC histotype, in the next step all ovarian cancer cell lines from CCLE were selected for TP53 mutations, since 97 % of HGSC cells exhibit mutated TP53 (Ahmed et al., 2010; TCGA, 2011), and were ranked for IGF2BP1 expression. Available cell lines are highlighted (Figure 6A). To study the role of IGF2BP1 promoting the mesenchymal

subtype, subsequently, the selected cell lines were classified into epithelial- and mesenchymal-like cell lines by a set of common EMT markers using the CCLE-provided RNA expression data. Thereby, cells were classified as epithelial upon expression of (i) the epithelial cell adhesion molecule EpCAM, (ii) the transmembrane anchor protein of epithelial AJs, E-cadherin (CDH1), (iii) the major structural component of epithelial intermediate filaments, cytokeratin 8 (KRT8) and (iv) the main component of the epithelial basement membrane type I, collagen (COL1A2). Mesenchymal criteria were the expression of (i) the extracellular matrix protein fibronectin (FN1), the classical mesenchymal intermediate filament component vimentin (VIM), (ii) the mesenchymal adherens junction component N-cadherin (CDH2), (iii) the EMT-inducing growth factor TGFBI and (iv) EMT associated transcription factors like TWIST1, ZEB2 or SNAI2. Moreover, a shift within integrin (ITGA and ITGB) expression could also be observed indicating a difference in focal adhesion priming epithelial cells for attachment and mesenchymal cells for migration. In addition, IGF2BP1 expression for each cell line is shown emphasizing its mesenchymal association (Figure 6B). In agreement with Busch et al. (Busch et al., 2016), showing a negative correlation of IGF2BP1 with CDH1 in a panel of pan-cancer cell lines, the IGF2BP1 protein expression exhibits a negative correlation with epithelial proteins CDH1 and KRT8 as well as a positive correlation with the mesenchymal marker proteins CDH2 and VIM (Figure 6C,D). Considering (i) the TP53 mutation status, (ii) the classification as suitable HGSC-model by (Domcke et al., 2013), (iii) its ability to perfectly grow in 3D cultures and (vi) its conspicuously mesenchymal expression pattern, ES-2 cells were selected as a mesenchymal model for further analyses. Accordingly, NIH:OVCAR-3 were chosen as the epithelial counterpart. GSEA was used to substantiate this selection. Therefore, the FC of selected cell lines was determined over all ovarian cancer cell lines in the CCLE-RNA-Seq cohort and used for ranking the expression values. This identified the hallmark gene set 'EMT' as significantly over-represented in ES-2, whereas the majority of genes within this gene set were down-modulated in NIH:OVCAR-3 (Figure 6E,F). This confirms ES-2 and NIH:OVCAR-3 with an unbiased approach as suitable mesenchymal or epithelial cell models, respectively.

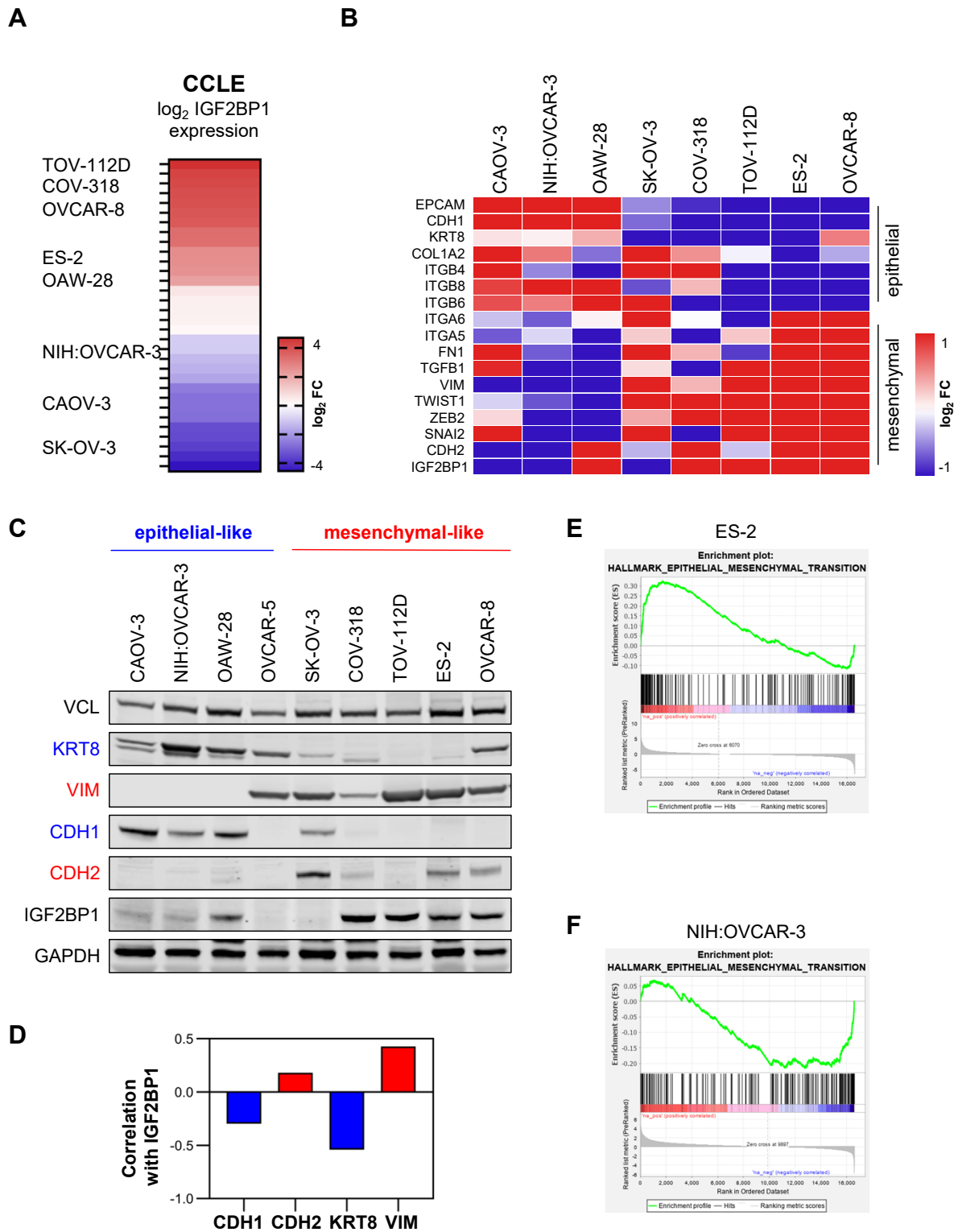


**Figure 6: Epithelial and mesenchymal classification of selected ovarian cancer cell lines.** (A) TP53 mutated ovarian cancer cell lines were selected and ranked by IGF2BP1 expression levels using the CCLC RNA sequencing data. Available cell lines with their corresponding IGF2BP1 expression are indicated as heatmap. (B) Expression of each shown cell line normalized by the median expression of all cell lines of the CCLC ovarian cohort (log<sub>2</sub>FC) is displayed in the heatmap for selected EMT-associated markers and IGF2BP1. (C) Protein expression of mesenchymal (red) and epithelial (blue) markers were recapitulated for the available cell lines next to IGF2BP1 expression by Western blot. VCL and GAPDH served as loading control. (D) Pearson correlation coefficients of IGF2BP1 with indicated mesenchymal marker markers (red) and epithelial markers (blue) from Western blot analyses in (C) are shown. (E,F) GSEA was performed with the median normalized expression values (log<sub>2</sub>FC; calculations according to (B)) based on the CCLC RNA sequencing data of the ES-2 (E) and NIH:OVCAR-3 (F) cell lines. The hallmark EMT is shown as enrichment plot. A positive enrichment (NES > 0) of EMT-associated genes was observed for ES-2, whereas a negative score was obtained for NIH:OVCAR-3.



To further investigate a functional connection of IGF2BP1 to EMT, phenotypical changes and alterations in gene expression were analyzed upon IGF2BP1 depletion. Alterations in morphology and cell-to-cell adhesion were observed by bright field microscopy within IGF2BP1-depleted ES-2 cells compared to a control siRNA-mediated knockdown (Figure 7A). Thereby, the IGF2BP1 depletion induced the formation of cell colonies and switched the usually spindle-shaped ES-2 cells towards a round-shaped morphology. Immunofluorescent imaging on F-actin cytoskeleton indicated that actin stress fibers in control ES-2 cells returned to a cortical actin cytoskeleton upon IGF2BP1 depletion. Likewise, the shape of the intermediate filament system stained by vimentin was re-organized (Figure 7B). Additionally, Western blot analysis revealed a significant reduction of several EMT-TFs when IGF2BP1 was absent after a transient depletion in ES-2 cells (Figure 7C). This indicates an IGF2BP1-dependent alteration in various EMT criteria shifting towards a mesenchymal cell state in the presence of IGF2BP1 which is in agreement with the findings in Zirkel et al. (Zirkel et al., 2013) while using here an alternative and more sophisticated knockdown approach based on a siRNA pool to diminish off-target effects (Hannus et al., 2014).

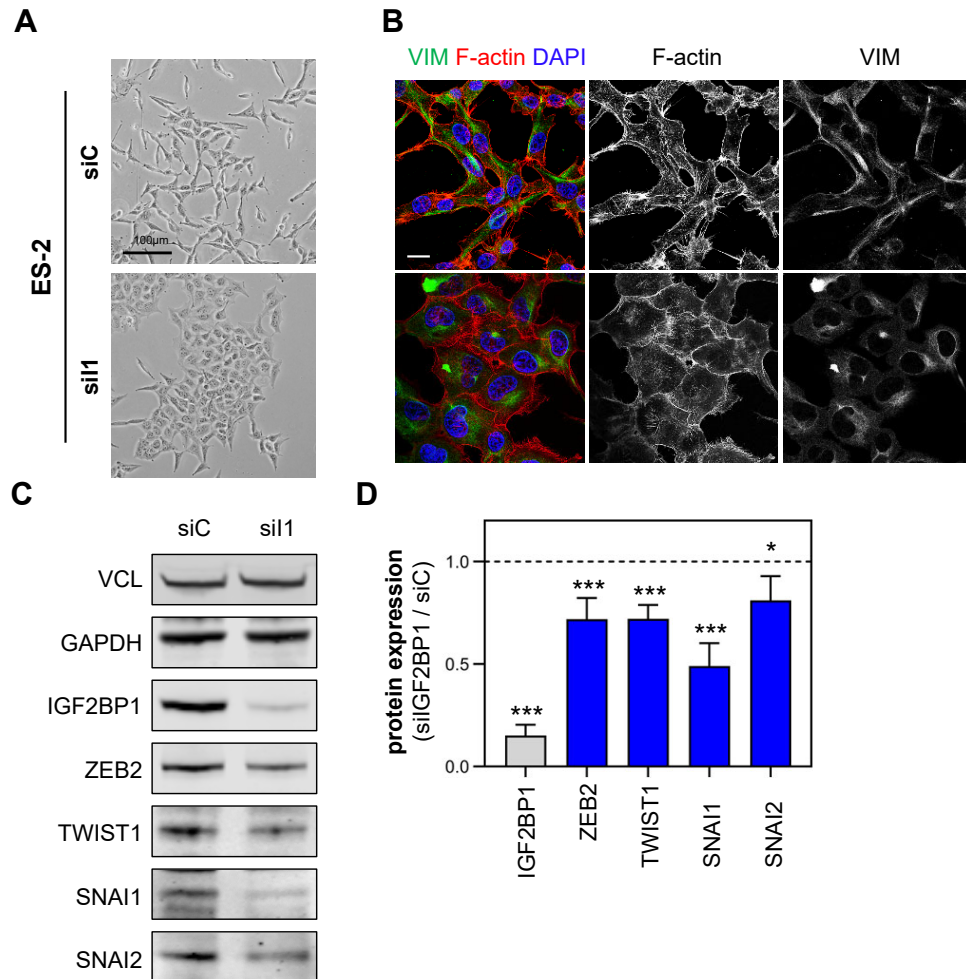


**Figure 7: IGF2BP1 diminishes mesenchymal cell characteristics.** (A) Bright field microscopy imaging shows cell morphology of ES-2 cells upon IGF2BP1 depletion (sil1) compared to control transfected cells (siC). (B) Immunofluorescence staining of Vimentin (VIM) and F-actin using Phalloidin-TRITC in ES-2 cells after an IGF2BP1 (sil1) and control (siC) knockdown were visualized by confocal microscopy. Nuclei are indicated with DAPI. Scale bar is equivalent to 25  $\mu$ m. Merged images and single stainings are shown. (C) Western blotting of indicated EMT-TFs upon IGF2BP1 (sil1) depletion is compared to its control (siC) in ES-2 cells. (D) The quantification of EMT-marker protein levels were determined using VCL and GAPDH as loading control. Error bars indicate standard deviation (SD) of at least three independent experiments. Statistical significance was assessed by Student's *t*-test. \*  $p < 0.05$ ; \*\*\*  $p < 0.001$ .

### 3.2 IGF2BP1 promotes AJ turnover without direct modulation of their mRNAs

EMT is always accompanied by a loss of cell-cell contacts and is of great relevance in ovarian cancer due to its frequent spread to the peritoneal cavity (Bowtell et al., 2015; Dongre and Weinberg, 2019). Focusing on the cell-cell adhesion structures termed adherens junctions (AJs), NGS analysis and quantitative proteomics conducted by Dr. Nadine Bley and Dr. Christian Ihling gave a first hint on the influence of IGF2BP1 on AJs (Bley et al., 2021). These analyses in the mesenchymal ovarian cancer cell line ES-2 revealed an upregulation of several AJ components upon transient IGF2BP1 depletion (Figure 8A). These alterations were mainly observed on protein but not RNA level. Although cells appeared more epithelial upon knockdown, the epithelial cadherin CDH1 was not detectably expressed in ES-2 cells. Unexpectedly, CDH2 and CDH5 expression was

increased. Elevated protein expression in the absence of IGF2BP1 was also monitored for the catenins, CTNNA1 and CTNNB1, while CTNND1 expression was hardly altered. This was validated by Western blot analyses confirming an upregulation of AJ proteins upon IGF2BP1 depletion in ES-2 cells which was already indicated during my master's thesis (Figure 8B). Since the expression of mesenchymal cadherins was increased upon IGF2BP1 depletion with cell phenotypical changes supporting rather epithelial characteristics, we investigated the localization of AJ components upon IGF2BP1 depletion.

Although there was no classical shift in the expression from mesenchymal to epithelial cadherins, imaging of immunofluorescence-labeled CDH2 together with CTNNB1 clearly revealed a restoration of CDH2-positive AJs in the absence of IGF2BP1 in ES-2 cells (Figure 8C) (Bley et al., 2021). CDH2 and CTNNB1 were increasingly recruited to the plasma membrane to build pre-mature, zipper-like cell-cell contacts. Quantification of fluorescence intensities of both proteins at the plasma membrane compared to their cytoplasmic abundance was calculated as described in Rietscher et al. (Rietscher et al., 2018) and reflected the observed alteration of IGF2BP1-dependent AJ protein localization (Figure 8D). To establish stable AJ contact structures, several factors are essential. Notably, CTNND1 serves as a stabilization factor of AJs. Here, it was shown that it localizes to AJ structures and is increasingly recruited to the contact site after IGF2BP1 depletion in ES-2 cells (Figure 8E,F) suggesting to promote the stabilization of the zipper-like contacts.

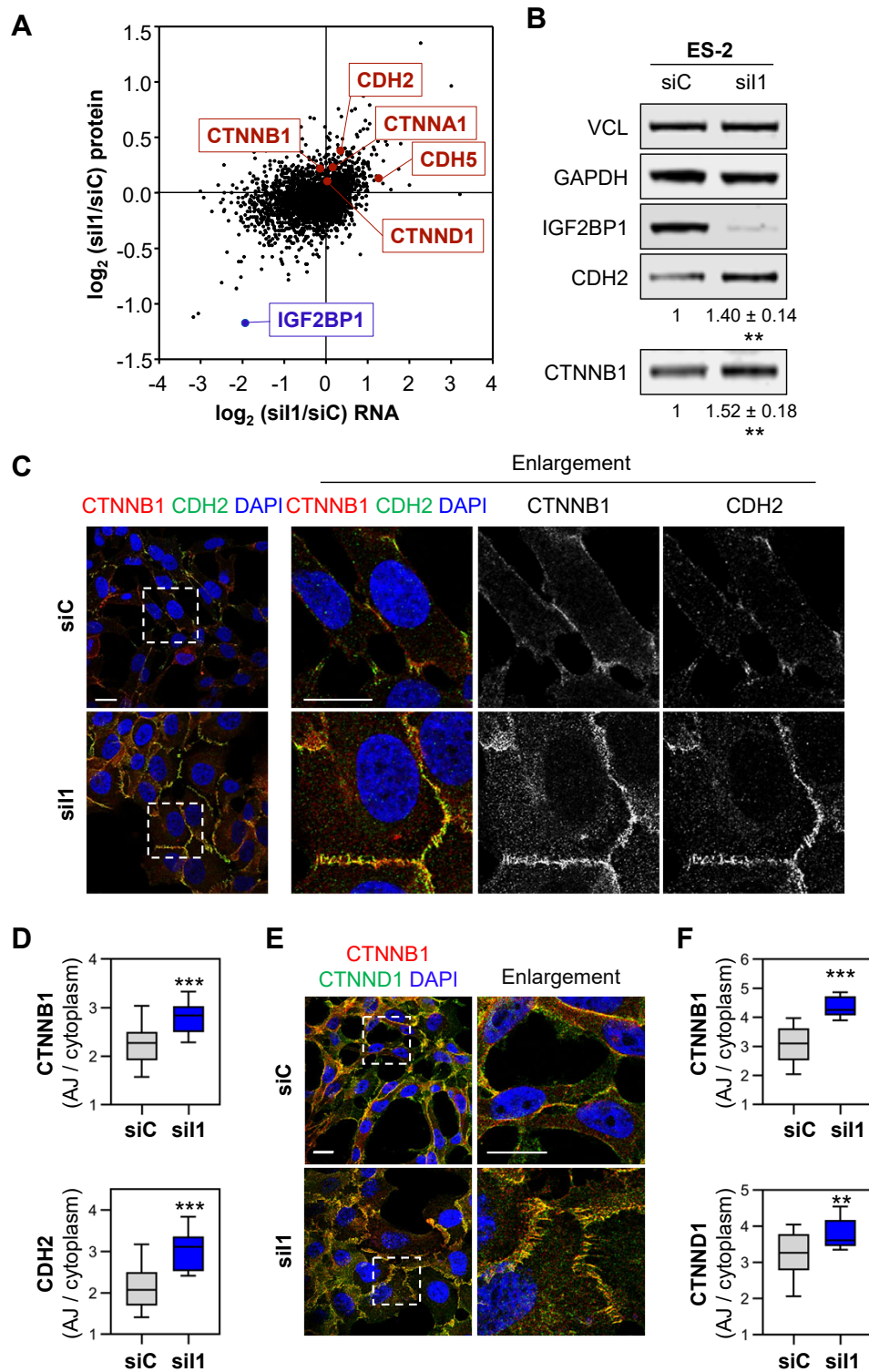


**Figure 8: A transient IGF2BP1 depletion restores AJs in ES-2 cells.** (A) RNA sequencing and quantitative proteomics of an IGF2BP1 depletion (sil1) compared to a control knockdown (siC) in ES-2 cells were performed by Dr. Nadine Bley and Dr. Christian Ihling. Fold changes in expression ( $\log_2FC$ ) of key AJ components are highlighted here next to IGF2BP1. (B) Western blotting of a control (siC) and an IGF2BP1 knockdown (sil1) shows changes of protein abundance of the two main components of AJs, CDH2 and CTNNB1, in ES-2 cells. (C-E) Immunofluorescent staining of CTNNB1 and CDH2 (C) or CTNND1 (E) in control (siC) and IGF2BP1 depleted (sil1) cells visualizes AJ structures while DAPI marks nuclei. Dashed boxes indicate enlarged regions of the following images. Scale bar is equivalent to 25  $\mu$ m. The ratio of CTNNB1, CDH2 or CTNND1 (D or F) localized to the plasma membrane compared to its cytoplasmic abundance was calculated via fluorescence intensities as described under (Rietscher et al., 2018). Data are partially taken from my master's thesis and published in (Bley et al., 2021). Statistical significance was assessed by Student's *t*-test. \*\*  $p < 0.01$ ; \*\*\*  $p < 0.001$ .

The transient effect in subcellular localization of CTNNB1 and CDH2 were confirmed by a CRISPR-Cas9-mediated knockout of IGF2BP1 in ES-2 cells (Figure 9A). Thereby, the stable deletion of IGF2BP1 resulted in the assembly of matured AJs and showed a significantly higher recruitment of the assessed proteins to the plasma membrane (Figure 9B). An over-expression of IGF2BP1 in the mesenchymal ES-2 cell line disassembled the rare contacts present in the wild type cell line as shown during my master's thesis. Especially, the rare mature contact structures turned into more zipper-like, loose connections. (Figure 9C). Quantification confirmed a significantly elevated disassembly of AJ structures (Figure 9D).

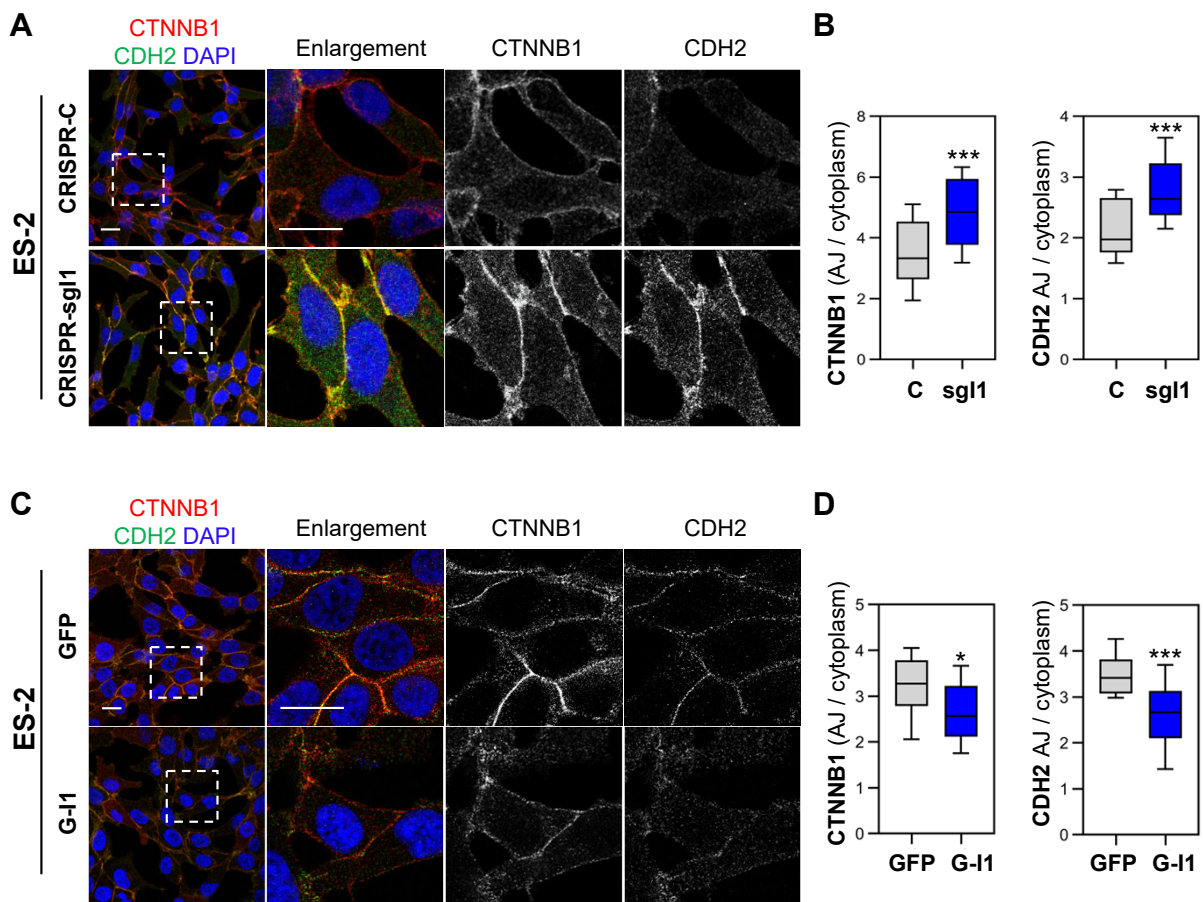


**Figure 9: Formation of matured AJs and its reduction in a stable cell system within ES-2 cells.** (A) Immunofluorescent imaging of CTNNB1 and CDH2 in ES-2 cells with a stable CRISPR-Cas9-mediated knockout of IGF2BP1 (sgl1) compared to control (C) cells. DAPI visualizes nuclei. Scale bar corresponds to 25  $\mu$ m. Dashed boxes depict enlarged regions. (B) Corresponding quantifications of fluorescence intensities display the ratio of the plasma membrane/cytoplasm localization of CTNNB1 and CDH2 in box plots. (C) Immunofluorescent imaging of CTNNB1 and CDH2 in a stable GFP-tagged over-expression of IGF2BP1 (G-11) and GFP-expressing control (GFP) was performed during my master's thesis. DAPI visualizes nuclei. Scale bar corresponds to 25  $\mu$ m. Dashed boxes depict enlarged regions. (D) Box plots show corresponding ratios of plasma membrane/cytoplasm localization of CTNNB1 or CDH2. Statistical significance was assessed by Student's *t*-test. \*  $p < 0.05$ ; \*\*\*  $p < 0.001$ .

The conservation of elevated AJ formation upon IGF2BP1 depletion was analyzed in a set of EOC-derived cell lines (Figure 10). Increased AJs and co-localization of CTNNB1 with the dominantly expressed cadherin of the respective cell line at the plasma membrane was reproducible in four likely HGSC cell lines, NIH:OVCAR-3 (CDH1) as well as OAW28, COV-318 and with fewer contact formation but still AJ induction in TOV-112D cells (CDH2).



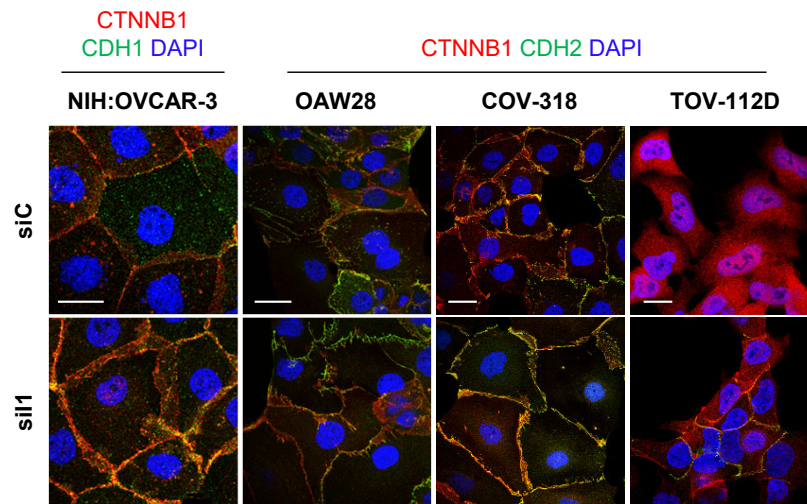


**Figure 10: Conservation of elevated AJs formation upon IGF2BP1 depletion.** Immunofluorescent imaging of CTNNB1 and CDH1 or CDH2, depending on its abundance, in the different indicated ovarian cancer cell lines after an IGF2BP1 (sil1) or control (siC) depletion was performed. DAPI visualizes nuclei. Scale bar corresponds to 25  $\mu$ m.

Conversely, a transient over-expression of IGF2BP1 in the epithelial NIH:OVCAR-3 cells partially disassembled cell colonies and single cells started to disseminate from usually dense clusters revealed by bright field microscopy (Figure 11A). The IGF2BP1 over-expression further led to a significantly increased disassembly of CDH1- and CTNNB1-positive AJs with elevated pre-mature contact structures (Figure 11C,D) accompanied by reduced AJ protein abundance (Figure 11B). With COV-318 cells, the IGF2BP1-induced disassembly of AJs was confirmed in a third EOC-derived cell line (Figure 11E,F).

In conclusion, microscopical imaging demonstrated a negative influence of IGF2BP1 expression on correct AJ protein localization and structure maintenance in a variety of ovarian cancer cell lines. AJ protein abundance was altered IGF2BP1-dependent while RNA levels determined by RNA sequencing were not changed upon IGF2BP1 depletion assuming no direct association of IGF2BP1 with CDH1 or CDH2 and CTNNB1 mRNAs in ES-2 cells. This is in contrast with the reported findings of a direct promotion of CTNNB1 and CDH1 mRNA expression by IGF2BP1 in breast cancer cell lines (Gu et al., 2008). However, the here shown data rather suggests an influence of IGF2BP1 in the early process of AJ assembly due to the zipper-like, pre-mature junctions in the knockdown experiments which are in agreement with Zirkel et al. (Zirkel et al., 2013).

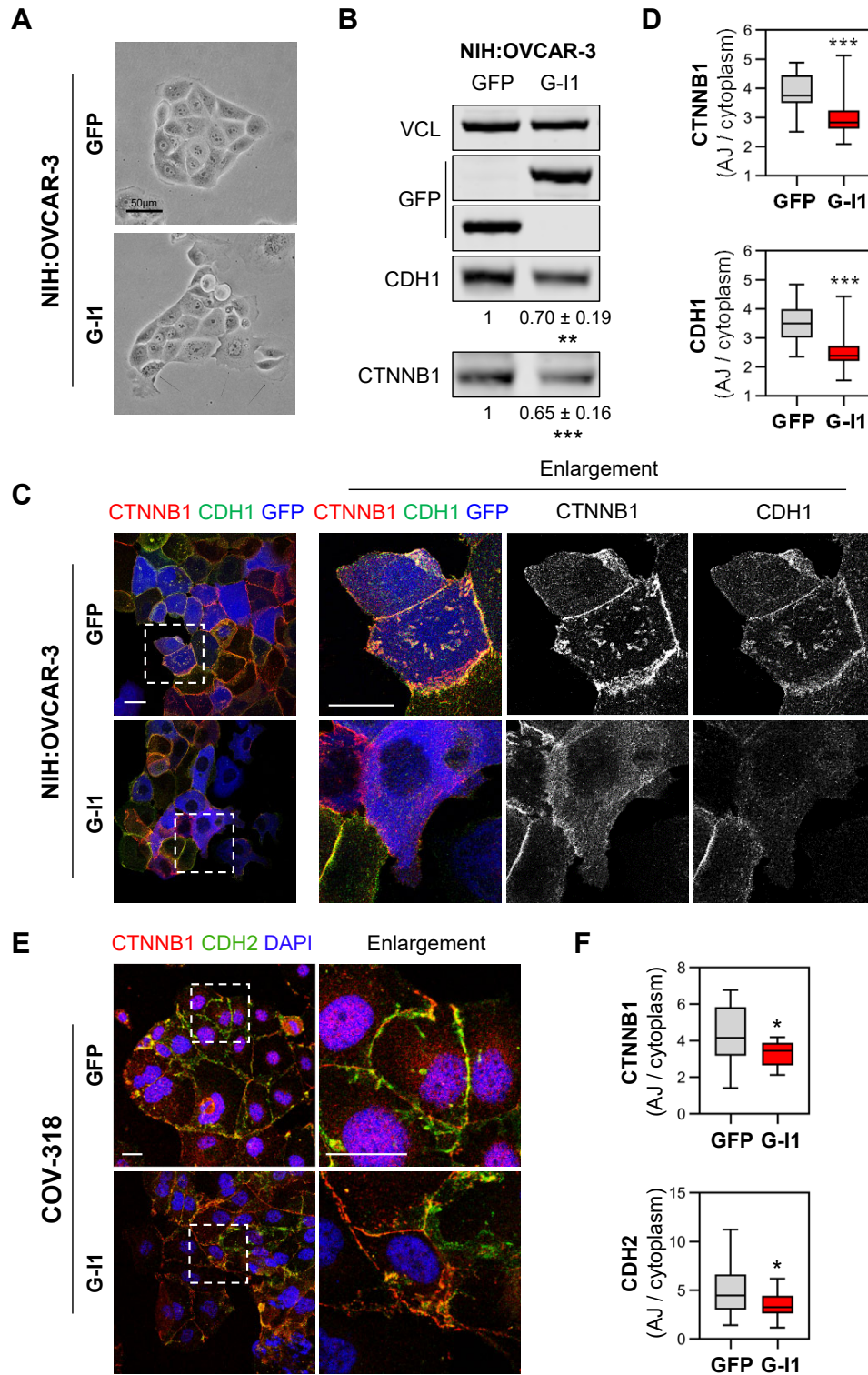


**Figure 11: IGF2BP1-promoted AJ disassembly is conserved in different cell lines.** (A) Bright field images of NIH:OVCAR-3 cells transiently over-expressing GFP-tagged IGF2BP1 (G-I1) or GFP alone serving as control are shown. Colony-detaching cells are marked with arrowheads. (B) Respective NIH:OVCAR-3 cells with GFP and GFP-IGF2BP1 (G-I1) over-expression are analyzed by Western blot displaying CDH1 and CTNNB1 protein levels with VCL as loading control. (C) Immunofluorescent imaging of CTNNB1 and CDH1 in NIH:OVCAR-3 cells with a transient GFP or GFP-IGF2BP1 (G-I1) over-expression that is pseudo-colored in blue. Scale bar corresponds to 25  $\mu$ m. Dashed boxes depict enlarged regions. (D) Corresponding quantification of fluorescence intensities display the ratio of plasma membrane/cytoplasm localization of CTNNB1 and CDH1 in box plots. (E) COV-318 with a stable over-expression of GFP or GFP-IGF2BP1 (G-I1) was analyzed as in (C,D) using CDH2 and CTNNB1 directed antibodies. Statistical significance was assessed by Student's *t*-test. \*  $p < 0.05$ ; \*\*  $p < 0.01$ ; \*\*\*  $p < 0.001$ .

Nonetheless, I investigated potential IGF2BP1-driven effects on the mRNA of AJ components in our cell model ES-2. First, RNA turnover experiments were carried out by adding actinomycin D at different time points to IGF2BP1-depleted and control transfected ES-2 cells and the degradation of CDH2 and CTNNB1 mRNA was analyzed (Figure 12A). Although these AJ components exhibit in a few experiments with other cell lines IGF2BP1 CLIP binding sites in their 3'UTR, the mRNA decay for CTNNB1 and CDH2 remained unchanged upon IGF2BP1 depletion compared to its control. Further supporting an RNA-independent regulation of AJ maintenance by IGF2BP1, the activity of the 3'UTR binding reporter for CTNNB1 and CDH2 were not reduced upon IGF2BP1 depletion which indicates that IGF2BP1 unlikely binds the 3'UTR of these mRNAs in this setting (Figure 12B). In addition, a standard technique to verify a direct association of an RBP with target mRNAs is the RNA immunoprecipitation (RIP) experiment. Therefore, over-expressed and immunoprecipitated GFP-IGF2BP1 vs. GFP and the RNA-binding deficient mutant of IGF2BP1 (KH) in ES-2 cells were analyzed for its bound mRNAs. In comparison to the known mRNA target of IGF2BP1, HMGA2, the quantification of CDH2 and CTNNB1 mRNA upon IGF2BP1 immunoprecipitation suggested no direct binding of IGF2BP1 to CTNNB1 or CDH2 mRNA (Figure 12C). In the next step, protein turnover experiments were carried out under similar conditions by treating knockdown and control ES-2 cells with emetine over the stated period to analyze the protein decay of CDH2 and CTNNB1. As expected, Western blot analysis demonstrated a stabilization of AJ proteins in the absence of IGF2BP1 referring to a stabilization of these components by contact incorporation (Figure 12D,E).

Thus, these data demonstrate that a 3'UTR-dependent regulation of CTNNB1- and CDH2-mRNA by IGF2BP1 is mainly excluded in the ES-2 cell line. IGF2BP1 promotes AJ disassembly rather by indirect destabilization of contact structures implying its internalization and turnover and thereby facilitating a mesenchymal cell morphology in EOC-derived cell lines.



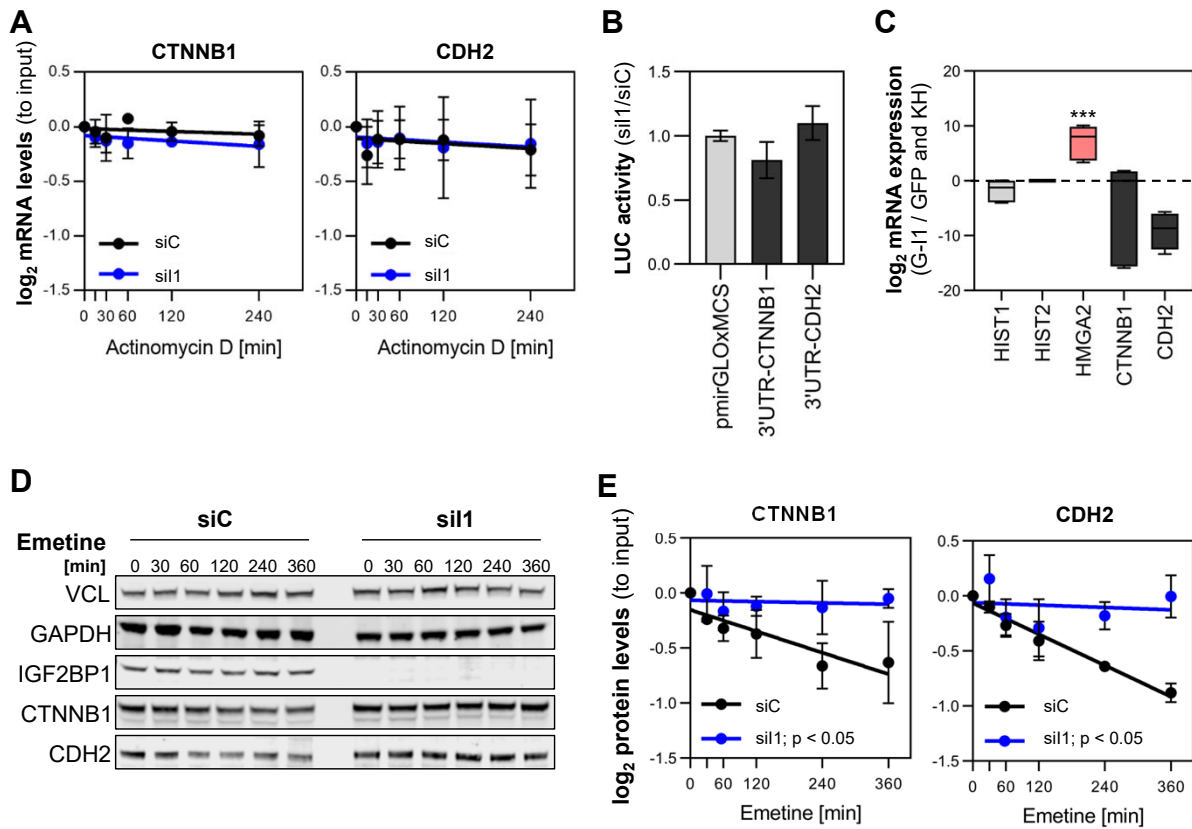


**Figure 12: AJ proteins are indirectly stabilized upon IGF2BP1 depletion.** (A) RNA turnover was determined in ES-2 cells with an IGF2BP1 (sil1) and control knockdown (siC) for CTNNB1 and CDH2 by adding actinomycin D for indicated periods and relative RNA abundance to input level was quantified. (B) Luciferase reporter, containing the 3'UTR of CTNNB1 or CDH2, were measured in dependence of IGF2BP1 (siC or sil1) to reflect IGF2BP1's ability to bind to the 3'UTR of the respective mRNAs. (C) RNA immunoprecipitation experiment, comparing GFP-IGF2BP1 (G-I1) over-expressing ES-2 cells to cells expressing the GFP-tagged full-length, RNA-binding deficient mutant of IGF2BP1 (KH) and GFP alone, shows the binding ability of IGF2BP1 to the indicated mRNAs. Levels of pulled mRNAs were normalized to input and HIST2H3A. HMG2 served as positive control for IGF2BP1 binding. (D) Protein turnover of CTNNB1 and CDH2 was assessed in the ES-2 cell line with an IGF2BP1 (sil1) and control (siC) depletion. Therefore, emetine was added for indicated periods and protein amount was analyzed by Western blot. (E) GAPDH and VCL served as loading control to quantify the degradation of both proteins relative to their inputs. Error bars indicate SD of at least three independent experiments. Statistical significance was assessed by Student's *t*-test. \*\*\*  $p < 0.001$ .

In view of the RNA-independent modulation of AJ proteins through IGF2BP1, important signaling events were further investigated. It is known that post-translational phosphorylation events are essential regulation mechanism of AJ stability and maintenance (Bertocchi et al., 2012). To substantiate an IGF2BP1-dependent destabilization of AJ proteins, phospho-sites of different AJ components were investigated by Western blot. Phosphorylation of CTNNB1 at Ser33, 37 and Thr41 by GSK3B indicates disassembled, cytoplasmic CTNNB1 priming it for degradation (Sakanaka, 2002). Upon IGF2BP1 depletion, this phosphorylation was decreased referring to less cytoplasmic CTNNB1 due to contact incorporation and thus less CTNNB1 turnover (Figure 13A). Although protein abundance of CTNNB1 was not altered by IGF2BP1, interestingly, phosphorylation of Tyr228 was significantly reduced in IGF2BP1 knockdown cells (Figure 13B). This phosphorylation site is known to contribute to a destabilization of AJs and is mainly

phosphorylated by the SRC kinase (Davis et al., 2003; Ishiyama et al., 2010).

The SRC kinase is referred to play an important role in AJ turnover while the GTPase RAC1 is an essential mediator of early, zipper-like AJ assembly (Figure 2). Interestingly, previously published data from our group suggested an indirect alteration of RAC1 activity by IGF2BP1 where a shifted PIP<sub>3</sub>/PIP<sub>2</sub> ratio promoted RAC1-dependent cell polarization leading to elevated cell migration (Stohr et al., 2012). To directly address if IGF2BP1 interferes with the AJ assembly process, RAC1 activity was assessed. Therefore, I performed an activity assay in cooperation with the group of Prof. Dr. Mechthild Hatzfeld where active, GTP bound RAC1 was pulled in ES-2 cells with an IGF2BP1 knockdown in comparison to control transfections. In this GST pulldown the TIAM1-GEF domain was used as bait. Input and pulldown fractions were analyzed by Western blotting and revealed that RAC1 activity is increased in the absence of IGF2BP1 shifting the balance of AJ maintenance to an elevated AJ formation (Figure 13C). Quantifications of GTP bound RAC1 compared to the input levels of RAC1 were significantly upregulated demonstrating an RAC1 activation in the absence of IGF2BP1 (Figure 13D) while overall expression of RAC1 remained unchanged upon IGF2BP1 depletion (Figure 13E,F). However, the main activator of RAC1, TIAM1, and its functional activity is published to be regulated by the SRC kinase interfering with the dynamic AJ maintenance by phosphorylating TIAM1 and thereby preventing the formation of new AJs leading to reduced AJ structures (Woodcock et al., 2009). Together, this implies an involvement of the SRC kinase unbalancing AJ protein localization and its turnover in an IGF2BP1-dependent manner.

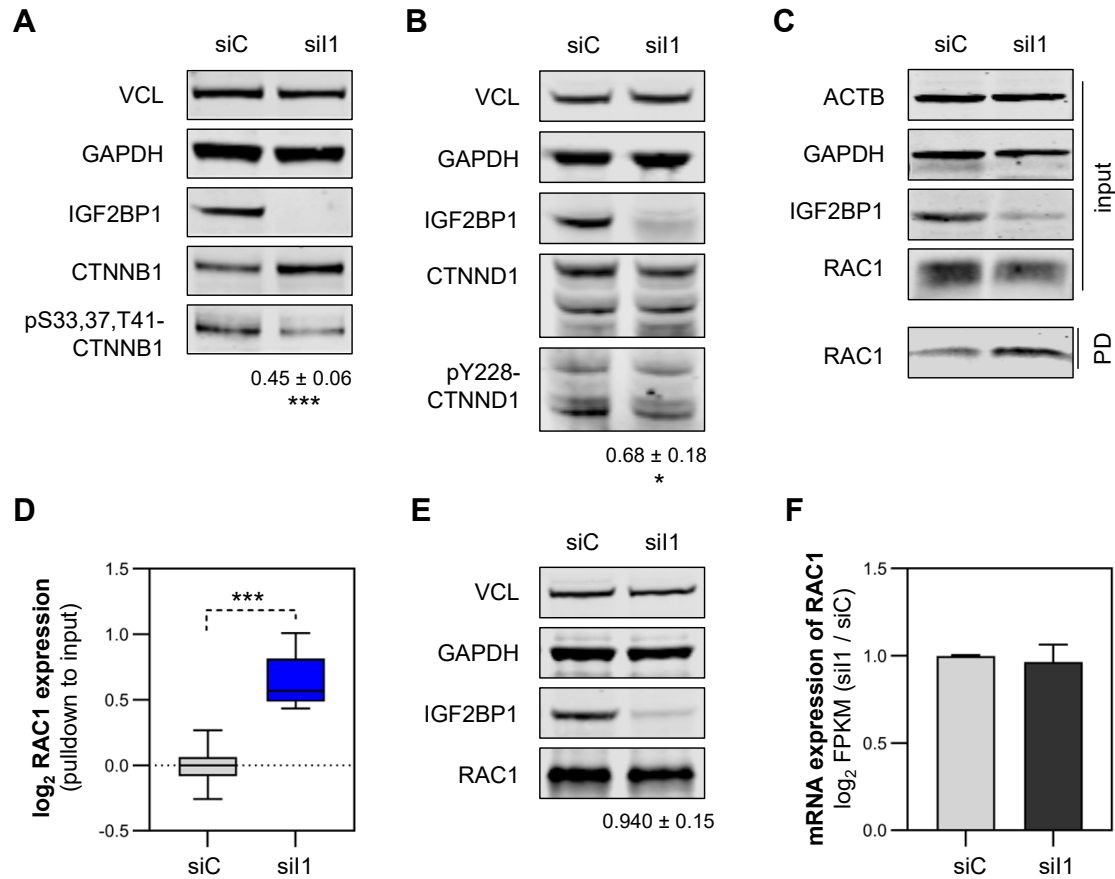


**Figure 13: Imbalanced AJ-promoting signaling upon IGF2BP1 depletion.** (A) Western blotting of CTNNB1 and its phosphorylation at Ser33,37 and Thr41 upon IGF2BP1 depletion in ES-2 cells (sil1) is compared to their control (siC). (B) Protein abundance of CTNND1 and its phosphorylation at Tyr228 is analyzed by Western blot in transient knockdown experiments as described before. VCL and GAPDH served as loading control (A,B). (C) Pull-down of active, GTP bound RAC1 protein using TIAM1-GEF domain as bait upon IGF2BP1 depletion (sil1) is compared to its control (siC) in ES-2 cells. Western blot analysis shows input and pulled RAC1 (PD) abundance while ACTB and GAPDH served as input control. (D) Precipitated, active RAC1 is normalized to input RAC1 abundance of the prior pull-down experiment in dependence on IGF2BP1. (E) IGF2BP1 knockdown in ES-2 cells was analyzed by Western blot for RAC1 protein abundance as described in (A,B). (F) RNA sequencing data of sil1 vs. siC knockdown experiments in ES-2 cells, carried out by Dr. Nadine Bley, were analyzed for RAC1 mRNA levels. Error bars indicate SD of at least three independent experiments. Statistical significance was assessed by Student's *t*-test. \*  $p < 0.05$ ; \*\*\*  $p < 0.001$ .

### 3.3 IGF2BP1-dependent SRC activation mediates AJ disassembly

One major driver of AJ disassembly is the direct phosphorylation of AJ proteins by the SRC kinase accompanied by protein internalization and turnover (Daugherty and Gottardi, 2007; Matsuyoshi et al., 1992; Qi et al., 2006; Roura et al., 1999; Woodcock et al., 2009). In its active form, SRC is phosphorylated at Tyr419 and can then further phosphorylate other proteins like CDH2, CTNNB1 or CTNND1 (Martin, 2001). Inhibition of SRC activity restores AJs as I could previously show in my master's thesis with the inhibitor PP2 in ES-2 cells (Figure 14A-C) or previously reported in other systems (Dosch et al., 2019; Nam et al., 2002). Immunofluorescence analyses clearly demonstrate an elevated formation of mature AJs after SRC inhibition with PP2 (Figure 14A,B). Slightly elevated AJ protein abundance after treatment supports the hypothesis that AJ stabilization in the absence of IGF2BP1 could be due to protein incorporation into contact structures (Figure 14C).

In view of the reported association of SRC via its SH3 domain with IGF2BP1 (Huttelmaier et al., 2005), it appeared tempting to speculate that IGF2BP1 directly regulates SRC activity (Huttelmaier et al., 2005). This is supported by an IGF2BP1-dependent shift of the occurrence of SRC phosphorylation within CTNND1 which was shown before (Figure 13F). Using Western blot analyses, I could verify that SRC activity, indicated by Tyr419-phosphorylation, is changed upon IGF2BP1 perturbation, which was already evidenced during my master's thesis, while SRC abundance remains unchanged by knockdown studies in EOC-derived cell lines (Figure 14D,F). Conversely, transient over-expression of IGF2BP1 in the NIH:OVCAR-3 cell line increased SRC's Tyr419-phosphorylation (Figure 14E). In sum, these findings imply an IGF2BP1-directed activation of the SRC kinase which can further phosphorylate and destabilize AJs.

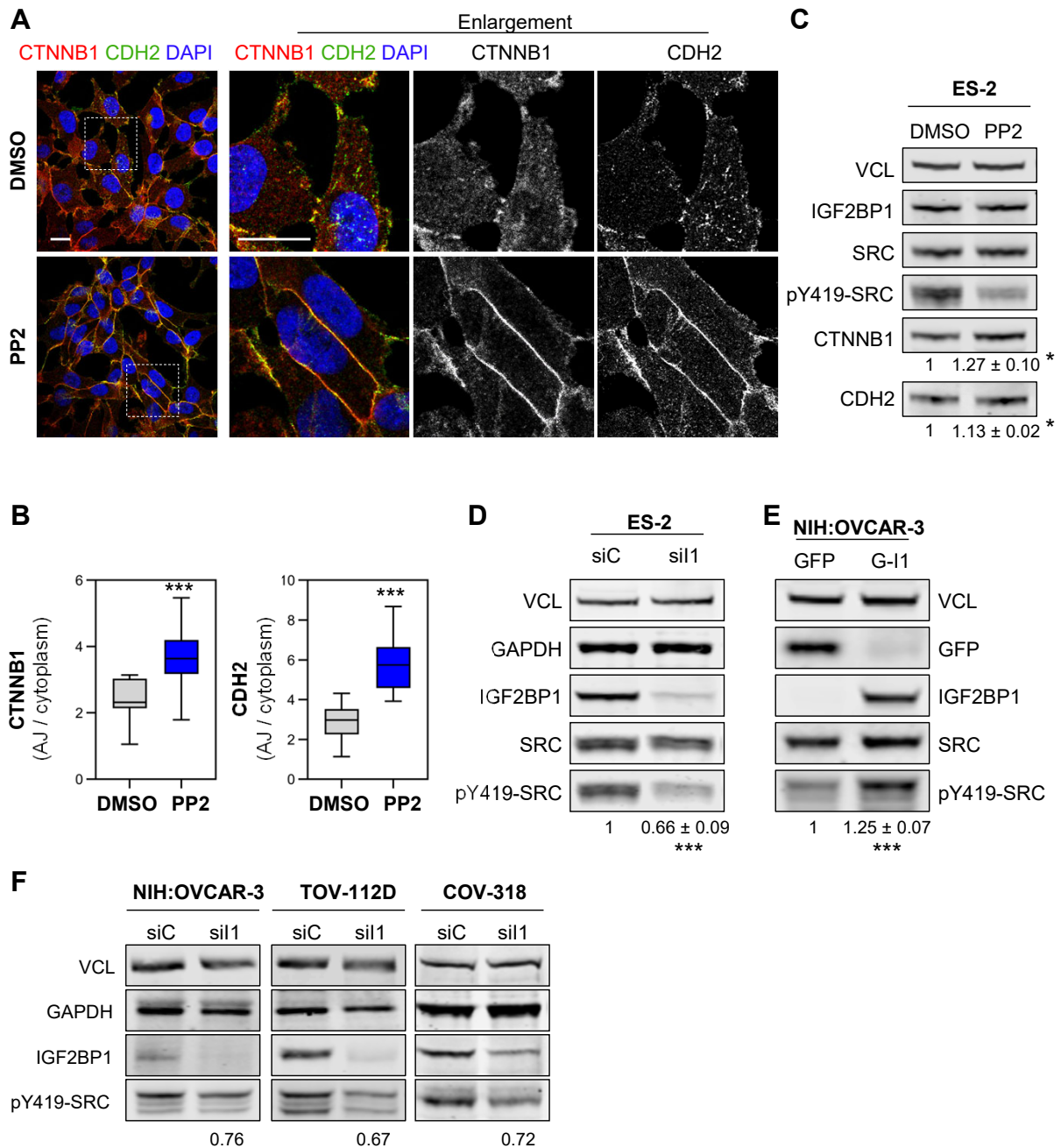


**Figure 14: SRC activity is associated with IGF2BP1 expression in ovarian cancer cell lines.** (A) Immunofluorescence images, generated during my master's, visualize CTNNB1 and CDH2 upon treatment of ES-2 cells with the SRC inhibitor PP2 (100 nM) compared to control treatment with DMSO. Nuclei are stained with DAPI. Enlarged regions are indicated by dashed boxes. Scale bar is equivalent to 25  $\mu$ m. (B) Corresponding quantifications of plasma membrane/cytoplasm ratios for the respective proteins were assessed via fluorescence intensities. (C-F) Western blotting of PP2 (100 nM) vs. DMSO (control) treated ES-2 cells (C), indicated EOC-derived cell lines with an IGF2BP1 depletion (sil1 vs. siC; D; F (n = 1)) or over-expression of IGF2BP1 (G-I1 vs. GFP; E) with indicated antibodies. SRC activity, analyzed through Tyr419 phosphorylation, was normalized to overall SRC abundance. VCL served as loading control. Unless otherwise stated, error indicates SD from at least three independent experiments. Statistical significance was assessed by Student's *t*-test. \*  $p < 0.05$ ; \*\*\*  $p < 0.001$ .

Further investigation on the mechanism of IGF2BP1-dependent SRC activation refers to the reported binding between SRC and IGF2BP1 suggesting an association of the SH3 domain of SRC with the VP<sub>4</sub>SS motif in IGF2BP1 (Huttelmaier et al., 2005). This motif is identical to the SRC binding site in the adhesion protein paxillin (Huttelmaier et al., 2005; Schaller, 2001) and is found in the linker region between KH2 and KH3 domain of the

IGF2BP1 protein (Figure 15A). It is highly conserved among other species within IGF2BP1 but exclusively encoded by IGF2BP1 within the IGF2BP family (Figure 15A). Activation of SRC can be mediated through a variety of mechanisms. One of these is a ligand-binding induced conformational change to enable its autophosphorylation at Tyr419 in an open conformation (Yadav and Miller, 2007). As putative ligand for SRC activation, IGF2BP1 was mutated to investigate if the VP<sub>4</sub>SS motif or its RNA binding capacity are responsible for SRC activation. First, GFP-fused wild type IGF2BP1 (GFP-IGF2BP1<sub>WT</sub>; WT), IGF2BP1 lacking the VP<sub>4</sub>SS motif (GFP-IGF2BP1<sub>ΔSH3</sub>; ΔSH3) by replacing it through GS and the full-length RNA-binding deficient IGF2BP1 (GFP-IGF2BP1<sub>KH</sub>; KH) with mutations in the GXXG loop of all four KH domains (Wachter et al., 2013) were generated and analyzed for its capability of RNA binding. While intact RNA binding was proven for the ΔSH3 mutant, the KH mutant lost its ability to bind targets transcripts (HMGA2, ERK2) compared to the WT (Figure 15B). Subsequently, increasing amounts of these variants were transiently over-expressed and compared to control transfected GFP (Figure 15C,D). Monitored SRC activity via its Tyr419-phosphorylation by Western blot analysis revealed a dose-dependent upregulation with WT or KH over-expression. In contrast, deletion of the VP<sub>4</sub>SS motif in IGF2BP1 within the ΔSH3 mutant resulted in unaltered SRC phosphorylation while the GFP-fused VP<sub>4</sub>SS peptide (GFP-VP<sub>4</sub>SS; SH3motif) alone was able to stimulate SRC activity, although to a lesser extent. This demonstrates that IGF2BP1 promotes SRC activation via a ligand-binding induced but largely RNA-independent mechanism. Similar activation mechanism are reported for hnRNPK and Sam68 (Frisone et al., 2015; Ostareck-Lederer et al., 2002).

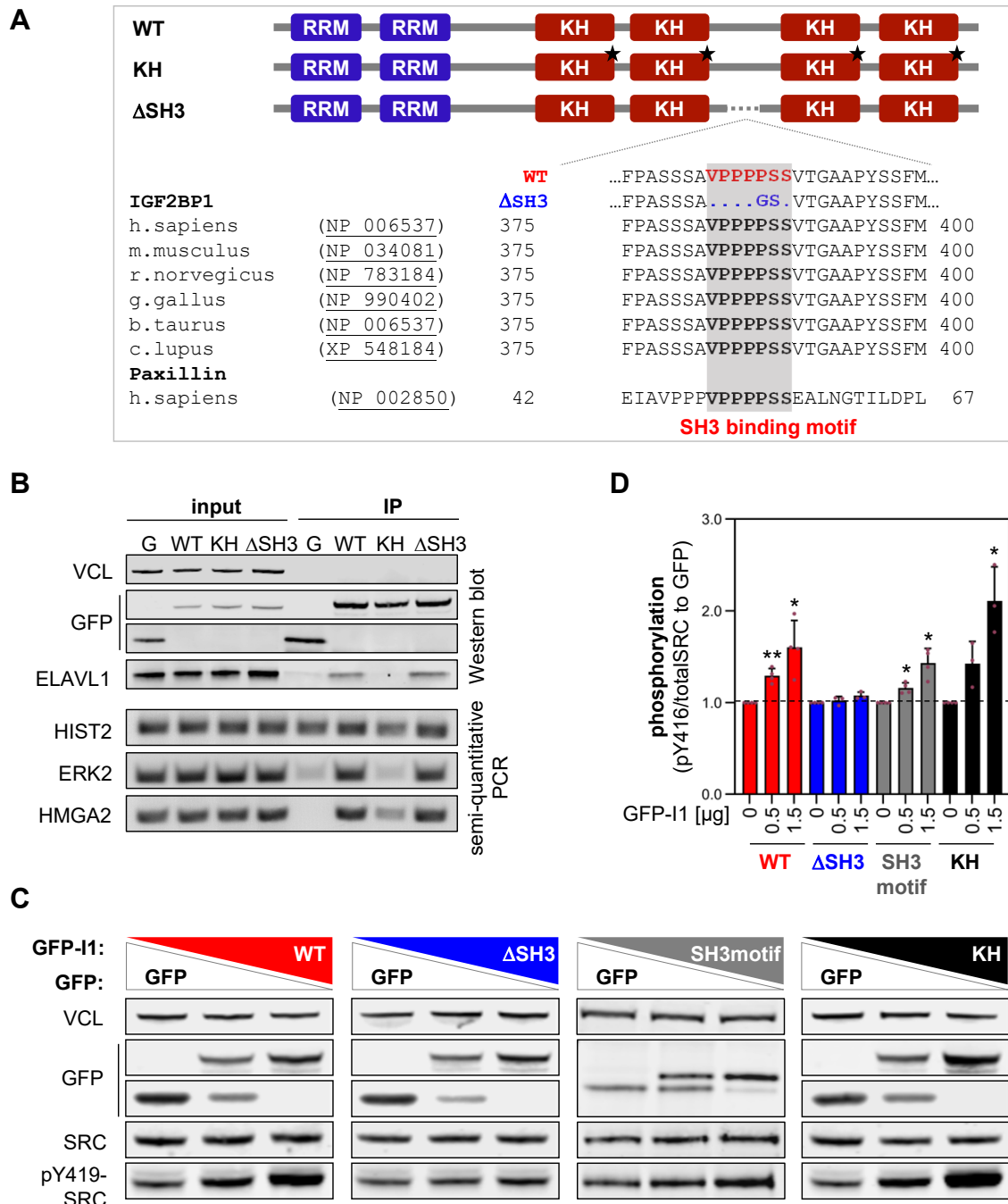


**Figure 15: IGF2BP1 promotes SRC activation via its SH3-binding VP<sub>4</sub>SS motif in an RNA-independent manner.** (A) Schematic showing IGF2BP1's domain structure (RRM, RNA recognition motif; KH, hnRNPk homology domain) with the localization of its VP<sub>4</sub>SS motif within the wild type (WT) protein, and its mutation in the ΔSH3 mutant. Conservation of the VP<sub>4</sub>SS motif is represented across different species and within paxillin. (B) A mutation in the GXXG loop of each KH domain of IGF2BP1 is responsible for the loss of RNA binding capability in the RNA binding deficient mutant (KH). The shown RNA immunoprecipitation of IGF2BP1 with a following semi-quantitative PCR analyzing its bound mRNAs served as confirmation for the loss of RNA binding capability within the mutant while intact RNA binding of the ΔSH3 mutant and wild type IGF2BP1 (WT) was shown. VCL served as loading control and ELAVL1 as a positive control. For the semi-quantitative PCR, HIST2 was the loading control while ERK2 and HMGA2 are reported mRNA targets of IGF2BP1 representing a positive control for mutant dependent binding. (C,D) Transient transfections of GFP-tagged wild type IGF2BP1 (GFP-IGF2BP1<sub>WT</sub>), IGF2BP1 lacking the VP<sub>4</sub>SS motif (GFP-IGF2BP1<sub>ΔSH3</sub>), the SH3 motif alone (GFP-VP<sub>4</sub>SS) and RNA-deficient KH mutant (GFP-IGF2BP1<sub>KH</sub>) in increasing amounts were analyzed by Western blotting (C). VCL served as loading control. The pY419-SRC levels were quantified relative to total SRC abundance and the respective GFP control (D). Error bars indicate SD of at least three independent experiments. Statistical significance was assessed by Student's *t*-test. \* *p* < 0.05; \*\* *p* < 0.01.



Due to distinct SRC activation upon over-expression of IGF2BP1 variants, the impact of the different IGF2BP1 mutant proteins on AJ integrity was monitored by immunofluorescence analysis in NIH:OVCAR-3 (Figure 16A) as well as in IGF2BP1-deleted ES-2 cells (Figure 16B). In both cell lines, WT expression interfered with AJ maintenance in comparison to the GFP control. Similarly, the KH mutant substantially promoted AJ disassembly. In contrast, upon over-expression of the  $\Delta$ SH3 mutant, AJ structures remained mainly unchanged. This clearly demonstrates that the IGF2BP1-dependent SRC activation promoting AJ disassembly depends on the presence of the VP<sub>4</sub>SS motif in IGF2BP1.

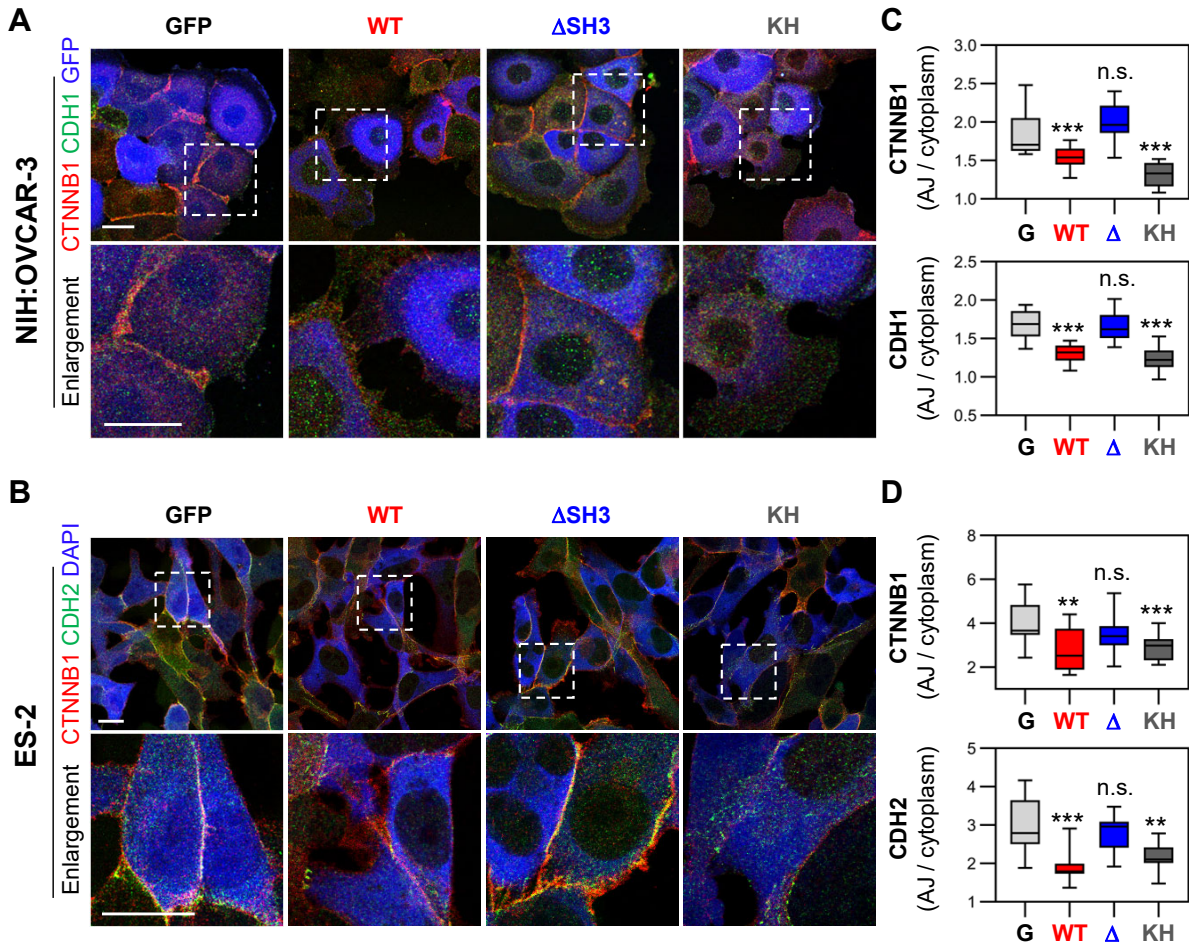


**Figure 16: IGF2BP1-dependent SRC activation impairs AJ maintenance.** (A,B) Immunofluorescent imaging visualized CTNNB1 and CDH1 or CDH2 localization in the epithelial NIH:OVCAR 3 and the mesenchymal ES 2 cell line deleted for IGF2BP1. Over-expression of the different mutants is pseudo-colored in blue. Dashed boxes indicate enlarged regions. Scale bar is equivalent to 25  $\mu$ m. (C,D) Quantification of the ratio between plasma membrane localized and cytoplasmic signals of the indicated proteins was calculated via fluorescence intensities. Statistical significance was assessed by Student's *t*-test. \*\*  $p < 0.01$ ; \*\*\*  $p < 0.001$ .



With focus on the physiological role of IGF2BP1 and its relevance in aggressive ovarian tumor cells, spheroid growth and invasion were observed in a panel of several ovarian cancer cell lines with either depleted or over-expressed IGF2BP1 (Figure 17A,B). Knockdown and over-expression experiments were based on the basal IGF2BP1 levels. Next to the ES-2 cell line, only the NIH:OVCAR-3 cells were able to invade under cell culture conditions. However, IGF2BP1 knockdown consequently reduced spheroid growth and invasion while the over-expression inverted those effects.

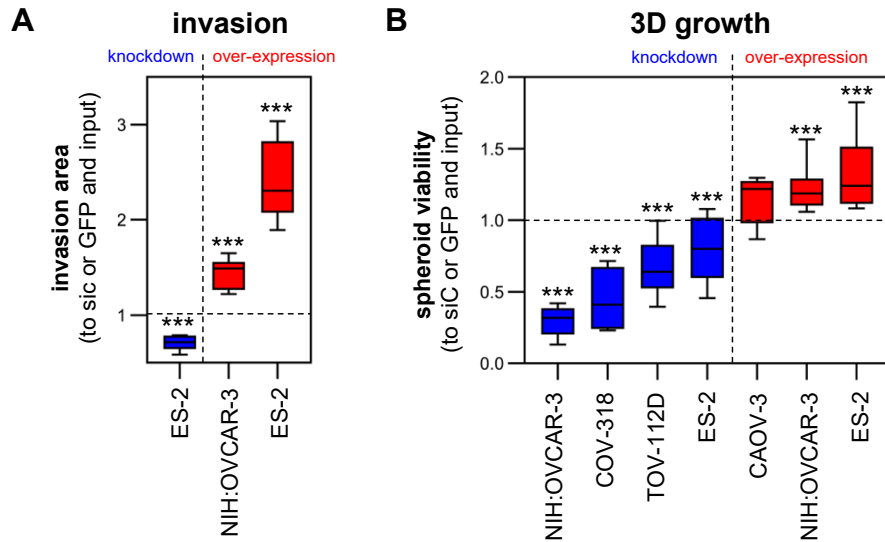


**Figure 17: IGF2BP1-promoted spheroid growth and invasion conserved in EOC-derived cell lines.** (A) Spheroid invasion of indicated cell lines either with an IGF2BP1 knockdown (blue) or an IGF2BP1 over-expression (red) was analyzed. Invasion was monitored via an Incucyte S3 and normalized to control and spheroid input. (B) Spheroid growth was analyzed using CellTiter-Glo® to determine relative cell viability for knockdowns (blue) and over-expressions (red) in the indicated cell lines with input normalization and relative to their respective control. Experiments were performed in cooperation with Dr. Nadine Bley (Bley et al., 2021). Statistical significance was assessed by Student's *t*-test. \*\*\*  $p < 0.001$ .

The mesenchymal ES-2 cell line served as model for further tumor assays with the different IGF2BP1 variants. Analyzing spheroid growth and invasion in 3D culture, the IGF2BP1 mutants showed a moderately enhanced effect in both phenotypic assays (Figure 18A,B). Only wild type IGF2BP1 was able to substantially increase invasion and spheroid growth in comparison to GFP control indicating that both SRC activation and mRNA binding are essential to promote mesenchymal cell properties. In agreement with previous findings (Busch et al., 2016; Muller et al., 2018), this demonstrates a role of IGF2BP1 in 3D growth and invasion upon its depletion. Moreover, this identifies for the first time a connection of IGF2BP1's SH3 motif to cancer-related cell properties.

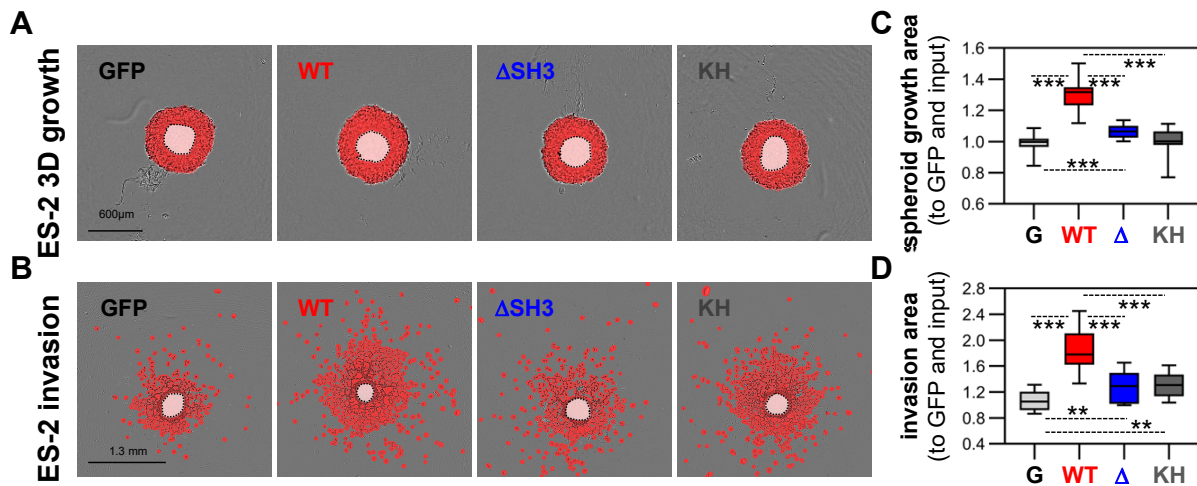


**Figure 18: IGF2BP1-dependent 3D growth and invasion require both, RNA binding and SRC activation.** (A,B) Spheroid growth and invasion of pre-formed Matrigel embedded spheroids of ES-2 cells stably expressing the indicated mutants of IGF2BP1 were monitored via an Incucyte S3 and compared to GFP over-expression alone. Representative images are shown. Overlaid red mask indicates growth (A) or invasion area (B) while the light red mask shows initial spheroid inputs. (C,D) Quantification of the segmentation area (red) between the different variants was normalized to GFP alone and input (light red). Statistical significance was assessed by Mann-Whitney rank-sum test. \*\* p < 0.01; \*\*\* p < 0.001.

In sum, IGF2BP1 induces AJ turnover through SRC activation and thereby promotes invasive growth. Lost cell-to-cell adhesion within tumors in turn enables cells to detach from the tumor allowing them to invade and metastasize (Polyak and Weinberg, 2009). Besides, the loss of intercellular connections disturbs signaling between those cells and the surrounding tissue including growth regulatory signals. Growth-factor receptors were reported to be subjected to the regulation by adhesion molecules and proliferation can be inhibited contact-dependently through intracellular signaling pathways (McClatchey and Yap, 2012). If the IGF2BP1-driven loss of adhesion leads to uncontrolled growth and proliferation will be addressed in the following.

### 3.4 Overcoming contact inhibition of proliferation with IGF2BP1 by directly modulating YAP1

The regulatory mechanism preventing uncontrolled growth is called contact inhibition of proliferation (CIP). When cells come in contact with each other and reach a certain density, growth is inhibited through CIP which is an important strategy to limit organ growth or during regeneration (McClatchey and Yap, 2012). In tumors, proliferation is often continued even under high density conditions leading to uncontrolled tumor growth (Hanahan and Weinberg, 2011).

Previous studies during my master's thesis provided the first evidence for an influence of IGF2BP1 in contact inhibition of proliferation by elevated proliferation and translation rates as well as a higher content of polysomal bound transcripts in the presence of IGF2BP1. However, the Click-iT® technique (2.2.5, 2.4.3) allows to directly monitor CIP by

calculating the translation rate through labelling newly synthesized proteins over a set period under different cell density conditions. A comparison of these conditions reflects which cell population is contact inhibited by arresting growth and translation. To test this, control and IGF2BP1 over-expressing ES-2 cells were cultured under normal, confluent conditions with approximately 20.000 cells / cm<sup>2</sup> and compared to a cell culture with a higher cell density containing about 60.000 cells / cm<sup>2</sup> within the same cavity (Figure 19A). The cultivation in a methionine-free medium allowed the subsequent addition of the methionine analog L-azidohomoalaine (AHA) and its incorporation within newly synthesized proteins which can then be covalently linked with biotin. Via streptavidin the biotin-labeled proteins can be visualized by Western blotting, quantified and normalized to ponceau staining, VCL and ACTB as it was done here (Figure 19B,C). Under high-density conditions, control cells were observed to stop translation while IGF2BP1 over-expressing cells continue with protein biosynthesis.

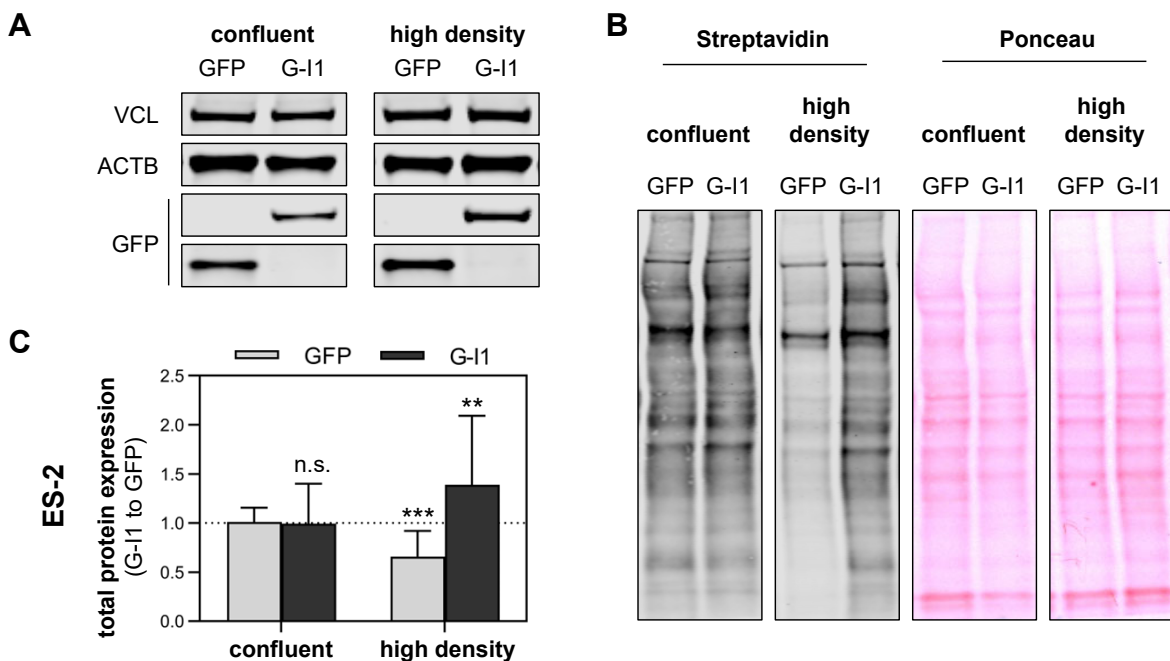


**Figure 19: IGF2BP1 overcomes contact inhibition of proliferation in ES-2 cells.** (A) Over-expression of IGF2BP1 in ES-2 cells growing in a confluent (20.000 cells / cm<sup>2</sup>) and in a high-density culture (60.000 cells / cm<sup>2</sup>), in which the three-fold number of cells were seeded in the same cavity, was compared to its GFP control. (B) Monitoring total protein biosynthesis of GFP and GFP-IGF2BP1 (G-I1) over-expression in ES-2 cells under confluent and high cell density conditions via Western blot using Click-iT® chemistry as described (2.2.5, 2.4.3). The methionine analog AHA was incorporated in newly synthesized proteins, subsequently covalently linked with biotin and visualized via Streptavidin. Ponceau staining served as loading control. (C) Newly synthesized proteins to overall protein amount labeled via Ponceau as well as ACTB and VCL shown in (A). Error bars indicate SD of at least three independent experiments. Statistical significance was assessed by Student's *t*-test. \*\*  $p < 0.01$ ; \*\*\*  $p < 0.001$ .

One major pathway regulating contact inhibition of growth is the hippo pathway consisting of a core phosphorylation cascade built of MST1/2, LATS1/2, SAV1, MOB1A/B and the key transcriptional activator YAP1. Thereby, active hippo signaling promotes phosphorylation of YAP1 to restrain it in the cytoplasm and preventing the stimulation of proliferative gene expression in cooperation with WWTR1 and the TFs TEAD1-4 (Figure 20A). To investigate alterations of the hippo signaling outcome, first, IGF2BP1 knockdown

RNA sequencing data (NCBI GEO: GSE116059) conducted by Simon Müller (Muller et al., 2019) was analyzed for the published gene sets of YAP1/WWTR1/TEAD-stimulated transcription of proliferative genes (Zanconato et al., 2015). Thereby, the majority of genes, included in this gene set, were downregulated upon IGF2BP1 depletion (Figure 20B). In a subsequent experiment, a YAP1/WWTR1-responsive reporter system containing four repetitive TEAD binding sites was cloned according to (Dupont et al., 2011) and analyzed in the IGF2BP1-dependent setting of different cell densities as described before (Figure 20C,D). Under confluent conditions (20.000 cells / cm<sup>2</sup>) YAP1 transcriptional activity correlated with IGF2BP1 levels referring to an increased proliferation. Under high density conditions (60.000 cells / cm<sup>2</sup>), the effect was even stronger (Figure 20C) whereas an IGF2BP1 depletion reduced YAP1 transcriptional activity (Figure 20D). Taken together, an IGF2BP1-dependent elevated overall translation rate and concomitantly a stimulated, transcriptional YAP1 activity support the hypothesis that IGF2BP1 enables cells to overcome CIP. Thereby, it seems that not only the IGF2BP1-promoted AJ turnover rather a deregulation of the hippo pathway enables IGF2BP1-containing cells to overcome CIP.

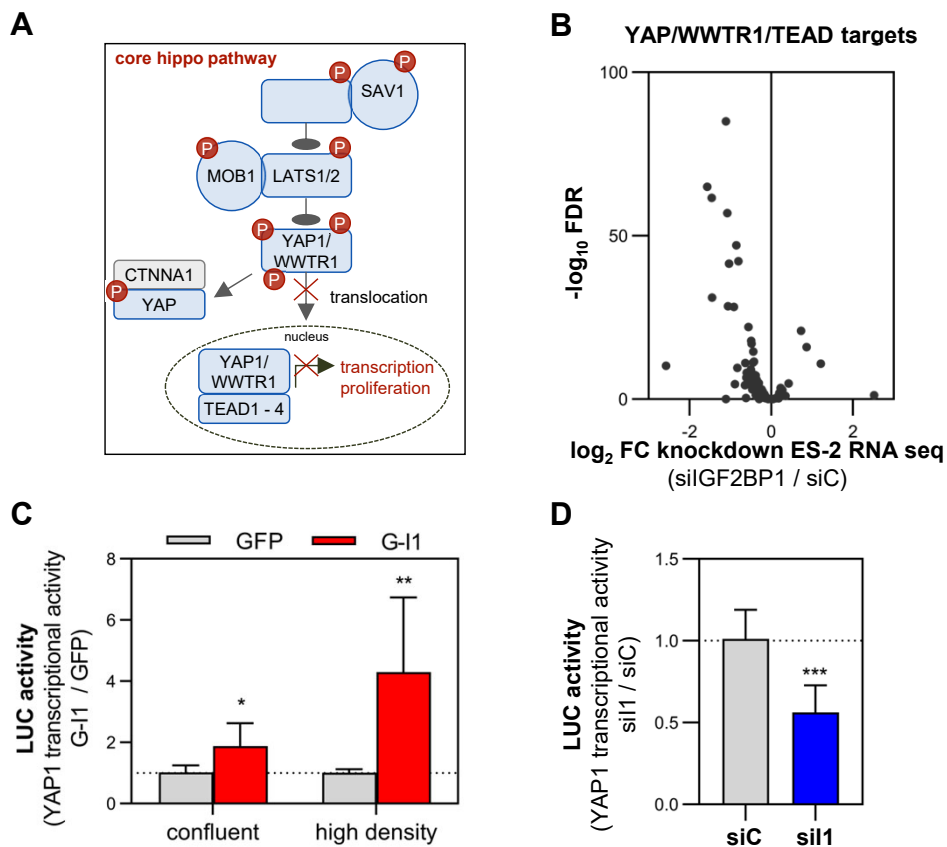


**Figure 20: IGF2BP1-dependent stimulation of YAP1-dependent transcription in ES-2 cells.** (A) Schematic represents the core hippo pathway with its phosphorylation cascade and the transcriptional activator YAP1/WWTR1 which can stimulate proliferative gene expression. (B) FCs and FDRs of the RNA sequencing data of the IGF2BP1 knockdown (NCBI GEO: GSE116059), performed by Simon Müller (Muller et al., 2019), within the gene set of proliferative genes directly stimulated by YAP1/WWTR1/TEAD axis from (Zanconato et al., 2015) are shown. (C,D) Luciferase activity of a YAP1/WWTR1-responsive reporter, containing four repetitive TEAD binding sites, was performed with GFP vs. GFP-IGF2BP1 (G-11)-expressing ES-2 cells under confluent (20.000 cells / cm<sup>2</sup>) and high-density conditions (60.000 cells / cm<sup>2</sup>; C) or upon IGF2BP1 depletion under confluent conditions (D). Reporter activity refers to the transcriptional activity of YAP1. Error bars indicate SD of at least three independent experiments. Statistical significance was assessed by Student's *t*-test. \* *p* < 0.05; \*\* *p* < 0.01; \*\*\* *p* < 0.001.

The core hippo pathways gene set described above (Figure 20A) can be divided into ‘tumor-suppressive’ genes responsible for cytoplasmic retention and ‘proto-oncogenes’ which can stimulate proliferative gene expression. Their expression was analyzed in dependency of IGF2BP1 within published RNA sequencing data sets of an IGF2BP1 knockdown, performed by Simon Müller (Muller et al., 2019), and of ovarian tumors of the TCGA-OV cohort (TCGA, 2011). While the expression of the ‘proto-oncogenic’ genes is upregulated within the tumors, the genes of the phosphorylation cascade are reduced (Figure 21A). In contrast, knockdown studies suggest the reverse effects. A potentially negative association of hippo factors in the TCGA-OV tumors versus the IGF2BP1 knockdown was tested by Pearson correlation identifying a significantly negative correlation (Figure 21B). Incorporation of the 3’UTR CLIP score of IGF2BP1 (Conway et al., 2016; Hafner et al., 2010; Van Nostrand et al., 2016), referring to the number out of eight cross-linking and immunoprecipitation (CLIP) experiments in which mRNA binding sites of IGF2BP1 for each gene within the 3’UTR were identified, is indicated by bubble size (Figure 21C). In this analysis, YAP1 emerges as one with the highest downregulation upon IGF2BP1 depletion, with moderate upregulation within the tumor and one of the highest CLIP scores tempting to hypothesize YAP1 as direct target of IGF2BP1. In brief, this implies an IGF2BP1-dependent shift of the hippo pathway with potential direct modulation of YAP1.

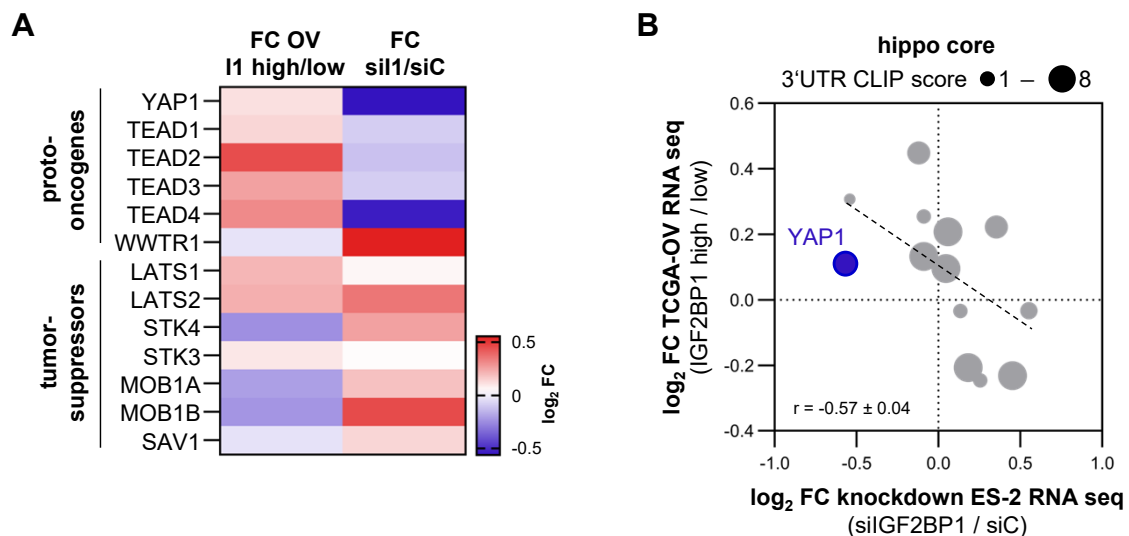


**Figure 21: Association of IGF2BP1 with genes of the core hippo pathway.** (A) Genes involved in the core hippo pathway are separated in ‘proto-oncogenes’ and ‘tumor-suppressive’ genes within this heatmap. Expression of these genes is analyzed within the RNA sequencing data of ovarian tumors from TCGA-OV cohort, where FCs of IGF2BP1-high and IGF2BP1-low expressing tumors are shown in comparison to RNA sequencing data of an IGF2BP1 knockdown experiment (sil1) relative to its control (siC) performed by Simon Müller (Muller et al., 2019). Upregulation is marked in red while blue indicates downregulation of the respective genes. (C) A Pearson correlation of the hippo core factors of the TCGA-OV tumors versus the IGF2BP1 knockdown was performed with the corresponding FCs and is indicated by linear regression and the  $r$  value. Bubble size of each gene refers to the IGF2BP1 CLIP score of eight CLIP experiments (Conway et al., 2016; Hafner et al., 2010; Van Nostrand et al., 2016) in total.

Since IGF2BPs are closely related with partially overlapping roles in cancer, RNA sequencing data sets, generated by Simon Müller, of isoform specific knockdowns were analyzed for alterations in hippo signaling (Figure 22A). Although all three IGF2BPs seem

to some extent alter the expression of hippo related genes, IGF2BP1 shows the strongest effect, especially on YAP1 mRNA expression. In support of this, the median 3'UTR CLIP scores of the proto-oncogenes of the core hippo factors, normalized to their number of CLIP experiments (Conway et al., 2016; Degrauwe et al., 2016a; Hafner et al., 2010; Van Nostrand et al., 2016), is elevated for IGF2BP1 compared to IGF2BP2 and IGF2BP3 (Figure 22B). Furthermore, a GSEA was performed with the gene set of YAP1/WWTR1/TEAD stimulated expression of proliferative genes (Zanconato et al., 2015) using the FCs of the RNA sequencing data of IGF2BP1-3 knockdown experiments from Simon Müller (Figure 22C). The calculated NES scores reflect an impact of all three IGF2BPs on hippo signaling while IGF2BP1 shows the strongest association.

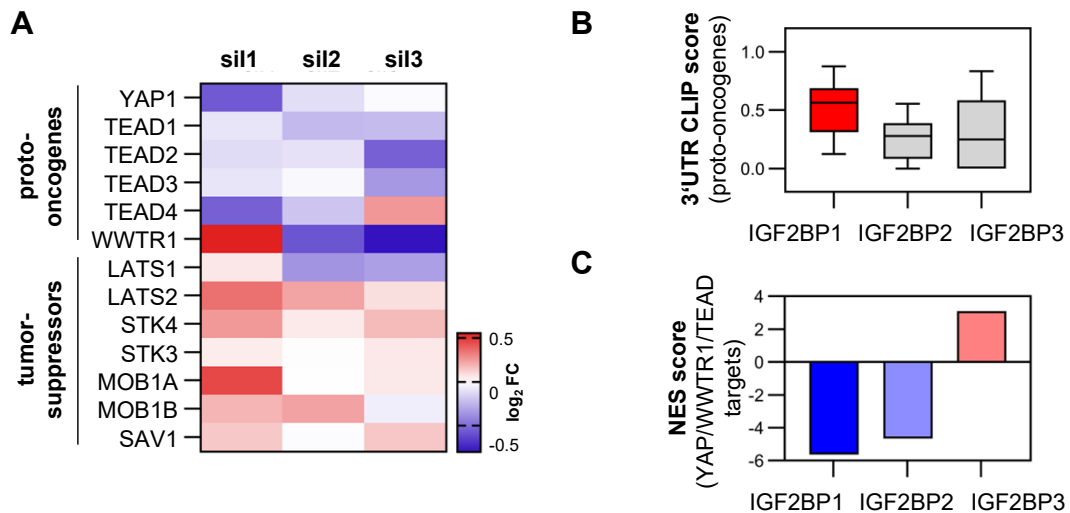


**Figure 22: The impact of IGF2BP1-3 on hippo signaling.** (A) Heatmap displays the FCs of RNA sequencing data from Simon Müller of knockdowns of all IGF2BPs separately in ES-2 cells for the selected genes of the core hippo pathway. Genes are divided into 'proto-oncogenic' and 'tumor-suppressive' association. (B) The relative CLIP score for the core hippo pathway genes for all three IGF2BPs normalized to their number of CLIP experiments (IGF2BP1: 8, IGF2BP2: 9, IGF2BP3: 6) are shown (Conway et al., 2016; Hafner et al., 2010; Van Nostrand et al., 2016). (C) GSEA was performed with the gene set from (Zanconato et al., 2015), containing directly YAP1/WWTR1/TEAD stimulated genes associated with proliferation, and the FCs of the RNA sequencing data of IGF2BP1-3 knockdown experiments from Simon Müller. NES scores are shown.

Focusing only on IGF2BP1, downregulation of YAP1 mRNA level upon IGF2BP1 depletion from RNA sequencing data was validated on the mRNA and protein level (Figure 23A,B). Moreover, an association of YAP1 abundance with IGF2BP1 could be further demonstrated in ES-2 cells with an CRISPR-Cas9-mediated knockout of IGF2BP1 and a stable re-expression of WT and KH mutant IGF2BP1 (Figure 23C). Reduced YAP1 protein expression within KH over-expression indicates an RNA-dependent regulation of YAP1. Besides, an IGF2BP1-dependent expression of YAP1 was further shown in the COV-318 cell lines performing knockdown and over-expression studies (Figure 23D,E).



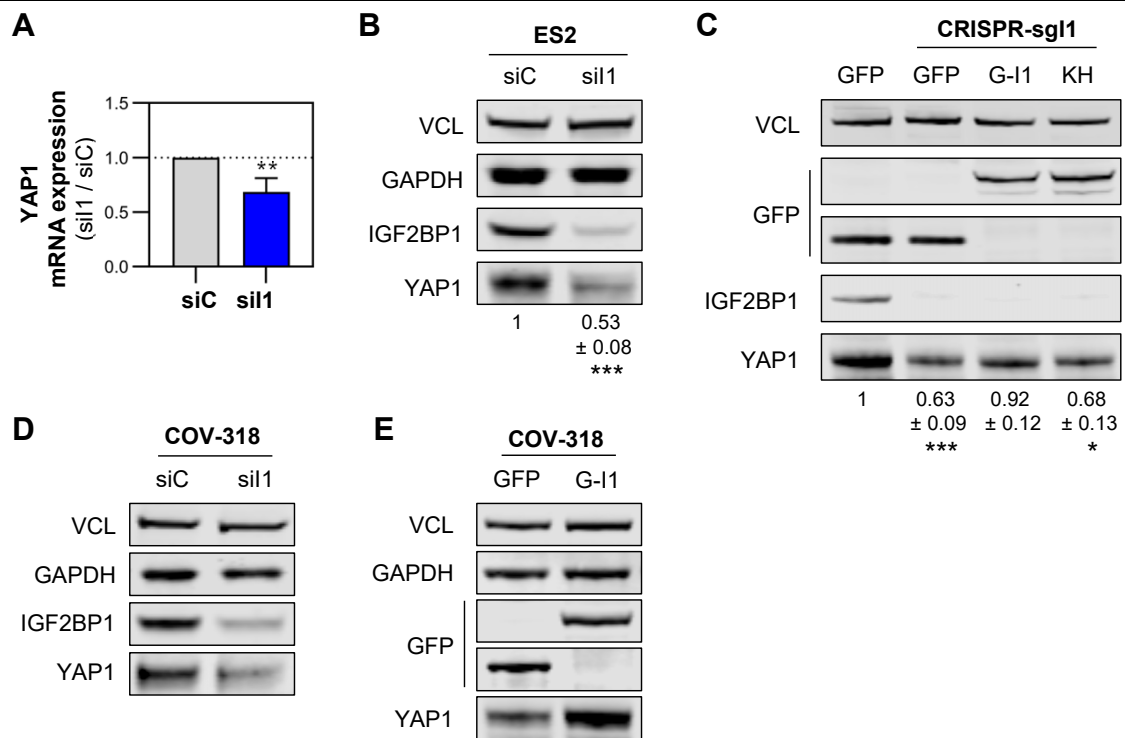


**Figure 23: YAP1 expression correlates with IGF2BP1 abundance.** (A) YAP1 mRNA expression upon an IGF2BP1 depletion (sil1) compared to its control transfection (siC) in ES-2 cells. (B-E) Western blotting of YAP1 protein expression: (B) after control (siC) and IGF2BP1 (sil1) knockdown; (C) stable deletion of IGF2BP1 (sg11-GFP), re-expression of wild type GFP-IGF2BP1 (sg11-G-I1) and its RNA binding deficient mutant (sg11-KH) compared to wild type ES-2 cells expressing GFP alone; (D,E) transient depletion of IGF2BP1 (sil1; D) and over-expression of IGF2BP1 (G-I1; E) in the ovarian cancer cell line COV-318 compared to their respective control (n = 1). VCL and GAPDH served as loading control. Errors indicate SD of at least three independent experiments unless otherwise stated. Statistical significance was assessed by Student's *t*-test. \*  $p < 0.05$ ; \*\*  $p < 0.01$ ; \*\*\*  $p < 0.001$ .

To test a direct regulation of YAP1 abundance by IGF2BP1, first, an RNA immunoprecipitation (RIP) was performed to quantify bound YAP1 mRNA by over-expressed, GFP-tagged wild type IGF2BP1 compared to the RNA binding deficient KH mutant and the GFP control (Figure 24A). YAP1 mRNA was similarly enriched as the positive control HMGA2 which is reported to be a direct target of IGF2BP1 (Busch et al., 2016). RNA turnover of YAP1 mRNA was increased upon IGF2BP1 deletion while a re-expression of IGF2BP1 was able to reduce it (Figure 24B). To investigate a 3'UTR dependent regulation, the 3'UTR of YAP1 was deleted via CRISPR-Cas9 as previously described (Muller et al., 2020; Muller et al., 2019) and the IGF2BP1-dependent regulation was analyzed by knockdown experiments (Figure 24C). Thereby, YAP1 abundance was reduced independently of control or IGF2BP1 depletion compared to cells exhibiting the full-length YAP1 mRNA. This implies that the 3'UTR of YAP1 is bound by IGF2BP1, complexes its mRNA in an RNP complex and thereby prevents degradation of YAP1 mRNA. Similarly, luciferase activity of the reporter containing the 3'UTR of YAP1 was significantly decreased upon IGF2BP1 depletion (Figure 24D). Taken together, this demonstrates binding of IGF2BP1 to the 3'UTR of YAP1 to stabilize its mRNA leading to an increased protein abundance and thereby presumably shifting its activity. As reported for other mRNA targets (Muller et al., 2018), through binding of a target mRNA sequence within the 3'UTR,

IGF2BP1 can shield the mRNA from miRNA attack. A crosstalk between hippo signaling and miRNAs is reported, although YAP1 seems not the most important miRNA target compared to other hippo genes (Li et al., 2017; Wang et al., 2018). In EOC, there are two miRNAs, of the here shown conserved miRNA sites within the 3'UTR of YAP1 (Figure 24E), reported to target YAP1, miR-199-3p and miR-375 (He et al., 2021). Both antagonizing YAP1 function and are associated with a tumor-suppressive role in ovarian cancer. Due to the overlap of the miRNA site of miR-199-3p with the IGF2BP1 CLIP peak, an IGF2BP1-dependent shielding of this miRNA should be addressed in continuative studies in detail.

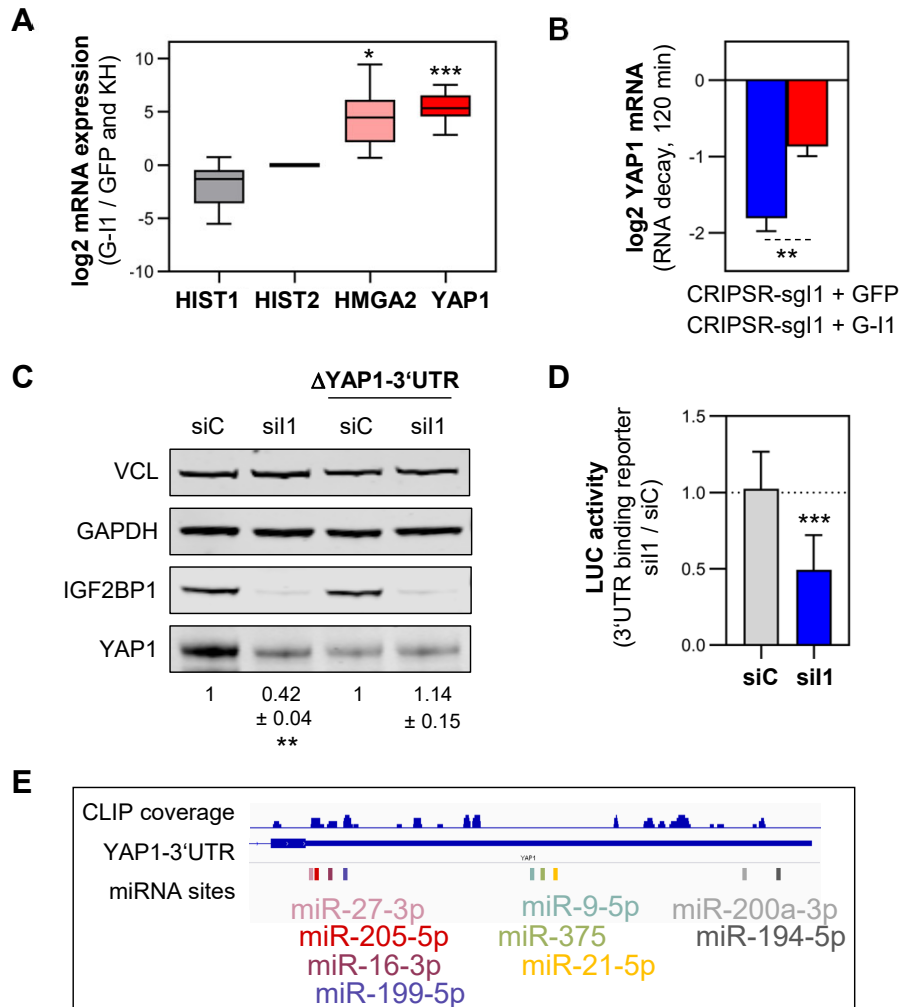


**Figure 24: YAP1 is directly regulated via its 3'UTR by IGF2BP1 in ES-2 cells.** (A) RNA immunoprecipitation of over-expressed GFP-IGF2BP1 (G-I1) and its bound mRNAs were analyzed by qRT-PCR and normalized to HIST2H3A as well as over-expressed GFP alone and the RNA binding deficient mutant of IGF2BP1 (KH). HMGA2, reported as direct target of IGF2BP1, served as positive control. (B) RNA turnover was determined between ES-2 cells exhibiting a IGF2BP1 deletion (sg1 + GFP) and IGF2BP1-deleted ES-2 cells re-expressing GFP-IGF2BP1 (sg1 + G-I1) by adding actinomycin D for the indicated time. YAP1 mRNA was normalized to RPLP0 and HIST2H3A. (C) CRISPR-Cas9-mediated deletion of the 3'UTR of YAP1 in ES-2 cells with an additional depletion of IGF2BP1 ( $\Delta$ YAP1-3'UTR-sil1) was analyzed by Western blot in comparison to the shown controls. VCL and GAPDH served as loading control and for quantification next to siC. (D) Luciferase activity of a 3'UTR binding reporter was measured after an IGF2BP1 (sil1) and a control (siC) knockdown to monitor binding of IGF2BP1 to the YAP1 3'UTR. (E) Schematic showing IGF2BP1 CLIP peaks within YAP1 3'UTR of eight CLIP experiments in total (Conway et al., 2016; Hafner et al., 2010; Van Nostrand et al., 2016) and localization of predicted conserved miRNA sites obtained from TargetScan. Error bars indicate SD of at least three independent experiments. Statistical significance was assessed by Student's *t*-test. \*  $p < 0.05$ ; \*\*  $p < 0.01$ ; \*\*\*  $p < 0.001$ .



Finally, an influence of SRC on the hippo pathway via direct phosphorylation of LATS1 or even YAP1 directly is reported which favors YAP1's nuclear activity and thus proliferation (Li et al., 2016; Si et al., 2017). To test in our setting if SRC activation is responsible for the increased transcriptional activity of YAP1 seen in (Figure 20D), reporter assays were performed within ES-2 cells. The inhibition of SRC activity with saracatinib reduced the transcriptional activity of YAP1 (Figure 25A) only down to 90 % while the IGF2BP1 knockdown decreased YAP1 activity by half (Figure 20D). As a control Western blotting showed that YAP1 protein abundance also remained unaffected after SRC inhibition (Figure 25B). Together, these experiments give first hints that the shown IGF2BP1-dependent alteration in YAP1 activity in ES-2 cells could rather be mediated directly by IGF2BP1 then through SRC stimulation alone. The shifted abundance of YAP1 upon IGF2BP1 depletion or over-expression possibly contributes to a shifted balance of cytoplasmic restrained and transcriptional active YAP1. Nonetheless, the dependency of the SRC kinase in YAP1 signaling in ovarian cancer needs to be addressed in further studies including its connection with IGF2BP1.

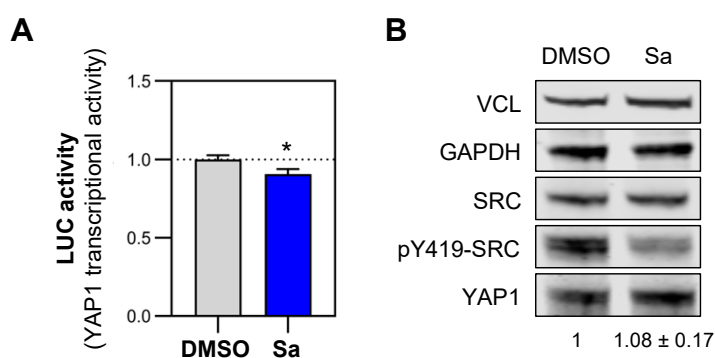


**Figure 25: SRC inhibition rarely interferes with YAP1 activity in ES-2 cells.** (A) Transcriptional activity of YAP1 was monitored upon inhibition of SRC activity with saracatinib (Sa, 6  $\mu$ M) in ES-2 cells via a luciferase reporter. DMSO served as control. (B) Western blotting of saracatinib inhibited ES-2 cells is compared to the DMSO control to analyze YAP1 protein abundance. VCL and GAPDH served as control. Error bars indicate SD of at least three independent experiments. Statistical significance was assessed by Student's *t*-test. \*  $p < 0.05$ .

### 3.5 Combined treatment of saracatinib and selumetinib effectively impairs IGF2BP1-driven invasive growth *in vitro* and *in vivo*

For targeting the IGF2BP1-promoted invasive growth, several inhibitor combinations can be beneficial in ovarian cancer. Due to frequent resistances in HGSC, combining drugs are a chance to achieve a higher efficacy, less toxicity and especially address or even overcome drug resistance. Figuring out which inhibitors are the most beneficial combinations becomes widely used. Before assessing different drug combinations,  $EC_{50}$ s (half maximal effective concentration) of the single drugs were calculated by measuring cell viability in 2D for different concentrations in ES-2 cells in advance (Figure 26). BTYNB, a novel described compound specifically inhibiting RNA binding of IGF2BP1 exhibits an  $EC_{50}$

of 6.4  $\mu\text{M}$  (Figure 26A). For verteporfin, a potent inhibitor of the YAP1-TEAD association, an  $\text{EC}_{50}$  of 11.3  $\mu\text{M}$  was determined (Figure 26C). Saracatinib which inhibits SRC activation, reveals anti-tumor activity within HGSC tumors (Simpkins et al., 2012) and was approved in different clinical trials, showed the lowest  $\text{EC}_{50}$  value with 5  $\mu\text{M}$  (Figure 26B).

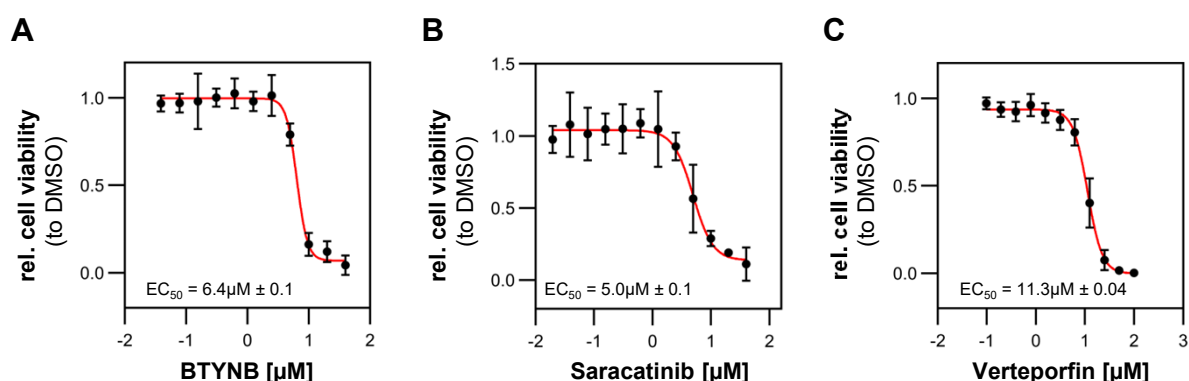


**Figure 26:  $\text{EC}_{50}$  calculations for BTYNB, saracatinib and verteporfin.** (A,B,C) Determination of  $\text{EC}_{50}$  values for the IGF2BP1 inhibitor (BTYNB, A), the SRC inhibitor (saracatinib, B) as well as the YAP1 inhibitor (verteporfin, C, carried out by Claudia Misiak) in ES-2 cells was performed by measuring relative cell viability in 2D for 12 different inhibitor concentrations normalized to DMSO. Error bars indicate SD of at least three independent experiments.

A standard application of combination studies are dose-dependent drug matrixes using different reference models to calculate the combinatorial over the single agent effect. In the left panel, the inhibition map with indicated inhibitor concentrations within this drug matrix visualizes the underlying measurements while the right panel shows synergy maps calculated by different models (Figure 27). The resulting effects of the applied synergy scoring from SynergyFinder (Ianevski et al., 2017) are clearly defined by additivity, synergy and antagonism reflecting a higher or lesser effect of drug combinations over the expected additive single drug effects. Synergistic effects are assumed when an additional effect is measured over the expected effect depending on the reference model. The here performed calculations are based on the principle of the three following reference models. The HSA (highest single agent) model simply compares the difference between the highest effect of a single drug with the effect of a combination. The Bliss Independence model is built on the concept that the different drugs have independent target sites but resulting in the same effect. Bliss calculations rely on the multiplication of single drug effects (Foucquier and Guedj, 2015). The ZIP (zero interaction potency) model is based on the comparison of changes in potency of individual drugs with their combinations including different drug doses. The assumption, that the individual drugs have zero interaction and are consequently rarely interfering with the potency of each other, lead to expected additivity of the single drugs. (Brooks et al., 2019; Yadav et al., 2015). Referring to the used web application SynergyFinder (Ianevski et al., 2017), antagonism is presented in green with a synergy score smaller than -10, synergism is indicated in red with a synergy score over 10 and additivity is assumed in between. The calculated synergy score for each model represents the average overall concentrations of the matrix, exhibiting maximal synergistic

regions indicated by a black frame. To test synergistic or additive drug combinations, different drug matrices with indicated concentrations measuring cell viability in 2D were performed for: (A) BTYNB + verteporfin, (B) BTYNB + saracatinib and (C) saracatinib + verteporfin (Figure 27). All assessed drug combinations show overall additive effects, while BTYNB in combination with verteporfin or saracatinib exhibits the lowest ones (Figure 27A,B). As BTYNB is unable to impair the RNA-independent activation of SRC kinase, BTYNB and saracatinib initially seemed to be a promising combination to target IGF2BP1's function, but overall synergy is missing. Saracatinib and verteporfin almost achieved overall synergy (Figure 27C). However, considering the maximal synergistic regions only, the combination of saracatinib and verteporfin has an average synergy score of 29 while BTYNB and verteporfin reached 22 and BTYNB and saracatinib 16. The synergy score thereby refers to the maximal percentage of a response effect beyond the expectations.

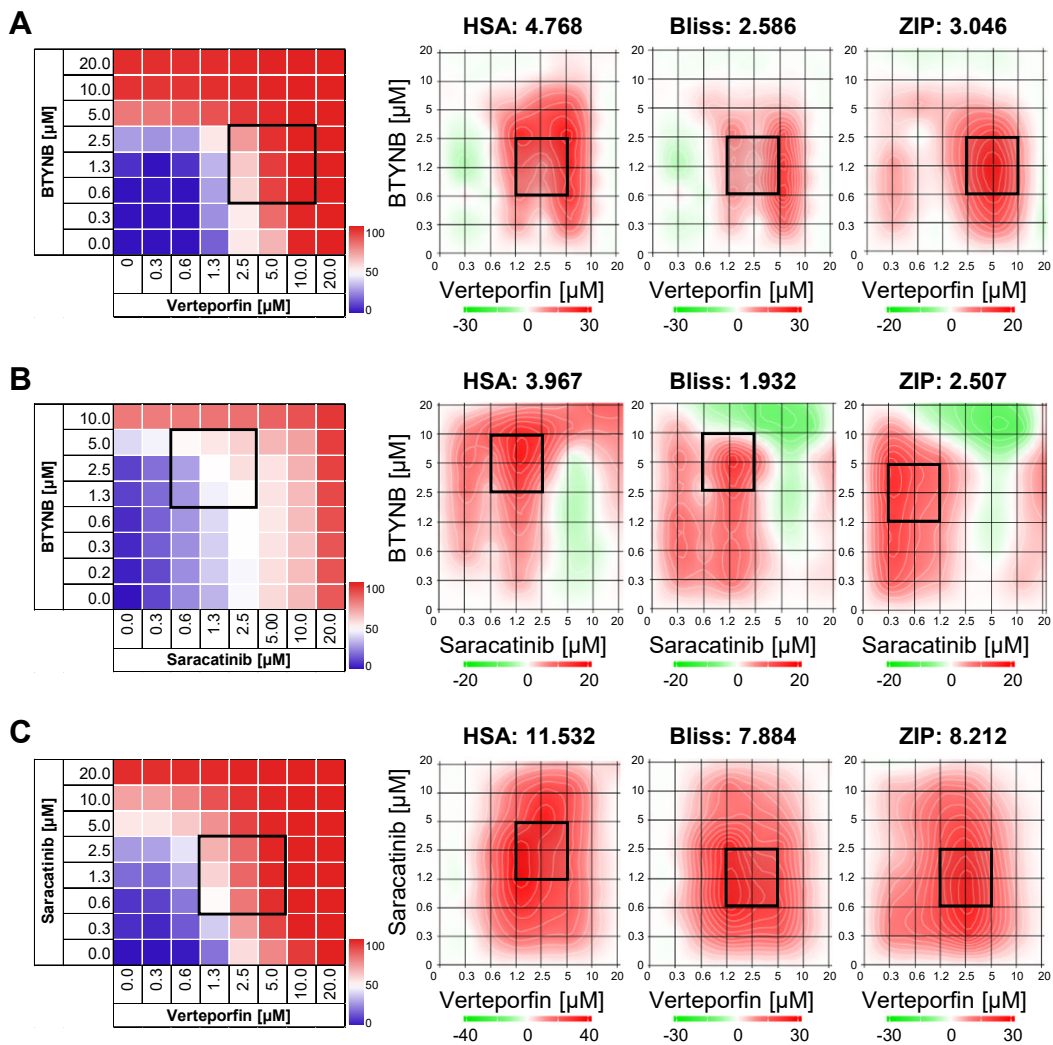


**Figure 27: Synergy scores of various drug combinations in ES-2 cells.** (A,B,C) Inhibition maps (left panel) of a drug matrix screen with the stated concentrations and inhibitors reflect the relative cell viability in percentage (%) measured with CellTiter-Glo® of a 2D growth assay with ES-2 cells. Three different synergy models (HSA, Bliss, ZIP; right panel) were applied via SynergyFinder to calculate an overall synergy score for each drug combination. Synergistic regions are marked in red and indicated with scores > 10, antagonistic areas are colored in green with synergy scores < 10 while additive effects are assumed between > -10 and < 10. Dashed boxes indicate regions with maximal synergy scoring. Experiments were carried out by Dr. Nadine Bley and reflect three independent experiments.

To further address drug resistance, finding the pathways which are activated alongside established monotherapies or newly developed drugs are important. Although saracatinib and verteporfin represent a potential combination, occurring resistances to saracatinib were previously associated with the activation of the MAPK pathway and should be further investigated. It is reported that inhibition of MEK re-sensitized saracatinib-resistant cells (McGivern et al., 2018) and a suitable inhibitor is, in contrast to verteporfin, approved in clinical trials. Co-activation of both, MEK and SRC, was found in HGSC patients and combined inhibition proved to be beneficial on tumor growth *in vivo* over single drug therapies (Simpkins et al., 2018). Since IGF2BP1 is upregulated in a subset of HGSC accompanied with SRC activation and ERK2 is reported to be upregulated mRNA-dependently through IGF2BP1 (Muller et al., 2018; Muller et al., 2019), combined inhibition SRC and ERK in an IGF2BP1-dependent manner should be further addressed. First, western blot analysis proved efficiency of both single inhibitors using 6  $\mu$ M and their combinations with only 3  $\mu$ M of each (Figure 28A). Next to the reported IGF2BP1-dependent effect on ERK2 abundance, its activity was shown to be enhanced with an over-expression of IGF2BP1 indicated by Thr202-/Tyr204-phosphorylation (Figure 28B). An IGF2BP1 knockdown decreases the phosphorylation and activity of ERK2 (Figure 28C,D) confirming the reduced transcriptional activity of the SRE luciferase reporter upon IGF2BP1 depletion (Muller et al., 2019). Additionally, effects of reduced ERK abundance could be recapitulated in two other EOC-derived cell lines (Figure 28E). To finally assess the synergy and the physiological relevance of combined saracatinib and selumetinib in the following, the  $EC_{50}$  of selumetinib alone in 2D was determined at 4.9  $\mu$ M.

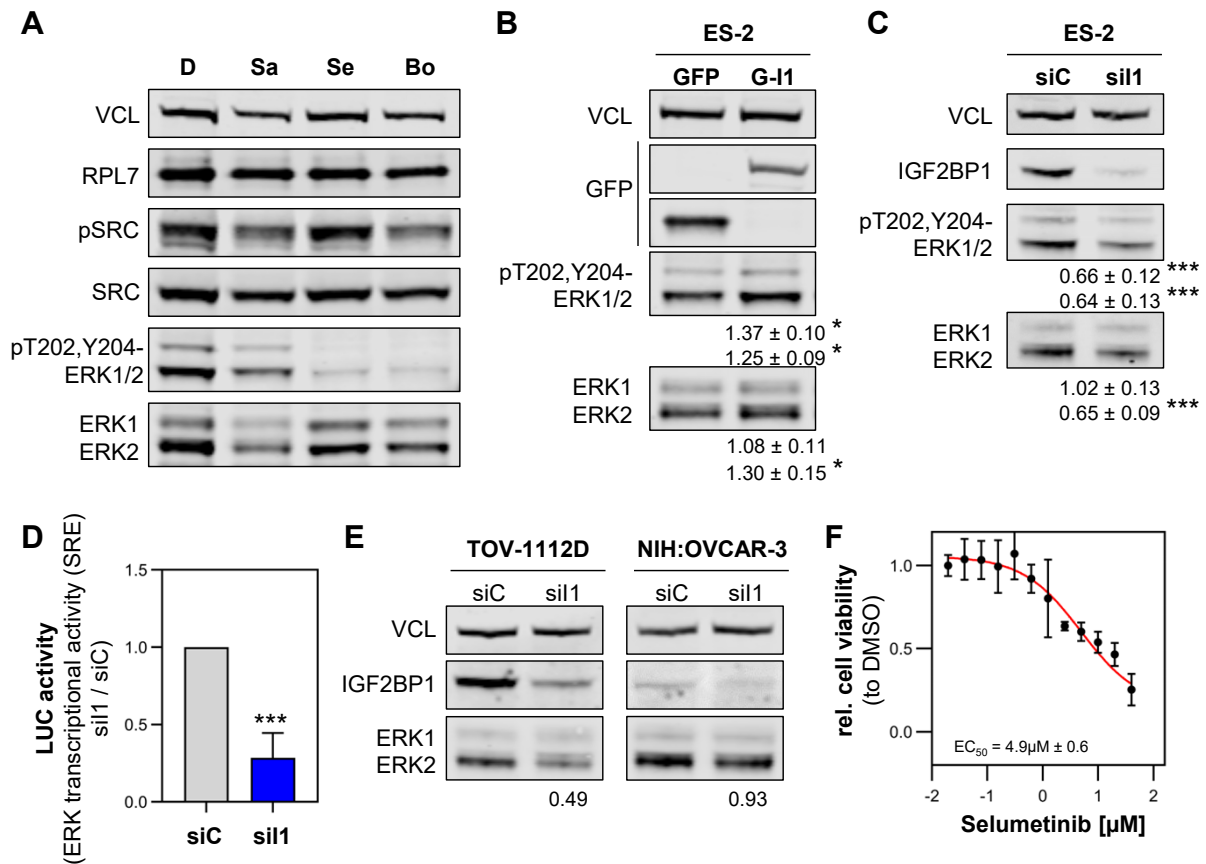


**Figure 28: IGF2BP1-dependent regulation of ERK2.** (A) The SRC inhibitor saracatinib (Sa, 6 μM), MEK inhibitor selumetinib (Se; 6 μM) and a combination of both (Bo, 3 μM Sa + 3 μM Se) are investigated for their inhibitory potential in ES-2 cells on Western blot compared to the DMSO control. VCL and RPL7 served as loading control. (B,C) Western blotting of ERK1/2 and their activating phosphorylation on T202/Y204 was performed in ES-2 after over-expressing GFP-IGF2BP1 (G-I1) next to GFP (B) and accordingly after an IGF2BP1 (sil1) and control (siC) depletion (C). VCL served as loading control for quantification. (D) A SRE reporter monitored transcriptional activity of ERK in IGF2BP1 knockdown experiments. (E) ERK1/2 protein abundance is investigated via Western blot in two other ovarian cancer cell lines, TOV-1112D and NIH:OVCAR-3, after a transient IGF2BP1 depletion compared to its control (n = 1). (F) The EC<sub>50</sub> value for selumetinib in ES-2 cells under 2D growth conditions was determined by measuring cell viability for indicated concentrations relative to DMSO. Error indicates SD of at least three independent experiments unless otherwise stated. Statistical significance was assessed by Student's *t*-test. \* *p* < 0.05; \*\*\* *p* < 0.001.

Since both drugs together already proved to be efficient to overcome resistances with saracatinib alone (McGivern et al., 2018), here we wanted to address if both drugs act in a synergistic or additive manner and which role IGF2BP1 plays in this setting. Analysis of this drug combination with the SynergyFinder revealed additive overall effect exhibiting the benefit of reducing the applied inhibitor concentrations by half compared to single drug treatment (Figure 29). Average synergy scores of around 7 for the IGF2BP1 over-expression and about 9 for the GFP control were calculated with the three models, ZIP, HSA and Bliss. Maximal scores were indicated by the black frame. Thereby, maximal synergy scores of about 35 in average were achieved reflecting a maximal 35 % response effect beyond the expectations. In comparison to the drug combinations evaluated before, saracatinib and selumetinib yield the highest synergistic effect. Interestingly, the regions of maximal synergy scoring were shifted within the two conditions. The IGF2BP1 over-expression (Figure 29C,D) needs a higher concentration of both drugs to achieve maximal





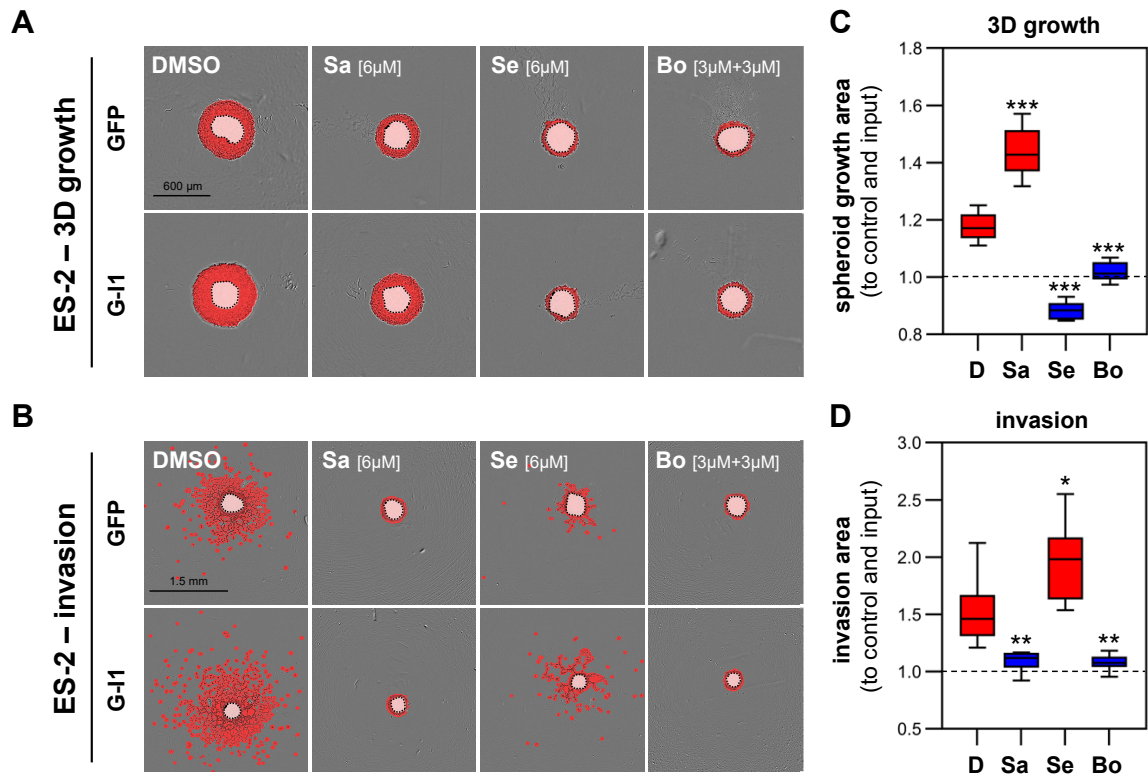


**Figure 30: Combination of saracatinib and selumetinib effectively targets IGF2BP1-driven phenotypes.** (A,B) Spheroid growth and invasion was analyzed upon treating ES-2 cells exhibiting a stable GFP or GFP-IGF2BP1 (G-I1) over-expression with saracatinib (Sa, 6  $\mu$ M), selumetinib (Se, 6  $\mu$ M) or both in combination with reduced concentrations of each drug (Bo, 3  $\mu$ M Sa + 3  $\mu$ M Se) for 72 h. Overlaid red mask indicates growth (A) or invasion area (B) while the light red mask shows initial spheroid inputs. Representative images collected with an Incucyte S3 are shown. (C,D) For quantification, growth area and invasion area were normalized to GFP control and input. Experiments were performed in cooperation with Dr. Nadine Bley (Bley et al., 2021) and reflect three independent experiments. Statistical significance was assessed by Mann-Whitney rank-sum test. \*  $p < 0.05$ ; \*\*  $p < 0.01$ ; \*\*\*  $p < 0.001$ .

Having a closer look on the different tolerances in the respective assays in dependency on IGF2BP1,  $EC_{50}$  calculations within the two assays were performed by measuring cell viability or invasion area over a concentration range. Confirming the prior suggested resistance, over-expressing IGF2BP1 led to an increase of the calculated  $EC_{50}$  about 60 % (from 3.5 to 5.8  $\mu$ M) for saracatinib under 3D growth conditions compared to the GFP control (Figure 31A). Comparably, the  $EC_{50}$  of selumetinib was four-fold increased within invasion assays (Figure 31B). Impairment of 3D growth by selumetinib was achieved with almost equal potency as invasion by saracatinib between GFP and GFP-IGF2BP1 (Figure 31C,D).

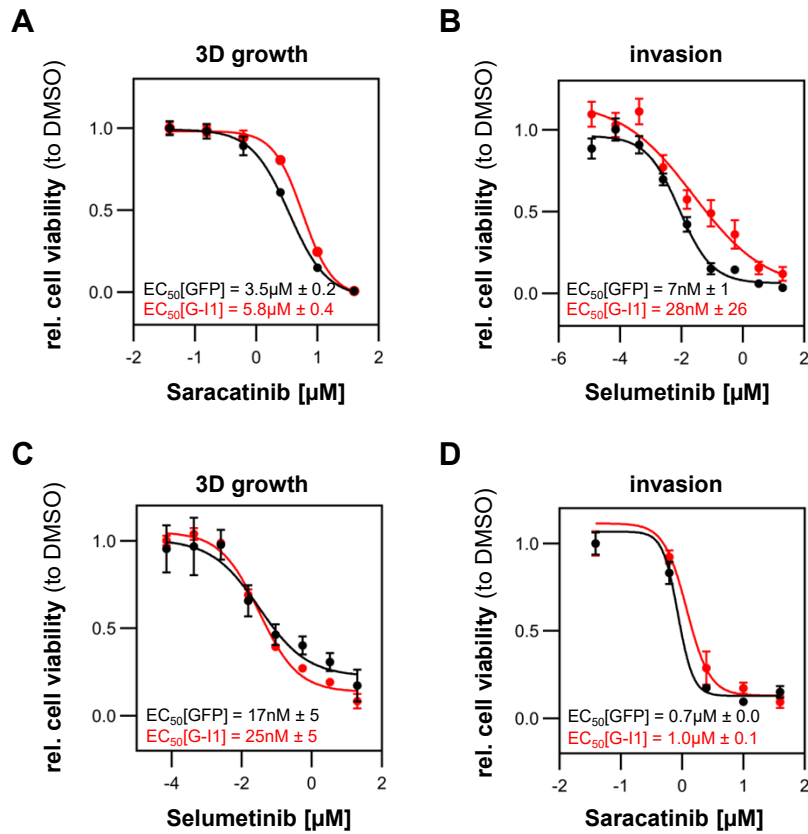


**Figure 31: IGF2BP1-dependent effects of saracatinib and selumetinib on spheroid growth and invasion.** EC50 values of ES-2 cells with a GFP or GFP-IGF2BP1 (G-I1) over-expression under 3D growth conditions were determined with a normalization to DMSO and input. (A,C) For spheroid growth relative cell viability was measured with CellTiter-Glo®. (B,D) Spheroid invasion was monitored via a Incucyte S3 and invasion area was quantified. Error bars indicate standard error of mean (SEM) of at least three independent analyses. Experiments were performed in cooperation with Dr. Nadine Bley (Bley et al., 2021).

Supporting data, generated by Dr. Nadine Bley, was shown within different EOC-derived cell lines performing similar phenotypic analyses. An IGF2BP1 depletion increased sensitivity of the respective cell lines to saracatinib in spheroid growth while an over-expression of IGF2BP1 enhanced resistance (Figure 32A). Similarly, cells were sensitized with an IGF2BP1 knockdown against selumetinib within the invasion assay and became more resistant with an increase of IGF2BP1 abundance (Figure 32B).



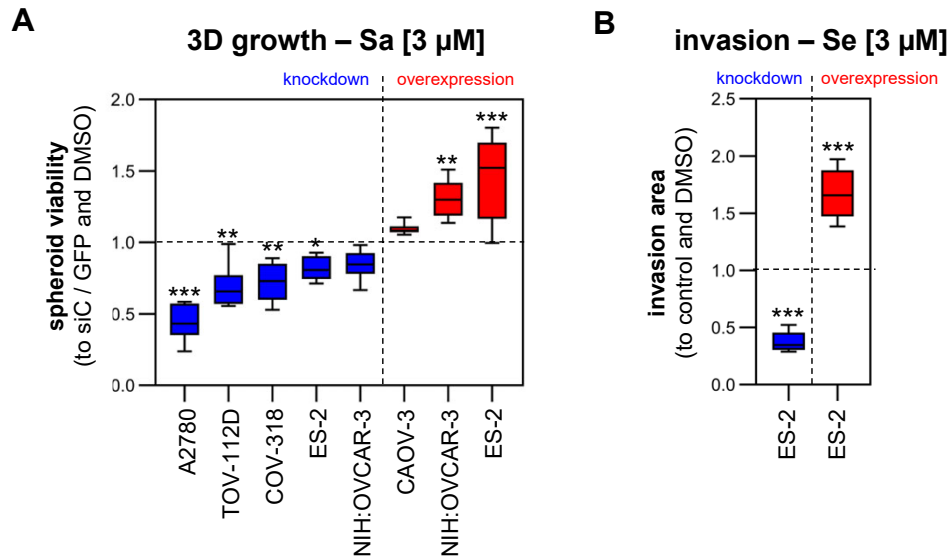


**Figure 32: IGF2BP1 contributes to resistances in single drug treatment of several EOC-derived cell lines.** (A,B) Spheroid growth analysis under saracatinib treatment (Sa, 3 μM, A) and an invasion assay with selumetinib treated cells (Se, 3 μM, B) were performed upon knockdown (siC, sil1) and overexpression (GFP, G-I1) of IGF2BP1 in different ovarian cancer cell lines. Effects were normalized to DMSO and their respective control (siC or GFP). Experiments were carried out by Dr. Nadine Bley (Bley et al., 2021) and represent three independent experiments. Statistical significance was assessed by Student's *t*-test. \*  $p < 0.05$ ; \*\*  $p < 0.01$ ; \*\*\*  $p < 0.001$ .

Due to late diagnosis of HGSC, it is often accompanied by metastasizing to the peritoneum. The potential of single cells to grow anchorage-independent and form spheroids favoring this process. As IGF2BP1 is mediating invasive growth *in vitro*, iRFP-labelled ES-2 cells either expressing GFP or GFP-IGF2BP1 were pre-treated with 3 μM of each inhibitor, saracatinib and selumetinib, or DMSO and IP-injected into nude mice in the presence of equal amounts of these drugs. To study the *in vivo* relevance of these drugs under varying IGF2BP1 conditions, tumor growth was assessed for two weeks post injection of these tumor cells by monitoring the iRFP signal in the peritoneum. An elevated tumor growth driven by the IGF2BP1 over-expression compared to GFP control within the DMSO treatment was observed (Figure 33A) fitting to the previously reported role of IGF2BP1 promoting tumor growth (Muller et al., 2020; Muller et al., 2018). The combination of saracatinib and selumetinib almost abolished tumor growth within the GFP control and strongly reduced tumor size under the IGF2BP1 over-expression (Figure 33B). In sum, the *in vivo* studies, thoroughly performed by Simon Müller, Tommy Fuchs and Dr. Nadine Bley, confirmed the reported *in vitro* benefit of combined treatment with saracatinib and selumetinib. Additionally, the combination of saracatinib and selumetinib demonstrated effective targeting of IGF2BP1-driven invasive growth *in vivo* (Bley et al., 2021).

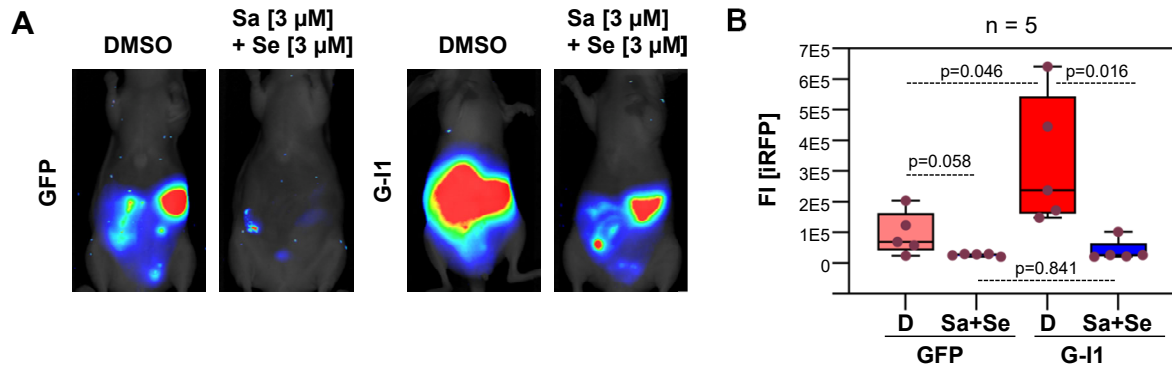


**Figure 33: SRCi and MEKi inhibition effectively targets IGF2BP1-driven phenotypes *in vivo*.** GFP or GFP-IGF2BP1 (G-11) over-expressing ES-2 cells, labelled with iRFP, were pre-treated with saracatinib (3  $\mu$ M) and selumetinib (3  $\mu$ M) or DMSO for 48 h and IP-injected into nude mice with stated inhibitor concentrations. Tumor growth in the abdomen was monitored by infrared imaging for 2 weeks. Representative images are shown. (B) Quantification of infrared images was calculated with five mice per condition. The *in vivo* experiment was carried out by Simon Müller, Tommy Fuchs and Dr. Nadine Bley (Bley et al., 2021). Statistical significance was assessed by Mann-Whitney rank-sum test.

In conclusion (Figure 34), associated with the C5 subtype of HGSC of the ovary, the oncofetal mRBP IGF2BP1 is suggested as novel marker for therapy selection. Stimulating SRC and ERK signaling, IGF2BP1 promotes a mesenchymal phenotype associated with the loss of AJs and thereby contributing to EMT. Next to the SRC-dependent disassembly of AJs, IGF2BP1 interferes with ERK and hippo signaling by directly promoting ERK2 and YAP1 expression and transcriptional activity. Subsequently, with the expression of proliferative genes stimulated by ERK2 or YAP1, IGF2BP1 promotes proliferation and concomitantly overcomes contact inhibition of proliferation. Uncontrolled, invasive growth enables metastasis to the peritoneum which is a frequent complication within HGSC. A combined treatment with the clinically approved drugs saracatinib and selumetinib, effectively targets the IGF2BP1-driven spheroid growth and invasion *in vitro* as well as tumor growth *in vivo* implying a benefit of this therapy in patients with IGF2BP1-positive tumors.

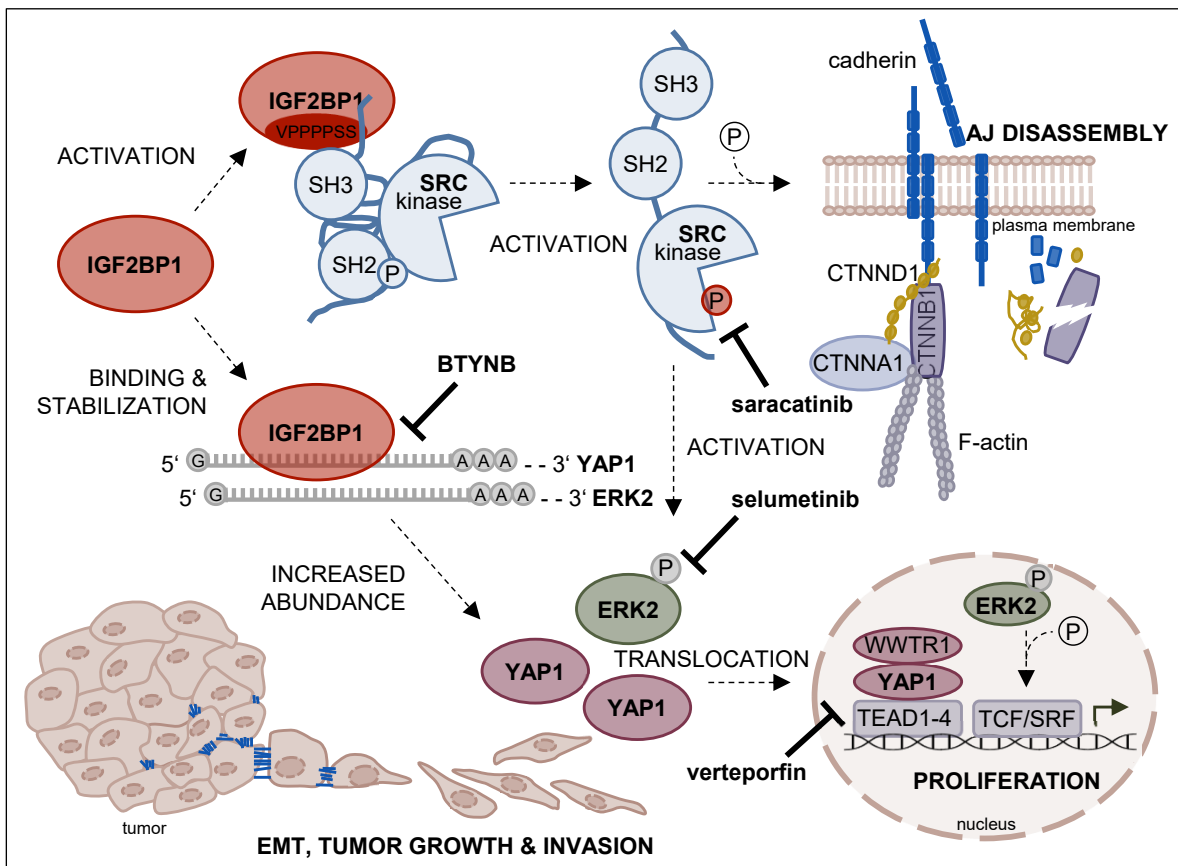


**Figure 34: IGF2BP1 targeting SRC, ERK2 and YAP1.** The schematic summarizes the here revealed insights of IGF2BP1 promoting AJ disassembly and overcoming contact inhibition of proliferation to enable EMT, tumor growth and invasion in ovarian cancer. On one site, the IGF2BP1-driven AJ disassembly is mediated through a ligand-binding dependent, RNA-independent activation of SRC kinase which can further phosphorylate AJ components to facilitate its turnover. On the other site, IGF2BP1 directly binds to YAP1 and ERK2 mRNA, increasing their abundance by stabilizing their mRNAs and thereby allowing them to stimulate gene expression via the TFs TEAD1-4 or TCF/SRF for cancer progression. Potential drugs inhibiting mRNA binding of IGF2BP1 (BTYNB), SRC activation (saracatinib), MEK and subsequently ERK activation (selumetinib) and YAP1-TEAD association (verteporfin) are shown. Schematic according to (Lavoie et al., 2020; Martin, 2001; Meng and Takeichi, 2009; Willert and Jones, 2006; Zhao et al., 2010).

## 4 DISCUSSION

Ovarian cancer is one of the most lethal gynecological malignancies due to its late diagnosis and its frequent metastatic spread (Sung et al., 2021). Over the last decades, it became clear that ovarian cancer resembles many disease entities, but targeted treatment opportunities are limited (Vaughan et al., 2011). Cytoreductive surgery and broad chemotherapeutics are still the standard treatment for all subtypes (du Bois et al., 2009). Except for PARP inhibitors, the improvement of PFS and overall survival remains dismal. Recurrence and developing resistances to first-line chemotherapeutics are a frequent problem which requests novel and more specific combination treatment strategies targeting adaption processes. Elucidating the molecular mechanisms of resistance and identifying subtype-specific oncogenic drivers creates a rationale for targeted therapies and biomarkers selecting patients benefitting from these therapies (Bowtell et al., 2015).

RBPs are essential regulators of mRNA fate controlling several cellular processes on the post-translational level (Gerstberger et al., 2014; Hentze et al., 2018). The highly tumor-selective expression and upregulation of IGF2BP1 in EOC (Bell et al., 2013; Kobel et al., 2007) provides the basis for this study aiming to elucidate the molecular action mechanism of IGF2BP1 in ovarian cancer cells suggesting therapeutic approaches. Due to its mRNA binding capability, IGF2BP1 is already reported to be involved in various cellular processes promoting tumor progression and forces mesenchymal properties (Bell et al., 2013; Bley et al., 2021; Degrauwe et al., 2016b; Gutschner et al., 2014; Muller et al., 2018; Zirkel et al., 2013). Here, IGF2BP1 is shown to be elevated in mesenchymal ovarian cancer and associated with the disassembly of AJs. Surprisingly, this revealed a novel, RNA-independent mechanism of IGF2BP1 stimulating SRC activation in a protein ligand binding-dependent manner to promote AJ turnover and thereby enabling EMT. The loss of AJs was further associated with a reduced contact inhibition of proliferation. At the same time, IGF2BP1 was shown to directly stabilize the mRNA of the main effector of the hippo pathway YAP1 to sustain proliferative gene expression.

However, the IGF2BP1-driven invasive growth essentially relied on SRC activation as well as on its mRNA binding capacity and thereby potentially contributes to cancer metastasis. Elevated SRC activity was observed in EOC and its inhibition was shown to significantly diminish invasion and induce apoptosis (Konecny et al., 2009; Simpkins et al., 2012; Wiener et al., 1999). The concomitant stimulation of ERK2 signaling was reported to confer resistances to the initially promising treatment with SRC inhibitors (McGivern et al., 2018; Simpkins et al., 2018). Nevertheless, kinase inhibitors are of increasing interest in resistant EOCs as kinases are involved in various signaling cascades allowing a fast tumor adaption (Katopodis et al., 2019). A combination of various kinase inhibitors thereby seems a beneficial strategy in targeting resistance mechanism. Here, IGF2BP1 was identified as

a marker for dual activation of SRC and ERK signaling while ERK2 expression was enhanced in an RNA-dependent mechanism through IGF2BP1 (Bley et al., 2021; Muller et al., 2018). Combined inhibition of SRC with saracatinib and ERK with the MEK inhibitor selumetinib effectively overcame the IGF2BP1-driven phenotype and showed anti-tumor activity. Thus, patients selected for IGF2BP1-positive tumors presumably benefit from a combinatorial SRC and MEK inhibition in mesenchymal HGSC.

#### **4.1 Upregulation of IGF2BP1 impairs AJ maintenance and promotes EMT in EOC**

HGSC is characterized by a high occurrence of peritoneal metastases. Its categorization into different molecular subtypes revealed the mesenchymal, proliferative C5 subtype which represents a dedifferentiated gene expression signature reflecting a mesenchymal shift (Tan et al., 2013; TCGA, 2011; Tothill et al., 2008). Above, the C5 subtype was associated with an upregulation of the cancer-related genes HMGA2 and LIN28B and the loss of miRNA let-7 (Helland et al., 2011). Apart from this, IGF2BP1 was shown to enhance these factors in an RNA-dependent manner by shielding their mRNAs from miRNA let-7 attack (Busch et al., 2016). Suggesting a pivotal role for IGF2BP1 in the C5 subtype, correlation analyses in three independent transcriptome datasets and immunohistochemical staining revealed a strong association of IGF2BP1 with the C5 gene expression signature (Bley et al., 2021). Together with the reported loss of CDH1-positive contacts within the C5 subtype (Tothill et al., 2008) and the here demonstrated IGF2BP1-driven AJ disassembly, this strengthens the hypothesis that IGF2BP1 essentially regulates the mesenchymal shift within the C5 subtype of HGSC promoting EMT which creates the basis for metastasis.

In detail, IGF2BP1 was shown to be associated with an EMT signature in a GSEA analysis and increases protein expression of several EMT-TFs which fits to the reported finding that IGF2BP1 stabilizes SNAI2 mRNA and promotes mesenchymal properties in a LEF1-dependent manner (Zirkel et al., 2013). An IGF2BP1-dependent modulation of cell morphology in epithelial-like NIH:OVCAR-3 and mesenchymal-like ES-2 cells favoring mesenchymal cell properties was observed. Moreover, immunostaining of CTNNB1 and CDH2 or CDH1 revealed that IGF2BP1 impairs the localization of these proteins to the plasma membrane and its assembling into contact structures. This demonstrates that IGF2BP1 interferes with AJ integrity in several EOC-derived cells. While a depletion of IGF2BP1 was only able to reassemble premature AJ contacts characterized through its zipper-like contact structures, the stable depletion of IGF2BP1 could establish mature CDH2-positive contacts. These two stages of the maturation process essentially differ in their arrangement of actin fibers and stability. The zipper-like or punctuate junctions are

usually found at the edge of cell colonies preferentially between mesenchymal-like cells enabling a fast and dynamic contact modulation. Linear junctions are mainly found in the interior of stable cell colonies (Takeichi, 2014). Thus, the different AJ structure between depleted and deleted IGF2BP1 suggests that lost IGF2BP1 abundance enables the establishment of mature cell contacts while only reduced IGF2BP1 levels seems to interfere with the assembly process leaving contacts in a premature state. However, the loss of IGF2BP1 expression failed to induce a shift from the mesenchymal CDH2 to the epithelial CDH1 within contact structures which could be observed by immunostaining so far. This suggests that a partially MET was induced which refers to gained epithelial properties while also some mesenchymal factors remained. Notably, the process of MET or EMT often occurs in an incomplete state and several factors should be taken into consideration to characterize the process (Dongre and Weinberg, 2019; Yang et al., 2020). Along with this, the absence of IGF2BP1 here positively modulated intercellular adhesion, induced an epithelial cell morphology and reduced EMT-TF expression. In contrast, over-expression of IGF2BP1 promoted AJ disassembly, partially cell detachment and invadopodia formation. For future analysis it would be interesting to visualize to which extent IGF2BP1 abundance reverts matured AJs to a zipper-like contact structure or if it induced a complete loss of adhesion within whole spheroids or tumors to weaken intercellular adhesion and enabling metastasis. So far, the immunofluorescent visualization was only performed in 2D growth.

The increase of cellular junctions under lost IGF2BP1 abundance further seems to slightly elevate the expression of AJ proteins seen in protein decay analysis of knockdown studies suggesting their stabilization through incorporation of these proteins into contact structures. This is further supported by the decreased phosphorylation of the stabilization factor CTNND1 which favors contact stabilization (Davis et al., 2003) while a direct control of the mRNAs of AJ components by IGF2BP1 was excluded. In particular, although a direct binding of IGF2BP1 to the CTNNB1 mRNA was reported in breast cancer cells and IGF2BP1 CLIPs were identified for CDH2 and CTNNB1 in four non-ovarian cell types (Gu et al., 2008), an association of IGF2BP1 with the CDH2 or CTNNB1 mRNA in the ovarian cancer cell line ES-2 could neither be detected via 3'UTR reporter analysis nor RNA decay or RIP analyses.

To further investigate the mechanism, how IGF2BP1 interferes with AJ integrity, the dynamic and fine-tuned balance of permanent AJ assembly and recycling was closer examined. The finding that IGF2BP1 drives the velocity and persistence of cell migration by constraining PIP<sub>3</sub>-directed RAC1 activation through direct binding to PTEN and MAPK4, has additionally drawn attention to the regulator of early step AJ assembly, RAC1 (Stohr et al., 2012). Accordingly, in this study pulldown assays of active RAC1 have shown an upregulation of RAC1 activity after an IGF2BP1 depletion. This directly links IGF2BP1 to the regulation of RAC1 activity without controlling RAC1 mRNA fate as indicated by RNA

sequencing analysis. Activation of RAC1 can be sustained directly through various GEFs process-dependently (Marei and Malliri, 2017). Thereby, the GEF TIAM1 essentially confers RAC1 activation during AJ assembly (Harris and Tepass, 2010). TIAM1 expression neither correlated with IGF2BP1 within the TCGA-OV cohort nor possess any IGF2BP1 CLIP sites. Interestingly, it was shown that TIAM1 was subjected to the regulation of the SRC kinase which is demonstrated to interfere with AJ integrity and their associated functions (Matsuyoshi et al., 1992; Woodcock et al., 2009; Yeatman, 2004).

Taken together, IGF2BP1 could be assigned with a pivotal role in promoting EMT by inducing AJ disassembly in an indirect manner, altering cell morphology and favoring mesenchymal cell properties. Concomitantly, it stimulated EMT-TF expression to maintain the mesenchymal cell state and was above associated with an EMT signature. An elevated EMT signature identified by single cell sequencing of HGSC cells was shown to correlate with poor prognosis as well as the abundance of IGF2BP1 in EOC (Hu et al., 2020; Kobel et al., 2007). The mechanism how IGF2BP1 interferes with AJs integrity further pointed to its described association with the SRC kinase which functions as a key regulator in adhesion (Huttelmaier et al., 2005).

## 4.2 The cooperation of the two oncogenic drivers SRC & IGF2BP1

The well characterized oncogene SRC was found to be associated with a set of cancer entities and SRC-directed inhibitors were in clinical trials as tumor therapy including ovarian cancer (Irby and Yeatman, 2000; McNeish et al., 2014). Already in 2005, SRC was shown to phosphorylate IGF2BP1 to release the bound ACTB mRNA from the mRNP complex controlling the spatial and temporal translation of actin in developing neurons (Huttelmaier et al., 2005). If IGF2BP1 in turn can activate SRC via a ligand binding induced mechanism was tested in this study. Interestingly, wild type IGF2BP1 promoted Tyr419-phosphorylation and thus activation of SRC in a dose-dependent manner. In contrast, SRC activation failed when the full length IGF2BP1 protein lacks the VP<sub>4</sub>SS motif, a binding motif identical to the SRC binding site in the adhesion molecule paxillin (Huttelmaier et al., 2005; Weng et al., 1993). This implies that binding of IGF2BP1 via its VP<sub>4</sub>SS motif to the SH3 domain of the SRC kinase effectively promotes SRC's open conformation which in turn enables autophosphorylation for the full activation of the kinase. Similar mechanisms were described for the mRBPs hnRNPK and SAM68 which specifically associate via proline-rich motifs with SRC, stimulate SRC activation and underly the control of SRC-dependent phosphorylation to activate translation of the bound mRNAs (Frisone et al., 2015; Ostareck-Lederer et al., 2002). Thus, the upregulation of IGF2BP1 induces SRC activation which in turn controls the release of the bound mRNAs based on the SRC-mediated alterations of IGF2BP1's binding affinities. This potentially creates a feedback loop of IGF2BP1 and SRC, both controlling

the activities of each other. Importantly, it could be further demonstrated that the IGF2BP1-driven SRC activation via the VP<sub>4</sub>SS motif is essential for AJ disassembly and equally required as its mRNA binding capacity to fulfill its full potential in promoting invasive growth.

Conversely, SRC inhibition phenocopied the AJ alteration observed upon IGF2BP1 depletion (Dosch et al., 2019; Nam et al., 2002). SRC was thereby described to function as key regulator in AJ turnover through directly phosphorylating AJ proteins promoting its internalization and degradation as it was indicated by the altered phosphorylation of CTNNB1 and CTNND1 within this study (Daugherty and Gottardi, 2007; Matsuyoshi et al., 1992; Qi et al., 2006; Roura et al., 1999; Woodcock et al., 2009). Besides, SRC modulates FAs to enable migration, invasion and thus metastasis (Boyer et al., 2002; Fincham and Frame, 1998; Playford and Schaller, 2004; Wozniak et al., 2004) as it is reported for IGF2BP1 (Bell et al., 2013; Degrauwe et al., 2016b; Muller et al., 2018). Both proteins act as oncogenic drivers and force similar cellular processes to promote cancer progression and thereby cooperate with each other. Likewise, it was previously reported for IGF2BP1 to act in concert with LIN28B and HMGA2 in an oncogenic and self-sustaining network in EOC-derived cells (Busch et al., 2016). However, here we identified for the first time an RNA-independent mechanism.

The inhibition of SRC activity with the approved inhibitor saracatinib was able to abolish the IGF2BP1-driven invasion which fits to reported findings (Guarino, 2010). In support of this, in *in vivo* settings SRC was further associated to essentially contribute to metastasis but not tumor growth (Criscuoli et al., 2005). Together, the interplay of IGF2BP1 and SRC controls a multitude of cellular processes and signaling cascades thereby shifting from an epithelial cell state to a more mesenchymal one allowing cells to migrate and invade the surrounding tissue.

Further investigations should extend the linkage between SRC activity and IGF2BP1 abundance beyond correlation data to reliable and comparable data within tumors. Phosphorylation events, which are used to indicate SRC activity, are post-translational protein modifications which enable a fast adaption to the microenvironment by transducing various signals into intracellular signaling cascades. These highly dynamic modifications are regulated through several different kinases and phosphatases and thus underly a high susceptibility to variations especially within *in vitro* assays. Promising tools are under current development which directly monitor SRC activity *in vivo*. For instance, the fluorescence resonance energy transfer (FRET) technique was used to visualize SRC activity in living cells via a genetically encoded SRC reporter and is already applied in various settings (Koudelkova et al., 2019; Ouyang et al., 2008; Wang et al., 2005). In the future, this could be extended to analyze HGSC cells with various IGF2BP1 wild type and mutant expression monitoring SRC activity and its localization as well as in combination with other cells. Another idea was based on bioluminescence imaging using split-



luminescence complementation for directly monitoring SRC activity in xenograft tumors but the successful establishment needs further evaluation (Leng et al., 2016). Nevertheless, bioluminescent imaging has a huge potential to monitor cellular processes and signaling via a non-invasive method and gets increasing interest (Manni et al., 2019; Su et al., 2020). A realization of conformation-dependent monitoring of SRC activity offers the potential of a real-time visualization of SRC signaling *in vivo* without detracting during sample preparation. This would allow associations with various microenvironmental factors, including drug application and immune responses, but could also reflect SRC activity during tumor development or even metastasis. Besides, classical bioluminescent assays analyzing mice tumor samples after surgery for SRC activity represent a more direct and faster technique and deliver more precise data that can link SRC activity and IGF2BP1 abundance within xenografts.

### **4.3 The strategies of IGF2BP1 to counter contact inhibition of proliferation**

The loss of adhesion is usually followed by a loss of contact inhibition of proliferation (CIP). It was early assumed that cell proliferation was inhibited as soon as cells reach a certain density and this process is mainly facilitated through cell-cell contacts (McClatchey and Yap, 2012). Thereby, different cadherins were associated to play an essential role in transducing these extracellular stimuli to intracellular responses (Grazia Lampugnani et al., 2003; Kim et al., 2011; Ozawa and Kemler, 1998; Perrais et al., 2007). Interestingly, during my master's thesis ribosomal profiling implied an overall shift of translation rate in an IGF2BP1-dependent manner indicating that IGF2BP1 potentially overcomes CIP. Here, the analysis of the overall translation rate by CLICK experiments demonstrated that the presence of IGF2BP1 sustains proliferation and overcomes CIP. This reflects a potential role of IGF2BP1 in uncontrolled growth during tumor initiation and progression, although the time point of IGF2BP1 upregulation within ovarian cancer development remains unknown.

The molecular mechanisms by which IGF2BP1 counter CIP can be manifold. Based on the here demonstrated induction of AJ turnover and the observed reduction of CIP through the upregulation of IGF2BP1 in ovarian cancer cells, modulating adhesion represents one potential strategy. Thereby, the IGF2BP1-induced SRC activation could impair hippo signaling through the loss of cadherin-based intercellular adhesion. Since the FRMD6-NF2-WWC1 complex usually co-localizes with AJs to classically activate the hippo pathway (Kim and Jho, 2018; Yu and Guan, 2013), a turnover and loss of AJs presumably will lead to mislocalized FRMD6-NF2-WWC1 complexes and a disruption of hippo signaling inducing YAP1's nuclear activity. Continuative studies could therefore visualize the intracellular

localization of these proteins in dependence of IGF2BP1 in various HGSC cell lines. Especially, the reported negative feedback loop of YAP1/WWTR1-stimulated LATS2 expression and its concomitant activation through NF2 could be another interesting point for future analysis (Kim and Jho, 2018; Moroishi et al., 2015; Yu and Guan, 2013). Therefore, it is worth investigating putative IGF2BP1 targets associated with adhesion since the cell polarity as well as the subcellular localization have huge impact on the complex regulation mechanisms of YAP1.

Next to the FRMD6-NF2-WWC1 complex, the apical polarity complex Crumbs and the TJs associated protein AMOT confer spatial inhibition of YAP1 activity by either activating the hippo pathway or sequestering YAP1 at the apical plasma membrane (Fulford et al., 2018; Ho et al., 2010; Kim and Jho, 2018; Yu and Guan, 2013; Yu et al., 2010). Depending on its phosphorylation status, AMOT was described to bind ACTB under cytoskeletal tension and is thereby unable to inhibit YAP1 activity. Additionally, hyperphosphorylation was seen to induce the nuclear entry of AMOT to promote the association of the co-activator YAP1 with the TEAD TFs (Chan et al., 2013; Fulford et al., 2018; Mana-Capelli et al., 2014). The basal polarity complex composed of SCRIB, DLG, and LGL antagonizing the apical one mediates the inhibition of hippo signaling through MARK kinases (Fulford et al., 2018; Heidary Arash et al., 2017; Mohseni et al., 2014; Wu and Griffin, 2017). Above, cell rearrangements including cytoskeletal tension, mechanical stimuli such as ECM stiffness and integrin activation were reported to favor the nuclear accumulation of YAP1 and thus its activity involving Rho-GTPases. In turn, YAP1 co-activates genes essential for FAs formation which creates a feedback loop to sustain tissue integrity (Dupont et al., 2011; Fulford et al., 2018). Together with the observation that YAP1's spatial localization and thus its activity was temporal coupled on cell shape in migrating fibroblasts depending on ACTB and SRC (Ege et al., 2018), this collectively highlights that YAP1's action is controlled by cell morphology, polarity and adhesion. Moreover, this suggests a putative linkage to IGF2BP1 as it is associated with a role in regulating cell morphology, adhesion and SRC activity (Bley et al., 2021; Huttelmaier et al., 2005; Zirkel et al., 2013). Next to elucidating further direct mRNA targets of IGF2BP1 including loss-of-function studies, immunofluorescence imaging of YAP1 seems to be a promising tool to further unravel the site of spatial regulation in an IGF2BP1-dependent manner.

One factor that is already negatively associated with YAP1 activity and IGF2BP1 abundance is the AJ protein CTNNA1. It was described to confer spatial inhibition of YAP1 activity at the site of AJs through binding via the 14-3-3 proteins the phosphorylation site of YAP1 preventing its nuclear translocation (Schlegelmilch et al., 2011; Silvis et al., 2011). Notably, one member of the 14-3-3 protein family, YWHAZ, was recently described as novel IGF2BP1 target (Glass et al., 2021) and should be considered next to its orthologs for further studies regarding IGF2BP1 in the regulation of the hippo pathway.

Besides, SRC activation represents an alternative strategy since previous findings have shown that the SRC kinase can uncouple YAP1 from the classical regulation via the hippo pathway. Apart from its role in adhesion, SRC's direct phosphorylation of the transcription activation domain within YAP1 inducing its nuclear activity and preventing its nuclear export in activated fibroblasts has led to nuclear accumulation of YAP1 (Ege et al., 2018; Lamar et al., 2019; Li et al., 2016). Additionally, it is assumed that altered focal adhesion and elevated SRC activation favor YAP1 nuclear localization through the inhibition of LATS1 caused by direct SRC phosphorylation (Si et al., 2017). To get first insights if the increased nuclear activity of YAP1 depends on SRC activation in our setting, inhibitor studies diminishing SRC activity with saracatinib were performed but rarely draw any conclusion. Considering the not fully understood conditions under which SRC directly or the classical hippo pathway control the action of YAP1 and the sensitive density-dependent regulation of both proteins, the experimental setting should be refined for future analyses. Thereby, different cell densities including 3D growth and microenvironmental factors should be addressed to better reflect the physiological conditions. To further test if the shifted YAP1 activity is mediated through SRC-dependent adhesion modulation or direct phosphorylation of hippo components, the phosphorylation status of LATS1 and YAP1 through SRC as well as inhibitor studies in dependence of IGF2BP1 need to be investigated.

Despite alternative regulation mechanisms, the main pathway facilitating CIP is the hippo pathway which was also seen to be affected through the presence of IGF2BP1 and thereby displays another strategy of IGF2BP1 overcoming CIP. Characterized by a phosphorylation cascade, the hippo pathway regulates YAP1 localization and action. As main effector of the hippo pathway, phosphorylated YAP1 restrains in the cytoplasm inhibiting proliferation while unphosphorylated YAP1 translocates to the nucleus and functions as a co-activator of TEAD-driven transcription of proliferative genes (Yu and Guan, 2013). Evaluating the activation of the hippo pathway, YAP1 activity was monitored by reporter assays described by (Dupont et al., 2011) within this study. Consistent with the CLICK experiments, IGF2BP1 abundance stimulated YAP1's transcriptional activity. To test if this effect is only due to the IGF2BP1-driven SRC activation and thus AJ disassembly or directly elicited by IGF2BP1, correlation studies with knockdown and tumor cohort RNA sequencing data as well as CLIP analysis of the core hippo components were performed. Surprisingly, a direct binding and thus stabilization of the YAP1 mRNA by IGF2BP1 was found. This association led to elevated YAP1 protein abundance which further shifted to a higher transcriptional activity of YAP1 which is supported by the correlation of IGF2BP1 expression to the YAP1/TEAD/WWTR1-driven gene expression signature postulated by (Zanconato et al., 2015). This directly links IGF2BP1 to the regulation of YAP1. Hence, the seen effects of YAP1 activity could also be assumed to be mediated directly through the

IGF2BP1-driven enhancement of YAP1 abundance. A fine-tuned stabilization of YAP1 through IGF2BP1 could possibly favor the upregulation of unphosphorylated YAP1 which is primed to enter the nucleus for the stimulation of gene transcription. A concomitant reduced hippo signaling through SRC phosphorylation within AJ or on hippo components directly thereby encourages the nuclear accumulation of YAP1. This could imply an interplay of all described strategies of IGF2BP1 to overcome CIP. However, further analyses are needed to evaluate the possibility of additional putative factors shifting the ratio of phosphorylated and unphosphorylated YAP1 and thereby influencing YAP1 activity in an IGF2BP1-dependent manner. Importantly, distinguishing to which extend the IGF2BP1-dependent SRC activation is responsible for a shifted YAP1 activity or the IGF2BP1-dependent post-transcriptional control of YAP1 mRNA contributes to a nuclear YAP1 accumulation, will be of future interest. Therefore, analyses of the nuclear activity of YAP1 and overall translation rate referring to CIP with the different IGF2BP1 mutants from this study in concert with inhibitor experiments could be beneficial.

Taken together, upregulation of IGF2BP1 in a subset of HGSC as well as its function in SRC activation and turnover of intercellular cadherin-based junctions interferes with CIP. At the same time, IGF2BP1 directly associates and stabilizes the YAP1 mRNA to further enhances YAP1-stimulated transcription. In concert, reduced adhesion potentially leads to less stimulation of the hippo pathway which in turn shifts the balance of increased YAP1 abundance to more unphosphorylated, nuclear YAP1 in an IGF2BP1-dependent manner. Based on this, IGF2BP1 essentially impacts proliferation by tackling YAP1, a key point controlling intracellular signal transduction. This versatile approach of IGF2BP1 facilitates uncontrolled growth and thereby disrupts tissue integrity.

Apart from this, several studies connected hippo and TP53 signaling on various levels. For instance, LATS2 was seen to protect TP53 from degradation through MDM2 resulting in TP53 accumulation and activation. An interaction between mutant TP53 and YAP1 seems to transcriptionally stimulate cell cycle-related gene expression in breast cancer cells while this association is non-existent with wild type TP53 conformation-dependently (Di Agostino et al., 2016; Furth et al., 2018; Raj and Bam, 2019). Considering the mutational background of TP53 in HGSC and the reported upregulation of YAP1 in these tumors (Cho et al., 2017; Wang et al., 2020), this additionally could contribute to the reported enrichment of the cell cycle gene set within the gene enrichment analyses next to IGF2BP1's impact on cell cycle (Muller et al., 2020). However, both are critical regulators of cellular adaption aiming to maintain genome and tissue integrity. Together with the early occurring mutation of TP53 in HGSC, YAP1 could cooperate with TP53 in HGSC tumorigenesis.

#### 4.4 Targeted treatment strategies for IGF2BP1-driven ovarian tumors

HGSC is characterized by a high genomic instability, cellular heterogeneity and frequent relapse accompanied by occurring resistances. The high genomic instability of HGSC makes it sensitive to platinum-based chemotherapy and PARP inhibition but concomitantly the high plasticity allows a fast adaption of the tumor leading to the development of resistances (Bowtell et al., 2015; Patch et al., 2015). Investigating resistance mechanism advances the establishment of targeted therapies. Intercellular adhesion thereby creates a basis for the transduction of extracellular stimuli from the microenvironment to various intracellular signaling pathways enabling tumor adaption. However, the high frequency of TP53 mutations within HGSC tumors also contributes to genomic instability, proliferation, stemness and drug resistance (Shetzer et al., 2014). Multidrug chemoresistance by mutant TP53 was referred to the transcriptional upregulation of the drug efflux pump MDR1 (Zhu et al., 2020).

Interestingly, Taxol-based therapy resistance was associated with the mRNA stabilization and upregulation of MDR1 through IGF2BP1 presumably shielding it from let-7g miRNA attack. Consistently, an upregulation of MDR1 and IGF2BP1 was frequently observed in relapsed ovarian cancer patient and seems to predict an early recurrence (Boyerinas et al., 2012). Considering the tumor-selective expression of the oncogenic driver IGF2BP1 and its upregulation within ovarian cancer, targeting of IGF2BP1 seems tempting. The recently developed small molecule inhibitor BTYNB specifically inhibits the binding of IGF2BP1 to its target mRNAs and showed promising anti-proliferative effects in ovarian preclinical studies (Mahapatra et al., 2017).

Along with this, an upregulated YAP1 expression was observed in HGSC patients (Cho et al., 2017; Wang et al., 2020) and its activity could be connected to resistance to the current chemotherapeutics in ovarian cancer. In particular, YAP1 was shown to confer resistance to Cisplatin and Taxol in 2D viability assays (Hall et al., 2010; Song et al., 2018; Xia et al., 2014; Zhang et al., 2011). Additionally, the above-mentioned association of YAP1 with mutant TP53 (Di Agostino et al., 2016; Furth et al., 2018; Raj and Bam, 2019) possibly indicates a cooperative role in early steps of HGSC development. Together with its association in facilitating chemoresistance, YAP1 also represents as an interesting therapeutic target.

Besides, the oncogene SRC was shown to be upregulated in ovarian cancer (Simpkins et al., 2012). A proteome-wide analysis of tyrosine phosphorylation in ovarian tumor samples revealed 19 dysregulated tyrosine kinases, including several SRC family members which were significantly enriched. Following immunohistochemical staining verified the enhanced abundance of SRC in ovarian tumor tissue sections compared to normal ovary tissue (Song et al., 2019). The here demonstrated IGF2BP1-dependent but RNA-

independent stimulation of SRC activity driving invasiveness *in vitro* and its known function in tumorigenesis (Summy and Gallick, 2003) assign SRC with a critical role in metastasis which is a frequent problem in HGSC. Although monotherapies with saracatinib failed to improve PFS in platinum-resistant ovarian cancer (McNeish et al., 2014), a subtype-specific inhibition of SRC in EMT-high tumors (Hu et al., 2020) could be beneficial to reduce metastasis and early recurrence. The identification of cellular adaptation responses and their key drivers are essential to develop targeted treatment strategies. The signaling molecules YAP1 and SRC as well as the post-transcriptional modulator IGF2BP1, which either possess exceptional expression or activity in ovarian cancer or were already associated with chemoresistance, are key regulators that can enable a fast adaptation within tumors. The broad impact of these proteins creates a rationale targeting them in cancer therapy.

In this study different drug combinations were evaluated in first line for their efficacy and synergy in 2D growth assays using drug matrices. The interplay of IGF2BP1 and YAP1 and their role in chemoresistance in ovarian cancer emphasized the evaluation of the inhibitor combination for their synergy. Inhibition of the two proteins were carried out by the combination of BTYNB and verteporfin but failed to show synergistic effects. Similar results were seen for the combination of saracatinib and BTYNB, although targeting the dual functions of IGF2BP1, its mRNA binding capacity and the SRC activation, seemed promising. Interestingly, targeting the two independently IGF2BP1-stimulated signaling molecules SRC and YAP1 with a combination of saracatinib and verteporfin exhibited potentially synergistic effects for some concentration combinations.

SRC inhibition alone initially proved promising, especially in sensitizing cells to paclitaxel treatment in preclinical *in vitro* and *in vivo* studies (Le et al., 2011). Unfortunately, under clinical evaluation there was neither an improvement of paclitaxel activity in patients with platinum-resistant ovarian cancer nor on PFS and overall survival (McNeish et al., 2014). The finding that saracatinib treatment often comes along with frequently occurring resistance to saracatinib shadowed the initial benefits. Concomitant with saracatinib resistance, ERK activation (MAPK pathway activation) was observed linking its upregulation to the developed resistance while dual inhibition beneficially targeted tumor growth in an ovarian mouse model (McGivern et al., 2018).

Further studies which aimed to characterize adaptive responses to chemotherapy by reverse-phase protein arrays further revealed that PARP inhibition also induced the activation of the MAPK pathway mediating PARP resistance. Dual inhibition showed synergistic effect *in vitro* and *in vivo* while an ongoing clinical trial is evaluating the combination of the PARP inhibitor olaparib and the MEK inhibitor selumetinib in ovarian and other solid cancers including PARP-resistant ones (Sun et al., 2020). Due to the reported finding that IGF2BP1 enhances ERK2 and SRF expression and thereby their transcriptional activity, this emphasized the need to test the recommended combination of saracatinib and

selumetinib against the IGF2BP1-driven phenotype (McGivern et al., 2018; Muller et al., 2018; Muller et al., 2019).

Although YAP1 was shown to promote resistance to MEK-targeted therapy in non-small lung cancer (Lin 2015), dual inhibition of SRC and MEK could potentially inhibit YAP1 activity as it responds to SRC inhibition, previously described. In particular, the SRC inhibitor dasatinib was shown to effectively inhibit YAP1 activity in *in vitro* studies of renal cell carcinoma (Sun et al., 2018). If similar effects can be achieved in ovarian cancer, needs to be investigated in future analyses. Nevertheless, uncontrolled YAP1 enforces a tremendous impact in tumorigenesis but its inhibition also diminishes its beneficial function in tissue repair and regeneration required for instance after cytoreductive surgery (Johnson and Halder, 2014). This requests the benefit of YAP1 inhibition. Consequently, the combined inhibition of SRC and ERK with saracatinib and selumetinib seems to unroll a higher clinical potential and was further evaluated and tested for its synergy and potential in targeting the IGF2BP1-driven phenotypes.

Synergistic effects of dual drug treatment with saracatinib and selumetinib was already described in 2D colony growth assays (McGivern et al., 2018). Here, we shifted the assays to 3D cell culture to better reproduce the tumor surrounding which was requested in an opinion article although a co-cultivation with fibroblasts and mesothelial cell was not applied here (Bowtell et al., 2015). The spheroids were grown matrix-embedded and matrix-free. Applying a drug matrix to assess synergy of the combination allows the accurate identification of the lowest concentration with the highest efficacy. The 3D cultivation was especially important in regard of the demonstrated role of IGF2BP1 in intercellular junctions referring to a comparison of 2D and 3D cell cultures that revealed that the extent of cell-cell contacts depends on their microenvironment. Surprisingly, it could be shown that tumor spheroids established less cell-cell contacts compared to its monolayer cultures of ovarian cancer cells and this correlates with its drug resistance (Kutova et al., 2020).

However, the combination of both inhibitors was able to effectively overcome the IGF2BP1-driven invasive growth *in vitro* and the tumor growth *in vivo*. While saracatinib showed a higher sensitivity in inhibiting invasion, selumetinib was more effective in the inhibition of spheroid growth in monotherapies. Consequently, saracatinib was able to abolish the IGF2BP1-driven spheroid invasion while spheroid growth was only modestly reduced fitting to its role in invasion and metastasis shown in previous publications (Boyer et al., 2002; Criscuoli et al., 2005; Guarino, 2010). The reverse effect was seen for selumetinib which is in accordance with the associated function of ERK in proliferation (Lavoie et al., 2020). Obviously, IGF2BP1 abundance correlated with an increased drug tolerance. In both cases, IGF2BP1 over-expression seems to confer resistance while an IGF2BP1 depletion sensitized the cells in the respective phenotype. Using only half of the drug concentration in a combination therapy compared to the monotherapy, combined

treatment was effective in inhibiting both phenotypes independent of IGF2BP1 abundance. The drug combination overall showed additive effects with clearly synergistic effects for some concentration combinations fitting to the reported synergy in 2D assays (McGivern et al., 2018).

In support of this, similar experiments with dual SRC and MEK inhibition were reported in the NIH:OVCAR-3, SK-OV3, OVCAR5 cell line. The combined inhibition partially restored CDH1 levels, altered cell morphology and was connected to the absence of active RAC1. Moreover, expression of constitutively active MEK and SRC induced TWIST1, ZEB1 and ZEB2 expression. Consistently, the combinatorial effect was much stronger as the one of the single agents (Fang et al., 2017). Together, these data and our observations strongly suggest that the combined treatment of ovarian tumors with SRC and MEK inhibitors can encounter EMT-driven tumors and metastasis. Due to the tumor-selective expression of IGF2BP1 (Bell et al., 2013), its association with the mesenchymal/proliferative C5 subtype of HGSC (Bley et al., 2021) and its interplay with the SRC kinase, IGF2BP1 can be recommended as a biomarker for selecting patients potentially benefitting from a combined therapy of SRC and MEK inhibitors.

Coming back to the mutational background of HGSC, TP53 mutations are known as the earliest occurring alteration in the initiation of HGSC (Ahmed et al., 2010; TCGA, 2011). The time point and mechanism of IGF2BP1 upregulation in a subset of HGSC tumors is unknown. Interestingly, next to the cooperation of mutant TP53 with YAP1, it was shown that mutant TP53 also represses the transcription of let-7i miRNA thereby leading to enhanced migration and invasion under the repression E2F5, LIN28B, MYC and NRAS (Subramanian et al., 2015). An almost identical target set and involvement was found for IGF2BP1 indicating a potential interconnection or overlaid functions of both (Busch et al., 2016; Mackedenski et al., 2018; Muller et al., 2020; Weidensdorfer et al., 2009). In regard of this, a first connection was drawn in murine ID8 cells in which the deleted expression of TP53 induced IGF2BP1 expression. Above, this forced expression suggests an upregulation of SRC activity while a deletion of IGF2BP1 on top again reduced SRC activation. Together, this makes it worth to additionally consider the IGF2BP1 inhibitor BTYNB or its derivatives for further mechanistical evaluation. The data therefore can be found in the appendix (Figure 37). The used CRISPR/Cas9-edited cells were kindly provided by Prof. Iain McNeish. The results are completely preliminary but represent an interesting observation and important research tool which should further investigated in future analyses. The induction of several HGSC-related mutations such as TP53 in the murine ID8 cells, derived from ovarian surface epithelium, allows the establishment of a transplantable murine mouse model suitable to address the biology of HGSC, potential treatment strategies, the microenvironment and immune responses (Walton et al., 2016), also in dependence of IGF2BP1.



To broaden the view, TP53 mutations are found across different entities of human cancers and therapeutic targeting of mutated TP53 protein is of great interest involving various strategies to restore wild type conformation, induce targeted degradation or synthetic lethality. Under preclinical evaluation are immunotherapies, RNAi, small molecular compounds and synthetic peptides. To highlight is the small peptide-based therapy aiming to restore TP53 wild type function and showed promising anti-cancer effects in *in vivo* models for ovarian cancer. These ambitious tools specifically encountering the multiple functions of mutant TP53 are still in its infancy but seems to be promising for future applications in HGSC (Zhu et al., 2020). For now, combination therapy including kinase inhibitors are more feasible and could be beneficial in targeting resistance mechanism. Thereby, making advantage of the already evaluated tolerability and partially efficacy in clinical trials, this allows a fast way of incorporation into clinical utility. Importantly, the C5-selective expression of IGF2BP1 accompanied by the dual activation of SRC and ERK signaling here proposes a subtype-specific targeted treatment strategy.

## 5 SUMMARY

High-grade serous ovarian carcinomas (HGSCs), the most common form of ovarian cancers, are characterized by frequent metastasis and occurring resistances to the current standard therapies. The upregulation within the mesenchymal C5 subtype of HGSC and the almost mutually exclusive expression within tumors, suggest a pivotal role of the post-translational regulator IGF2BP1 in HGSC.

Here, IGF2BP1 was found to essentially regulate key signaling molecules such as SRC, ERK2 and YAP1 to control a plethora of cellular processes facilitating tumor progression in ovarian cancer cells. In detail, IGF2BP1 promotes SRC activation in an unexpected ligand binding induced, RNA-independent mechanism to interfere with AJ integrity. The SRC kinase thereby induces the phosphorylation and disassembly of AJ components. Concomitantly, IGF2BP1 enhances EMT-TF expression and affects the activity of the early step regulator of AJ assembly, RAC1, to promote EMT and sustain a mesenchymal cell state. The IGF2BP1-driven loss of AJs thereby creates the basis for invasive growth and tumor spreading. Next to the diminished intercellular adhesion, the direct stabilization of the YAP1 mRNA through IGF2BP1 leads to a deregulation of the hippo pathway and reduces contact inhibition of proliferation. Thereby, YAP1 is forced to translocate to the nucleus and activate proliferative gene expression. Similarly, the reported association of IGF2BP1 with the ERK2 mRNA triggers the activation of ERK signaling and the expression of multiple genes involved in cancer progression and resistance mechanisms. Together, this links the interconnected stimulation of SRC and ERK2 signaling, reported in ovarian cancer, to the post-transcriptional action of IGF2BP1. Consistently, the IGF2BP1-driven invasive growth, which essentially relies on the RNA-independent SRC activation as well as on the mRNA binding capacity of IGF2BP1, was targetable by dual inhibition of SRC and ERK. Compared to its monotherapies, only the combinatorial inhibition of SRC with saracatinib and ERK with the MEK inhibitor selumetinib was able to effectively overcome the IGF2BP1-driven phenotype *in vitro* and *in vivo*.

Thus, the findings of this study highlight the relevance of IGF2BP1 within mesenchymal-like HGSC and gave insights into its various molecular action allowing a fast adaption of the tumor to its microenvironment, important during metastasis and resistance development. Thereby, IGF2BP1 is proposed as a biomarker for dual SRC/ERK activation in mesenchymal HGSC. Targeting IGF2BP1-positive tumors with a combination of SRC and MEK inhibitors seems a beneficial, subtype-specific treatment strategy and is recommended for further evaluation.

## REFERENCES

- Adhikari, S., Moran, J., Weddle, C., and Hinczewski, M. (2018). Unraveling the mechanism of the cadherin-catenin-actin catch bond. *PLoS Comput Biol* *14*, e1006399.
- Ahmed, A.A., Becker, C.M., and Bast, R.C., Jr. (2012). The origin of ovarian cancer. *BJOG* *119*, 134-136.
- Ahmed, A.A., Etemadmoghadam, D., Temple, J., Lynch, A.G., Riad, M., Sharma, R., Stewart, C., Fereday, S., Caldas, C., Defazio, A., *et al.* (2010). Driver mutations in TP53 are ubiquitous in high grade serous carcinoma of the ovary. *J Pathol* *221*, 49-56.
- Balda, M.S., and Matter, K. (2008). Tight junctions at a glance. *J Cell Sci* *121*, 3677-3682.
- Bast, R.C., Jr., Lu, Z., Han, C.Y., Lu, K.H., Anderson, K.S., Drescher, C.W., and Skates, S.J. (2020). Biomarkers and Strategies for Early Detection of Ovarian Cancer. *Cancer Epidemiol Biomarkers Prev* *29*, 2504-2512.
- Bast, R.C., Jr., Matulonis, U.A., Sood, A.K., Ahmed, A.A., Amobi, A.E., Balkwill, F.R., Wielgos-Bonvallet, M., Bowtell, D.D.L., Brenton, J.D., Brugge, J.S., *et al.* (2019). Critical questions in ovarian cancer research and treatment: Report of an American Association for Cancer Research Special Conference. *Cancer* *125*, 1963-1972.
- Behrens, B.C., Hamilton, T.C., Masuda, H., Grotzinger, K.R., Whang-Peng, J., Louie, K.G., Knutsen, T., McKoy, W.M., Young, R.C., and Ozols, R.F. (1987). Characterization of a cis-diamminedichloroplatinum(II)-resistant human ovarian cancer cell line and its use in evaluation of platinum analogues. *Cancer Res* *47*, 414-418.
- Bell, J.L., Turlapati, R., Liu, T., Schulte, J.H., and Huttelmaier, S. (2015). IGF2BP1 harbors prognostic significance by gene gain and diverse expression in neuroblastoma. *J Clin Oncol* *33*, 1285-1293.
- Bell, J.L., Wachter, K., Muhleck, B., Pazaitis, N., Kohn, M., Lederer, M., and Huttelmaier, S. (2013). Insulin-like growth factor 2 mRNA-binding proteins (IGF2BPs): post-transcriptional drivers of cancer progression? *Cellular and molecular life sciences* : *CMLS* *70*, 2657-2675.
- Berrier, A.L., and Yamada, K.M. (2007). Cell-matrix adhesion. *J Cell Physiol* *213*, 565-573.
- Bertocchi, C., Vaman Rao, M., and Zaidel-Bar, R. (2012). Regulation of adherens junction dynamics by phosphorylation switches. *J Signal Transduct* *2012*, 125295.
- Bjorge, J.D., Pang, A., and Fujita, D.J. (2000). Identification of protein-tyrosine phosphatase 1B as the major tyrosine phosphatase activity capable of dephosphorylating and activating c-Src in several human breast cancer cell lines. *J Biol Chem* *275*, 41439-41446.
- Bley, N., Schott, A., Muller, S., Misiak, D., Lederer, M., Fuchs, T., Assmann, C., Glass, M., Ihling, C., Sinz, A., *et al.* (2021). IGF2BP1 is a targetable SRC/MAPK-dependent driver of invasive growth in ovarian cancer. *RNA Biol* *18*, 391-403.
- Bowtell, D.D. (2010). The genesis and evolution of high-grade serous ovarian cancer. *Nat Rev Cancer* *10*, 803-808.
- Bowtell, D.D., Bohm, S., Ahmed, A.A., Aspuria, P.J., Bast, R.C., Jr., Beral, V., Berek, J.S., Birrer, M.J., Blagden, S., Bookman, M.A., *et al.* (2015). Rethinking ovarian cancer II: reducing mortality from high-grade serous ovarian cancer. *Nat Rev Cancer* *15*, 668-679.
- Boyer, B., Bourgeois, Y., and Poupon, M.F. (2002). Src kinase contributes to the metastatic spread of carcinoma cells. *Oncogene* *21*, 2347-2356.

- Boyerinas, B., Park, S.M., Murmann, A.E., Gwin, K., Montag, A.G., Zillhardt, M., Hua, Y.J., Lengyel, E., and Peter, M.E. (2012). Let-7 modulates acquired resistance of ovarian cancer to Taxanes via IMP-1-mediated stabilization of multidrug resistance 1. *Int J Cancer* *130*, 1787-1797.
- Bromann, P.A., Korkaya, H., and Courtneidge, S.A. (2004). The interplay between Src family kinases and receptor tyrosine kinases. *Oncogene* *23*, 7957-7968.
- Brooks, E.A., Galarza, S., Gencoglu, M.F., Cornelison, R.C., Munson, J.M., and Peyton, S.R. (2019). Applicability of drug response metrics for cancer studies using biomaterials. *Philos Trans R Soc Lond B Biol Sci* *374*, 20180226.
- Brulet, P., Babinet, C., Kemler, R., and Jacob, F. (1980). Monoclonal antibodies against trophectoderm-specific markers during mouse blastocyst formation. *Proc Natl Acad Sci U S A* *77*, 4113-4117.
- Busch, B., Bley, N., Muller, S., Glass, M., Misiak, D., Lederer, M., Vetter, M., Strauss, H.G., Thomssen, C., and Huttelmaier, S. (2016). The oncogenic triangle of HMGA2, LIN28B and IGF2BP1 antagonizes tumor-suppressive actions of the let-7 family. *Nucleic acids research* *44*, 3845-3864.
- Calautti, E., Cabodi, S., Stein, P.L., Hatzfeld, M., Kedersha, N., and Paolo Dotto, G. (1998). Tyrosine phosphorylation and src family kinases control keratinocyte cell-cell adhesion. *J Cell Biol* *141*, 1449-1465.
- Chan, S.W., Lim, C.J., Guo, F., Tan, I., Leung, T., and Hong, W. (2013). Actin-binding and cell proliferation activities of angiomin family members are regulated by Hippo pathway-mediated phosphorylation. *J Biol Chem* *288*, 37296-37307.
- Chang, F., Lemmon, C., Lietha, D., Eck, M., and Romer, L. (2011). Tyrosine phosphorylation of Rac1: a role in regulation of cell spreading. *PLoS One* *6*, e28587.
- Chen, C.S., Hong, S., Indra, I., Sergeeva, A.P., Troyanovsky, R.B., Shapiro, L., Honig, B., and Troyanovsky, S.M. (2015). alpha-Catenin-mediated cadherin clustering couples cadherin and actin dynamics. *J Cell Biol* *210*, 647-661.
- Chen, X., and Macara, I.G. (2005). Par-3 controls tight junction assembly through the Rac exchange factor Tiam1. *Nat Cell Biol* *7*, 262-269.
- Cheung, L.W., Leung, P.C., and Wong, A.S. (2010). Cadherin switching and activation of p120 catenin signaling are mediators of gonadotropin-releasing hormone to promote tumor cell migration and invasion in ovarian cancer. *Oncogene* *29*, 2427-2440.
- Cho, S.Y., Kim, K., Park, M.S., Jang, M.Y., Choi, Y.H., Han, S., Shin, H.M., Chung, C., Han, H.Y., Yang, J.B., *et al.* (2017). Expression of Yes-associated protein 1 and its clinical significance in ovarian serous cystadenocarcinoma. *Oncol Rep* *37*, 2620-2632.
- Choi, S.H., Estaras, C., Moresco, J.J., Yates, J.R., 3rd, and Jones, K.A. (2013). alpha-Catenin interacts with APC to regulate beta-catenin proteolysis and transcriptional repression of Wnt target genes. *Genes & development* *27*, 2473-2488.
- Chung, Y.C., Wei, W.C., Huang, S.H., Shih, C.M., Hsu, C.P., Chang, K.J., and Chao, W.T. (2014). Rab11 regulates E-cadherin expression and induces cell transformation in colorectal carcinoma. *BMC Cancer* *14*, 587.
- Cleynen, I., Brants, J.R., Peeters, K., Deckers, R., Debiec-Rychter, M., Sciot, R., Van de Ven, W.J., and Petit, M.M. (2007). HMGA2 regulates transcription of the *Imp2* gene via an intronic regulatory element in cooperation with nuclear factor-kappaB. *Mol Cancer Res* *5*, 363-372.
- Coates, J.C. (2003). Armadillo repeat proteins: beyond the animal kingdom. *Trends Cell Biol* *13*, 463-471.
- Coleman, R.L., Monk, B.J., Sood, A.K., and Herzog, T.J. (2013). Latest research and treatment of advanced-stage epithelial ovarian cancer. *Nat Rev Clin Oncol* *10*, 211-224.

- Conway, A.E., Van Nostrand, E.L., Pratt, G.A., Aigner, S., Wilbert, M.L., Sundararaman, B., Freese, P., Lambert, N.J., Sathe, S., Liang, T.Y., *et al.* (2016). Enhanced CLIP Uncovers IMP Protein-RNA Targets in Human Pluripotent Stem Cells Important for Cell Adhesion and Survival. *Cell Rep* *15*, 666-679.
- Cortes-Reynosa, P., Robledo, T., Macias-Silva, M., Wu, S.V., and Salazar, E.P. (2008). Src kinase regulates metalloproteinase-9 secretion induced by type IV collagen in MCF-7 human breast cancer cells. *Matrix Biol* *27*, 220-231.
- Criscuoli, M.L., Nguyen, M., and Eliceiri, B.P. (2005). Tumor metastasis but not tumor growth is dependent on Src-mediated vascular permeability. *Blood* *105*, 1508-1514.
- Curtis, M.W., Johnson, K.R., and Wheelock, M.J. (2008). E-cadherin/catenin complexes are formed cotranslationally in the endoplasmic reticulum/Golgi compartments. *Cell Commun Adhes* *15*, 365-378.
- Dai, N., Rapley, J., Angel, M., Yanik, M.F., Blower, M.D., and Avruch, J. (2011). mTOR phosphorylates IMP2 to promote IGF2 mRNA translation by internal ribosomal entry. *Genes & development* *25*, 1159-1172.
- Daniel, J.M., and Reynolds, A.B. (1999). The catenin p120(ctn) interacts with Kaiso, a novel BTB/POZ domain zinc finger transcription factor. *Mol Cell Biol* *19*, 3614-3623.
- Daugherty, R.L., and Gottardi, C.J. (2007). Phospho-regulation of Beta-catenin adhesion and signaling functions. *Physiology (Bethesda)* *22*, 303-309.
- Davis, M.A., Ireton, R.C., and Reynolds, A.B. (2003). A core function for p120-catenin in cadherin turnover. *J Cell Biol* *163*, 525-534.
- Degrauwe, N., Schlumpf, T.B., Janiszewska, M., Martin, P., Cauderay, A., Provero, P., Riggi, N., Suva, M.L., Paro, R., and Stamenkovic, I. (2016a). The RNA Binding Protein IMP2 Preserves Glioblastoma Stem Cells by Preventing let-7 Target Gene Silencing. *Cell Rep* *15*, 1634-1647.
- Degrauwe, N., Suva, M.L., Janiszewska, M., Riggi, N., and Stamenkovic, I. (2016b). IMPs: an RNA-binding protein family that provides a link between stem cell maintenance in normal development and cancer. *Genes & development* *30*, 2459-2474.
- DeMali, K.A., Godwin, S.L., Soltoff, S.P., and Kazlauskas, A. (1999). Multiple roles for Src in a PDGF-stimulated cell. *Exp Cell Res* *253*, 271-279.
- Desai, R., Sarpal, R., Ishiyama, N., Pellikka, M., Ikura, M., and Tepass, U. (2013). Monomeric alpha-catenin links cadherin to the actin cytoskeleton. *Nat Cell Biol* *15*, 261-273.
- Di Agostino, S., Sorrentino, G., Ingallina, E., Valenti, F., Ferraiuolo, M., Biciato, S., Piazza, S., Strano, S., Del Sal, G., and Blandino, G. (2016). YAP enhances the pro-proliferative transcriptional activity of mutant p53 proteins. *EMBO Rep* *17*, 188-201.
- Dimitriadis, E., Trangas, T., Milatos, S., Foukas, P.G., Gioulbasanis, I., Courtis, N., Nielsen, F.C., Pandis, N., Dafni, U., Bardi, G., *et al.* (2007). Expression of oncofetal RNA-binding protein CRD-BP/IMP1 predicts clinical outcome in colon cancer. *Int J Cancer* *121*, 486-494.
- Domcke, S., Sinha, R., Levine, D.A., Sander, C., and Schultz, N. (2013). Evaluating cell lines as tumour models by comparison of genomic profiles. *Nat Commun* *4*, 2126.
- Dongre, A., and Weinberg, R.A. (2019). New insights into the mechanisms of epithelial-mesenchymal transition and implications for cancer. *Nat Rev Mol Cell Biol* *20*, 69-84.
- Dosch, A.R., Dai, X., Gaidarski Iii, A.A., Shi, C., Castellanos, J.A., VanSaun, M.N., Merchant, N.B., and Nagathihalli, N.S. (2019). Src kinase inhibition restores E-cadherin expression in dasatinib-sensitive pancreatic cancer cells. *Oncotarget* *10*, 1056-1069.

- Doyle, G.A., Betz, N.A., Leeds, P.F., Fleisig, A.J., Prokipcak, R.D., and Ross, J. (1998). The c-myc coding region determinant-binding protein: a member of a family of KH domain RNA-binding proteins. *Nucleic Acids Res* 26, 5036-5044.
- Drees, F., Pokutta, S., Yamada, S., Nelson, W.J., and Weis, W.I. (2005). Alpha-catenin is a molecular switch that binds E-cadherin-beta-catenin and regulates actin-filament assembly. *Cell* 123, 903-915.
- du Bois, A., Reuss, A., Pujade-Lauraine, E., Harter, P., Ray-Coquard, I., and Pfisterer, J. (2009). Role of surgical outcome as prognostic factor in advanced epithelial ovarian cancer: a combined exploratory analysis of 3 prospectively randomized phase 3 multicenter trials: by the Arbeitsgemeinschaft Gynaekologische Onkologie Studiengruppe Ovarialkarzinom (AGO-OVAR) and the Groupe d'Investigateurs Nationaux Pour les Etudes des Cancers de l'Ovaire (GINECO). *Cancer* 115, 1234-1244.
- DuBridge, R.B., Tang, P., Hsia, H.C., Leong, P.M., Miller, J.H., and Calos, M.P. (1987). Analysis of mutation in human cells by using an Epstein-Barr virus shuttle system. *Mol Cell Biol* 7, 379-387.
- Dupont, S., Morsut, L., Aragona, M., Enzo, E., Giulitti, S., Cordenonsi, M., Zanconato, F., Le Digabel, J., Forcato, M., Bicciato, S., *et al.* (2011). Role of YAP/TAZ in mechanotransduction. *Nature* 474, 179-183.
- Ege, N., Dowbaj, A.M., Jiang, M., Howell, M., Hooper, S., Foster, C., Jenkins, R.P., and Sahai, E. (2018). Quantitative Analysis Reveals that Actin and Src-Family Kinases Regulate Nuclear YAP1 and Its Export. *Cell Syst* 6, 692-708 e613.
- Elcheva, I., Goswami, S., Noubissi, F.K., and Spiegelman, V.S. (2009). CRD-BP protects the coding region of betaTrCP1 mRNA from miR-183-mediated degradation. *Molecular cell* 35, 240-246.
- Fakhraldein, S.A., Clark, R.J., Roopra, A., Chin, E.N., Huang, W., Castorino, J., Wisinski, K.B., Kim, T., Spiegelman, V.S., and Alexander, C.M. (2015). Two Isoforms of the RNA Binding Protein, Coding Region Determinant-binding Protein (CRD-BP/IGF2BP1), Are Expressed in Breast Epithelium and Support Clonogenic Growth of Breast Tumor Cells. *J Biol Chem* 290, 13386-13400.
- Faleiro-Rodrigues, C., Macedo-Pinto, I., Pereira, D., and Lopes, C.S. (2004). Prognostic value of E-cadherin immunoexpression in patients with primary ovarian carcinomas. *Ann Oncol* 15, 1535-1542.
- Fang, D., Chen, H., Zhu, J.Y., Wang, W., Teng, Y., Ding, H.F., Jing, Q., Su, S.B., and Huang, S. (2017). Epithelial-mesenchymal transition of ovarian cancer cells is sustained by Rac1 through simultaneous activation of MEK1/2 and Src signaling pathways. *Oncogene* 36, 1546-1558.
- Farina, K.L., Huttelmaier, S., Musunuru, K., Darnell, R., and Singer, R.H. (2003). Two ZBP1 KH domains facilitate beta-actin mRNA localization, granule formation, and cytoskeletal attachment. *J Cell Biol* 160, 77-87.
- Farley, J., Brady, W.E., Vathipadiekal, V., Lankes, H.A., Coleman, R., Morgan, M.A., Mannel, R., Yamada, S.D., Mutch, D., Rodgers, W.H., *et al.* (2013). Selumetinib in women with recurrent low-grade serous carcinoma of the ovary or peritoneum: an open-label, single-arm, phase 2 study. *Lancet Oncol* 14, 134-140.
- Fincham, V.J., and Frame, M.C. (1998). The catalytic activity of Src is dispensable for translocation to focal adhesions but controls the turnover of these structures during cell motility. *EMBO J* 17, 81-92.
- Fogh, J. (1986). Human tumor lines for cancer research. *Cancer Invest* 4, 157-184.
- Fogh, J., Fogh, J.M., and Orfeo, T. (1977). One hundred and twenty-seven cultured human tumor cell lines producing tumors in nude mice. *J Natl Cancer Inst* 59, 221-226.

- Fortis, S.P., Anastasopoulou, E.A., Voutsas, I.F., Baxevanis, C.N., Perez, S.A., and Mahaira, L.G. (2017). Potential Prognostic Molecular Signatures in a Preclinical Model of Melanoma. *Anticancer Res* 37, 143-148.
- Fouquier, J., and Guedj, M. (2015). Analysis of drug combinations: current methodological landscape. *Pharmacol Res Perspect* 3, e00149.
- Franzese, E., Diana, A., Centonze, S., Pignata, S., De Vita, F., Ciardiello, F., and Orditura, M. (2020). PARP Inhibitors in First-Line Therapy of Ovarian Cancer: Are There Any Doubts? *Front Oncol* 10, 782.
- Frisone, P., Pradella, D., Di Matteo, A., Belloni, E., Ghigna, C., and Paronetto, M.P. (2015). SAM68: Signal Transduction and RNA Metabolism in Human Cancer. *Biomed Res Int* 2015, 528954.
- Fujita, Y., Krause, G., Scheffner, M., Zechner, D., Leddy, H.E., Behrens, J., Sommer, T., and Birchmeier, W. (2002). Hakai, a c-Cbl-like protein, ubiquitinates and induces endocytosis of the E-cadherin complex. *Nat Cell Biol* 4, 222-231.
- Fulford, A., Tapon, N., and Ribeiro, P.S. (2018). Upstairs, downstairs: spatial regulation of Hippo signalling. *Curr Opin Cell Biol* 51, 22-32.
- Furth, N., Aylon, Y., and Oren, M. (2018). p53 shades of Hippo. *Cell Death Differ* 25, 81-92.
- Galli, G.G., Carrara, M., Yuan, W.C., Valdes-Quezada, C., Gurung, B., Pepe-Mooney, B., Zhang, T., Geeven, G., Gray, N.S., de Laat, W., *et al.* (2015). YAP Drives Growth by Controlling Transcriptional Pause Release from Dynamic Enhancers. *Molecular cell* 60, 328-337.
- Gerstberger, S., Hafner, M., and Tuschl, T. (2014). A census of human RNA-binding proteins. *Nat Rev Genet* 15, 829-845.
- Git, A., Allison, R., Perdiguero, E., Nebreda, A.R., Houlston, E., and Standart, N. (2009). Vg1RBP phosphorylation by Erk2 MAP kinase correlates with the cortical release of Vg1 mRNA during meiotic maturation of *Xenopus* oocytes. *RNA* 15, 1121-1133.
- Glass, M., Misiak, D., Bley, N., Muller, S., Hagemann, S., Busch, B., Rausch, A., and Huttelmaier, S. (2021). IGF2BP1, a Conserved Regulator of RNA Turnover in Cancer. *Front Mol Biosci* 8, 632219.
- Gordon, A.N., Fleagle, J.T., Guthrie, D., Parkin, D.E., Gore, M.E., and Lacave, A.J. (2001). Recurrent epithelial ovarian carcinoma: a randomized phase III study of pegylated liposomal doxorubicin versus topotecan. *J Clin Oncol* 19, 3312-3322.
- Gordon, A.N., Tonda, M., Sun, S., and Rackoff, W. (2004). Long-term survival advantage for women treated with pegylated liposomal doxorubicin compared with topotecan in a phase 3 randomized study of recurrent and refractory epithelial ovarian cancer. *Gynecol Oncol* 95, 1-8.
- Goswami, S., Tarapore, R.S., Teslaa, J.J., Grinblat, Y., Setaluri, V., and Spiegelman, V.S. (2010). MicroRNA-340-mediated degradation of microphthalmia-associated transcription factor mRNA is inhibited by the coding region determinant-binding protein. *The Journal of biological chemistry* 285, 20532-20540.
- Graham, F.L., Smiley, J., Russell, W.C., and Nairn, R. (1977). Characteristics of a human cell line transformed by DNA from human adenovirus type 5. *J Gen Virol* 36, 59-74.
- Grazia Lampugnani, M., Zanetti, A., Corada, M., Takahashi, T., Balconi, G., Breviario, F., Orsenigo, F., Cattelino, A., Kemler, R., Daniel, T.O., *et al.* (2003). Contact inhibition of VEGF-induced proliferation requires vascular endothelial cadherin, beta-catenin, and the phosphatase DEP-1/CD148. *J Cell Biol* 161, 793-804.
- Gu, W., Pan, F., and Singer, R.H. (2009). Blocking beta-catenin binding to the ZBP1 promoter represses ZBP1 expression, leading to increased proliferation and migration of metastatic breast-cancer cells. *J Cell Sci* 122, 1895-1905.

- Gu, W., Wells, A.L., Pan, F., and Singer, R.H. (2008). Feedback regulation between zipcode binding protein 1 and beta-catenin mRNAs in breast cancer cells. *Mol Cell Biol* 28, 4963-4974.
- Guarino, M. (2010). Src signaling in cancer invasion. *J Cell Physiol* 223, 14-26.
- Gutschner, T., Hammerle, M., Pazaitis, N., Bley, N., Fiskin, E., Uckelmann, H., Heim, A., Grobota, M., Hofmann, N., Geffers, R., *et al.* (2014). Insulin-like growth factor 2 mRNA-binding protein 1 (IGF2BP1) is an important protumorigenic factor in hepatocellular carcinoma. *Hepatology* 59, 1900-1911.
- Gyorffy, B., Lanczky, A., and Szallasi, Z. (2012). Implementing an online tool for genome-wide validation of survival-associated biomarkers in ovarian-cancer using microarray data from 1287 patients. *Endocr Relat Cancer* 19, 197-208.
- Haase, J., Misiak, D., Bauer, M., Pazaitis, N., Braun, J., Potschke, R., Mensch, A., Bell, J.L., Dralle, H., Siebolts, U., *et al.* (2021). IGF2BP1 is the first positive marker for anaplastic thyroid carcinoma diagnosis. *Mod Pathol* 34, 32-41.
- Hafner, M., Landthaler, M., Burger, L., Khorshid, M., Hausser, J., Berninger, P., Rothballer, A., Ascano, M., Jr., Jungkamp, A.C., Munschauer, M., *et al.* (2010). Transcriptome-wide identification of RNA-binding protein and microRNA target sites by PAR-CLIP. *Cell* 141, 129-141.
- Halbleib, J.M., and Nelson, W.J. (2006). Cadherins in development: cell adhesion, sorting, and tissue morphogenesis. *Genes & development* 20, 3199-3214.
- Hall, C.A., Wang, R., Miao, J., Oliva, E., Shen, X., Wheeler, T., Hilsenbeck, S.G., Orsulic, S., and Goode, S. (2010). Hippo pathway effector Yap is an ovarian cancer oncogene. *Cancer Res* 70, 8517-8525.
- Hamilton, K.E., Noubissi, F.K., Katti, P.S., Hahn, C.M., Davey, S.R., Lundsmith, E.T., Klein-Szanto, A.J., Rhim, A.D., Spiegelman, V.S., and Rustgi, A.K. (2013). IMP1 promotes tumor growth, dissemination and a tumor-initiating cell phenotype in colorectal cancer cell xenografts. *Carcinogenesis* 34, 2647-2654.
- Hamilton, T.C., Young, R.C., McKoy, W.M., Grotzinger, K.R., Green, J.A., Chu, E.W., Whang-Peng, J., Rogan, A.M., Green, W.R., and Ozols, R.F. (1983). Characterization of a human ovarian carcinoma cell line (NIH:OVCAR-3) with androgen and estrogen receptors. *Cancer Res* 43, 5379-5389.
- Hamilton, T.C., Young, R.C., and Ozols, R.F. (1984). Experimental model systems of ovarian cancer: applications to the design and evaluation of new treatment approaches. *Semin Oncol* 11, 285-298.
- Han, Y. (2019). Analysis of the role of the Hippo pathway in cancer. *J Transl Med* 17, 116.
- Hanahan, D., and Weinberg, R.A. (2011). Hallmarks of cancer: the next generation. *Cell* 144, 646-674.
- Hansen, C.G., Moroishi, T., and Guan, K.L. (2015). YAP and TAZ: a nexus for Hippo signaling and beyond. *Trends Cell Biol* 25, 499-513.
- Hansen, S.D., Kwiatkowski, A.V., Ouyang, C.Y., Liu, H., Pokutta, S., Watkins, S.C., Volkman, N., Hanein, D., Weis, W.I., Mullins, R.D., *et al.* (2013). alphaE-catenin actin-binding domain alters actin filament conformation and regulates binding of nucleation and disassembly factors. *Mol Biol Cell* 24, 3710-3720.
- Harris, T.J., and Tepass, U. (2010). Adherens junctions: from molecules to morphogenesis. *Nat Rev Mol Cell Biol* 11, 502-514.
- Hatanaka, K., Simons, M., and Murakami, M. (2011). Phosphorylation of VE-cadherin controls endothelial phenotypes via p120-catenin coupling and Rac1 activation. *Am J Physiol Heart Circ Physiol* 300, H162-172.



- Hatzfeld, M., Keil, R., and Magin, T.M. (2017). Desmosomes and Intermediate Filaments: Their Consequences for Tissue Mechanics. *Cold Spring Harb Perspect Biol* 9.
- Havin, L., Git, A., Elisha, Z., Oberman, F., Yaniv, K., Schwartz, S.P., Standart, N., and Yisraeli, J.K. (1998). RNA-binding protein conserved in both microtubule- and microfilament-based RNA localization. *Genes & development* 12, 1593-1598.
- He, Y., Yu, X., Tang, Y., Guo, Y., Yuan, J., Bai, J., Yao, T., and Wu, X. (2021). MicroRNA199a3p inhibits ovarian cancer cell viability by targeting the oncogene YAP1. *Mol Med Rep* 23.
- Heidary Arash, E., Shiban, A., Song, S., and Attisano, L. (2017). MARK4 inhibits Hippo signaling to promote proliferation and migration of breast cancer cells. *EMBO Rep* 18, 420-436.
- Helland, A., Anglesio, M.S., George, J., Cowin, P.A., Johnstone, C.N., House, C.M., Sheppard, K.E., Etemadmoghadam, D., Melnyk, N., Rustgi, A.K., *et al.* (2011). Dereglulation of MYCN, LIN28B and LET7 in a molecular subtype of aggressive high-grade serous ovarian cancers. *PLoS One* 6, e18064.
- Hentze, M.W., Castello, A., Schwarzl, T., and Preiss, T. (2018). A brave new world of RNA-binding proteins. *Nat Rev Mol Cell Biol* 19, 327-341.
- Ho, L.L., Wei, X., Shimizu, T., and Lai, Z.C. (2010). Mob as tumor suppressor is activated at the cell membrane to control tissue growth and organ size in *Drosophila*. *Dev Biol* 337, 274-283.
- Hong, J.Y., Oh, I.H., and McCrea, P.D. (2016). Phosphorylation and isoform use in p120-catenin during development and tumorigenesis. *Biochim Biophys Acta* 1863, 102-114.
- Hong, J.Y., Park, J.I., Cho, K., Gu, D., Ji, H., Artandi, S.E., and McCrea, P.D. (2010). Shared molecular mechanisms regulate multiple catenin proteins: canonical Wnt signals and components modulate p120-catenin isoform-1 and additional p120 subfamily members. *J Cell Sci* 123, 4351-4365.
- Hosking, C.R., Ulloa, F., Hogan, C., Ferber, E.C., Figueroa, A., Gevaert, K., Birchmeier, W., Briscoe, J., and Fujita, Y. (2007). The transcriptional repressor Glis2 is a novel binding partner for p120 catenin. *Mol Biol Cell* 18, 1918-1927.
- Hsia, D.A., Mitra, S.K., Hauck, C.R., Strebblow, D.N., Nelson, J.A., Ilic, D., Huang, S., Li, E., Nemerow, G.R., Leng, J., *et al.* (2003). Differential regulation of cell motility and invasion by FAK. *J Cell Biol* 160, 753-767.
- Hu, X., Wu, X., Xu, J., Zhou, J., Han, X., and Guo, J. (2009). Src kinase up-regulates the ERK cascade through inactivation of protein phosphatase 2A following cerebral ischemia. *BMC Neurosci* 10, 74.
- Hu, Z., Artibani, M., Alsaadi, A., Wietek, N., Morotti, M., Shi, T., Zhong, Z., Santana Gonzalez, L., El-Sahhar, S., KaramiNejadRanjbar, M., *et al.* (2020). The Repertoire of Serous Ovarian Cancer Non-genetic Heterogeneity Revealed by Single-Cell Sequencing of Normal Fallopian Tube Epithelial Cells. *Cancer Cell* 37, 226-242 e227.
- Huang, H., Weng, H., Sun, W., Qin, X., Shi, H., Wu, H., Zhao, B.S., Mesquita, A., Liu, C., Yuan, C.L., *et al.* (2018). Recognition of RNA N(6)-methyladenosine by IGF2BP proteins enhances mRNA stability and translation. *Nat Cell Biol* 20, 285-295.
- Huttelmaier, S., Zenklusen, D., Lederer, M., Dichtenberg, J., Lorenz, M., Meng, X., Bassell, G.J., Condeelis, J., and Singer, R.H. (2005). Spatial regulation of beta-actin translation by Src-dependent phosphorylation of ZBP1. *Nature* 438, 512-515.
- Ianevski, A., He, L., Aittokallio, T., and Tang, J. (2017). SynergyFinder: a web application for analyzing drug combination dose-response matrix data. *Bioinformatics* 33, 2413-2415.
- Irby, R.B., and Yeatman, T.J. (2000). Role of Src expression and activation in human cancer. *Oncogene* 19, 5636-5642.

- Ishiyama, N., Lee, S.H., Liu, S., Li, G.Y., Smith, M.J., Reichardt, L.F., and Ikura, M. (2010). Dynamic and static interactions between p120 catenin and E-cadherin regulate the stability of cell-cell adhesion. *Cell* *141*, 117-128.
- Ishiyama, N., Sarpal, R., Wood, M.N., Barrick, S.K., Nishikawa, T., Hayashi, H., Kobb, A.B., Flozak, A.S., Yemelyanov, A., Fernandez-Gonzalez, R., *et al.* (2018). Force-dependent allostery of the alpha-catenin actin-binding domain controls adherens junction dynamics and functions. *Nat Commun* *9*, 5121.
- Johnson, E., Seachrist, D.D., DeLeon-Rodriguez, C.M., Lozada, K.L., Miedler, J., Abdul-Karim, F.W., and Keri, R.A. (2010). HER2/ErbB2-induced breast cancer cell migration and invasion require p120 catenin activation of Rac1 and Cdc42. *J Biol Chem* *285*, 29491-29501.
- Johnson, R., and Halder, G. (2014). The two faces of Hippo: targeting the Hippo pathway for regenerative medicine and cancer treatment. *Nat Rev Drug Discov* *13*, 63-79.
- Johnson, S.W., Laub, P.B., Beesley, J.S., Ozols, R.F., and Hamilton, T.C. (1997). Increased platinum-DNA damage tolerance is associated with cisplatin resistance and cross-resistance to various chemotherapeutic agents in unrelated human ovarian cancer cell lines. *Cancer Res* *57*, 850-856.
- Karnezis, A.N., Cho, K.R., Gilks, C.B., Pearce, C.L., and Huntsman, D.G. (2017). The disparate origins of ovarian cancers: pathogenesis and prevention strategies. *Nat Rev Cancer* *17*, 65-74.
- Kato, T., Hayama, S., Yamabuki, T., Ishikawa, N., Miyamoto, M., Ito, T., Tsuchiya, E., Kondo, S., Nakamura, Y., and Daigo, Y. (2007). Increased expression of insulin-like growth factor-II messenger RNA-binding protein 1 is associated with tumor progression in patients with lung cancer. *Clin Cancer Res* *13*, 434-442.
- Katopodis, P., Chudasama, D., Wander, G., Sales, L., Kumar, J., Pandhal, M., Anikin, V., Chatterjee, J., Hall, M., and Karteris, E. (2019). Kinase Inhibitors and Ovarian Cancer. *Cancers (Basel)* *11*.
- Kim, N.G., Koh, E., Chen, X., and Gumbiner, B.M. (2011). E-cadherin mediates contact inhibition of proliferation through Hippo signaling-pathway components. *Proc Natl Acad Sci U S A* *108*, 11930-11935.
- Kim, W., and Jho, E.H. (2018). The history and regulatory mechanism of the Hippo pathway. *BMB Rep* *51*, 106-118.
- Klymenko, Y., Johnson, J., Bos, B., Lombard, R., Campbell, L., Loughran, E., and Stack, M.S. (2017). Heterogeneous Cadherin Expression and Multicellular Aggregate Dynamics in Ovarian Cancer Dissemination. *Neoplasia* *19*, 549-563.
- Kobel, M., Bak, J., Bertelsen, B.I., Carpen, O., Grove, A., Hansen, E.S., Levin Jakobsen, A.M., Lidang, M., Masback, A., Tolf, A., *et al.* (2014). Ovarian carcinoma histotype determination is highly reproducible, and is improved through the use of immunohistochemistry. *Histopathology* *64*, 1004-1013.
- Kobel, M., Weidensdorfer, D., Reinke, C., Lederer, M., Schmitt, W.D., Zeng, K., Thomssen, C., Hauptmann, S., and Huttelmaier, S. (2007). Expression of the RNA-binding protein IMP1 correlates with poor prognosis in ovarian carcinoma. *Oncogene* *26*, 7584-7589.
- Kommos, S., Gilks, C.B., du Bois, A., and Kommos, F. (2016). Ovarian carcinoma diagnosis: the clinical impact of 15 years of change. *Br J Cancer* *115*, 993-999.
- Kondrashova, O., Nguyen, M., Shield-Artin, K., Tinker, A.V., Teng, N.N.H., Harrell, M.I., Kuiper, M.J., Ho, G.Y., Barker, H., Jasin, M., *et al.* (2017). Secondary Somatic Mutations Restoring RAD51C and RAD51D Associated with Acquired Resistance to the PARP Inhibitor Rucaparib in High-Grade Ovarian Carcinoma. *Cancer Discov* *7*, 984-998.

- Konecny, G.E., Glas, R., Dering, J., Manivong, K., Qi, J., Finn, R.S., Yang, G.R., Hong, K.L., Ginther, C., Winterhoff, B., *et al.* (2009). Activity of the multikinase inhibitor dasatinib against ovarian cancer cells. *Br J Cancer* *101*, 1699-1708.
- Konecny, G.E., Wang, C., Hamidi, H., Winterhoff, B., Kalli, K.R., Dering, J., Ginther, C., Chen, H.W., Dowdy, S., Cliby, W., *et al.* (2014). Prognostic and therapeutic relevance of molecular subtypes in high-grade serous ovarian cancer. *J Natl Cancer Inst* *106*.
- Konecny, G.E., Winterhoff, B., and Wang, C. (2016). Gene-expression signatures in ovarian cancer: Promise and challenges for patient stratification. *Gynecol Oncol* *141*, 379-385.
- Koudelkova, L., Pataki, A.C., Tolde, O., Pavlik, V., Nobis, M., Gemperle, J., Anderson, K., Brabek, J., and Rosel, D. (2019). Novel FRET-Based Src Biosensor Reveals Mechanisms of Src Activation and Its Dynamics in Focal Adhesions. *Cell Chem Biol* *26*, 255-268 e254.
- Kourtidis, A., Ngok, S.P., and Anastasiadis, P.Z. (2013). p120 catenin: an essential regulator of cadherin stability, adhesion-induced signaling, and cancer progression. *Prog Mol Biol Transl Sci* *116*, 409-432.
- Kourtidis, A., Yanagisawa, M., Huvelde, D., Copland, J.A., and Anastasiadis, P.Z. (2015). Pro-Tumorigenic Phosphorylation of p120 Catenin in Renal and Breast Cancer. *PLoS One* *10*, e0129964.
- Kowalczyk, A.P., and Nanes, B.A. (2012). Adherens junction turnover: regulating adhesion through cadherin endocytosis, degradation, and recycling. *Subcell Biochem* *60*, 197-222.
- Kumar, N.M., and Gilula, N.B. (1996). The gap junction communication channel. *Cell* *84*, 381-388.
- Kurman, R.J., Carcangiu, M.L., Herrington, C.S., and Young, R.H. (2014). WHO Classification of Tumours of Female Reproductive Organs. 4th ed IARC, Lyon 6.
- Kuroki, L., and Guntupalli, S.R. (2020). Treatment of epithelial ovarian cancer. *BMJ* *371*, m3773.
- Kutova, O.M., Sencha, L.M., Pospelov, A.D., Dobrynina, O.E., Brilkina, A.A., Cherkasova, E.I., and Balalaeva, I.V. (2020). Comparative Analysis of Cell-Cell Contact Abundance in Ovarian Carcinoma Cells Cultured in Two- and Three-Dimensional In Vitro Models. *Biology (Basel)* *9*.
- Lamar, J.M., Xiao, Y., Norton, E., Jiang, Z.G., Gerhard, G.M., Kooner, S., Warren, J.S.A., and Hynes, R.O. (2019). SRC tyrosine kinase activates the YAP/TAZ axis and thereby drives tumor growth and metastasis. *J Biol Chem* *294*, 2302-2317.
- Landgren, E., Blume-Jensen, P., Courtneidge, S.A., and Claesson-Welsh, L. (1995). Fibroblast growth factor receptor-1 regulation of Src family kinases. *Oncogene* *10*, 2027-2035.
- Lau, D.H., Lewis, A.D., Ehsan, M.N., and Sikic, B.I. (1991). Multifactorial mechanisms associated with broad cross-resistance of ovarian carcinoma cells selected by cyanomorpholino doxorubicin. *Cancer Res* *51*, 5181-5187.
- Lavoie, H., Gagnon, J., and Therrien, M. (2020). ERK signalling: a master regulator of cell behaviour, life and fate. *Nat Rev Mol Cell Biol* *21*, 607-632.
- Le, T.L., Yap, A.S., and Stow, J.L. (1999). Recycling of E-cadherin: a potential mechanism for regulating cadherin dynamics. *The Journal of cell biology* *146*, 219-232.
- Le, X.F., Mao, W., He, G., Claret, F.X., Xia, W., Ahmed, A.A., Hung, M.C., Siddik, Z.H., and Bast, R.C., Jr. (2011). The role of p27(Kip1) in dasatinib-enhanced paclitaxel cytotoxicity in human ovarian cancer cells. *J Natl Cancer Inst* *103*, 1403-1422.

- Lee, M., Ji, H., Furuta, Y., Park, J.I., and McCrea, P.D. (2014). p120-catenin regulates REST and CoREST, and modulates mouse embryonic stem cell differentiation. *J Cell Sci* 127, 4037-4051.
- Lemm, I., and Ross, J. (2002). Regulation of c-myc mRNA decay by translational pausing in a coding region instability determinant. *Mol Cell Biol* 22, 3959-3969.
- Leng, W., Li, D., Chen, L., Xia, H., Tang, Q., Chen, B., Gong, Q., Gao, F., and Bi, F. (2016). Novel Bioluminescent Activatable Reporter for Src Tyrosine Kinase Activity in Living Mice. *Theranostics* 6, 594-609.
- Leong, H.S., Galletta, L., Etemadmoghadam, D., George, J., Kobel, M., Ramus, S.J., and Bowtell, D. (2015). Efficient molecular subtype classification of high-grade serous ovarian cancer. *J Pathol* 236, 272-277.
- Li, N., Xie, C., and Lu, N. (2017). Crosstalk between Hippo signalling and miRNAs in tumour progression. *FEBS J* 284, 1045-1055.
- Li, P., Silvis, M.R., Honaker, Y., Lien, W.H., Arron, S.T., and Vasioukhin, V. (2016). alphaE-catenin inhibits a Src-YAP1 oncogenic module that couples tyrosine kinases and the effector of Hippo signaling pathway. *Genes & development* 30, 798-811.
- Liberzon, A., Birger, C., Thorvaldsdottir, H., Ghandi, M., Mesirov, J.P., and Tamayo, P. (2015). The Molecular Signatures Database (MSigDB) hallmark gene set collection. *Cell Syst* 1, 417-425.
- Lilien, J., Balsamo, J., Arregui, C., and Xu, G. (2002). Turn-off, drop-out: functional state switching of cadherins. *Dev Dyn* 224, 18-29.
- Livak, K.J., and Schmittgen, T.D. (2001). Analysis of relative gene expression data using real-time quantitative PCR and the 2(-Delta Delta C(T)) Method. *Methods* 25, 402-408.
- Ma, L.W., Zhou, Z.T., He, Q.B., and Jiang, W.W. (2012). Phosphorylated p120-catenin expression has predictive value for oral cancer progression. *J Clin Pathol* 65, 315-319.
- Mackedenski, S., Wang, C., Li, W.M., and Lee, C.H. (2018). Characterizing the interaction between insulin-like growth factor 2 mRNA-binding protein 1 (IMP1) and KRAS expression. *Biochem J* 475, 2749-2767.
- Mahapatra, L., Andruska, N., Mao, C., Le, J., and Shapiro, D.J. (2017). A Novel IMP1 Inhibitor, BTYNB, Targets c-Myc and Inhibits Melanoma and Ovarian Cancer Cell Proliferation. *Transl Oncol* 10, 818-827.
- Malliri, A., van Es, S., Huveneers, S., and Collard, J.G. (2004). The Rac exchange factor Tiam1 is required for the establishment and maintenance of cadherin-based adhesions. *The Journal of biological chemistry* 279, 30092-30098.
- Mana-Capelli, S., Paramasivam, M., Dutta, S., and McCollum, D. (2014). Angiomotins link F-actin architecture to Hippo pathway signaling. *Mol Biol Cell* 25, 1676-1685.
- Manni, I., de Latouliere, L., Gurtner, A., and Piaggio, G. (2019). Transgenic Animal Models to Visualize Cancer-Related Cellular Processes by Bioluminescence Imaging. *Front Pharmacol* 10, 235.
- Marei, H., and Malliri, A. (2017). GEFs: Dual regulation of Rac1 signaling. *Small GTPases* 8, 90-99.
- Mariner, D.J., Anastasiadis, P., Keilhack, H., Bohmer, F.D., Wang, J., and Reynolds, A.B. (2001). Identification of Src phosphorylation sites in the catenin p120ctn. *J Biol Chem* 276, 28006-28013.
- Markman, M., Blessing, J., Rubin, S.C., Connor, J., Hanjani, P., and Waggoner, S. (2006). Phase II trial of weekly paclitaxel (80 mg/m<sup>2</sup>) in platinum and paclitaxel-resistant ovarian and primary peritoneal cancers: a Gynecologic Oncology Group study. *Gynecol Oncol* 101, 436-440.

- Martin-Belmonte, F., and Perez-Moreno, M. (2011). Epithelial cell polarity, stem cells and cancer. *Nat Rev Cancer* *12*, 23-38.
- Martin, G.S. (2001). The hunting of the Src. *Nat Rev Mol Cell Biol* *2*, 467-475.
- Matsuyoshi, N., Hamaguchi, M., Taniguchi, S., Nagafuchi, A., Tsukita, S., and Takeichi, M. (1992). Cadherin-mediated cell-cell adhesion is perturbed by v-src tyrosine phosphorylation in metastatic fibroblasts. *J Cell Biol* *118*, 703-714.
- Matulonis, U.A., Sood, A.K., Fallowfield, L., Howitt, B.E., Sehouli, J., and Karlan, B.Y. (2016). Ovarian cancer. *Nat Rev Dis Primers* *2*, 16061.
- McClatchey, A.I., and Yap, A.S. (2012). Contact inhibition (of proliferation) redux. *Curr Opin Cell Biol* *24*, 685-694.
- McCrea, P.D., and Gottardi, C.J. (2016). Beyond beta-catenin: prospects for a larger catenin network in the nucleus. *Nat Rev Mol Cell Biol* *17*, 55-64.
- McGivern, N., El-Helali, A., Mullan, P., McNeish, I.A., Paul Harkin, D., Kennedy, R.D., and McCabe, N. (2018). Activation of MAPK signalling results in resistance to saracatinib (AZD0530) in ovarian cancer. *Oncotarget* *9*, 4722-4736.
- McNeish, I.A., Ledermann, J.A., Webber, L., James, L., Kaye, S.B., Hall, M., Hall, G., Clamp, A., Earl, H., Banerjee, S., *et al.* (2014). A randomised, placebo-controlled trial of weekly paclitaxel and saracatinib (AZD0530) in platinum-resistant ovarian, fallopian tube or primary peritoneal cancer. *Ann Oncol* *25*, 1988-1995.
- Meng, W., and Takeichi, M. (2009). Adherens junction: molecular architecture and regulation. *Cold Spring Harb Perspect Biol* *1*, a002899.
- Mittica, G., Ghisoni, E., Giannone, G., Genta, S., Aglietta, M., Sapino, A., and Valabrega, G. (2018). PARP Inhibitors in Ovarian Cancer. *Recent Pat Anticancer Drug Discov* *13*, 392-410.
- Moarefi, I., LaFevre-Bernt, M., Sicheri, F., Huse, M., Lee, C.H., Kuriyan, J., and Miller, W.T. (1997). Activation of the Src-family tyrosine kinase Hck by SH3 domain displacement. *Nature* *385*, 650-653.
- Mohseni, M., Sun, J., Lau, A., Curtis, S., Goldsmith, J., Fox, V.L., Wei, C., Frazier, M., Samson, O., Wong, K.K., *et al.* (2014). A genetic screen identifies an LKB1-MARK signalling axis controlling the Hippo-YAP pathway. *Nat Cell Biol* *16*, 108-117.
- Mongroo, P.S., Noubissi, F.K., Cuatrecasas, M., Kalabis, J., King, C.E., Johnstone, C.N., Bowser, M.J., Castells, A., Spiegelman, V.S., and Rustgi, A.K. (2011). IMP-1 displays cross-talk with K-Ras and modulates colon cancer cell survival through the novel proapoptotic protein CYFIP2. *Cancer Res* *71*, 2172-2182.
- Moroishi, T., Park, H.W., Qin, B., Chen, Q., Meng, Z., Plouffe, S.W., Taniguchi, K., Yu, F.X., Karin, M., Pan, D., *et al.* (2015). A YAP/TAZ-induced feedback mechanism regulates Hippo pathway homeostasis. *Genes & development* *29*, 1271-1284.
- Mueller-Pillasch, F., Pohl, B., Wilda, M., Lacher, U., Beil, M., Wallrapp, C., Hameister, H., Knochel, W., Adler, G., and Gress, T.M. (1999). Expression of the highly conserved RNA binding protein KOC in embryogenesis. *Mech Dev* *88*, 95-99.
- Muller-McNicoll, M., and Neugebauer, K.M. (2013). How cells get the message: dynamic assembly and function of mRNA-protein complexes. *Nat Rev Genet* *14*, 275-287.
- Muller, S., Bley, N., Busch, B., Glass, M., Lederer, M., Misiak, C., Fuchs, T., Wedler, A., Haase, J., Bertoldo, J.B., *et al.* (2020). The oncofetal RNA-binding protein IGF2BP1 is a druggable, post-transcriptional super-enhancer of E2F-driven gene expression in cancer. *Nucleic Acids Res* *48*, 8576-8590.

- Muller, S., Bley, N., Glass, M., Busch, B., Rousseau, V., Misiak, D., Fuchs, T., Lederer, M., and Huttelmaier, S. (2018). IGF2BP1 enhances an aggressive tumor cell phenotype by impairing miRNA-directed downregulation of oncogenic factors. *Nucleic Acids Res* **46**, 6285-6303.
- Muller, S., Glass, M., Singh, A.K., Haase, J., Bley, N., Fuchs, T., Lederer, M., Dahl, A., Huang, H., Chen, J., *et al.* (2019). IGF2BP1 promotes SRF-dependent transcription in cancer in a m6A- and miRNA-dependent manner. *Nucleic Acids Res* **47**, 375-390.
- Nakagawa, M., Fukata, M., Yamaga, M., Itoh, N., and Kaibuchi, K. (2001). Recruitment and activation of Rac1 by the formation of E-cadherin-mediated cell-cell adhesion sites. *Journal of cell science* **114**, 1829-1838.
- Nam, J.S., Ino, Y., Sakamoto, M., and Hirohashi, S. (2002). Src family kinase inhibitor PP2 restores the E-cadherin/catenin cell adhesion system in human cancer cells and reduces cancer metastasis. *Clin Cancer Res* **8**, 2430-2436.
- Nero, C., Ciccarone, F., Pietragalla, A., Duranti, S., Daniele, G., Salutari, V., Carbone, M.V., Scambia, G., and Lorusso, D. (2021). Ovarian Cancer Treatments Strategy: Focus on PARP Inhibitors and Immune Check Point Inhibitors. *Cancers (Basel)* **13**.
- Nielsen, J., Christiansen, J., Lykke-Andersen, J., Johnsen, A.H., Wewer, U.M., and Nielsen, F.C. (1999). A family of insulin-like growth factor II mRNA-binding proteins represses translation in late development. *Molecular and cellular biology* **19**, 1262-1270.
- Nielsen, J., Kristensen, M.A., Willemoes, M., Nielsen, F.C., and Christiansen, J. (2004). Sequential dimerization of human zipcode-binding protein IMP1 on RNA: a cooperative mechanism providing RNP stability. *Nucleic Acids Res* **32**, 4368-4376.
- Noren, N.K., Liu, B.P., Burrridge, K., and Kreft, B. (2000). p120 catenin regulates the actin cytoskeleton via Rho family GTPases. *J Cell Biol* **150**, 567-580.
- Noubissi, F.K., Elcheva, I., Bhatia, N., Shakoory, A., Ougolkov, A., Liu, J., Minamoto, T., Ross, J., Fuchs, S.Y., and Spiegelman, V.S. (2006). CRD-BP mediates stabilization of betaTrCP1 and c-myc mRNA in response to beta-catenin signalling. *Nature* **441**, 898-901.
- Noubissi, F.K., Goswami, S., Sanek, N.A., Kawakami, K., Minamoto, T., Moser, A., Grinblat, Y., and Spiegelman, V.S. (2009). Wnt signaling stimulates transcriptional outcome of the Hedgehog pathway by stabilizing GLI1 mRNA. *Cancer Res* **69**, 8572-8578.
- Noubissi, F.K., Nikiforov, M.A., Colburn, N., and Spiegelman, V.S. (2010). Transcriptional Regulation of CRD-BP by c-myc: Implications for c-myc Functions. *Genes Cancer* **1**, 1074-1082.
- Oberman, F., Rand, K., Maizels, Y., Rubinstein, A.M., and Yisraeli, J.K. (2007). VICKZ proteins mediate cell migration via their RNA binding activity. *RNA* **13**, 1558-1569.
- Okada, M. (2012). Regulation of the SRC family kinases by Csk. *Int J Biol Sci* **8**, 1385-1397.
- Oleynikov, Y., and Singer, R.H. (2003). Real-time visualization of ZBP1 association with beta-actin mRNA during transcription and localization. *Curr Biol* **13**, 199-207.
- Ostareck-Lederer, A., Ostareck, D.H., Cans, C., Neubauer, G., Bomsztyk, K., Superti-Furga, G., and Hentze, M.W. (2002). c-Src-mediated phosphorylation of hnRNP K drives translational activation of specifically silenced mRNAs. *Mol Cell Biol* **22**, 4535-4543.
- Ouyang, M., Sun, J., Chien, S., and Wang, Y. (2008). Determination of hierarchical relationship of Src and Rac at subcellular locations with FRET biosensors. *Proc Natl Acad Sci U S A* **105**, 14353-14358.
- Owens, D.W., McLean, G.W., Wyke, A.W., Paraskeva, C., Parkinson, E.K., Frame, M.C., and Brunton, V.G. (2000). The catalytic activity of the Src family kinases is required to disrupt cadherin-dependent cell-cell contacts. *Mol Biol Cell* **11**, 51-64.

- Ozawa, M., and Kemler, R. (1998). Altered cell adhesion activity by pervanadate due to the dissociation of alpha-catenin from the E-cadherin.catenin complex. *J Biol Chem* **273**, 6166-6170.
- Park, J.I., Kim, S.W., Lyons, J.P., Ji, H., Nguyen, T.T., Cho, K., Barton, M.C., Deroo, T., Vleminckx, K., Moon, R.T., *et al.* (2005). Kaiso/p120-catenin and TCF/beta-catenin complexes coordinately regulate canonical Wnt gene targets. *Dev Cell* **8**, 843-854.
- Patch, A.M., Christie, E.L., Etemadmoghadam, D., Garsed, D.W., George, J., Fereday, S., Nones, K., Cowin, P., Alsop, K., Bailey, P.J., *et al.* (2015). Whole-genome characterization of chemoresistant ovarian cancer. *Nature* **521**, 489-494.
- Patel, A., Sabbineni, H., Clarke, A., and Somanath, P.R. (2016). Novel roles of Src in cancer cell epithelial-to-mesenchymal transition, vascular permeability, microinvasion and metastasis. *Life Sci* **157**, 52-61.
- Pereira, B., Billaud, M., and Almeida, R. (2017). RNA-Binding Proteins in Cancer: Old Players and New Actors. *Trends Cancer* **3**, 506-528.
- Peres, L.C., Cushing-Haugen, K.L., Anglesio, M., Wicklund, K., Bentley, R., Berchuck, A., Kelemen, L.E., Nazeran, T.M., Gilks, C.B., Harris, H.R., *et al.* (2018). Histotype classification of ovarian carcinoma: A comparison of approaches. *Gynecol Oncol* **151**, 53-60.
- Perrais, M., Chen, X., Perez-Moreno, M., and Gumbiner, B.M. (2007). E-cadherin homophilic ligation inhibits cell growth and epidermal growth factor receptor signaling independently of other cell interactions. *Mol Biol Cell* **18**, 2013-2025.
- Playford, M.P., and Schaller, M.D. (2004). The interplay between Src and integrins in normal and tumor biology. *Oncogene* **23**, 7928-7946.
- Plouffe, S.W., Lin, K.C., Moore, J.L., 3rd, Tan, F.E., Ma, S., Ye, Z., Qiu, Y., Ren, B., and Guan, K.L. (2018). The Hippo pathway effector proteins YAP and TAZ have both distinct and overlapping functions in the cell. *J Biol Chem* **293**, 11230-11240.
- Pokutta, S., and Weis, W.I. (2007). Structure and mechanism of cadherins and catenins in cell-cell contacts. *Annu Rev Cell Dev Biol* **23**, 237-261.
- Polyak, K., and Weinberg, R.A. (2009). Transitions between epithelial and mesenchymal states: acquisition of malignant and stem cell traits. *Nat Rev Cancer* **9**, 265-273.
- Potter, M.D., Barbero, S., and Cheresch, D.A. (2005). Tyrosine phosphorylation of VE-cadherin prevents binding of p120- and beta-catenin and maintains the cellular mesenchymal state. *J Biol Chem* **280**, 31906-31912.
- Prat, J. (2012). Ovarian carcinomas: five distinct diseases with different origins, genetic alterations, and clinicopathological features. *Virchows Arch* **460**, 237-249.
- Price, M.A. (2006). CKI, there's more than one: casein kinase I family members in Wnt and Hedgehog signaling. *Genes & development* **20**, 399-410.
- Provencher, D.M., Lounis, H., Champoux, L., Tetrault, M., Manderson, E.N., Wang, J.C., Eydoux, P., Savoie, R., Tonin, P.N., and Mes-Masson, A.M. (2000). Characterization of four novel epithelial ovarian cancer cell lines. *In Vitro Cell Dev Biol Anim* **36**, 357-361.
- Pujade-Lauraine, E., Hilpert, F., Weber, B., Reuss, A., Poveda, A., Kristensen, G., Sorio, R., Vergote, I., Witteveen, P., Bamias, A., *et al.* (2014). Bevacizumab combined with chemotherapy for platinum-resistant recurrent ovarian cancer: The AURELIA open-label randomized phase III trial. *J Clin Oncol* **32**, 1302-1308.
- Qi, J., Wang, J., Romanyuk, O., and Siu, C.H. (2006). Involvement of Src family kinases in N-cadherin phosphorylation and beta-catenin dissociation during transendothelial migration of melanoma cells. *Mol Biol Cell* **17**, 1261-1272.

- Qian, X., Karpova, T., Sheppard, A.M., McNally, J., and Lowy, D.R. (2004). E-cadherin-mediated adhesion inhibits ligand-dependent activation of diverse receptor tyrosine kinases. *EMBO J* 23, 1739-1748.
- Raj, N., and Bam, R. (2019). Reciprocal Crosstalk Between YAP1/Hippo Pathway and the p53 Family Proteins: Mechanisms and Outcomes in Cancer. *Front Cell Dev Biol* 7, 159.
- Raja, F.A., Chopra, N., and Ledermann, J.A. (2012). Optimal first-line treatment in ovarian cancer. *Ann Oncol* 23 *Suppl* 10, x118-127.
- Ren, F., Zhang, L., and Jiang, J. (2010). Hippo signaling regulates Yorkie nuclear localization and activity through 14-3-3 dependent and independent mechanisms. *Dev Biol* 337, 303-312.
- Rietscher, K., Keil, R., Jordan, A., and Hatzfeld, M. (2018). 14-3-3 proteins regulate desmosomal adhesion via plakophilins. *J Cell Sci* 131.
- Robinson, M.D., McCarthy, D.J., and Smyth, G.K. (2010). edgeR: a Bioconductor package for differential expression analysis of digital gene expression data. *Bioinformatics* 26, 139-140.
- Roby, K.F., Taylor, C.C., Sweetwood, J.P., Cheng, Y., Pace, J.L., Tawfik, O., Persons, D.L., Smith, P.G., and Terranova, P.F. (2000). Development of a syngeneic mouse model for events related to ovarian cancer. *Carcinogenesis* 21, 585-591.
- Ross, A.F., Oleynikov, Y., Kislauskis, E.H., Taneja, K.L., and Singer, R.H. (1997). Characterization of a beta-actin mRNA zipcode-binding protein. *Molecular and cellular biology* 17, 2158-2165.
- Roura, S., Miravet, S., Piedra, J., Garcia de Herreros, A., and Dunach, M. (1999). Regulation of E-cadherin/Catenin association by tyrosine phosphorylation. *J Biol Chem* 274, 36734-36740.
- Sakanaka, C. (2002). Phosphorylation and regulation of beta-catenin by casein kinase I epsilon. *J Biochem* 132, 697-703.
- Sato, K., Watanabe, T., Wang, S., Kakeno, M., Matsuzawa, K., Matsui, T., Yokoi, K., Murase, K., Sugiyama, I., Ozawa, M., *et al.* (2011). Numb controls E-cadherin endocytosis through p120 catenin with aPKC. *Mol Biol Cell* 22, 3103-3119.
- Schaller, M.D. (2001). Paxillin: a focal adhesion-associated adaptor protein. *Oncogene* 20, 6459-6472.
- Schlegelmilch, K., Mohseni, M., Kirak, O., Pruszek, J., Rodriguez, J.R., Zhou, D., Kreger, B.T., Vasioukhin, V., Avruch, J., Brummelkamp, T.R., *et al.* (2011). Yap1 acts downstream of alpha-catenin to control epidermal proliferation. *Cell* 144, 782-795.
- Shetzer, Y., Solomon, H., Koifman, G., Molchadsky, A., Horesh, S., and Rotter, V. (2014). The paradigm of mutant p53-expressing cancer stem cells and drug resistance. *Carcinogenesis* 35, 1196-1208.
- Si, Y., Ji, X., Cao, X., Dai, X., Xu, L., Zhao, H., Guo, X., Yan, H., Zhang, H., Zhu, C., *et al.* (2017). Src Inhibits the Hippo Tumor Suppressor Pathway through Tyrosine Phosphorylation of Lats1. *Cancer Res* 77, 4868-4880.
- Silvis, M.R., Kreger, B.T., Lien, W.H., Klezovitch, O., Rudakova, G.M., Camargo, F.D., Lantz, D.M., Seykora, J.T., and Vasioukhin, V. (2011). alpha-catenin is a tumor suppressor that controls cell accumulation by regulating the localization and activity of the transcriptional coactivator Yap1. *Sci Signal* 4, ra33.
- Simpkins, F., Hevia-Paez, P., Sun, J., Ullmer, W., Gilbert, C.A., da Silva, T., Pedram, A., Levin, E.R., Reis, I.M., Rabinovich, B., *et al.* (2012). Src Inhibition with saracatinib reverses fulvestrant resistance in ER-positive ovarian cancer models in vitro and in vivo. *Clin Cancer Res* 18, 5911-5923.



- Simpkins, F., Jang, K., Yoon, H., Hew, K.E., Kim, M., Azzam, D.J., Sun, J., Zhao, D., Ince, T.A., Liu, W., *et al.* (2018). Dual Src and MEK Inhibition Decreases Ovarian Cancer Growth and Targets Tumor Initiating Stem-Like Cells. *Clin Cancer Res* **24**, 4874-4886.
- Song, G., Chen, L., Zhang, B., Song, Q., Yu, Y., Moore, C., Wang, T.L., Shih, I.M., Zhang, H., Chan, D.W., *et al.* (2019). Proteome-wide Tyrosine Phosphorylation Analysis Reveals Dysregulated Signaling Pathways in Ovarian Tumors. *Mol Cell Proteomics* **18**, 448-460.
- Song, J., Xie, L.X., Zhang, X.Y., Hu, P., Long, M.F., Xiong, F., Huang, J., and Ye, X.Q. (2018). Role of YAP in lung cancer resistance to cisplatin. *Oncol Lett* **16**, 3949-3954.
- Sparanese, D., and Lee, C.H. (2007). CRD-BP shields c-myc and MDR-1 RNA from endonucleolytic attack by a mammalian endoribonuclease. *Nucleic Acids Res* **35**, 1209-1221.
- Stein, C., Bardet, A.F., Roma, G., Bergling, S., Clay, I., Ruchti, A., Agarinis, C., Schmelzle, T., Bouwmeester, T., Schubeler, D., *et al.* (2015). YAP1 Exerts Its Transcriptional Control via TEAD-Mediated Activation of Enhancers. *PLoS Genet* **11**, e1005465.
- Stohr, N., Kohn, M., Lederer, M., Glass, M., Reinke, C., Singer, R.H., and Huttelmaier, S. (2012). IGF2BP1 promotes cell migration by regulating MK5 and PTEN signaling. *Genes & development* **26**, 176-189.
- Stokoe, D., and McCormick, F. (1997). Activation of c-Raf-1 by Ras and Src through different mechanisms: activation in vivo and in vitro. *EMBO J* **16**, 2384-2396.
- Su, Y., Walker, J.R., Park, Y., Smith, T.P., Liu, L.X., Hall, M.P., Labanieh, L., Hurst, R., Wang, D.C., Encell, L.P., *et al.* (2020). Novel NanoLuc substrates enable bright two-population bioluminescence imaging in animals. *Nat Methods* **17**, 852-860.
- Subramanian, M., Francis, P., Bilke, S., Li, X.L., Hara, T., Lu, X., Jones, M.F., Walker, R.L., Zhu, Y., Pineda, M., *et al.* (2015). A mutant p53/let-7i-axis-regulated gene network drives cell migration, invasion and metastasis. *Oncogene* **34**, 1094-1104.
- Summy, J.M., and Gallick, G.E. (2003). Src family kinases in tumor progression and metastasis. *Cancer Metastasis Rev* **22**, 337-358.
- Sun, C., Fang, Y., Labrie, M., Li, X., and Mills, G.B. (2020). Systems approach to rational combination therapy: PARP inhibitors. *Biochem Soc Trans* **48**, 1101-1108.
- Sun, J., Wang, X., Tang, B., Liu, H., Zhang, M., Wang, Y., Ping, F., Ding, J., Shen, A., and Geng, M. (2018). A tightly controlled Src-YAP signaling axis determines therapeutic response to dasatinib in renal cell carcinoma. *Theranostics* **8**, 3256-3267.
- Sun, Y., Zhang, J., and Ma, L. (2014). alpha-catenin. A tumor suppressor beyond adherens junctions. *Cell cycle* **13**, 2334-2339.
- Sung, H., Ferlay, J., Siegel, R.L., Laversanne, M., Soerjomataram, I., Jemal, A., and Bray, F. (2021). Global Cancer Statistics 2020: GLOBOCAN Estimates of Incidence and Mortality Worldwide for 36 Cancers in 185 Countries. *CA Cancer J Clin* **71**, 209-249.
- Suyama, K., Shapiro, I., Guttman, M., and Hazan, R.B. (2002). A signaling pathway leading to metastasis is controlled by N-cadherin and the FGF receptor. *Cancer Cell* **2**, 301-314.
- Takeichi, M. (2014). Dynamic contacts: rearranging adherens junctions to drive epithelial remodelling. *Nat Rev Mol Cell Biol* **15**, 397-410.
- Tan, T.Z., Miow, Q.H., Huang, R.Y., Wong, M.K., Ye, J., Lau, J.A., Wu, M.C., Bin Abdul Hadi, L.H., Soong, R., Choolani, M., *et al.* (2013). Functional genomics identifies five distinct molecular subtypes with clinical relevance and pathways for growth control in epithelial ovarian cancer. *EMBO Mol Med* **5**, 1051-1066.
- TCGA (2011). Integrated genomic analyses of ovarian carcinoma. *Nature* **474**, 609-615.

- Tessier, C.R., Doyle, G.A., Clark, B.A., Pitot, H.C., and Ross, J. (2004). Mammary tumor induction in transgenic mice expressing an RNA-binding protein. *Cancer Res* **64**, 209-214.
- Thomas, J.W., Ellis, B., Boerner, R.J., Knight, W.B., White, G.C., 2nd, and Schaller, M.D. (1998). SH2- and SH3-mediated interactions between focal adhesion kinase and Src. *J Biol Chem* **273**, 577-583.
- Tice, D.A., Biscardi, J.S., Nickles, A.L., and Parsons, S.J. (1999). Mechanism of biological synergy between cellular Src and epidermal growth factor receptor. *Proc Natl Acad Sci U S A* **96**, 1415-1420.
- Timpson, P., Jones, G.E., Frame, M.C., and Brunton, V.G. (2001). Coordination of cell polarization and migration by the Rho family GTPases requires Src tyrosine kinase activity. *Curr Biol* **11**, 1836-1846.
- Torre, L.A., Trabert, B., DeSantis, C.E., Miller, K.D., Samimi, G., Runowicz, C.D., Gaudet, M.M., Jemal, A., and Siegel, R.L. (2018). Ovarian cancer statistics, 2018. *CA Cancer J Clin* **68**, 284-296.
- Tothill, R.W., Tinker, A.V., George, J., Brown, R., Fox, S.B., Lade, S., Johnson, D.S., Trivett, M.K., Etemadmoghadam, D., Locandro, B., *et al.* (2008). Novel molecular subtypes of serous and endometrioid ovarian cancer linked to clinical outcome. *Clin Cancer Res* **14**, 5198-5208.
- Tran, N.H., and Frost, J.A. (2003). Phosphorylation of Raf-1 by p21-activated kinase 1 and Src regulates Raf-1 autoinhibition. *J Biol Chem* **278**, 11221-11226.
- Vainer, G., Vainer-Mosse, E., Pikarsky, A., Shenoy, S.M., Oberman, F., Yeffet, A., Singer, R.H., Pikarsky, E., and Yisraeli, J.K. (2008). A role for VICKZ proteins in the progression of colorectal carcinomas: regulating lamellipodia formation. *J Pathol* **215**, 445-456.
- van de Ven, R.A., Tenhagen, M., Meuleman, W., van Riel, J.J., Schackmann, R.C., and Derksen, P.W. (2015). Nuclear p120-catenin regulates the anoikis resistance of mouse lobular breast cancer cells through Kaiso-dependent Wnt11 expression. *Dis Model Mech* **8**, 373-384.
- van den Berg-Bakker, C.A., Hagemeyer, A., Franken-Postma, E.M., Smit, V.T., Kuppen, P.J., van Ravenswaay Claasen, H.H., Cornelisse, C.J., and Schrier, P.I. (1993). Establishment and characterization of 7 ovarian carcinoma cell lines and one granulosa tumor cell line: growth features and cytogenetics. *Int J Cancer* **53**, 613-620.
- Van Nostrand, E.L., Pratt, G.A., Shishkin, A.A., Gelboin-Burkhart, C., Fang, M.Y., Sundararaman, B., Blue, S.M., Nguyen, T.B., Surka, C., Elkins, K., *et al.* (2016). Robust transcriptome-wide discovery of RNA-binding protein binding sites with enhanced CLIP (eCLIP). *Nat Methods* **13**, 508-514.
- Vaughan, S., Coward, J.I., Bast, R.C., Jr., Berchuck, A., Berek, J.S., Brenton, J.D., Coukos, G., Crum, C.C., Drapkin, R., Etemadmoghadam, D., *et al.* (2011). Rethinking ovarian cancer: recommendations for improving outcomes. *Nat Rev Cancer* **11**, 719-725.
- Venhuizen, J.H., Jacobs, F.J.C., Span, P.N., and Zegers, M.M. (2020). P120 and E-cadherin: Double-edged swords in tumor metastasis. *Semin Cancer Biol* **60**, 107-120.
- Vikesaa, J., Hansen, T.V., Jonson, L., Borup, R., Wewer, U.M., Christiansen, J., and Nielsen, F.C. (2006). RNA-binding IMPs promote cell adhesion and invadopodia formation. *EMBO J* **25**, 1456-1468.
- Wachter, K., Kohn, M., Stohr, N., and Huttelmaier, S. (2013). Subcellular localization and RNP formation of IGF2BPs (IGF2 mRNA-binding proteins) is modulated by distinct RNA-binding domains. *Biol Chem* **394**, 1077-1090.

- Walton, J., Blagih, J., Ennis, D., Leung, E., Dowson, S., Farquharson, M., Tookman, L.A., Orange, C., Athineos, D., Mason, S., *et al.* (2016). CRISPR/Cas9-Mediated Trp53 and Brca2 Knockout to Generate Improved Murine Models of Ovarian High-Grade Serous Carcinoma. *Cancer Res* 76, 6118-6129.
- Walton, J.B., Farquharson, M., Mason, S., Port, J., Kruspig, B., Dowson, S., Stevenson, D., Murphy, D., Matzuk, M., Kim, J., *et al.* (2017). CRISPR/Cas9-derived models of ovarian high grade serous carcinoma targeting Brca1, Pten and Nf1, and correlation with platinum sensitivity. *Sci Rep* 7, 16827.
- Wang, D., He, J., Dong, J., Meyer, T.F., and Xu, T. (2020). The HIPPO pathway in gynecological malignancies. *Am J Cancer Res* 10, 610-629.
- Wang, Y., Botvinick, E.L., Zhao, Y., Berns, M.W., Usami, S., Tsien, R.Y., and Chien, S. (2005). Visualizing the mechanical activation of Src. *Nature* 434, 1040-1045.
- Wang, Y., Xu, X., Maglic, D., Dill, M.T., Mojumdar, K., Ng, P.K., Jeong, K.J., Tsang, Y.H., Moreno, D., Bhavana, V.H., *et al.* (2018). Comprehensive Molecular Characterization of the Hippo Signaling Pathway in Cancer. *Cell Rep* 25, 1304-1317 e1305.
- Weidensdorfer, D., Stohr, N., Baude, A., Lederer, M., Kohn, M., Schierhorn, A., Buchmeier, S., Wahle, E., and Huttelmaier, S. (2009). Control of c-myc mRNA stability by IGF2BP1-associated cytoplasmic RNPs. *RNA* 15, 104-115.
- Weng, Z., Taylor, J.A., Turner, C.E., Brugge, J.S., and Seidel-Dugan, C. (1993). Detection of Src homology 3-binding proteins, including paxillin, in normal and v-Src-transformed Balb/c 3T3 cells. *The Journal of biological chemistry* 268, 14956-14963.
- Wheelock, M.J., Shintani, Y., Maeda, M., Fukumoto, Y., and Johnson, K.R. (2008). Cadherin switching. *J Cell Sci* 121, 727-735.
- Wiener, J.R., Nakano, K., Kruzelock, R.P., Bucana, C.D., Bast, R.C., Jr., and Gallick, G.E. (1999). Decreased Src tyrosine kinase activity inhibits malignant human ovarian cancer tumor growth in a nude mouse model. *Clin Cancer Res* 5, 2164-2170.
- Wiener, J.R., Windham, T.C., Estrella, V.C., Parikh, N.U., Thall, P.F., Deavers, M.T., Bast, R.C., Mills, G.B., and Gallick, G.E. (2003). Activated SRC protein tyrosine kinase is overexpressed in late-stage human ovarian cancers. *Gynecol Oncol* 88, 73-79.
- Wildenberg, G.A., Dohn, M.R., Carnahan, R.H., Davis, M.A., Lobdell, N.A., Settleman, J., and Reynolds, A.B. (2006). p120-catenin and p190RhoGAP regulate cell-cell adhesion by coordinating antagonism between Rac and Rho. *Cell* 127, 1027-1039.
- Willert, K., and Jones, K.A. (2006). Wnt signaling: is the party in the nucleus? *Genes & development* 20, 1394-1404.
- Wilson, A.P., Dent, M., Pejovic, T., Hubbard, L., and Radford, H. (1996). Characterisation of seven human ovarian tumour cell lines. *Br J Cancer* 74, 722-727.
- Wolf, A., Keil, R., Gotzl, O., Mun, A., Schwarze, K., Lederer, M., Huttelmaier, S., and Hatzfeld, M. (2006). The armadillo protein p0071 regulates Rho signalling during cytokinesis. *Nat Cell Biol* 8, 1432-1440.
- Woodcock, S.A., Rooney, C., Lontos, M., Connolly, Y., Zoumpourlis, V., Whetton, A.D., Gorgoulis, V.G., and Malliri, A. (2009). SRC-induced disassembly of adherens junctions requires localized phosphorylation and degradation of the rac activator tiam1. *Molecular cell* 33, 639-653.
- Wozniak, M.A., Modzelewska, K., Kwong, L., and Keely, P.J. (2004). Focal adhesion regulation of cell behavior. *Biochim Biophys Acta* 1692, 103-119.
- Wu, J.C., Chen, Y.C., Kuo, C.T., Wenshin Yu, H., Chen, Y.Q., Chiou, A., and Kuo, J.C. (2015). Focal adhesion kinase-dependent focal adhesion recruitment of SH2 domains directs SRC into focal adhesions to regulate cell adhesion and migration. *Sci Rep* 5, 18476.

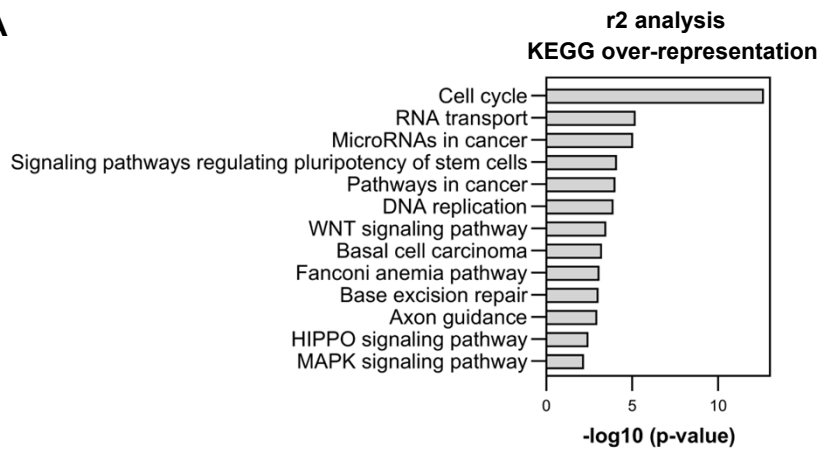
- Wu, Y., and Griffin, E.E. (2017). Regulation of Cell Polarity by PAR-1/MARK Kinase. *Curr Top Dev Biol* **123**, 365-397.
- Xia, Y., Chang, T., Wang, Y., Liu, Y., Li, W., Li, M., and Fan, H.Y. (2014). YAP promotes ovarian cancer cell tumorigenesis and is indicative of a poor prognosis for ovarian cancer patients. *PLoS One* **9**, e91770.
- Xing, Z., Chen, H.C., Nowlen, J.K., Taylor, S.J., Shalloway, D., and Guan, J.L. (1994). Direct interaction of v-Src with the focal adhesion kinase mediated by the Src SH2 domain. *Mol Biol Cell* **5**, 413-421.
- Yadav, B., Wennerberg, K., Aittokallio, T., and Tang, J. (2015). Searching for Drug Synergy in Complex Dose-Response Landscapes Using an Interaction Potency Model. *Comput Struct Biotechnol J* **13**, 504-513.
- Yadav, S.S., and Miller, W.T. (2007). Cooperative activation of Src family kinases by SH3 and SH2 ligands. *Cancer Lett* **257**, 116-123.
- Yamada, S., and Nelson, W.J. (2007). Localized zones of Rho and Rac activities drive initiation and expansion of epithelial cell-cell adhesion. *J Cell Biol* **178**, 517-527.
- Yamada, S., Pokutta, S., Drees, F., Weis, W.I., and Nelson, W.J. (2005). Deconstructing the cadherin-catenin-actin complex. *Cell* **123**, 889-901.
- Yamazaki, D., Oikawa, T., and Takenawa, T. (2007). Rac-WAVE-mediated actin reorganization is required for organization and maintenance of cell-cell adhesion. *Journal of cell science* **120**, 86-100.
- Yang, J., Antin, P., Berx, G., Blanpain, C., Brabletz, T., Bronner, M., Campbell, K., Cano, A., Casanova, J., Christofori, G., *et al.* (2020). Guidelines and definitions for research on epithelial-mesenchymal transition. *Nat Rev Mol Cell Biol* **21**, 341-352.
- Yaniv, K., and Yisraeli, J.K. (2002). The involvement of a conserved family of RNA binding proteins in embryonic development and carcinogenesis. *Gene* **287**, 49-54.
- Yap, A.S., Niessen, C.M., and Gumbiner, B.M. (1998). The juxtamembrane region of the cadherin cytoplasmic tail supports lateral clustering, adhesive strengthening, and interaction with p120ctn. *J Cell Biol* **141**, 779-789.
- Yeatman, T.J. (2004). A renaissance for SRC. *Nat Rev Cancer* **4**, 470-480.
- Yisraeli, J.K. (2005). VICKZ proteins: a multi-talented family of regulatory RNA-binding proteins. *Biol Cell* **97**, 87-96.
- Yu, F.X., and Guan, K.L. (2013). The Hippo pathway: regulators and regulations. *Genes & development* **27**, 355-371.
- Yu, J., Zheng, Y., Dong, J., Klusza, S., Deng, W.M., and Pan, D. (2010). Kibra functions as a tumor suppressor protein that regulates Hippo signaling in conjunction with Merlin and Expanded. *Dev Cell* **18**, 288-299.
- Zanconato, F., Forcato, M., Battilana, G., Azzolin, L., Quaranta, E., Bodega, B., Rosato, A., Bicciato, S., Cordenonsi, M., and Piccolo, S. (2015). Genome-wide association between YAP/TAZ/TEAD and AP-1 at enhancers drives oncogenic growth. *Nat Cell Biol* **17**, 1218-1227.
- Zhang, X., George, J., Deb, S., Degoutin, J.L., Takano, E.A., Fox, S.B., Bowtell, D.D., and Harvey, K.F. (2011). The Hippo pathway transcriptional co-activator, YAP, is an ovarian cancer oncogene. *Oncogene* **30**, 2810-2822.
- Zhao, B., Li, L., Lei, Q., and Guan, K.L. (2010). The Hippo-YAP pathway in organ size control and tumorigenesis: an updated version. *Genes & development* **24**, 862-874.
- Zhao, B., Li, L., Wang, L., Wang, C.Y., Yu, J., and Guan, K.L. (2012). Cell detachment activates the Hippo pathway via cytoskeleton reorganization to induce anoikis. *Genes & development* **26**, 54-68.

- Zhao, B., Wei, X., Li, W., Udan, R.S., Yang, Q., Kim, J., Xie, J., Ikenoue, T., Yu, J., Li, L., *et al.* (2007). Inactivation of YAP oncoprotein by the Hippo pathway is involved in cell contact inhibition and tissue growth control. *Genes & development* *21*, 2747-2761.
- Zhu, G., Pan, C., Bei, J.X., Li, B., Liang, C., Xu, Y., and Fu, X. (2020). Mutant p53 in Cancer Progression and Targeted Therapies. *Front Oncol* *10*, 595187.
- Zirkel, A., Lederer, M., Stohr, N., Pazaitis, N., and Huttelmaier, S. (2013). IGF2BP1 promotes mesenchymal cell properties and migration of tumor-derived cells by enhancing the expression of LEF1 and SNAI2 (SLUG). *Nucleic Acids Res* *41*, 6618-6636.

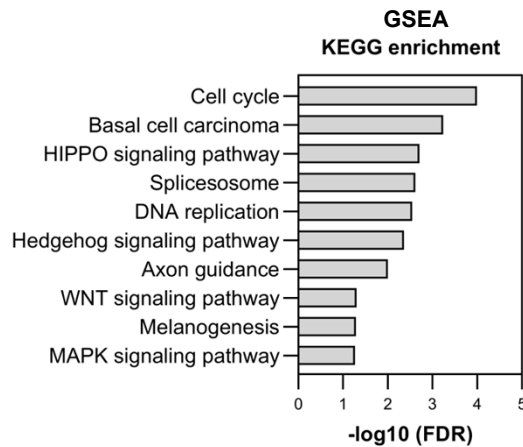
## APPENDIX

## Additional data

A



B



C

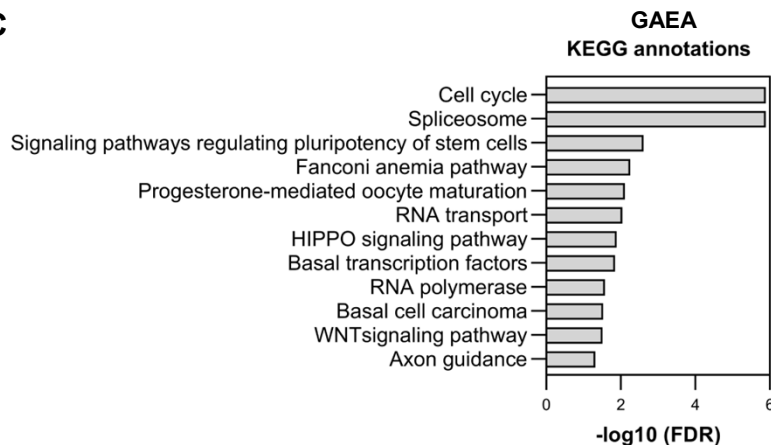


**Figure 35: Functional enrichment analysis.** (A) In an r2 ([http:// r2.amc.nl/](http://r2.amc.nl/)) gene set analysis IGF2BP1-positive correlated genes of the TCGA-OV cohort were analyzed for over-represented KEGG gene sets. The significant over-represented KEGG gene sets are shown. (B) An GSEA analysis was performed with the pre-ranked FCs of the IGF2BP1-high expressing population compared to the IGF2BP1-low expressing group of the TCGA-OV cohort using GSEA v4.0.3 software with a permutation number of 1000 and classical enrichment statistics. Population separation was achieved at around 5 FPKM. Significant enriched KEGG pathways of the GSEA analysis are shown. (C) Significant IGF2BP1-correlated genes of the TCGA-OV cohort were investigated for the KEGG gene sets in a GAEA analysis using Cytoscape v3.8.0 and the ClueGo plugin v2.5.7. A two-side hypergeometric enrichment was applied and a cut-off-value for Benjamini-Hochberg corrected p-values of 0.05 was set. Annotated cancer-related KEGG pathways are shown.

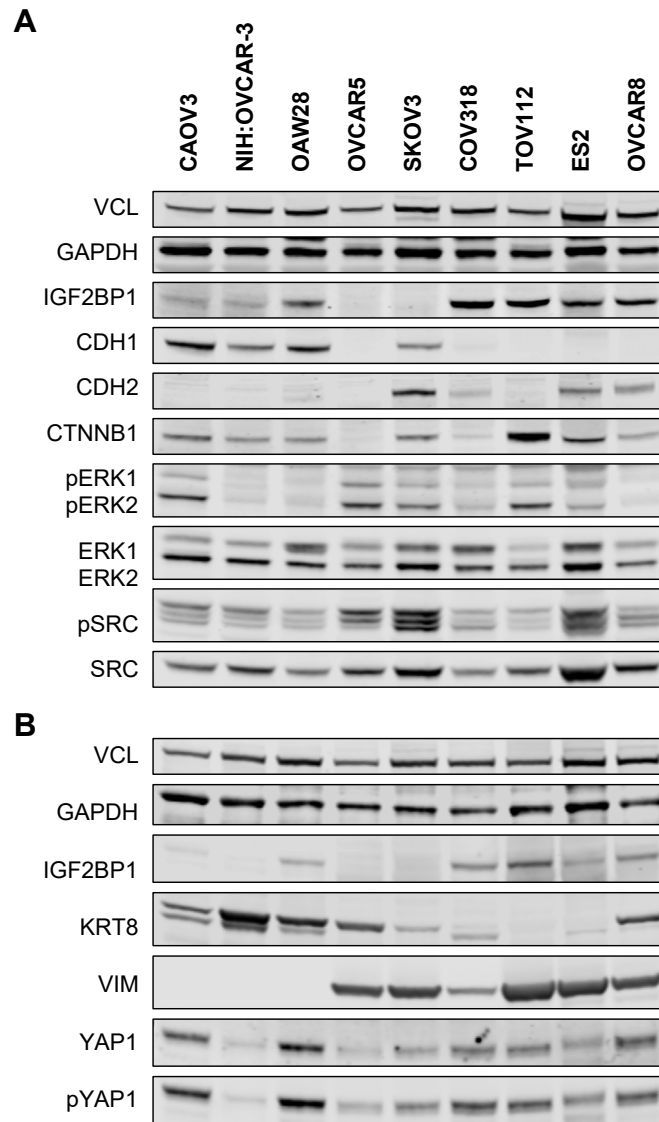


**Figure 36: Cell line overview.** The western blot analyses of different ovarian cancer cell lines, available in our laboratories, give an overview of the expression of several proteins which were important in the here presented study including AJ components (CDH1, CDH2, CTNNB1), signaling molecules (ERK, SRC), epithelial and mesenchymal marker of the intermediate filament system (KRT8, VIM), the main effector of the hippo pathway (YAP1) and the investigated RBP (IGF2BP1) next to the loading controls (VCL, GAPDH). Due to the number of used antibodies two separate Western blots were performed and are shown in (A) and (B).

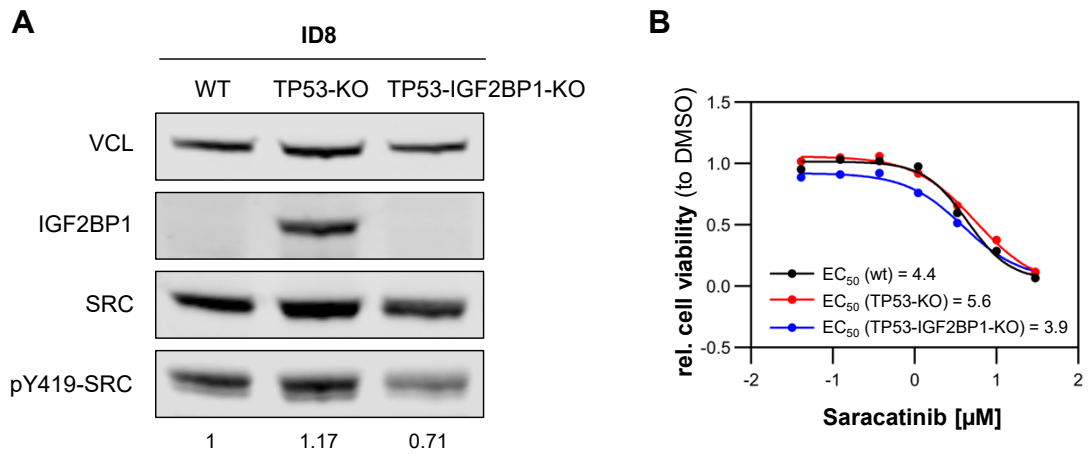


**Figure 37: The murine ID8 cells.** (A) Western blot analysis indicated an upregulation of IGF2BP1 after a TP53 knockout (TP53-KO) in the murine ID8 cells. Concomitantly, pSRC levels compared to SRC abundance were quantitatively slightly elevated while a dual depletion of TP53 and IGF2BP1 seems to reduce SRC phosphorylation again in comparison to the wild type ID8 cells (wt).  $n = 1$  (B)  $EC_{50}$  values of saracatinib were measured by determining the cell viability of ID8 cells with wild type background (wt), TP53 knockout (TP53-KO) and TP53 and IGF2BP1 knockout (TP53-IGF2BP1-KO). Calculated  $EC_{50}$  values are indicated in the diagram suggesting a higher saracatinib tolerance under TP53-KO conditions while an additional depletion of IGF2BP1 (TP53-IGF2BP1-KO) seems to sensitize the ID8 cells to saracatinib.



## List of figures

Figure 1: Origin and histotypes of epithelial ovarian cancer (EOC).....	2
Figure 2: Adherens junction assembly and disassembly.....	10
Figure 3: Activation of the SRC kinase.....	14
Figure 4: The hippo pathway and its extracellular stimulation.....	18
Figure 5: The proto-oncogenic mRNA binding protein IGF2BP1 suffers from a high re-expression in ovarian carcinoma and is associated with EMT as well as various cancer signaling pathways.....	49
Figure 6: Epithelial and mesenchymal classification of selected ovarian cancer cell lines.....	51
Figure 7: IGF2BP1 diminishes mesenchymal cell characteristics.....	53
Figure 8: A transient IGF2BP1 depletion restores AJs in ES-2 cells.....	55
Figure 9: Formation of matured AJs and its reduction in a stable cell system within ES-2 cells.....	56
Figure 10: Conservation of elevated AJs formation upon IGF2BP1 depletion.....	57
Figure 11: IGF2BP1-promoted AJ disassembly is conserved in different cell lines.....	58
Figure 12: AJ proteins are indirectly stabilized upon IGF2BP1 depletion.....	60
Figure 13: Imbalanced AJ-promoting signaling upon IGF2BP1 depletion.....	62
Figure 14: SRC activity is associated with IGF2BP1 expression in ovarian cancer cell lines.....	64
Figure 15: IGF2BP1 promotes SRC activation via its SH3-binding VP <sub>4</sub> SS motif in an RNA-independent manner.....	66
Figure 16: IGF2BP1-dependent SRC activation impairs AJ maintenance.....	67
Figure 17: IGF2BP1-promoted spheroid growth and invasion conserved in EOC-derived cell lines.....	68
Figure 18: IGF2BP1-dependent 3D growth and invasion require both, RNA binding and SRC activation.....	69
Figure 19: IGF2BP1 overcomes contact inhibition of proliferation in ES-2 cells.....	70
Figure 20: IGF2BP1-dependent stimulation of YAP1-dependent transcription in ES-2 cells.....	72
Figure 21: Association of IGF2BP1 with genes of the core hippo pathway.....	73
Figure 22: The impact of IGF2BP1-3 on hippo signaling.....	74
Figure 23: YAP1 expression correlates with IGF2BP1 abundance.....	75
Figure 24: YAP1 is directly regulated via its 3'UTR by IGF2BP1 in ES-2 cells.....	76
Figure 25: SRC inhibition rarely interferes with YAP1 activity in ES-2 cells.....	77
Figure 26: EC <sub>50</sub> calculations for BTYNB, saracatinib and verteporfin.....	78
Figure 27: Synergy scores of various drug combinations in ES-2 cells.....	79
Figure 28: IGF2BP1-dependent regulation of ERK2.....	81

Figure 29: Additive effects of saracatinib and selumetinib in combination. ....	82
Figure 30: Combination of saracatinib and selumetinib effectively targets IGF2BP1-driven phenotypes. ....	83
Figure 31: IGF2BP1-dependent effects of saracatinib and selumetinib on spheroid growth and invasion.....	84
Figure 32: IGF2BP1 contributes to resistances in single drug treatment of several EOC-derived cell lines. ....	85
Figure 33: SRCi and MEKi inhibition effectively targets IGF2BP1-driven phenotypes <i>in vivo</i> . ....	86
Figure 34: IGF2BP1 targeting SRC, ERK2 and YAP1.....	87
Figure 35: Functional enrichment analysis. ....	122
Figure 36: Cell line overview.....	123
Figure 37: The murine ID8 cells.....	124

## List of tables

Table 1: Overview of parental cell lines. ....	25
Table 2: Generated cell clones by CRISPR-Cas9 system.....	26
Table 3: Primary antibodies for Western blot and immunofluorescence staining. ....	26
Table 4: Secondary, fluorescence labelled antibodies for Western blot detection and immunofluorescence imaging. ....	27
Table 5: Commercial plasmids. ....	28
Table 6: Oligodesoxynucleotides for cloning. ....	29
Table 7: Oligodesoxynucleotides for qRT-PCR. ....	30
Table 8: Oligonucleotides for siRNA-mediated inhibition of gene expression. ....	30
Table 9: sgRNAs for establishment CRISPR-Cas9-mediated cell clones. ....	31
Table 10: Oligonucleotides for sequencing.....	31
Table 11: Commercial kits used. ....	31
Table 12: Composition of standard buffers.....	32
Table 13: Manufacturer's list of used devices.....	32

---

## List of abbreviations

%	percent
% (v/v)	percent by volume
% (w/v)	percent weight per volume
°C	centigrade
µg	microgram
µL	microliter
µM	micromolar
µm	micrometer
AHA	L-azidohomoalaine
AJs	adherens junctions
as	antisense
ATP	adenosintriphosphate
bo	both; saracatinib and selumetinib
bp	base pairs
BSA	bovine serum albumin
C	control
C1 subtype	stroma reactive / mesenchymal cluster of HGSC
C2 subtype	immunoreactive cluster of HGSC
C4 subtype	differentiated cluster of HGSC
C5 subtype	mesenchymal / proliferative cluster of HGSC
CCC	clear cell carcinoma
CCLE	Cancer Cell Line Encyclopedia
cDNA	complementary DNA
CDS	coding sequence
CIP	contact inhibition of proliferation
CLIP	cross-linking immunoprecipitation
cm	centimeter
CPM	counts per million mapped reads
CRISPR	clustered regularly interspaced short palindromic repeats
DAPI	4',6-diaminidino-2-phenylindole
DMEM	Dulbecco's modified Eagle's medium
DMSO	dimethylsulfoxid
DNA	desoxyribonucleic acid
dNTP	desoxynucleoside triphosphate
ΔSH3 (mutant)	full-length, GFP-tagged IGF2BP1 without VP <sub>4</sub> SS motif
dT	desoxythymidine

---

EC	endometroid carcinoma
EC <sub>50</sub>	half maximal effective concentration
eCLIP	enhanced CLIP
ECM	extracellular matrix
EDTA	ethylenediaminetetraacetate
EMT	epithelial-to-mesenchymal transition
EOC	epithelial ovarian carcinoma
FA	focal adhesion
FACS	fluorescence-activated cell sorting
FBS	fetal bovine serum
FC	fold change
FDR	false discovery rate
FPKM	fragments per kilobase million mapped reads
FTE	fallopian tube epithelium
g	relative centrifugal force
GAEA	gene annotation enrichment analyses
GAP	GTPase activating protein
GAPDH	glyceraldehyde 3-phosphate dehydrogenase
gDNA	genomic desoxyribonucleic acid
GEF	guanine nucleotide exchange factor
GFP	green fluorescent protein
G-11	GFP-tagged wildtype IGF2BP1
gPCR	genomic PCR
GSEA	gene set enrichment analysis
GTE <sub>x</sub>	the genotype-tissue expression
GTP	guanosine triphosphate
h	hours
HGSC	high-grade serous carcinoma
HR	homologous recombination
HR	hazard ratio
HSA	highest single agent
I1/2/3 or IGF2BP1/2/3	insulin-like growth factor 2 mRNA binding protein 1/2/3
IC <sub>50</sub>	half maximal inhibitory concentration
iCLIP	individual-nucleotide resolution CLIP
IHC	immunohistochemistry
IP	intraperitoneal
iRFP	near-infrared fluorescent protein
kb	kilobase pairs

---

kDa	kilodalton
KEGG	Kyoto Encyclopedia of Genes and Genomes
KH (mutant)	full-length, RNA-binding deficient, GFP-tagged IGF2BP1
KH1-4	hnRNPK homology domain 1 - 4
KO	CRISPR-Cas9-mediated knockout
L	liter
LGSC	low-grade serous carcinoma
log	logarithm
M	molar
m6A	N6-methyladenosine
MC	mucinous carcinoma
MEKi	MEK inhibitor selumetinib
mg	milligram
min	minutes
miRISC	miRNA-induced silencing complex
miRNA /miR	microRNA
mL	milliliter
mM	millimolar
mRNA	messenger RNA
mRNP	messenger RNP
n	number
NES	normalized enrichment score
nM	nanomolar
nm	nanometer
PAGE	polyacrylamide gel electrophoresis
PAR-CLIP	photoactivatable ribonucleoside-enhanced CLIP
PARP	poly (ADP-ribose) polymerase
PARPi	poly (ADP-ribose) polymerase inhibitor
PBS	phosphate-buffered saline
PCR	polymerase chain reaction
PD	pulldown
PFS	progression-free survival
pH	potential of hydrogen
qRT-PCR	quantitative real-time polymerase chain reaction
RBP	RNA binding protein
RFP	red fluorescent protein
RIP	RNA-co-immunoprecipitation
RNA	ribonucleic acid

---

RNP	ribonucleoprotein
rpm	revolutions per minute
RRM	RNA recognition motif
RSEM	RNA-seq by expectation maximization
RT	reverse transcription
s	sense
sa	saracatinib
SD	standard deviation
SDS	sodium dodecylsulfate
se	selumetinib
sec	seconds
SEM	standard error of mean
Seq	sequencing
Ser / S	serine
sgRNA	single guide RNA
SH2+3	SRC homology 2+3
si	siRNA knockdown
siRNA	small interfering RNA
SRCi	SRC inhibitor saracatinib
STIC	serous tubal intraepithelial carcinoma
TCGA	The Cancer Genome Atlas
TCGA-OV	ovarian tumor cohort of the TCGA
TFs	transcription factors
Thr / T	threonine
TJs	tight junctions
TMM	trimmed mean of the M-values
TPM	transcripts per million mapped reads
Tyr / Y	tyrosine
UTR	untranslated region
UV	ultraviolet
V	volt
VCL	vinculin
WB	Western blot
WHO	world health organization
WT	wildtype
ZIP	zero interaction potency

# DANKSAGUNG

An dieser Stelle möchte ich mich bei allen bedanken, die mich während meiner Promotion unterstützt, inspiriert und begleitet haben.

Als Erstes möchte ich Stefan Hüttelmaier für die Möglichkeit der Promotion und die geschaffene methodisch vielseitige und offene Forschungsumgebung danken. Danke auch für Dein Engagement, Dein Enthusiasmus und die konstruktiven und motivierenden Diskussionen, die mich stets vorangebracht haben. Durch die Mitgliedschaft im GRK1591 konnte ich zudem von regelmäßigem fachlichem Rat durch Mechthild Hatzfeld zum Thema Zellkontakte sowie kooperativen Experimenten mit Andrej Mun und René Keil profitieren, an Kongressen teilnehmen und mein Wissen im Bereich der Mikroskopie in Workshops vertiefen. Besten Dank dafür!

Ein besonderer Dank gilt Nadine Bley – für Deinen Antriebsgeist, Deinen Einsatz, das Teilen deines fachlichen Wissens und vor allem die effektive Zusammenarbeit, die eine sehr produktive Durchführung von mehreren umfassenden Experimenten gleichzeitig ermöglicht hat. Die Teamarbeit habe ich sehr genossen und hat mich stets motiviert.

Großer Dank geht auch an die gesamte AG für die tägliche fachliche Unterstützung, den schönen Laboralltag sowie die amüsanten Pausen und Ausflüge fernab der Wissenschaft. Danke Euch! Besonders möchte ich mich bei Simon Müller, Jacob Haase und Hendrik Täuber bedanken, die mir stets bei Fragen und Problemen zur Seite standen. Ein Dankeschön gebührt auch Markus Glaß. Danke für Deine Geduld, die konstruktiven bioinformatischen Lösungsansätze, die schnelle Bearbeitung und Deine Anleitung zur eigenständigen Durchführung von Analysen. Vielen Dank, Nadine Bley und Simon Müller, für die Bereitstellung der generierten NGS-Daten, die ich für zahlreiche Analysen nutzen konnte.

Zuletzt bin ich auch sehr dankbar für die Weiterführung und Beendigung einiger Experimente während meiner Schwangerschaft durch Nadine Bley, Simon Müller, Claudia Misiak und Tommy Fuchs. Ihr habt es mir ermöglicht meine Arbeit im Labor noch in dieser Zeit abzuschließen. Vielen Dank dafür!

Ganz herzlich möchte ich mich auch noch bei meiner kleinen Familie bedanken für Verständnis, Aufmunterung und die ermöglichten produktiven Nachtschichten während der Schreibphase. Vielen Dank an meine Eltern für die große Unterstützung im letzten Jahr. Max Schott und Anna Unger danke ich für Korrekturlesen und Layout. Ein großes Dankeschön gilt auch meinen Hallenser Freunden – für Motivation, Ablenkung & eine unvergessliche Zeit.

# CURRICULUM VITAE

## PERSONAL DETAILS:

Name: Annekatri Schott  
Date of birth, birthplace: 22/04/1993, Rodewisch  
Nationality: German

## EDUCATION:

08 / 2020 – 09 / 2021

**Maternity & parental leave**

since 05 / 2017

**Doctoral studies** in the laboratory of Prof. Dr. Stefan Hüttelmaier at the Institute of Molecular Medicine (IMM) at the Martin Luther University of Halle-Wittenberg, member of the RTG 1591

10 / 2014 – 03 / 2017

**Master of Science (M.Sc.) studies in Biochemistry** at the Martin Luther University Halle-Wittenberg

10 / 2011 – 09 / 2014

**Bachelor of Science (B.Sc.) studies in Biochemistry** at the Martin Luther University Halle-Wittenberg

08 / 2003 – 06 / 2011

**High-school diploma (Abitur)** at Johann-Heinrich-Pestalozzi Gymnasium, Rodewisch



## LIST OF PUBLICATIONS & CONFERENCES

Nadine Bley\*, Annekatriin Schott\*, Simon Müller, Danny Misiak, Marcell Lederer, Tommy Fuchs, Chris Aßmann, Markus Glaß, Christian Ihling, Andrea Sinz, Nikolaos Pazaitis, Claudia Wickenhauser, Martina Vetter, Olga Ungurs, Hans-Georg Strauss, Christoph Thomssen & Stefan Hüttelmaier (2021) IGF2BP1 is a targetable SRC/MAPK-dependent driver of invasive growth in ovarian cancer, *RNA Biology*, 18:3, 391-403.

\* shared first authorship

Annekatriin Schott, Nadine Bley, Danny Misiak, Marcell Lederer, Christian Ihling, Andreas Sinz, Stefan Hüttelmaier (2018) The IGF2 mRNA binding protein 1 (IGF2BP1) impairs the formation of adherens junctions in cancer cells by promoting SRC activity. 23<sup>rd</sup> Annual RNA Meeting (RNA society), University of California, Berkeley, USA (poster).

# EIDESSTATTLICHE ERKLÄRUNG

Hiermit versichere ich, dass ich die vorliegende Dissertation selbstständig und ohne fremde Hilfe verfasst habe. Ich habe keine anderen als die von mir angegebenen Quellen und Hilfsmittel benutzt. Die eingereichte schriftliche Fassung der Arbeit entspricht der auf dem elektronischen Speichermedium. Mit der vorliegenden Arbeit bewerbe ich mich erstmals um die Erlangung des Doktorgrades *doctor rerum naturalium*.

---

Ort, Datum

---

Unterschrift